Universidade do Minho
Escola de Engenharia

Ana Isabel Morais Neto

High-Throughput Processing and Analysis of Marine-based Biomaterials and Cells

Junho de 2016

High-Throughput Processing and Analysis of Marine-based Biomaterials and Cells
Ana Isabel Morais Neto
Uminho | 2016

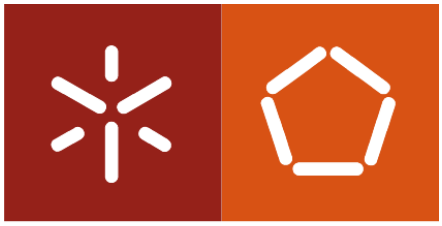

Universidade do Minho

Escola de Engenharia

Ana Isabel Morais Neto

High-Throughput Processing and Analysis of Marine-based Biomaterials and Cells

Tese de Doutoramento em Engenharia Biomédica

Trabalho efetuado sob a orientação do

Professor Doutor João Filipe Colardelle da Luz Mano

Junho de 2016

STATEMENT OF INTEGRITY

I hereby declare having conducted my thesis with integrity. I confirm that I have not used plagiarism or any form of falsification of results in the process of the thesis elaboration.

I further declare that I have fully acknowledged the Code of Ethical Conduct of the University of Minho

Universidade do Minho, / /

(Ana Isabel Morais Neto)

ACKNOWLEDGMENTS

During my PhD, several people have contributed to the accomplishment of this thesis, both professionally and personally.

Primarily, I would like to present my sincere gratitude to my parents and my brother for their endless support. Everything I did was for them. They always believed in me and never questioned my choices. Unquestionably, the autonomy and responsibility that they have handed me since my youth have been vital in my personal development not only as an individual but also as a scientist.

My first scientific acknowledgement goes to my supervisor Prof. João Mano, without whom this thesis would not be possible. Thanks for giving me the opportunity to join the 3Bs Research Group and also for providing me all the tools and means to perform my scientific work. All over these seven years that we have been working together, he always gave me an invaluable guidance, attention, confidence that made me feel proud for working under his supervision. I could never accomplish the scientific merit of my publications without his constant and positive encouragement, "crazy" but useful brainstorms and future prospects. My sincere thanks.

I would like to acknowledge Dr. Pavel Levkin. I really appreciate of having had the opportunity to have gone to Germany and have worked on Institute of Technology and Genetic of the prestigious KIT University. I would like to thank for the support and the enlightening scientific discussions that always left me with more to think about and work to do. For his patience and willing to provide me an eye-opening view, with clever solutions always towards a much-needed reality check.

I would also like to acknowledge the 3B's Research Group and its director, Prof. Rui Reis, for the possibility of developing my PhD work in such well-equiped facilities and highly reputed institution.

I would like to acknowledge Prof. Nuno Neves who, as a representative of the Doctoral Program in Biomedical Engineering, helped me through the academic process related to the University of Minho.

A huge thank to the whole team of Prof. João Mano for all the productive meetings with valuable discussions. My special thanks are directed to Mariana Oliveira, Clara Correia, Catarina Custódio, Sara Oliveira, Natália Vasconcelos, Gisela Luz and Isabel Hermida, who directly contributed with their specific expertise to the work presented in this thesis.

To all my 3Bs colleagues that directly or indirectly contributed for this thesis and the staff for their help and friendship.

I would like to thank all my lab mates of Levkin lab, especially Anna, Konnie, Tina and Danuta who made a rainy and cloudy Germany a very warm place to be. Thanks for all the support on the lab, but mainly for all the peculiar moments and laughs. You definitely made my journey even better and funnier.

To the Portuguese Foundation for Science and Technology for the financial support through a Ph.D. grant with the reference SFRH/BD/73119/2010

To my “ressabiadas” friends, for all the travels and good moments that we shared. I am really glad and pleased to have people that I can trust and share my life. No matter the distance, they always encourage me to keep going and care about my positive and negative feelings.

A special thanks goes to Nuno Relvas, for all the time that he spent helping me, supporting every decision that I made, and for all his patience that contributed positively to my work.

The last and undoubtedly the deepest gratitude go to my family. Thanks for all unconditional love, care, aid, patience and emotional support. I am so fortunate to have all of you with me, always. Thanks for being the best.

My final words go to my grandmother. Thank you for all the candles and prayers. Thank you for never give up and be always on my side when I most needed. The education and values that you taught me, made me who I am today. I had promised you that one day I would finish my graduation and I did it. To you, my dear grandmother, I dedicate this thesis.

ABSTRACT

As the field of Tissue Engineering (TE) progresses, new technology are essential to accelerate the identification of potentially translatable approaches for the repair of tissues damaged due to disease or trauma. The development of high-throughput and combinatorial technologies is helping to speed up research that is applicable to all aspects of the TE paradigm. In this thesis, interactions of cells with many diverse materials in both two- and three-dimensions was assessed rapidly through the use of superhydrophobic (SH) chips for rapid outcome measurements of cell-material or cell-cell combinations. The main hypothesis is that flat biomimetic SH surfaces patterned with transparent superhydrophilic (SL) spots were used to individual pattern biomaterials with precise shape and pre-determined height, by controlling the volume dispensed in each wettable spot. Initially, distinct combinations of nanostructured films were produced using layer-by-layer methodology and their morphological, physicochemical, and biological properties were analyzed using glass slides and then validated on-chip. Inspired by the composition of the adhesive proteins in mussels, thin films containing dopamine-modified hyaluronic acid were studied. The flat configuration of the SH chip allowed to perform a series of nondestructive and non-conventional measurements directly on the individual spots. *In situ* adhesion properties were directly measured in each wettable spot, showing that nanostructured films richer in dopamine promote the adhesion compared to control films (hyaluronic acid and alginate films – two polysaccharides often regarded as good natural adhesives – were assembled in parallel). *In vitro* tests showed an enhanced cell adhesion for the films with more catechol groups.

Combining two biomimetic concepts we developed devices with multifunctional capabilities. One approach was based on two-sided film made almost entirely from polystyrene onto which the properties of both lotus leaves and mussel adhesive were incorporated. On one side of the film, imparting micro and nanometer scale hierarchical roughness yields superhydrophobicity and water repellency, providing rapid fluid flow and the basis for microfluidic devices, as such synthetic blood or fluid flow vessels. On second approach, SH microarray based on the so-called lotus effect were produced, onto which arrays of micro-indentations allow the fixing of liquid droplets, based on the rose-petal effect. Such platforms were able to sustain arrays of quasi-spherical microdroplets, allowing the isolation and confinement of different combinations of substances and living cells. Distinct compartmentalized physical, chemical, and biological processes were monitored individually in each droplet. In addition, taking the advantage of controlled positional adhesion and minimum contact with a solid substrate, we developed a novel hanging

spherical drop system for anchoring arrays of droplets of cell suspension. By facing the chip downward it was possible to generate independent spheroids bodies in a high throughput manner, in order to mimic *in vivo* tumor models in a lab-on-chip scale. The system was validated for drug screening purposes and the toxicity of the anti-cancer drug doxorubicin in cell spheroids was tested and compared to monolayer cells culture.

Finally, high-throughput fabrication of alginate hydrogel particles of specific sizes and shapes was developed using a droplet microarray. The method was based on the formation of arrays of droplets of pre-hydrogel solutions on SH-SL patterns using the process of discontinuous de-wetting, followed by their gelation via the parallel addition of the crosslinker to the individual droplets via the sandwiching method. The viability of living cells incorporated within the hydrogel particles was evaluated showing to be higher during the long-term cultivation than in the case of cells cultured in the bulk three-dimensional hydrogel matrix.

In conclusion, SH platforms patterned with wettable spots used in this thesis proved to be compatible with a complete study of both two- and three-dimensional biomaterial-cell interactions, comprising a wide set of factors as biomaterials characterization and *in vitro* testing. Although much of the work performed is only applicable for *in vitro* studies, future methods may translate into rapid screening of these approaches *in vivo*.

RESUMO

Com o progresso da área de engenharia de tecidos (ET), novas tecnologias são essenciais para acelerar a identificação de abordagens potencialmente adaptáveis para a reparação de tecidos danificados devido a doenças ou traumatismo. O desenvolvimento de testes expeditos e tecnologias combinatórias está a ajudar a acelerar a investigação que é aplicável para todos os exemplos dos paradigmas de ET. Nesta tese, as interações das células com vários materiais, tanto em duas como em três dimensões, foram rapidamente analisadas através de *chips* superhidrofóbicos (SH), de modo a obter medições rápidas das combinações entre células-materiais ou células-células. A hipótese principal é que superfícies planas SH padronizadas com regiões superhidrofílicas (SL) transparentes foram usadas para depositar biomateriais com forma e altura precisas, controlando o volume depositado em cada área molhável. Inicialmente, combinações distintas de filmes nano-estruturados foram produzidos através da metodologia de camada-sobre-camada, e as suas propriedades morfológicas, físico-químicas e biológicas foram analisadas em lâminas de vidro, e posteriormente, validadas em *chip*, tendo como inspiração a composição das proteínas adesivas existente nos mexilhões. Filmes finos compostos por ácido hialurónico modificado com dopamina foram alvo de estudo. A configuração plana do *chip* SH permitiu executar uma série de medições não-destrutivas e não-convencionais diretamente sobre as regiões molháveis. As propriedades de adesão *in situ* foram diretamente medidas em cada região hidrofílica, mostrando que os filmes nano-estruturados com mais dopamina promovem a adesão, em comparação com filmes usados como controlo (filmes de ácido hialurónico e de alginato - dois polissacarídeos considerados como bons adesivos naturais - foram construídos em paralelo). Os testes *in vitro* mostraram uma melhor adesão celular para os filmes com mais grupos *catechol*.

A combinação de dois conceitos bio-miméticos permitiu desenvolver dispositivos com capacidades multifuncionais. Uma primeira abordagem foi baseada num filme contendo duas faces, feito inteiramente a partir de poliestireno, integrando as tanto as propriedades das folhas de lótus as adesivas do mexilhão. Um lado do filme obtém superhidrofobicidade e alta repelência à água devido à rugosidade hierárquica e à escala micro e nano-métrica, proporcionando um fluxo de fluido rápido e uma base para novos dispositivos para microfluídica, como tal sangue sintético ou fluxo de fluidos nos canais. Na segunda abordagem, as superfícies SH baseadas no efeito de lótus foram padronizadas com micro-indentações para fixar gotas líquidas, mimetizando o efeito das pétalas de rosas. Estas plataformas foram capazes de suportar matrizes de micro-gotas quase esféricas, permitindo o isolamento e aderência de diferentes

combinações de substâncias e células vivas. Diversos processos, tais como, físicos, químicos e biológicos foram monitorizados individualmente em cada gota. Além disso, tendo em conta a vantagem da adesão controlada da posição e contacto mínimo da gota com a superfície sólida, desenvolvemos um novo sistema de gota esférica pendurada de modo a fixar matrizes de gotas contendo suspensão de células. Voltando a superfície sólida para baixo, foi possível gerar corpos independentes de esferoides de uma forma expedita, de modo a mimetizar modelos *in vivo*, a uma escala *lab-on-chip*. O sistema foi validado para fins de rastreio de fármacos e a toxicidade da doxorubicina nos esferoides foi testada e comparada com a cultura de células em monocamada.

Finalmente, o fabrico expedito de hidrogeis de alginato com o tamanho e forma especifica foi desenvolvido usando superfícies padronizadas de gotas. O método foi baseado na formação de matrizes de gotas de soluções pré-hidrogel nas superfícies padronizadas SH com regiões SL usando um processo molhável descontinuo. O processo de formação de gel foi obtido através da adição paralela de um agente reticulante a cada gota individualmente, usando um método "sandwich". A viabilidade das células incorporadas dentro do hidrogel foi avaliada para um longo tempo de cultura mostrando ser mais elevada em comparação com as células incorporadas dentro de uma matriz 3D de hidrogel em massa.

Em conclusão, as superfícies padronizadas SH com regiões molháveis provaram ser compatíveis com um estudo completo de interações 2D e 3D entre células e biomateriais, compreendendo um vasto conjunto de factores como a caracterização de biomateriais e testes *in vitro*. Embora a maioria do trabalho realizado só tem aplicabilidade para estudos *in vitro*, métodos futuros podem transpor para uma seleção rápida destas abordagens *in vivo*.

TABLE OF CONTENTS

LIST OF ABBREVIATIONS AND ACRONYMS

μCT microcomputed tomography

μL microliter

μm micrometer

$\Delta f/\upsilon$ normalized frequency

υ overtone

ΔD dissipation

ω angular frequency

ρ density

h thickness

η viscosity

θ angle

γ interfacial tensions

2D two-dimensional

3D three-dimensional

A

AFMatomic force microscopy

ALG alginate

ATR attenuated total reflectance

C

CAHcontact angle hysteresis

CHTChitosan

cm centimetre

C-NMR carbon-13 nuclear magnetic resonance

$CuSO_4$ cooper sulphate

D

D_2O deuterated water

DMA droplet microarray

DMPAP 2,2-dimethoxy-2- phenylacetophenone

DMEM Dubelcco's Modified Eagle Medium

DN dopamine

DOPA 3,4-dihydroxyphenylalanine

Dox doxorubicin

E

E young's modulus

ECM extracellular matrix

EDMA ethylene dimethacrylate

ethylcarbodiimide hydrochloride

EDTA ethylenediaminetetraacetic acid

ePTFE poly(tetrafluoroethylene)

F

FBS fetal bovine serum

FTIRFourier-transform infrared

H

HA hyaluronic acid

HA-DN dopamine-modified HA

HCl hydrochloric acid

HeLa-GFP human cervical tumor cell line expressing GFP

HEMA 2-hydroxyethyl methacrylate

H-NMR proton nuclear magnetic resonance

HTS high-throughput screening

L

LbL layer-by-layer

L929 lung fibroblastic cell line

M

M molar

MAPs mussel adhesive proteins

mg milligram

min minute

mL mililiter

mm milimeter

MHz megahertz

MTS(3-(4,5-dimethyl-2-yl)-5-(3-carboxy-methoxyphenyl)-2-(4-sulfophenyl)-2H-tetrazolium

MTT 3-(4,5-Dimethylthiazol-2-yl)- 2,5-diphenyltetrazolium bromide

MLIy-CMV-mCherry-neo Red fluorescent rat mammary carcinoma

MW molecular weight

N

n number of samples

NaCl sodium chloride

$NaIO_4$ sodium periodate

NMR nuclear magnetic resonance

P

PBS phosphate buffered saline

PDMS polydimethylsiloxane

PS polystyrene

PVC polyvinyl chloride

Q

QCM-D Quartz crystal microbalance

R

Ra average roughness

Rq root mean Square

S

SEM scanning electron microscopy

SH superhydrophobic

SL superhydrophilic

SaOs-2 human primary osteosarcoma cell line

T

THF tetrahydrofuran

U

UVO ultraviolet/ozone

W

WCA water contact angle

LIST OF FIGURES

CHAPTER 1. PATTERNED SUPERHYDROPHOBIC SURFACES TO PROCESS AND CHARACTERIZE BIOMATERIALS AND 3D CELL CULTURES

CHAPTER 2. MATERIALS AND METHODS

LIST OF TABLES

LIST OF PUBLICATIONS AND COMMUNICATIONS

The work performed under the scope of this thesis resulted in the publications listed bellow:

Papers in international scientific journals with referees

1. **Neto A. I.**, Levkin P. and Mano J. F. Patterned superhydrophobic surfaces to process and characterize biomaterials and 3d cell cultures. 2016. Submitted.

2. **Neto A. I.**, Demir K., Popova A. A., Oliveira M. B., Mano J. F. and Levkin P. A. Fabrication of Hydrogel Particles of Defined Shapes using Hydrophilic-Superhydrophobic Micropatterns. Advanced Materials. 2016, Accepted manuscript.

3. **Neto A. I.**, Vasconcelos N. L., Oliveira S.M., Ruiz-Molina D. and Mano J. F. High-throughput topographic, mechanical and biological screening of multilayer films containing mussel-inspired biopolymers. Advanced Functional Materials, 26, 2745-2755, 2016.

4. **Neto A. I.**, Correia C. R., Oliveira M. B., Rial-Hermida I., Alvarez-Lorenzo C., Reis R. L. and Mano J. F. A novel hanging spherical drop system for the generation of cellular spheroids and high throughput combinatorial drug screening. Biomaterials Science, 3, 581-585, 2015.

5. **Neto A. I.**, Correia C. R., Custódio C. A., and Mano J. F. Biomimetic Miniaturized Platform Able to Sustain Arrays of Liquid Droplets for High-Throughput Combinatorial Tests. Advanced Functional Materials, 24, 5096–5103, 2014.

6. **Neto A. I.**, Cibrão A. C., Correia C. R., Carvalho R. R., Luz G. M., Ferrer G. G., Botelho G., Picart C., Alves N. M., and Mano J. F. Nanostructured Polymeric Coatings Based on Chitosan and Dopamine-Modified Hyaluronic Acid for Biomedical Applications. Small, 12, 2459–2469, 2014.

7. **Neto A. I.**, Meredith H. J., Jenkins C. L., Wilker J. J., and Mano J. F. Combining Biomimetic Principles from the Lotus Leaf and Mussel Adhesive: Polystyrene Films with Superhydrophobic and Adhesive Layers. RSC Advances, 3, 9352-9356, 2013.

Publications resulting from collaborative work

1. Oliveira, M.B., **Neto A. I.**, Correia C. R., Rial-Hermida M. I., Álvarez-Lorenzo C., and Mano J. F. Superhydrophobic Chips for Cell Spheroids High-Throughput Generation and Drug Screening. ACS Appl. Mater. Interfaces, 6, 9488-9495, 2014.

2. Oliveira M. B., Ribeiro M. P., Miguel S. P., **Neto A. I.**, Coutinho P., Correia I. J., and Mano J. F., "In Vivo High-Content Evaluation of Three-Dimensional Scaffolds Biocompatibility", Tissue Engineering Part C - Methods, 20, 851-864, 2014.

3. Costa R. R., **Neto A. I.**, Calgeris I., Correia C. R., Pinho A. C. M., Fonseca J., Öner E. T., and Mano J. F. Adhesive nanostructured multilayer films using a bacterial exopolysaccharide for biomedical applications. Journal of Materials Chemistry B, 1, 2367-2374, 2013

4. Silva J. M., Duarte A. R. C., Custódio C. A., Sher P., **Neto A. I.**, Pinho A. C. M., Fonseca J., Reis R. L., and Mano J. F. Nanostructured Hollow Tubes Based on Chitosan and Alginate Multilayers. Advanced Healthcare Materials, 3, 433–440, 2013.

Conference abstract published in international scientific journals

1. **Neto A. I.**,Correia C. R., Custódio C. A. and Mano J. F. Miniaturized droplets-based microarray of chemical and biological high-throughput tests. Journal of Tissue Engineering and Regenerative Medicine, vol. 7, issue 1, pp. 6-52, DOI: 10.1002/term.1822, 2013.

2. **Neto A. I.**, Vasconcelos N. L., Oliveira S. M. and Mano J. F. Combinatorial analysis of marine based biomaterials: High-throughput analysis of the effect of nanostructured multilayers on cell behavior. Journal of Tissue Engineering and Regenerative Medicine, vol. 7, issue 1, pp. 6-52, DOI: 10.1002/term.1822, 2013.

3. **Neto A. I.**, Cibrão A. C. ,Correia C. R., Carvalho R. R. Luz G. M, Ferrer G. G. , Botelho G., Picart C., Alves N. M. and Mano J. F. Polymeric layer-by-layer films composed by natural polymers and based on the adhesive properties of mussels for biomedical applications. Journal of Tissue Engineering and Regenerative Medicine, vol. 7, issue 1, pp. 6-52, DOI: 10.1002/term.1822, 2013.

4. Oliveira M. B., **Neto A. I.**, Rial-Hermida M. I., Alvarez-Lorenzo C. and Mano J. F. High-throughput drug screening using cell spheroids in superhydrophobic patterned chips. Journal of Tissue Engineering and Regenerative Medicine, vol. 7, issue 1, pp. 6-52, DOI: 10.1002/term.1822, 2013.

5. Silva J. M., Duarte A.R.C., Custódio C. A., Sher P., **Neto A. I.**, Reis R. L. and Mano J. F. Nanostructured hollow tubes based on Chitosan and alginate multilayers. Journal of Tissue Engineering and Regenerative Medicine, vol. 7, issue 1, pp. 6-52, DOI: 10.1002/term.1822, 2013.

Oral communications

1. **Neto A. I.**, Vasconcelos N. L., Oliveira S. M. and Mano J. F. Combinatorial analysis of nanostructured multilayers films using mussel adhesive inspired polymer, Cost Action TD0906, Istanbul, Turkey, May 2014.

2. **Neto A. I.**, Cibrão A. C. , Luz G. M, Ferrer G. G. , Botelho G., Picart C., Alves N. M. and Mano J. F. Layer-by-layer coatings inspired by the adhesive properties of marine mussels., 25th European Conference on Biomaterials and 10th Young Scientific Forum, Madrid, Spain. September, 2013

3. Costa R. R., **Neto A. I.**, Calgeris I., Correia C. R., Pinho A. C. M., Fonseca J., Öner E. T., and Mano J. F. Layer-by-layer assembly using bacterial Levan adhesive polymer. Cost Action TD0906, WG3 & WG4 Scientific Workshop, Biological Adhesives: from Biology to Biomimetics, Cluj-Napoca, Romania May, 2013.

Poster communications

1. **Neto A. I.**, Vasconcelos N. L., Oliveira S. M. and Mano J. F. High-throughput analysis of nanostructured multilayers films on cell behavior and adhesiveness. TERMIS, Genova, Italy, June 2014.

2. **Neto A. I.**, Cibrão A. C., Luz G. M, Ferrer G. G. , Botelho G., Picart C., Alves N. M. and Mano J. F. Nanostructured Polymeric Coatings Based on Chitosan and Dopamine-modified Hyaluronic Acid for Biomedical Applications. TERMIS, Istanbul, Turkey, June, 2013.

3. Costa R. R., **Neto A. I.**, Calgeris I., Correia C. R., Pinho A. C. M., Fonseca J., Öner E. T., and Mano J. F. Bacterial Levan-Derivatives: An Alternative Adhesive Biomaterial for Medical and Tissue Engineering Applications. TERMIS, Istanbul, Turkey, June, 2013.

4. **Neto A. I.**, Cibrão A. C. ,Correia C. R., Carvalho R. R. Luz G. M, Ferrer G. G. , Botelho G., Picart C., Alves N. M. and Mano J. F. Mussel-inspired adhesive multilayers coatings for biomedical applications. 2nd meeting ICVS/3Bs, Braga, Portugal, June, 2013.

5. **Neto A. I.**, Cibrão A. C. , Luz G. M, Ferrer G. G. , Botelho G., Picart C., Alves N. M. and Mano J. F. Nanostructured multilayer films exhibiting using mussel adhesive inspired polymers. 1st ERC-BIOMIM Congress, Minatec, Grenoble Institute of Technology, France, April, 2013

6. **Neto A. I.**, Wilker, J.J., Mano, J.F.,High-throughput screening aproach based on patterned superhydrophobic substrates: a possible platform for combinatorial nanostructures multilayer films using marine-inspired macromolecules, 124th BASF International Summer Course, Ludwigshafen, Germany, August 2012.

7. **Neto A. I.,** Cibrão, A.C., Alves, N.M. and Mano, J.F., Nanostructured multilayer films exhibiting adhesive properties using dopamine modified- hyaluronic acid and Chitosan, II Meeting of ICVS/3B's Associate Laboratory, Braga, Portugal, May, 2012.

8. **Neto A. I.**, Wilker, J.J., Mano, J.F.,Learning twice with nature to produce new polystyrene-based biomimetic films, 1st International Conference on Biological and Biomimetic Adhesives, Cost Action TD0906, Lisbon, Portugal, May, 2012.

9. **Neto A. I.**, Cibrão, A.C., Alves, N.M. and Mano, J.F., Nanostructured films exhibiting adhesive properties using dopamine-modified, hyaluronic acid and Chitosan, 1st International Conference on Biological and Biomimetic Adhesives, Cost Action TD0906, Lisbon, Portugal, May, 2012.

10. **Neto A. I.**, Custódio, C.A., Song, W. and Mano J.F., Patterned superhydrophobic surfaces as a new platform for high-throughput evaluation of biomaterials interactions with proteins and cells, Competition World day of Materials, Faculty of Science and technology, New University of Lisbon, Lisbon, Portugal, November 2011.

11. **Neto A. I.**, Custódio, C.A., Song, W. and Mano J.F., Combinatory assessement of interactions between biomaterials, proteins and cells using patterned superhydrophobic substrates, TERMIS Europe, Granada, Spain, June 2011.

12. **Neto A. I.**, Custódio, C.A., Song, W. and Mano J.F., High-throughput characterization of materials on patterned superhydrophobic substrates: a possible platform for combinatorial tests of biological adhesives, 2nd scientific meeting of Biological and biomimetic adhesives, Cost action TD0906, Mons, Belgium, May 2011.

Awards

1. COST Action: TD0906, Training School Title: Nanomechanics in biomolecular adhesion. Venice, Italy, January, 2014

2. 124th BASF International Summer Course, Ludwigshafen, Germany, August 2012.

3. 1st SPM Award (Portuguese Society of Materials), Competition of the World day of Materials, Faculty of Science and Technology, New University of Lisbon, Lisbon, Portugal, November 2011.

INTRODUCTION TO THE STRUCTURE OF THE THESIS

This thesis is organized in 4 sections, in a total of 9 Chapters. The first section provides a general introduction to the thesis. It is based on review paper submitted for publication. The second section comprises a single Chapter addressing the materials and methods performed to accomplish the experimental work giving rise to this thesis. The third section is based on a set of 6 research articles accepted for publication in international peer-reviewed journals. The forth section summarizes the main outcomes of this thesis and explores future perspectives on the research field. The identification of the original publications regarding submitted/accepted articles can be found in the presenting page of each Chapter.

Section I – General Introduction

Chapter 1. Patterned superhydrophobic surfaces to process and characterize biomaterials and 3D cell cultures. The evolution of up-scaling microarray platforms are reviewed for 3D cell culture in order to meet the criteria of complex biological environments for tissue engineering and disease models.

Section II – Experimental Section

Chapter 2. Materials and Methods. The experimental setups used to produce the materials used in this thesis are presented. The techniques performed for biomaterials physicochemical, morphological and cellular interaction analysis are also addressed.

Section III – Optimization of multilayer films and superhydrophobic microarrays for high-throughput tissue engineering studies

Chapter 3. Nanostructured Polymeric Coatings Based on Chitosan and Dopamine-modified Hyaluronic Acid for Biomedical Applications. Inspired by the structure and composition of adhesive proteins in mussels, dopamine-modified hyaluronic acid is used to form thin and surface-adherent multilayer films that present an enhance cell adhesion, demonstrating their potential for biomedical applications.

Chapter 4. Combining Biomimetic Principles from the Lotus Leaf and Mussel Adhesive: Polystyrene Films with Superhydrophobic and Adhesive Layers. Two biomimetic concepts are used for developing devices

with multifunctional capabilities. The superhydrophobic properties of a lotus leaf is joined with the permanent adhesive bonding of marine mussels.

Chapter 5. High-throughput topographic, mechanical and biological screening of multilayer films containing mussel-inspired biopolymers. Inspired by the structure of mussel adhesive proteins, layer-by-layer coatings are developed. Many combinations of multilayers films are individually disposed on isolated transparent spots, patterned onto biomimetic superhydrophobic substrates. The adhesion properties of the coatings are analyzed in a high-throughput way. *In vitro* tests are carried out to evaluate the biological performance of the multilayer films that could be useful in distinct biomedical applications.

Chapter 6. Biomimetic miniaturized platform able to sustain arrays of liquid droplets for high-throughput combinatorial tests. A flat platform is developed for high throughput screening of multiplexed and accelerated evaluations of physical, chemical and biological processes in lab-on-chip scale. The device permits to confine and analyze different combinations of elements and conditions in spherical aqueous-based environments.

Chapter 7. A novel hanging spherical drop system for the generation of cellular spheroids and high throughput combinatorial drug testing. Flat SH substrates is used to arrange arrays of quasi-spherical cell culture droplets with the capability to build-up 3D spheroids in a high throughput manner, in order to mimic *in vivo* tumour models in a lab-on-chip scale.

Chapter 8. Fabrication of Hydrogel Particles of Defined Shapes using Hydrophilic-Superhydrophobic Micropatterns. High-throughput fabrication of free-standing hydrogel particles with defined geometry and size for 3D cell culture, cell screenings and modular tissue engineering. The method employs discontinuous de-wetting using superhydrophobic-hydrophilic micropatterns.

Section IV – Concluding Remarks and Future Perspectives

Chapter 9 - Conclusions and Future Perspectives. This Chapter finalizes the thesis by comprising its major conclusions and exploring future perspectives and needs in the field.

SECTION I. GENERAL INTRODUCTION

CHAPTER 1. PATTERNED SUPERHYDROPHOBIC SURFACES TO PROCESS AND CHARACTERIZE BIOMATERIALS AND 3D CELL CULTURES

1.1 Abstract

Cell-based microarrays are powerful experimental tools for high throughput screening of large numbers of test samples. We review the evolution of up-scaling microarray platforms for three-dimensional cell culture in order to meet the criteria of complex biological environments for tissue engineering and disease models. Recently, patterned microarrays with extreme wettabilities are suggested as a sophisticated platform for high-throughput assays to generate cell environments, as well as, characterize and analyze biomaterials properties and cell-cell and cell–biomaterial interactions. We conclude that among the emerging high throughput approaches, platforms with extreme wettabilities holds a great potential to provide three-dimensional cell based constructs with high temporal, spatial control and versatility, which makes these miniaturized systems very attractive for regenerative medicine and drug screening applications.

1.2 Introduction

In the field of regenerative medicine, smart and intelligent biomaterials that mimic the complex environment of native tissues have been developed [1, 2]. Current approaches on the design of biomimetic biomaterials with appropriate physical, chemical, and biological properties are costly, inaccurate and inefficient. This is attributed to complex cell-matrix and cell-cell interactions, which are difficult to mimic under *in vitro* conditions. Cell-based assays offer the opportunity to perform screens of chemical libraries for molecules that modulate a broad range of biological events [3, 4]. Despite exciting progress in multiplexed cell screening, most of these studies have focused on cellular responses on two-dimensional (2D) surfaces, and the associated cost of throughput phenotypic cell-based screening using conventional well-plate platforms can be unaffordable [5, 6]. To address this critical issue, microarray technologies for high-throughput screening (HTS) of multiplexed biomaterials and cells analysis have been widely proposed [7-18]. Given its throughput and data-rich nature, HTS is very much influenced by advances in automation and miniaturization, and is under constant development [18-22]. However, cells grown 2D on flat and rigid substrates are facing an unnatural environment and behave differently compared with cells grown in their native three-dimensional (3D) environment [16, 23-27]. The dimensionality of the system in which cells are studied can influence a number of cell functions, including polarity, morphology, motility, and cell–cell interactions, as reviewed by Baker and Chen [28]. Many of these shortcomings have been overcome through the use of arrays of cell-biomaterial and cell-cell

interactions in 3D microenvironment to guarantee a successful therapeutic outcome [23]. These interactions are able to recapitulate important *in vivo* conditions and thereby help us to design smart and bio-responsive materials to tailor the differentiation and commitment potential of encapsulated stem cells [1, 29, 30]. Structural, physical, and chemical properties of biomaterials play a major role in controlling cellular fate. The use of miniaturized cell-based microarrays, in which cells are grown in biomaterial surfaces, will significantly improve the ability in identifying the right material combinations for different tissue engineering approaches [12, 13, 26, 31].

Over the last years, miniaturized devices have demonstrated their potential and benefits for many applications, including point-of-care diagnostics, genomic and proteomic research, analytical chemistry, environmental monitoring, and the detection of biohazards [32-35]. Several technologies have enabled the fabrication of 3D biomaterial microarrays for high-throughput screening of cellular fates within 3D microenvironments [11, 36-38]. Such technologies present many advantages compared to bulkier and conventional analytical instruments: the precise control of liquids, minimize consumption of reagents and samples, favor short reaction times, enable highly parallel and multiplexed analysis, require little or less power to operate, are portable, and potentially have low cost of production.

The unique properties of nanostructure surfaces with extremes in wettability have motivated the researchers on the development of a novel generation of 3D biomaterial and cell microarrays and microfluidics [39-42].

This review focuses on the recent advances in superhydrophobic (SH) microarrays for 3D HTS cell assays, and its impact on cell biology, tissue engineering and regenerative medicine and drug screening. We highlight that bioinspired substrates with extreme and controllable wettability ranging from SH to superhydrophilic (SL) regimes could bring the possibility of new investigations of cell–biomaterial and cell-cell interactions. The range of applications is remarkably broad and including the formation of 3D cell niches using biomaterials, microgels particles, scaffolds or as cell spheroids. This article focus on the main motivations and requirements in the biomedical field that pushed for the utilization of SH platforms as suitable alternative device for HTS analysis, as well as the great evolution of applications that have emerged in the last few years. We conclude by outlining some of the future prospects using 3D microarray technology to promote the development of complex macroscale 3D networks or combinations of building blocks on timescales previously unseen using current HTS technologies.

1.3 Evolution of high-throughput screening platforms

HTS approaches are powerful tools to fabricate and probe extremely large combinations of structural, biophysical and biochemical parameters and thus elucidate some of the mechanisms that dictate cell biology. The premise of HTS is to automate and miniaturize the assay process, thereby significantly decreasing the cost and time promises of screening a biological target against thousands of biomaterials and compounds.

HTS assays are used for screening of different types of libraries, including combinatorial chemistry, genomics, protein, and peptide libraries [10, 43-45]. At present, most of HTS studies in biomedical research areas such as drug toxicology and cell-based screening have been carried out mainly in 2D environment [8, 10, 17, 18, 46, 47]. Such models are used for evaluating the effectiveness and safety of libraries of drugs and other bioactive or potentially therapeutic molecules [48]. Recent studies have focused on supporting the growth and controlling the differentiation of stem cells, due to the enormous therapeutic benefits that stem cells offer [10, 13, 30, 49-53]. However, conventional *in vitro* cellular microenvironments based on flattened 2D substrates (e.g. culture dish or multi-well plate) are far from being capable to recapitulate the complexity of the native cellular microenvironments. Cells seeded onto 2D substrates are polarized maintaining one part of their surface anchored and the rest exposed to the culture media. This contrast with the natural micro-environment of the tissues where cells interact with different cells and ECM. Therefore, considerable efforts have been made to upgrade *in vitro* cellular niches from 2D to 3D network. A variety of 3D culture systems, as well as the adoption of 3D cell culture systems in drug discovery, cancer cell biology, stem cell study, engineered functional tissues for implantation, and other cell-based analysis have been proposed [26, 54]. Such systems provide more reliable *in vitro* models, allowing to investigate multiple cell types, extracellular matrices and bioactive soluble factors with well-defined 3D microscale arCHTtectures and specific functions [55]. A more accurate prediction of drug responses is also aCHTeved [56, 57].

Biomaterial-assisted 3D cell culture (Figure 1.1) is widely used to construct 3D cellular microenvironments by encapsulating cells in 3D matrices, usually in the form of aqueous hydrogels [58-61] or porous scaffolds [23, 62, 63]. Moreover, *in vivo* cells lie in a 3D configuration organized in the self-secreted microenvironment, the ECM, both in organs and tumor masses. In this milieu, cells interact in a totally natural manner, without the intervention of foreign factors, such as biomaterials. The use of cell spheroids has been also suggested as a potential link to bridge the gap between monolayer cultures and animal model studies [56, 63, 64].

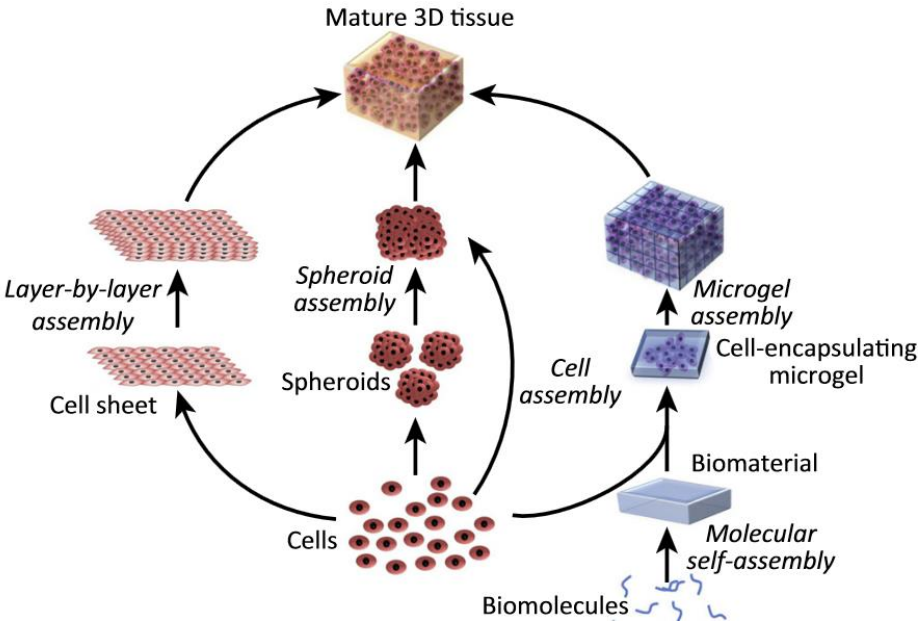

Figure 1.1 Schematic of 3D strategies from the bottom to the top for engineering 3D tissue constructs [65].

Micro-well plates and robotic spotting are examples of well-established technologies for high throughput applications [52]. Standard HTS assays are currently run in 96-well micro-titer plates in batch formats, since automation and detection instruments have been designed to be compatible with these plates. Although combinatorial chemical synthesis can also be carried out assays in plates with 384 and 1536-wells format which use the same plate dimensions and are being widely implemented, which would increase the throughput and reduce reagent costs [49, 56, 63, 64, 66, 67]. However, these methods are typically labor-intensive, time-consuming, and extremely expensive. In addition, the shape of such commercially available well plates present stiff and high walls, impairing several characterization analysis that require the insertion of probes, passage of beams through the biomaterials or image analysis. Plenty of researches have been reported about the study of drug metabolism and drug-induced cytotoxicity [8, 13, 31, 49, 66, 68-70] but the characterization of metabolites and cytotoxicity assays could not be realized on the same platform. Among the types of 3D cultures that use 96-well formats are those that assay cell aggregates, or cells in gel particles, suspended in wells, and those that assay cells grown in thin gels on the surface of 96-well plates or 96-well inserts [26]. The majority of these methods use 3D constructs that are typically non-uniform in dimensions, and fail to provide information about cells in different areas within a single 3D construct. In addition, using 3D culture in multi-well formats unable to recreate the pre-defined microscale arCHTtectural features of the native tissue niches (e.g. bifurcated vasculature, neuronal networks, or hexagonal lobules in the liver), which is of great importance in enabling the resulting functions [54]. The integration of microfabrication techniques enables construction of 3D

cellular microenvironments with precisely controlled arCHTtectural features, which can pattern the matrices and the encapsulated cells in pre-defined locations recreating the complex tissue networks [12, 26, 71]. Meanwhile, the micro-patterned biomaterial-based 3D cellular microenvironments can be readily replicated in a HTS manner to allow parallel cell-based assays, which could generate a huge amount of information for systematic studies in modern biology, regenerative medicine and drug discovery [12, 21, 31, 56].

Miniaturized devices for cellular experiments and cell-based assays on chip have expanded dramatically in the last decade [3, 4, 10, 31, 50, 53, 72-76]. The majority of the research within the field of the miniaturization has been directed toward the biological and life sciences. Biochips, cell/protein/DNA arrays, microfluidics, micro-systems, micro-reactors, and medical MEMS are frequently used terms [57, 74, 77-80].

Miniaturization of assay technologies coupled with automation of HTS combinatorial synthesis is helping to set the stage for screening 50 - 100,000 samples/ day in an ultra HTS mode [81]. In a straightforward approach, the concept of HTS would ideally rely on the maximum miniaturization of each individual unit to be studied. Innovative solutions resulting in a broadening of the biological questions answerable by micro-engineered platforms and progress towards ambitious applications, such as stimulated neurogenic repair or the creation of functional organs from stem cells, both of which include a 3D biological-material interaction [62, 82-84].

1.3.1 Miniaturized micro-engineering techniques: current approaches

Recent reviews outline a host of techniques that hold great promise for tailored cellular microenvironments with high spatio-temporal control over the mechanical and biochemical cues to regulate cellular behavior [13, 21, 31, 85-87].

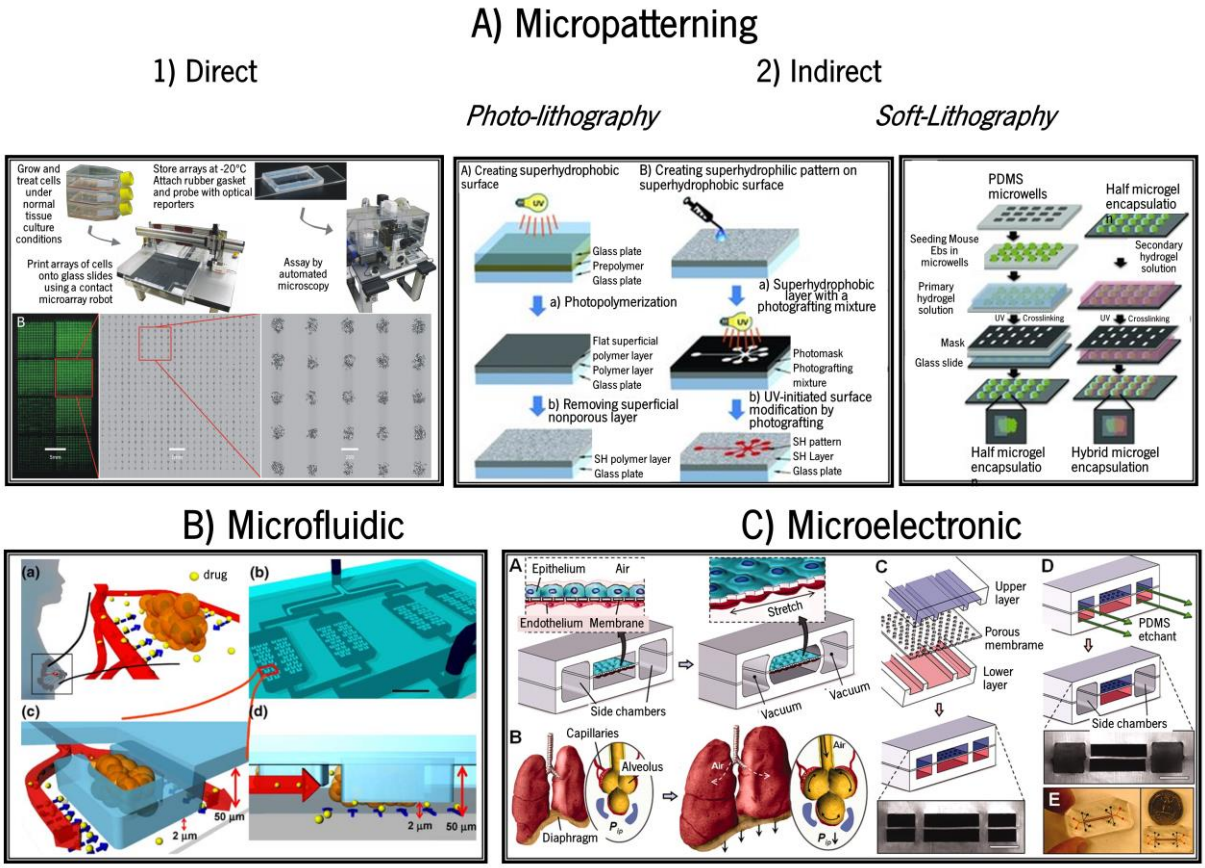

Figure 1.2 Examples of current microfabrication approaches to process supports for HTS and lab-on-Chip. A) Micropatterning approaches are based on direct (A.1) or indirect technologies (A.2). Using a direct technology based on robotic microarray spotting device (A.1), cells are printed onto streptavidin-coated slides, to obtain a high-density cell Chip. An 8-pin print of 4,608 replicate spots, each containing a microsample of HeLa cells, is shown by imaging with a microarray scanner [88]. Using an indirect technology based, superhydrophobic-superhydrophilic porous polymer films on a glass can be produced by UV-initiated photolithography [89]. Individual embryonic bodies was successively encapsulated in PEG and GelMA microgel by photolithography [90]. Scale bar: 1000µm. B) Microfluidic technology was used to generate spheroid culture array [91]. The spheroid culture chamber was formed by bonding the PDMS device to a glass slide. In each chamber, there are U-shape traps arrayed in the density of 7,500 traps per square centimeter. C) Using microelectronic approaches a human breathing lung-on-a-Chip microdevice was developed [92]. The micro-fabricated lung mimic device uses compartmentalized microchannels to form an alveolar-capillary barrier on a thin, porous, flexible PDMS membrane coated with ECM. The device recreates physiological breathing movements by applying vacuum to the side chambers and causing mechanical stretching of the PDMS membrane forming the alveolar-capillary barrier.

Micropatterning, microfluidics and microelectronics technologies enable the development of novel miniaturized platforms physiologically relevant for *in vitro* tissue models [38, 40, 70, 74, 78, 80, 93-97]. Such micro-engineered devices have been widespread proposed in the field of biomedical engineering, including drug discovery [68], stem cell biology [95], cancer biology [49] and experimental cell culture and processing [98] and single cell assays [99]. The first biomaterial microarray was developed by Anderson et al. [9] consisted of polymeric network for seeding embryonic stem cells. Since then, many other applications of this technique have been introduced. 2D microarrays have been the most used platforms to reveal specific hits and control the cell attachment, proliferation, migration and differentiation

[76]. A recent example used cell microarray technology and a method of reverse transfection, where transfection mixtures were pre-spotted onto a glass slide prior to seeding the cell monolayer [78]. The size of each microarray spot is about 120-150 μm in diameter and consists of a cluster of 30-80 fluorescent cells. Such innovative approach allowed spotting up to 10,000 transfection mixtures improving the throughput and decreasing the reagent consumption. However, cells under *in vivo* milieu are organized into a complex 3D microenvironment and thus, recent significant efforts have been directed toward engineering microarrays for screening cellular fates within 3D niches.

Micro-patterning approaches, based on direct or indirect technologies, have been proposed to demonstrate that different ECM proteins, biomolecules, and drugs can be entrapped within 3D biomaterial microarrays and the effect of these components on cellular behavior can be monitored in a combined approach [31].

In direct manufacturing (Figure 1.2 A), cell-laden biomaterials are deposited with either a contact or inkjet printer. A broad range of different molecules (small molecules, polymers, antibodies, proteins) can be arrayed using robotic spotting technology [79]. Using robotic fluid-dispensing devices, cells can be directly spotted onto functionalized glass surfaces [88]. With this strategy, it was possible to generate patterns of cells encapsulated within 3D hydrogel matrices promoting support for cell growth at the micro-scale. One example proposed by Lee and colleagues [11] involves the use of glass slides that are spin-coated with a polymeric material to increase the hydrophobicity of the surface while providing reactive functional groups to attach a hydrogel matrix. Hart et al. [88] used a robotic microarray spotting device (pin printing) to print cells onto streptavidin-coated slides in an array format. With this method, high density has been achieved with approximately 4,700 discrete HeLa cells printed on a single slide using an 8-ejector printer (Figure 1.2 A.1). Recently, cell printing has been used to directly deposit cell-laden scaffolding materials (e.g., ECM materials such as collagen, alginate, elastin, and agarose) at high throughput to 3D cell microarrays [63]. The scaffolding materials can support cells mechanically and allow for perfusion of nutrients, thus enabling long-term cell culture. For example, cells can be encapsulated in nano-sized drops of collagen or alginate, which are mounted onto a functional glass slide by a robotic system to form 3D cell microarrays [47].

Indirect techniques require the pre-production of a template to pattern biomaterials. Lithographic methods are particularly advantageous when complex designs for integration of bioreactors on-chip are required [100, 101]. In photo-lithography a substrate is irradiated with a high energy through a photo-mask and a high-density array of wells with microscale well sizes (e.g., tens to hundreds of micrometers) can be fabricated [101]. Levkin group have shown over the last years a simple method based on UV-initiated free

radical polymerization and photolithography to create SH and SL porous polymer films (Figure 1.2 A.2) using different monomers and porogen ratios to control the bulk chemistry, morphology and porosity [89, 102]. Beyond most of the work performed were toward 2D cell culture [102-105], recently they have shown that SH-SL micro-patterns is becoming a promising approach for 3D cell culture [40]. In soft-lithography, PDMS is applied in a pre-designed mold and further crosslinked, producing a pattern array that corresponds with the template. Then cells are seeded inside the micro-wells and stimulated into 3D cellular constructs for high-throughput studies [33, 35]. An example is the work performed by Figallo et al. in which twelve independent micro-bioreactors were fabricated [106]. Human embryonic stem cell-encapsulated hydrogels were crosslinked inside the micro-bioreactors and each bioreactor was exposed to a different media flow configuration. Recently, Zhao et al. [38] developed an inexpensive, off-the-shelf surface patterning method to fabricate cell microarrays. The method is based on a 3D cell-based assay based on off-the-shelf microsponge arrays with tailored microarchtectures (e.g. micropillar/ well arrays or bifurcated vascular network) and highly porous that enables the automatic and uniform loading of cellular niche components (cells, matrices and soluble factors). The hydrogel grids were used to guide cell seeding on a glass slide to form cell microarrays at a density of 21,000 spots/cm^2 (single cell array) or 6,000 spots/cm^2 (multi-cellular array). Khademhosseini group used micromolding and photolithography to encapsulate individual embryoid bodies within hybrid microgels to regulate stem cell differentiation [90]. The use of micro-wells chips has been shown to be beneficial in avoiding crosstalk and contamination between biomaterials [107] and more recently, micro-wells based platforms for single-cell analysis has gained increased attention in the field of miniaturization [57]. However, the presence of walls may impair easy on-chip mechanical characterization of the samples. Tayalia et al. utilized two-photon microscopy to precisely control the pore microstructures within acrylate-based polymeric 3D scaffolds for investigation of cell migration [108]. Gauvin et al. adopted 3D projection to micro-fabricate gelatin-based scaffolds with complex architectures for tissue engineering applications [109]. These platforms could be potentially used to micro-fabricate 3D scaffolds for miniaturized cell-based assays despite of the high cost and low throughput of the microfabrication approaches

The combination of photolithography replica molding with robotic printing is well-suited to create structures with defined shapes and positions on the micrometer scale that can be used to position cells and tissues, control cell shape and function, and create highly structured 3D culture microenvironments [31]. Robotic printing combined with soft lithography permit to print cell-laden hydrogels loaded with small molecules inside micro-wells [14, 16]. Such kind of platforms showed significant promise in multiplexed microarray studies with almost no spot-to-spot crosstalk. By varying the size, shape and depth of micro-

wells, single cell arrays can be fabricated to evaluate cellular behavior at a single cell level [57]. Cell aggregated with controlled size can also be produced inside the micro-wells cavities [110-112]. High-throughput assays of single cell responses and cell aggregates in form of micro-masses are thus essential for a variety of applications including drug screening, toxicology and cell biology [56, 63, 64].

Microfluidic systems enable enhanced dynamic control over the cellular microenvironment within on-chip tissue models, such as providing nutrients and dissolved gasses and applying mechanical stimulation to cultured tissues [31]. In a recent example, 3D co-culture cell microarray was performed by integrating microfluidics and timeshared holographic optical trapping [113]. In this method, E. coli cells were manipulated using 3D arrays of optical traps, and then conveyed to an assembly area using a microfluidic network. In addition, Wu et al. [91] formed a microfluidic platform allowing self-assembly of spheroids of tumor cells and characterized the dynamics of spheroid formation. In this study, U-shape traps were designed and integrated in the microfluidic array device. It was observed that MCF-7 breast cancer cells formed spheroids with a density of 7,500 spheroids per cm^2, which can be potentially used to evaluate anti-cancer drugs in a high-throughput manner (Figure 1.2 B). Moreover, combinations of hydrogels and microfluidics have been used to fabricate 3D cell microarrays, which may provide new methods for drug screening in a physiologically relevant environment. For example, Tan and Takeuchi developed a bead-based dynamic 3D cell microarray by introducing cell encapsulating alginate beads into a microfluidic system, and arraying the beads using a fluidic trap [114].

Moving forward, incorporating stimulation and sensing technologies on-chip and interfacing these with cultured cells is another important step for the real-time manipulation and detection of cellular behavior. Recent developments in stem cell research, regenerative medicine, biomaterials and tissue engineering could be integrated into new 3D *in vitro* models closely mimicking human organs and tissues. Organs-on-chip devices could provide not only the biological relevance but also the requisite high throughput applications [54]. The challenge is to develop more sophisticated micro-systems that incorporate multiple tissues and vascular channels with active interfaces between them for transporting fluids, nutrients, immune cells and other regulatory factors - see Figure 1.2 C [92]. Moreover, controlling spatio-temporal mechanical forces to such microsystems permit to simulate the physiological environment, such as breathing in the lung, shear within blood vessels, and peristalsis in the gut and tension in the skin [54]. For example, a micro total bioassay system containing micro-intestine, micro-liver and target cells was developed to evaluate the overall properties of oral medicines and food constituents [115].

1.3.2 Miniaturized 3D cell-based culture platforms: advantages and drawbacks

There are many reasons why miniaturized platforms are beneficial could become the next-generation of 3D cell-based for HTS assays:

a) Using smaller volumes of expensive reagents and cell consumption, economical saving can be made;
b) Compatibility with low and ultrahigh throughput;
c) The molecules of interest are micro-nanometer scale implying the small-sized tools for analysis should be better suited than conventional laboratory beakers and test tubes (cm);
d) Small amounts of biological sample enable more experiments to be run, leading to better result interpretation;
e) The time consumed during the throughput allow large sets of data to be generated for statistical analysis;
f) Scalability and control over construct size;
g) Compatible with microscopy imaging enabling 3D cell images;
h) Ease-of-use, repeatability, and broad access to the assembly technology;
i) Mechanical stability and cellular ECM remodeling;
j) Dynamic temporal and spatial control over precision and 3D complexity;
k) Produce complex 3D structures in architecture and facilitates the establishment of tissue hierarchy.

However, some of the technology platforms require either expensive equipment or sophisticated set-ups that are not commercially available and need to be designed or custom manufactured as prototypes (e.g., bio-printing, laser printing requiring lasers, robotics, and microscopy systems). It would be desirable for these miniaturized technologies to be easily adapted broadly to laboratories around the globe with minimal investment, minimizing operator-to-operator variability and enabling repeatable outcomes. A general drawback with many microwells is the lack of functionality to measure dynamic rapid cellular responses as a result of instant interaction with a reagent. Since reagents often are distributed across the entire well chip, difficulties in practical liquid dispensing might collide with the requirements for simultaneous detection. For example, in microfluidics devices, this is often not a problem as exemplified by live-cell imaging of apoptotic phenotype heterogeneity [57]. In addition, in HTS engineering relies on the effects of eventual crosstalk between spots immersed under the same cell culture medium. The development of new platforms for a high-throughput study of biomaterials and respective interactions with cells must take into consideration three different aspects: (i) the easy fabrication of the platform where the different materials are deposited with controlled volumes; (ii) the easy and homogeneous generation of combinatorial biomaterial arrays and combinations in the desired shape and organizational structure, such as scaffolds or hydrogels, optionally combined with other tissue engineering components such as

soluble factors or cells; (iii) on-chip biomaterial and cell characterization and reliable collection of results, ideally avoiding the destruction of the platform; (iv) enable non-conventional high throughput analysis implementing new 3D culture conditions, such as under mechanical forces (compression or shear stress) to better simulate physiological environments.

1.4 Advances in the design of HTS platforms based on surfaces with extreme wettability

With the advent of micro- and nano-fabrication, biomaterials for drug delivery, tissue engineering, biomedical implant and diagnostics have rapidly evolved. One of the primary techniques used in the fabrication of biomaterials is surface modification to achieve micrometric surface features, down to the molecular scale, in order to achieve the desired interfacial characteristics. The first contact between the material and the biological milieu occurs at the surface of the material, where this triggers a cascade of complex interactions [116]. The characteristics of the surfaces such as chemistry, charge, topography and wettability, play crucial roles on the biological response [73]. Although these factors usually work together to have a cooperation effect, surface wettability is a parameter of utmost importance affecting the uses in biological applications, such as cell adhesion/detachment and protein absorption [117]. Inspired by natural structures, great attention has been devoted to the study and development of surfaces with extreme wettable properties [118-123]. The meticulous study of natural systems revealed that the micro/nano-topography of the surface is critical to obtaining unique wettability features, including superhydrophobicity. Materials exhibiting extreme wetting properties, such as SL and SH surfaces have attracted considerable attention because of their potential use in several industrial applications, such as self-cleaning fabrics, anti-fog windows, anti-corrosive coatings, drag-reduction systems, and efficient water transportation [121, 123]. In particular, engineering of surface wettability by manipulating chemical properties and structure opens emerging biomedical applications, e.g. implantable biomaterials with anti-adherent properties for vascular graft or with anti-bacterial properties [124, 125] as well as potential microarrays and microfluidic devices for simple and economical diagnosis /monitoring of cell assays [126].

Non-wettable surfaces with high water contact angles (WCAs) and facile sliding of drops, called SH or ultra-hydrophobic, have received tremendous attention in recent years [118, 123, 127-130]. SH surfaces are typically composed of materials with a low intrinsic surface energy with a hierarchical structural configuration [131]. The surface topography decrease the contact area of water droplets and the surface, thereby increasing the extent of the air/water interface, resulting in WCA greater than 150°. Since Tsujii et al. [132] first demonstrated biomimetic SH surfaces in the mid-1990s, various smart methods for

obtaining rough surfaces exhibiting extreme water repellency have been reported, such as phase separation [133, 134], electrochemical deposition [135], crystallization control [136], chemical vapor deposition [137], wet chemical reaction [138], sol–gel processing [139], lithography [140], electrospinning [137], and so on. With the developments of nanotechnology, various surface features such as the self-cleaning ability [141], anisotropic wetting of rice leaves [142], water-collection behavior of desert beetles and spider silk [143] and liquid repellency of pitcher plants [144] have been mimicked by engineering surface topology and chemistry.

Hierarchical micro- and nano-structuring of the surface is responsible for superhydrophobicity. Rough surface not only enhance its hydrophobicity due to the increase in the solid–liquid interface [145] but also when air can be trapped on a rough surface between the surface and the liquid droplet. There are two types of non-wettable surfaces differing in their adhesive properties. If the contact angle hysteresis (CAH) is higher than 10°, meaning the difference between the advancing and receding contact angles, the water droplet stay preferentially adhered onto the surface. Otherwise, if the CAH is less than 10°, the surface is non-adhesive, and the water droplet rolls off the surface at a minimum inclination. In the case of non-adhesive SH surfaces (Cassie-Baxter state) the existence of a hierarchical morphology from the nano- to the micro-scale leads to minimal contact between the liquid and the surface. The water dispensed onto this type of surfaces acquires an almost spherical shape in order to minimize the energy, being suspended on the top of the micro- and nano-structures that compose the surface, and at minimal inclinations the droplets roll off [146]. In high-adhesive surfaces (Wenzel state), the droplets also acquire a near-spherical shape due the presence of micro- and nano-structures, but do not roll off easily. High adhesive SH surfaces present a larger pitch leading the liquid to impregnate partially within the nanostructures [145]. Over the last decade, many authors have studied the effect of the wettability and excellent reviews describing the Cassie-Baxter and Wenzel models can be found in the literature [120, 121, 147-149]. Based on these methods, artificial SH surfaces have been developed inspired by the microstructure surface of the natural flowers; e.g. lotus leaf as non-adhesive surface and rose petals as adhesive surface [122]. Their superhydrophobicity is attributed to the hierarchical roughness of the randomly oriented, small, hydrophobic wax tubules on top of convex cell papillae [119]. However, differently from the lotus leave, the micro- and nanostructures of rose petals provide a sufficient roughness for superhydrophobicity, but at the same time a high adhesive force with water. When compared with the lotus leaf surface, rose petals have higher distances between the microstructures. A water droplet on the surface of the petals appears spherical in shape; however, it cannot roll off even when the petal is turned upside down [144]. This phenomenon is usually defined as the “petal effect” as compared with the

popular “lotus effect”. To mimic the liquid adhesion function of the rose petal, Feng *et al.* replicated the rose petal’s micro/nanostructures using the solvent-evaporation-driven nano-imprint pattern transfer process [119]. Combining the principles of lotus and rose-petal effect, Neto et *al.* developed an array of microindentations on a superhydrophobic surface [150]. The concept of using an array of ‘‘defects’’ on a SH surface was used to deposit a droplet, which served as a microreactor for chemical or biological reactions or for cell culture. Since it is difficult to control surface roughness on the nanometer scale, only a few groups have attempted the preparation of transparent SH coatings. For example, transparent SH films have been obtained by coating TiO_2 with fluoroalkylsilanes [151, 152]; while evaporation of solvent from a solution of fluoropolymer covered by a layer of water droplets was used to generate a transparent SH nanoporous polymer film. Bravo et al. created transparent SH films by a layer-by-layer deposition of differently sized silica nanoparticles on a glass substrate [153].

1.4.1 Bio-inspired patterning with extreme wettability contrast for 3D cell culture

In this Chapter, we describe several paradigms concerning the throughput to rapidly and efficiently modulate the interaction between the various components of the cellular microenvironment in 3D space. SH microarrays as platforms for 3D cell-based assays are presented, offering a very recent approach to HTS cellular analysis (Figure 1.3). Such microarrays containing 3D cell cultures can be incubated for long period and the obtained data significantly help the design of synthetic biomaterials, implant surfaces and tissue-engineering scaffolds by finding correlations between their chemical structure and their biological performance. The flexibility of using microarrays analysis not only greatly refines our knowledge of multitude of 3D cell-biomaterial interactions but could also be used in biocompatibility assessments as novel biomarkers. Herein we show that 3D functional patterns would represent a versatile platform in a wide range of applications, especial for biomedical devices such as, selection of hydrogels or scaffolds for site-selective cell attachment and protein absorption and the targeted drug delivery for site-specific and high-sensitivity cancer cell assays.

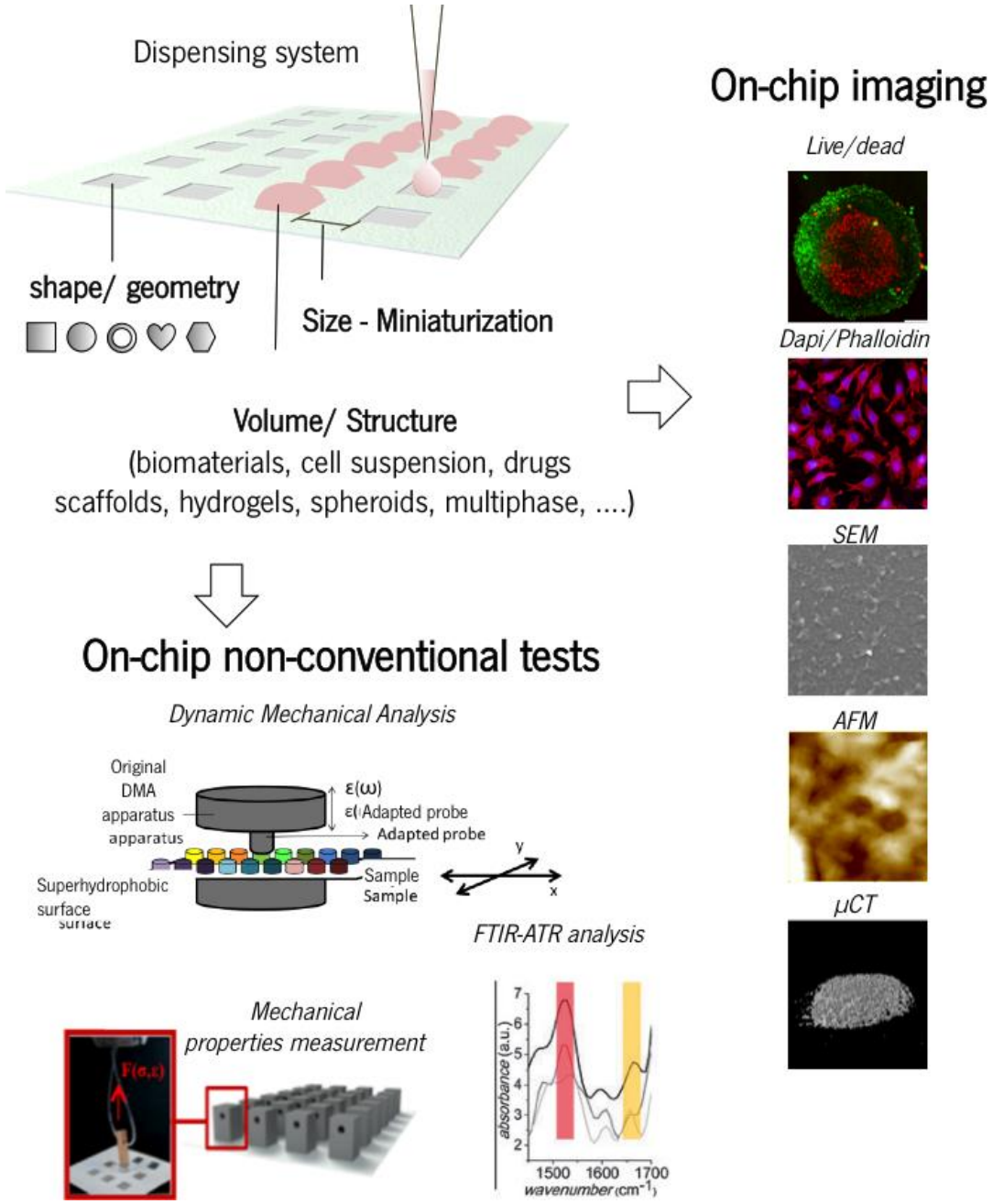

Figure 1.3 Schematic representation of the main functions of SH-SL microarrays, including the control over the size, geometry, volume of the biomaterial with applicability for *in-vitro* HTS (e.g. live/dead, dapi/phalloidin, scanning electron microscope (SEM), atomic force microscope (AFM), and micro–computed tomography (μCT)) and non-conventional testing (e.g. dynamic mechanical analysis, in-situ mechanical tests and attenuated total reflectance Fourier transform infrared spectroscopy (ATR-FTIR) analysis)

Table 1.1 shows the advantages and limitations of the use of patterned SH microarrays in comparison with conventional microarrays widely used for 3D cell culture on research or clinical field.

Table 1.1 Description of the main advantages and drawbacks using distinct 3D cell culture systems

3D cell culture system		Advantages	Disadvantages
Superhydrophobic - superhydrophilic microarrays	*General*	Precise control of liquids; Minimize consumption of reagents and samples; Short reaction times; Enable parallel and multiplexed analysis; Low cost of production; High encapsulation efficiency; Prevention of particle aggregation; Possibility to produce complex spherical systems; Scalability and control over construct size and geometry; Each spot serve as a reservoir for individual experiment with biomaterials, drugs or cells; Non-conventional HTS analysis; Long culture time.	Opaque spots limit on-chip tests, are based on image analysis; Possible cross-contamination of soluble factors between the spots; Adaptation of conventional equipments for the analysis.
	Hydrogels	Large variety of natural or synthetic materials; Co-cultures possible; Control over size and geometry; HTS capable; High cellular survival (low volumes).	Gel-to-gel variation and structural changes over time; Media replacement is difficult; Possible detachment of the microgels.
	Scaffolds	Large variety of materials; possible for desired properties; Co-cultures possible; Control over size and geometry.	Possible scaffold-to-scaffold variation; Cell removal may be difficult; HTS options is limited; Media replacement is difficult; Limited miniaturization (depending on the pore size)
	Spheroids	No added materials; Consistent spheroid formation; Control over size; Co-cultures possible; HTS capable.	Culture edia replacement is difficult.
Conventional microarrays and culture Micro-well plates		Longer culture time; Control over spheroid/ hydrogel size; Culture multiple cell types; Screening applications; Compatible with liquid handling tools.	Expensive equipment; Sophisticated set-ups; Specialized equipment compatible with micro-well infrastructure; Often cross contamination between microarray spots, Measure dynamic rapid cellular responses. Some characterization techniques requiring flat substrates cannot be used.
Microfluidic devices		Offer control of fluids over cell, locations to specific regions; Culture multiple cell lines; Generation of chemical gradients; Tubeless microfluidics do not need external connectors, pumps and valves and are suitable for drug applications.	Cells are difficult to isolate from culture regions; Limited quantitative analysis; Difficult microscopy analysis; Short term cell culture; Media replacement is difficult; Measure dynamic rapid cellular responses.

1.4.1.1 Formation of tissue spheroids

A first insight related to 3D cell structures was presented using SH platforms to obtain cell spheroids [150, 154-159]. Spheroids are 3D spherical structures composed of cancer cells, which are used as *in-vitro* models of avascular tumor nodules, micro-metastases and the extravascular space of solid tumors [160]. Such micro-masses develop many features similar to *in vivo* tumors such as diffusion limitations of oxygen, glucose, and other nutrients, including hypoxia and central necrosis and 3D interactions [161]. Due to the closer representation of physiological tumoral conditions, spheroids became a promising model for drug discovery and are expected to fill the gap between 2D monolayer culture models and animal testing [162]. Studies have shown that tumor cells when evaluated in a 3D format are less sensitive to anti-cancer agents and the results are more predictive than when the same cells are cultured in 2D formats [163]. Technologies have been developed to generate 3D homogeneous or heterogeneous spheroids, such as hanging drop techniques, rotating wall vessels, magnetic levitation, and suspension culture in low adhesion/attachment plates [155, 164-166]. Non-adhesive micro titer plates becoming popular platform for culturing spheroids since they allow for formation of homogeneous spheroids in one-spheroid-per-well format and compatible with standard liquid handling robotics [167]. The main problem of such platforms is high costs of experiments due to relatively large volume of wells and requirement of pipetting robotics for HTS experiments. Recently, SH surfaces have been proposed to arrange quasi-spherical cell culture droplets with the capability to build-up 3D spheroids in a HTS manner on the lab-on-chip scale. A SH platform so-called “spheroform” inspired by the back surface of the desert beetle allowed to form islet cell spheroids with enhanced therapeutic efficacy for angiogenesis and insulin secretion [157]. A different approach based on SH platform containing wells with various shapes were fabricated using photolithography technique. Such platform was used for miniaturized 3D culture of individual or groups of cell types. Cell suspension was dispensed on the SH microwells, allowing them to settle via gravity. Uniform multicellular tumor spheroid formation was demonstrated with the ability to control the spheroid diameter in microwells for HTS of drugs [156]. The therapeutic efficacy of 3D stem cell spheroids using SH surfaces was also investigated [158]. The authors used a switchable water-adhesive SH nanowire surface for the formation of functional human adipose-derived stem cell spheroids, of which the sizes were readily controllable on the surface. It increased cell-cell and cell-matrix interaction, and thus improved viability and paracrine secretion of the spheroids. They also observed that human adipose-derived stem cell spheroids produced on the surface exhibited significantly enhanced angiogenic efficacy. Based on the same principle of enabling droplet fixation (rose petals‘effect), flat SH surfaces were patterned with microindentations in which liquid droplets containing cells were immobilized. 3D

agglomerates of cells were obtained facing down the platforms with the droplets (Figure 1.4 A). The gravity effect allowed the deposition of the cells and their aggregation into clusters [150, 155]. Such a device was hypothesized to be applicable in the biomedical field as a micro-bioreactor in which chemical and biological combinatorial tests may be performed (e.g., screening of the cytotoxicity of drugs on micro-tissues).

Instead of suspending aqueous spherical droplets containing cells, semispherical droplets were dispensed over transparent wettable spots distributed in SH PS surfaces [168]. By inverting the system, spheroids could also be generated for drug screening tests. In this case, the transparent windows existing in each spot facilitated the visualization of the individual spheroid and the independent liquid exchange in each droplet.

1.4.1.2 Cell-laden scaffold microarray

Scaffolds provide the necessary support for cells to proliferate and maintain their differentiation function, and its architecture defines the ultimate shape of the new bone and cartilage [23].

Bio-inspired micropatterned SH titanium dioxide nanotube surface array can act as a good scaffold for site-selective cell immobilization on the SL regions in a highly selective manner [126]. Such SH-SL micro-patterns offer a versatile template enabling the loading of calcium phosphate, silver nano-particles, drug and biomolecules in a highly selective manner. Recently, a polymethylmethacrylate micro-scaffold array chip allow fast medium exchange and arrayed drug administration directly on the hydrophilic spots of the platform [169]. The drug administration was achieved by producing a drug-loaded PEG microsponge array and then aligned with high precision with the cell-laden micro-scaffold array chip, using a sandwich approach. Importantly, arrays of dried porous scaffolds may be an interesting way of commercializing biomaterial sets in ready-to-use, off-the-shelf platforms for cell–biomaterial testing [38]. Lim *et al.* fabricated a photo-switchable nanoporous multilayer film with wettability that can be reversibly switched between superhydrophobicity and superhydrophilicity triggered by UV/visible irradiation [170]. They combined surface roughness control with an electrostatic self-assembly process and photo-responsive molecular switching of fluorinated azobenzene molecules. A patterned SH-SL surface was produced by using selective UV light irradiation through an aluminum mask. Prior to UV irradiation the substrates are SH all over, but after UV irradiation the selectively exposed regions become SL and the masked areas maintain the SH properties.

A pre-requisite on the design of miniaturized platforms for 3D cell culture is scalability. Platform for HTS analysis have been proposed with spots size less than 200 μm in diameter [78]. However, for 3D cell-

biomaterial interaction, the size of the 3D tissue engineering structure where cells are encapsulated must be suitable without interfering the cellular integrity. Thus, scaffold needs an adequate mechanical stability and strength containing highly open porous structure. The pore size distribution in 3D matrices is of outmost importance for cellular growth, proliferation as well as freely transport of nutrients within the matrix [171]. Endothelial cells, for example, show favorable attachment to pores in the range of 30–80 μm [172], whereas osteoblasts require pores larger than 100 μm for bone formation [173]. Due to the micrometric size of the spots of the conventional microarray, most commercially available microarray scanners are inverted florescent microscopes that acquire data at two wavelengths (generally used to record a test and a control signal) using 532 nm and 635 nm lasers [174]. Additionally, the scaffold needs to be easily fabricated into a variety of shapes and sizes. Using SH-SL flat platform, the size of the porous scaffold can be easily varied, simply by varying the size of the SL spot and the volume of the liquid precursors. Since the size of cells are in micrometric scale, miniaturizes porous scaffolds with representative number of pores and truly interconnected structure required a minimum size of 1-2 mm [175, 176]. The versatility of controlling the sizes of the hydrophilic spots open the possibility to produce scaffold structures with hierarchical organization exhibiting pore sizes adequate for tissue engineering applications. The ability to create arrays of on-chip dried porous scaffolds or even scaffold platforms may be promising for commercializing ready-to use platforms for HTS cell-biomaterial testing [38, 177]. The production of 3D scaffolds was performed *in situ* over the SH microarray [176]. The structures were characterized regarding mechanical properties, porosity and pore size. The proportions between materials (sodium alginate and Chitosan) were varied and cell–material interactions were also evaluated by looking at the metabolic activity and cell number using both destructive methods and direct image-based analysis (Figure 1.4 B). Such SH-SL microarray could be considered as a reliable platform for *in vitro* screening of the main properties currently assessed in scaffold characterization, as well as for preliminary biological studies. Using freeze-drying technique, polymer solutions can be easily dispensed directed on the wettable spots, instead of the need to cross-link any monomers. This process avoids several rinsing steps since dispersed water and polymer solvents can be removed directly. In addition, the pores structure of the scaffolds can be controlled by varying the freezing temperature. However, the ability to produce HTS homogeneous porous scaffolds by freeze-drying is still limited. With the advances of modern technologies, a new method should be developed to produce porous scaffolds with better control of pore sizes, pore morphology, and porosity of matrix as compared with other fabrication methods using flat microarrays. To overcome this challenge, we suggest the use of 3D printing (never shown before). We believe that could be particularly advantageous for on the design of complex structures that are not cost effective in

conventional manufacturing methods. Moreover, automated 3D printing promises to produce complex biomedical devices with defined shape and size, as well as, controlled scaffold position on the microarray platform, according to computer design.

1.4.1.3 Formation of hydrogel microparticles

Hydrogels are hydrated 3D cross-linked polymers resembling natural ECM that provide soft 3D support for cellular growth and tissue formation [178]. Due to their unique properties such as high porosity, permeability for gases, nutrients and metabolites, as well as their compatibility with physiological conditions, hydrogels have been extensively studied as material support for immobilizing and cultivating cells in 3D, biomedical applications, drug delivery and tissue engineering [179]. Hydrogels such as fibrin, collagen, alginate, and PEG-based biomaterials are extensively used in tissue engineering due to their biocompatibility, porous structure, and their biological, chemical and mechanical properties [59]. Although recent studies have provided initial efforts in implementing combinatorial approaches to 3D cell culture, they have been limited in scope due to constraints in the ability to generate large-scale libraries of microenvironments, limited systems-level analysis and lack of cell recovery. The use of concepts of patterning hydrogels in a 3D manner [60] is an elegant way to study biomaterials allowing or avoiding the crosstalk of soluble factors between distinct patterned biomaterials by varying the distance between each patterned spot and the density of the polymeric matrix separating each spot. 3D cell-biomaterial microarray was developed by pipetting cell-loaded precursor solutions onto SH micropatterned surfaces with SL regions in order to form cell-laden hydrogel arrays [39]. A combinatorial array of Chitosan, collagen and hyaluronic acid with alginate to control the cell distribution on a SH polystyrene surface was formed. Due to the high contrast of wettability between the patterned SL spots and the SH background, the biological performance of encapsulated cells inside the hydrogels were tested in an *in vitro* 3D environment on a flat platform [39]. Some of the advantages associated with this method are the easy fabrication process, low cost, and high efficiency. Moreover, the biomaterials dispensed in each wettable spot were kept and fixed separated from each other due to the highly repellent character of the surrounding area, even when the entire chip is immersed in cell culture medium. One limitation of this strategy is the difficulty of use for analyzing opaque materials, as the on-chip tests are based on image analysis. SH-SL transparent titanium dioxide surfaces could solve the existent problems [152], creating a microarrays containing alginate hydrogel particles, with features as small as 5 μm. Tumarkin et al. showed a straightforward operational platform for the co-encapsulation of a controlled number of cells of different lineages in well-defined microgel environments. Cells co-encapsulated in each individual microgel

are separated from cells encapsulated in different microgels, which enables interrogation of interactions between two types of cells encapsulated in the same microgel [180]. Hancock et al. used a similar approach to create gradients of soluble factors, cells, and microspheres in 3D hydrogels by photo-crosslinking pre-polymeric solutions in the SL stripes [181].

Most of the methods used for the formation of droplets on patterned SH surfaces are based on multiple pipetting or a liquid handling device, which can be inconvenient due to the time consuming and the liquid volume precise. The handling of small volumes of droplets requires fewer reagents than with conventional microplates. Levkin group developed a "DropletMicroarray" platform able to form thousands of spatially separated pico- to microliter-sized droplets with defined geometry and volume using SH-SL surface [40]. High-density of hydrogel/cell arrays were formed in the SL spots without requiring pipetting in single individual spots. Using a phenomenon of discontinuous de-wetting, as long as liquid moved along the patterned surface, the trailing edge of the liquid became pinned at the borders between the SH-SL regions, and the liquid film thinned and finally broke to form a droplet in each SL spot. Hydrogels containing cells were only formed within the SL spots, and no cells were observed outside the hydrogel on the SH barriers (Figure 1.4 C).

The promising hydrogel microarrays could be functionalized or incorporated with extracellular matrix proteins, signaling molecules, drugs, and other small molecules for 3D cell screenings. After the hydrogel is formed, the array of hydrogel particles encapsulating cells can be immersed in cell culture medium, or droplets of medium can be formed in the SL spots to isolate each hydrogel microparticles for further culturing. The SH barriers promote very high-densities of microdroplets containing bioactive molecules, non-adherent cells, or microorganisms and could be fully isolated microdroplets for HTS, or in the hydrogel microparticles for screening in 3D microenvironments.

In future, the use of concepts such as patterning of hydrogels in a 3D manner, as proposed for other applications may be an elegant way to study biomaterials allowing or avoiding the crosstalk of soluble factors between patterned biomaterials by varying the distance between each SL spot. The development of miniaturized platforms to produce diverse combinations of biomaterials for 3D cell culture must be followed with the development of HTS or high-content methods for data collection to assess cell–biomaterial interactions/therapeutic effects [75].

Hydrogels with complex geometries: Microscale building blocks for modular tissue engineering

Engineered tissues remain challenging to create, especially if the goal is to spatially position multiple cell types in a heterogeneous pattern in 3D. The combination of 3D microarray technology along with microfabrication technology is a promising new approach to engineering heterogeneous structures [182].

The ability to control the shapes of the cell microcarriers allows for the production of shape-coded arrays, which can offer a cost-effective and versatile platform for high-throughput and multiplexed bioassays. SH-SL patterns provide a precisely control over the geometry and shape of liquids. Hancock et al. used microarray pattern to shape liquids into more complex geometries, at both the macro- and microscale, to control the deposition of micro- particles and cells or to create shaped hydrogels [183]. By using finite element simulations to predict the liquid shapes, they could pre-design the SH-SL patterns based on the desired particle deposition or gradient formation. A range of droplet shapes, such as sine waves, linear gradients, and spiral gradients were produced to validate the combined experimental and theoretical investigation. Addition of surfactant was needed to lower the surface tension of the liquid in order for it to completely fill the complex pattern geometries at the microscale. This could be improved by using a SL surface that rapidly and uniformly spreads the solution, eliminating the need for surfactant. Also, increasing the hydrophobicity and using a surface with low WCA hysteresis as the background could eliminate the extra droplets after liquid patterning. Recently, Kobaku and co-authors had developed a simple wettability engendered templated self-assembly methodology for preparing monodisperse, multiphasic micro- and nanoparticles [184]. The method is based on the construction of a SH substrate patterned with SL domains of different sizes and shapes by taking advantage of photo-catalytic activity of TiO_2. Multi-phasic assemblies with precisely control over the geometry and composition through multiple, layered, depositions of polymers and/or particles were constructed simply by dip-coating the template with dispersed polymer or particle solutions, which preferentially self-assembled within the wettable regions. Such SL regions could be further reused for the synthesis of a new batch of particles, enabling an easily reproducible method for scalable manufacturing of multi-phasic functional particles. In addition, microgel arrays could be produced by combining surface-wettability-guided assembly and microdroplet-array-based operations, using widely accessible PDMS stamping approach [185]. It was shown the assembly of thousands of heterogeneous 3D cell microenvironments with precise control over individual shapes and sized including circles, squares, octagons, crosses, triangles, as well as complex interconnected microgel networks, as well as control of chemical concentrations, cell density, and 3D spatial distribution of multiple components (Figure 1.4 C). Khademhosseini group presented a micromolding approach for 3D cell-encapsulating hydrogels with controlled shapes and sizes in the form of harvestable free particles [174]. Cells were suspended in a hydrogel precursor solution containing photoinitiator, deposited onto hydrophilic PDMS patterns, crosslinked under UV radiation, and retrieved upon hydration. The cells distributed homogeneously within two types of hydrogels (methacrylated hyaluronic acid and poly(ethylene glycol) diacrylate (PEGDA)). The control over the shape and size of the

microgels were useful since shape-fitting microgels could then be placed adjacent to one another and assembled into larger structures or tissues. Later, authors from the same group achieved directed-assembly of cell-laden microgels into tissue sheets on surfaces patterned with hydrophobic and hydrophilic regions [186]. They were able to regulate the architecture of the microgel assembly by controlling the size and shape of the patterns on the surface. In order to stabilize the assembled microgels, a secondary crosslinking reaction was used to encapsulate the assembled microgels into a bulk hydrogel material. The stabilized assembled microgels could be readily harvested from the surface as multi-cellular tissue constructs.

In vivo, cells are embedded in a 3D niche comprising ECM and neighboring cells with a well-defined spatial distribution. Biomaterials mimicking the native ECM are critically important to form cell-encapsulating building blocks for the bioengineering of artificial tissues. Generating heterogeneous 3D cell microenvironment arrays *in vitro* with controlled and spatially organized components over individual microenvironments is still challenging. The shape of the 3D structures is extremely important for constructing macro assemblies with diverse architectures, inter-particulate distances or particle-to-particle interactions. SH-SL microarray patterns can be proposed for the formation of engineered 3D tissues with robust mechanical properties to withstand clinical implantation and interact appropriately with native tissues, and be used as a toolbox of cell bearing hydrogel bricks of different shapes to enable diversity of multi-particle assemblies for modular tissue engineering [58, 187, 188]. 3D shaped hydrogel particles can be adapted for cell co-culturing that provides a more relevant *in vivo*-like tissue model, and which enables the high-throughput screening and in-depth monitoring of other molecules' effects on cell-to–cell interactions.

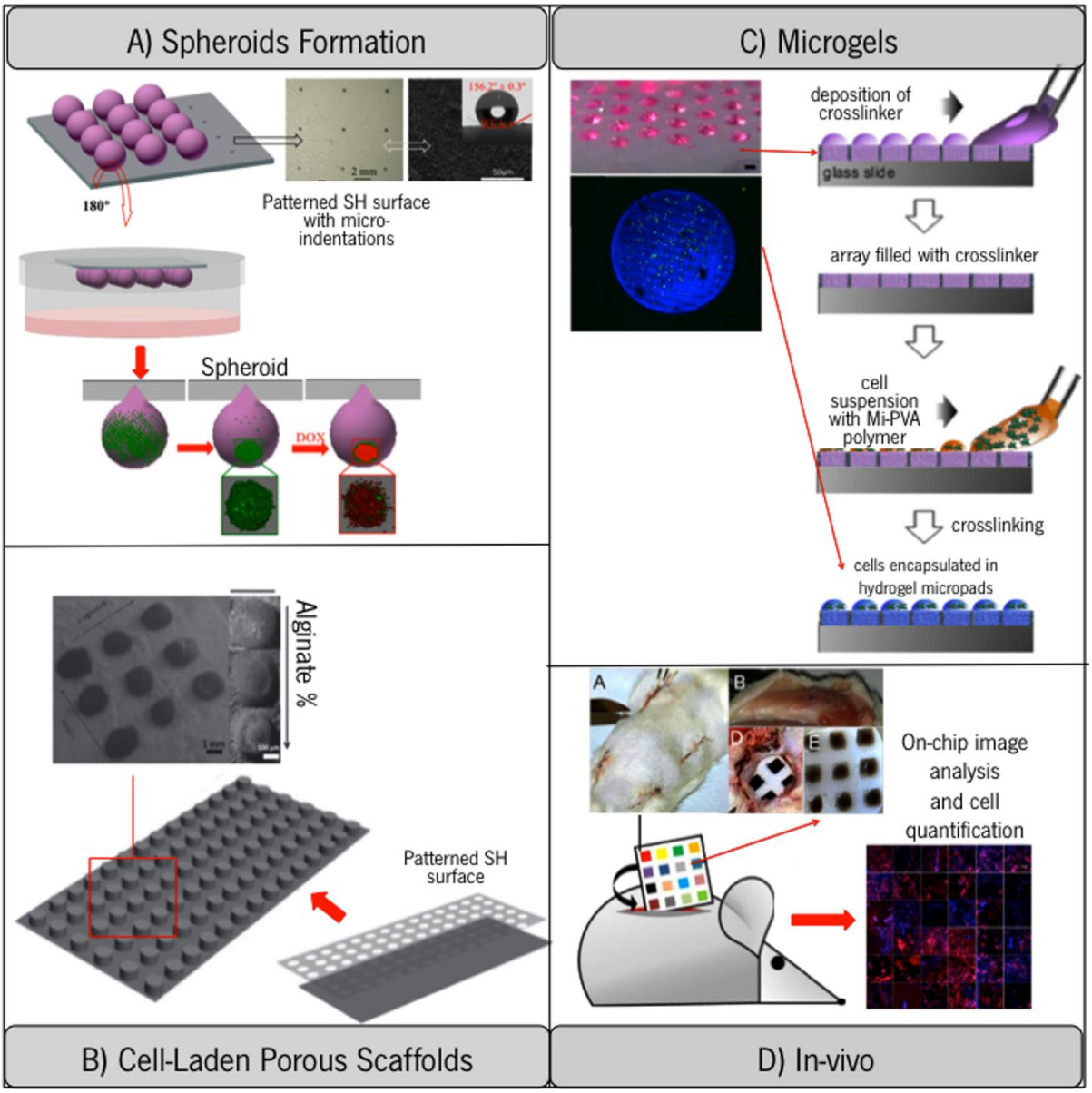

Figure 1.4 Emerging applications using patterned SH surfaces in order to produce a more relevant *in vivo*-like tissue 3D model. A) Spheroids formation using patterned SH surfaces with microindentations, mimicking rose petal effect, able to suspended arrays of droplets containing cells. Turning the platform 180°, the cell suspension inside the droplet lead to a formation of individual spheroids due to the gravitational forces applied to the cells. Drug screening test were performed using anti-cancer cell drug, doxorubicin [155]. B) Formation of MI-PVA microgels incorporating cells using the rolling droplet method on SH-SL droplet microarray [40]. C) HTS formation of porous Scaffolds with distinct compositions [176]. D) Arrays of combinatorial biomaterials were implanted subcutaneously in a Wistar rat model [189].

1.5 In-vivo HTS testing of biomaterials

Clinical trials are a crucial step towards probing the foreign-body response and toxicity of newly developed biomaterials. Conventional *in vivo* screening of materials involves their implanting one by one, often requiring a large number of animals, which in turn triggers ethical questions and elevates experimental costs. Patterned devices with areas of contrast wettabilities produced on flat and flexible films were hypothesized to be powerful tools for the detection of hotspots with promising properties and excluding

materials with uninteresting characteristics. By implanting biomaterial microarrays, a large number of biomaterial combinations can be investigated using fewer animals. This high-throughput clinical testing offers a major advancement in biomaterial development and a great ethical improvement in the field of biomaterials science. A firstly developed SH microarray chip containing 36 different scaffolds was implanted in Wistar rats [189]. The microarray chip was used to study the immune response towards the implanted biomaterials in a cost-effective manner. The results obtained on chip were compared with conventional individual implantation of the scaffolds and showed that such SH-SL microarray could be used for high-content evaluation of *in vivo* biomaterial responses (Figure 1.4 D). The inflammatory response of the individual scaffolds was accessed after implantation (up to 7 days) by examining the recruitment of macrophages and lymphocytes to the respective scaffolds. The implanted micro-scaffolds elucidated different inflammatory responses depending on their physical and chemical properties. Moreover, through a histology analysis of the tissue surrounding the microchips it was evident that the inflammatory response in each scaffold was independent between the implanted scaffolds. The employment of cheap approach as HTS devices for *in vivo* screening clearly marks an important step in biomaterials development. It was referred that only the inflammatory response caused by the biomaterials was explored in this work. Although such unique *in vivo* HTS testing of biomaterials is a very promising approach, additional experiments and new platforms are needed to further validate this system. In the future, hybrid structures combining cells and materials should be tested in order to extend this methodology towards future discovers for tissue engineering and regenerative medicine.

1.6 Conclusions and future perspectives

Over the last decades, miniaturized devices have achieved tremendous advances to facilitate applied and basic cell-based biological research. Significant developments in micro-fabrications greatly changed various aspects, including science and engineering. Compared with conventional cell-culture methods, 3D microarray systems are growing at a remarkable speed aid in the identification of such magical formulations in the shortest possible time, enabling the HTS of cell-biomaterial, cell-ECM, and cell-drug interactions within tissue-like microenvironments. The development of heterogeneous cell-laden microarrays holds significant range of different physical, biological, and geometrical settings in a cost-effective manner. The primary goal of these microarray platforms is to identify combinations of biomaterials that can stimulate and reorganize cells into artificial tissues structures for regenerative medicine or drug screening applications. While some of the techniques outlined in this manuscript of micro-engineered approaches for 3D cell culture are well documented, the uses of biomimetic strategies

for creating 3D cell niches of the microarrays are still relatively new. Recent advances on surfaces with extreme contrast of wettabilities have contributed for the design of flat microarrays for HTS of cellular fates within 3D microenvironments. Despite exiting progress in multiplexed biomaterial screening, SH platforms with wettable regions have enabling rapid assembly of thousands of heterogeneous 3D tissue-like structure (polymer-based scaffolds and/or spheroids) with precise control over individual shapes, sizes, chemical concentrations, cell density, and 3D spatial distribution of multiple components. The emerging strategies for directly production of microscale tissue units reviewed here have potential to create complex 3D tissue building blocks with specific micro-architectural features for modular tissue engineering applications. Modular tissue engineering possesses immense potential for advancing the fields of tissue engineering while bringing us closer to the ultimate goal of creating clinically relevant engineered tissues for human implantation and the treatment of disease. In the future engineer arrays of more sophisticated hierarchical and multiphasic environments to permit to recapitulate more closely the complexity of stem cell niches or, at larger scale, humanized organoids. Other culturing conditions should also be implemented, including under mechanical forces (compression, or shear stress) to simulate relevant physiological conditions. Another future approach is the ability to create biomaterial microchips that can be implanted clinically for cost-effective screening of the host response to new biomaterials. It would be interesting to investigate whether a biomaterial microchip can also be used to examine the tissue regeneration potential of scaffolds in a high-throughput manner. A further downscaling of such implantable microchips could lead to a rapid breakthrough in tissue engineering and bring the field closer to meeting its clinical potential.

1.7 References

[1] M.P. Lutolf, J.A. Hubbell, Synthetic Biomaterials As Instructive Extracellular Microenvironments For Morphogenesis In Tissue Engineering, Nature Biotechnology, 23 (2005) 47-55.

[2] J.F. Mano, G.A. Silva, H.S. Azevedo, P.B. Malafaya, R.A. Sousa, S.S. Silva, L.F. Boesel, J.M. Oliveira, T.C. Santos, A.P. Marques, N.M. Neves, R.L. Reis, Natural Origin Biodegradable Systems In Tissue Engineering And Regenerative Medicine: Present Status And Some Moving Trends, Journal Of The Royal Society Interface, 4 (2007) 999-1030.

[3] D. Falconnet, G. Csucs, H.M. Grandin, M. Textor, Surface Engineering Approaches To Micropattern Surfaces For Cell-Based Assays, Biomaterials, 27 (2006) 3044-3063.

[4] K. Korn, E. Krausz, Cell-Based High-Content Screening Of Small-Molecule Libraries, Current Opinion In Chemical Biology, 11 (2007) 503-510.

[5] J. Li, S.T. Crowley, J. Duskey, S. Khargharia, M. Wu, K.G. Rice, Miniaturization Of Gene Transfection Assays In 384-And 1536-Well Microplates, Analytical Biochemistry, 470 (2015) 14-21.

[6] J. Rajasarkka, M. Virta, Miniaturization Of A Panel Of High Throughput Yeast-Cell-Based Nuclear Receptor Assays In 384-And 1536-Well Microplates, Combinatorial Chemistry & High Throughput Screening, 14 (2011) 47-54.

[7] C.G. Simon, S. Lin-Gibson, Combinatorial And High-Throughput Screening Of Biomaterials, Advanced Materials, 23 (2011) 369-387.

[8] R. Macarron, M.N. Banks, D. Bojanic, D.J. Burns, D.A. Cirovic, T. Garyantes, D.V.S. Green, R.P. Hertzberg, W.P. Janzen, J.W. Paslay, U. Schopfer, G.S. Sittampalam, Impact Of High-Throughput Screening In Biomedical Research, Nature Reviews Drug Discovery, 10 (2011) 188-195.

[9] D.G. Anderson, S. Levenberg, R. Langer, Nanoliter-Scale Synthesis Of Arrayed Biomaterials And Application To Human Embryonic Stem Cells, Nature Biotechnology, 22 (2004) 863-866.

[10] A.L. Hook, D.G. Anderson, R. Langer, P. Williams, M.C. Davies, M.R. Alexander, High Throughput Methods Applied In Biomaterial Development And Discovery, Biomaterials, 31 (2010) 187-198.

[11] L. Meli, H.S.C. Barbosa, A.M. Hickey, L. Gasimli, G. Nierode, M.M. Diogo, R.J. Linhardt, J.M.S. Cabral, J.S. Dordick, Three Dimensional Cellular Microarray Platform For Human Neural Stem Cell Differentiation And Toxicology, Stem Cell Research, 13 (2014) 36-47.

[12] C.M. Dumont, P. Karande, D.M. Thompson, Rapid Assessment Of Migration And Proliferation: A Novel 3d High-Throughput Platform For Rational And Combinatorial Screening Of Tissue-Specific Biomaterials, Tissue Engineering Part C: Methods, 20 (2014) 620-629.

[13] T.G. Fernandes, M.M. Diogo, D.S. Clark, J.S. Dordick, J.M.S. Cabral, High-Throughput Cellular Microarray Platforms: Applications In Drug Discovery, Toxicology And Stem Cell Research, Trends In Biotechnology, 27 (2009) 342-349.

[14] M.Y. Lee, R.A. Kumar, S.M. Sukumaran, M.G. Hogg, D.S. Clark, J.S. Dordick, Three-Dimensional Cellular Microarray For High-Throughput Toxicology Assays, Proceedings Of The National Academy Of Sciences 105 (2008) 59-63.

[15] K.A. Power, K.T. Fitzgerald, W.M. Gallagher, Examination Of Cell–Host–Biomaterial Interactions Via High-Throughput Technologies: A Re-Appraisal, Biomaterials, 31 (2010) 6667-6674.

[16] A. Ranga, S. Gobaa, Y. Okawa, K. Mosiewicz, A. Negro, M.P. Lutolf, 3d Niche Microarrays For Systems-Level Analyses Of Cell Fate, Nature Communications, 5 (2014) 4324.

[17] S. Gobaa, S. Hoehnel, M. Roccio, A. Negro, S. Kobel, M.P. Lutolf, Artificial Niche Microarrays For Probing Single Stem Cell Fate In High Throughput, Nature Methods, 8 (2011) 949-955.

[18] A.K. Patel, M.W. Tibbitt, A.D. Celiz, M.C. Davies, R. Langer, C. Denning, M.R. Alexander, D.G. Anderson, High Throughput Screening For Discovery Of Materials That Control Stem Cell Fate, Current Opinion In Solid State And Materials Science, (2016) In Press.

[19] R.P. Hertzberg, A.J. Pope, High-Throughput Screening: New Technology For The 21st Century, Current Opinion In Chemical Biology, 4 (2000) 445-451.

[20] H. Mario Geysen, F. Schoenen, D. Wagner, R. Wagner, Combinatorial Compound Libraries For Drug Discovery: An Ongoing Challenge, Nature Reviews Drug Discovery, 2 (2003) 222-230.

[21] M.B. Oliveira, J.F. Mano, High-Throughput Screening For Integrative Biomaterials Design: Exploring Advances And New Trends, Trends In Biotechnology, 32 (2014) 627-636.

[22] Y.H. Wu, L.X. Li, P.A. Levkin, G. Davidson, Combinatorial Synthesis And High Throughput Screening Of Lipidoids For Gene Delivery, Journal Of Controlled Release, 213 (2015) E134-E134.

[23] E. Santos, R.M. Hernandez, J.L. Pedraz, G. Orive, Novel Advances In The Design Of Three-Dimensional Bio-Scaffolds To Control Cell Fate: Translation From 2d To 3d, Trends In Biotechnology, 30 (2012) 331-341.

[24] E. Cukierman, R. Pankov, D.R. Stevens, K.M. Yamada, Taking Cell-Matrix Adhesions To The Third Dimension, Science, 294 (2001) 1708-1712.

[25] K.M. Hakkinen, J.S. Harunaga, A.D. Doyle, K.M. Yamada, Direct Comparisons Of The Morphology, Migration, Cell Adhesions, And Actin Cytoskeleton Of Fibroblasts In Four Different Three-Dimensional Extracellular Matrices, Tissue Engineering Part A, 17 (2010) 713-724.

[26] B.A. Justice, N.A. Badr, R.A. Felder, 3d Cell Culture Opens New Dimensions In Cell-Based Assays, Drug Discovery Today, 14 (2009) 102-107.

[27] Y. Haraguchi, T. Shimizu, T. Sasagawa, H. Sekine, K. Sakaguchi, T. Kikuchi, W. Sekine, S. Sekiya, M. Yamato, M. Umezu, T. Okano, Fabrication Of Functional Three-Dimensional Tissues By Stacking Cell Sheets In Vitro, Nature Protocols, 7 (2012) 850-858.

[28] B.M. Baker, C.S. Chen, Deconstructing The Third Dimension–How 3d Culture Microenvironments Alter Cellular Cues, Journal Of Cell Science, 125 (2012) 3015-3024.

[29] T.G. Fernandes, S.-J. Kwon, S.S. Bale, M.-Y. Lee, M.M. Diogo, D.S. Clark, J.M.S. Cabral, J.S. Dordick, Three-Dimensional Cell Culture Microarray For High-Throughput Studies Of Stem Cell Fate, Biotechnology And Bioengineering, 106 (2010) 106-118.

[30] A. Dolatshahi-Pirouz, M. Nikkhah, A.K. Gaharwar, B. Hashmi, E. Guermani, H. Aliabadi, G. Camci-Unal, T. Ferrante, M. Foss, D.E. Ingber, A. Khademhosseini, A Combinatorial Cell-Laden Gel Microarray For Inducing Osteogenic Differentiation Of Human Mesenchymal Stem Cells, Scientific Reports, 4 (2014) 3896.

[31] F. Xu, J.H. Wu, S.Q. Wang, N.G. Durmus, U.A. Gurkan, U. Demirci, Microengineering Methods For Cell-Based Microarrays And High-Throughput Drug-Screening Applications, Biofabrication, 3 (2011) 034101.

[32] Y.N. Xia, G.M. Whitesides, Soft Lithography, Annual Review Of Materials Science, 28 (1998) 153-184.

[33] S. Brittain, K. Paul, X.M. Zhao, G. Whitesides, Soft Lithography And Microfabrication, Physics World, 11 (1998) 31-36.

[34] G.M. Whitesides, E. Ostuni, S. Takayama, X.Y. Jiang, D.E. Ingber, Soft Lithography In Biology And Biochemistry, Annual Review Of Biomedical Engineering, 3 (2001) 335-373.

[35] D. Qin, Y.N. Xia, G.M. Whitesides, Soft Lithography For Micro- And Nanoscale Patterning, Nature Protocols, 5 (2010) 491-502.

[36] A. Ranga, S. Gobaa, Y. Okawa, K. Mosiewicz, A. Negro, M.P. Lutolf, 3d Niche Microarrays For Systems-Level Analyses Of Cell Fate, Nature Communications, 5 (2014).

[37] A.K. Gaharwar, A. Arpanaei, T.L. Andresen, A. Dolatshahi-Pirouz, 3d Biomaterial Microarrays For Regenerative Medicine: Current State-Of-The-Art, Emerging Directions And Future Trends, Advanced Materials, 28 (2016) 771-781.

[38] S. Zhao, H. Zhao, X. Zhang, Y. Li, Y. Du, Off-The-Shelf Microsponge Arrays For Facile And Efficient Construction Of Miniaturized 3d Cellular Microenvironments For Versatile Cell-Based Assays, Lab On A Chip, 13 (2013) 2350-2358.

[39] C.L. Salgado, M.B. Oliveira, J.F. Mano, Combinatorial Cell-3d Biomaterials Cytocompatibility Screening For Tissue Engineering Using Bioinspired Superhydrophobic Substrates, Integrative Biology, 4 (2012) 318-327.

[40] E. Ueda, F.L. Geyer, V. Nedashkivska, P.A. Levkin, Droplet Microarray: Facile Formation Of Arrays Of Microdroplets And Hydrogel Micropads For Cell Screening Applications, Lab On A Chip, 12 (2012) 5218-5224.

[41] M.B. Oliveira, C.L. Salgado, J.F. Mano, Patterned Superhydrophobic Surfaces For The Combinatorial Assessment Of 3d Biomaterials-Cells Interactions, Journal Of Tissue Engineering And Regenerative Medicine, 6 (2012) 230-230.

[42] T. Limongi, F. Cesca, F. Gentile, R. Marotta, R. Ruffilli, A. Barberis, M. Dal Maschto, E.M. Petrini, S. Santoriello, F. Benfenati, E. Di Fabrizio, Nanostructured Superhydrophobic Substrates Trigger The Development Of 3d Neuronal Networks, Small, 9 (2013) 402-412.

[43] G. Rosse, E. Kueng, M.G.P. Page, V. Schauer-Vukasinovic, T. Giller, H.W. Lahm, P. Hunziker, D. Schlatter, Rapid Identification Of Substrates For Novel Proteases Using A Combinatorial Peptide Library, Journal Of Combinatorial Chemistry, 2 (2000) 461-466.

[44] M. Uttamchandani, J. Wang, S.Q. Yao, Protein And Small Molecule Microarrays: Powerful Tools For High-Throughput Proteomics, Molecular Biosystems, 2 (2006) 58-68.

[45] C. Maudet, M. Mano, U. Sunkavalli, M. Sharan, M. Giacca, K.U. Forstner, A. Eulalio, Functional High-Throughput Screening Identifies The Mir-15 Microrna Family As Cellular Restriction Factors For Salmonella Infection, Nature Communications, 5 (2014) 4718.

[46] Y. Mei, Microarrayed Materials For Stem Cells, Materials Today, 15 (2012) 444-452.

[47] T.G. Fernandes, S.-J. Kwon, M.-Y. Lee, D.S. Clark, J.M.S. Cabral, J.S. Dordick, On-Chip, Cell-Based Microarray Immunofluorescence Assay For High-Throughput Analysis Of Target Proteins, Analytical Chemistry, 80 (2008) 6633-6639.

[48] B.J. Battersby, M. Trau, Novel Miniaturized Systems In High-Throughput Screening, Trends In Biotechnology, 20 (2002) 167-173.

[49] L.A. Mathews, J.M. Keller, B.L. Goodwin, R. Guha, P. Shinn, R. Mull, C.J. Thomas, R.L. De Kluyver, T.J. Sayers, M. Ferrer, A 1536-Well Quantitative High-Throughput Screen To Identify Compounds Targeting Cancer Stem Cells, Journal Of Biomolecular Screening, 17 (2012) 1231-1242.

[50] S. Neuss, C. Apel, P. Buttler, B. Denecke, A. Dhanasingh, X. Ding, D. Grafahrend, A. Groger, K. Hemmrich, A. Herr, W. Jahnen-Dechent, S. Mastitskaya, A. Perez-Bouza, S. Rosewick, J. Salber, M. Woeltje, M. Zenke, Assessment Of Stem Cell/Biomaterial Combinations For Stem Cell-Based Tissue Engineering, Biomaterials, 29 (2008) 302-313.

[51] O.Z. Fisher, A. Khademhosseini, R. Langer, N.A. Peppas, Bioinspired Materials For Controlling Stem Cell Fate, Accounts Of Chemical Research, 43 (2010) 419-428.

[52] S. Ankam, B.K.K. Teo, M. Kukumberg, E.K.F. Yim, High Throughput Screening To Investigate The Interaction Of Stem Cells With Their Extracellular Microenvironment, Organogenesis, 9 (2013) 128-142.

[53] K. Johnson, S. Zhu, M.S. Tremblay, J.N. Payette, J. Wang, L.C. Bouchez, S. Meeusen, A. Althage, C.Y. Cho, X. Wu, P.G. Schultz, A Stem Cell-Based Approach To Cartilage Repair, Science, 336 (2012) 717-721.

[54] A.M. Ghaemmaghami, M.J. Hancock, H. Harrington, H. Kaji, A. Khademhosseini, Biomimetic Tissues On A Chip For Drug Discovery, Drug Discovery Today, 17 (2012) 173-181.

[55] E. Santos, R.M. Hernández, J.L. Pedraz, G. Orive, Novel Advances In The Design Of Three-Dimensional Bio-Scaffolds To Control Cell Fate: Translation From 2d To 3d, Trends In Biotechnology, 30 (2012) 331-341.

[56] Y. Yoshii, T. Furukawa, A. Waki, H. Okuyama, M. Inoue, M. Itoh, M.R. Zhang, H. Wakizaka, C. Sogawa, Y. Kiyono, H. Yoshii, Y. Fujibayashi, T. Saga, High-Throughput Screening With Nanoimprinting 3d Culture For Efficient Drug Development By Mimicking The Tumor Environment, Biomaterials, 51 (2015) 278-289.

[57] S. Lindstrom, H. Andersson-Svahn, Miniaturization Of Biological Assays - Overview On Microwell Devices For Single-Cell Analyses, Biochimica Et Biophysica Acta-General Subjects, 1810 (2011) 308-316.

[58] U.A. Gurkan, S. Tasoglu, D. Kavaz, M.C. Demirel, U. Demirci, Emerging Technologies For Assembly Of Microscale Hydrogels, Advanced Healthcare Materials, 1 (2012) 149-158.

[59] Y.S. Song, R.L. Lin, G. Montesano, N.G. Durmus, G. Lee, S.S. Yoo, E. Kayaalp, E. Haeggstrom, A. Khademhosseini, U. Demirci, Engineered 3d Tissue Models For Cell-Laden Microfluidic Channels, Analytical And Bioanalytical Chemistry, 395 (2009) 185-193.

[60] S. Khetan, J.A. Burdick, Patterning Hydrogels In Three Dimensions Towards Controlling Cellular Interactions, Soft Matter, 7 (2011) 830-838.

[61] C.A. Deforest, K.S. Anseth, Photoreversible Patterning Of Biomolecules Within Click-Based Hydrogels, Angewandte Chemie-International Edition, 51 (2012) 1816-1819.

[62] T. Dvir, B.P. Timko, D.S. Kohane, R. Langer, Nanotechnological Strategies For Engineering Complex Tissues, Nature Nanotechnology, 6 (2011) 13-22.

[63] Y. Yoshii, A. Waki, K. Yoshida, A. Kakezuka, M. Kobayashi, H. Namiki, Y. Kuroda, Y. Kiyono, H. Yoshii, T. Furukawa, T. Asai, H. Okazawa, J.G. Gelovani, Y. Fujibayashi, The Use Of Nanoimprinted Scaffolds As 3d Culture Models To Facilitate Spontaneous Tumor Cell Migration And Well-Regulated Spheroid Formation, Biomaterials, 32 (2011) 6052-6058.

[64] Y.C. Tung, A.Y. Hsiao, S.G. Allen, Y.S. Torisawa, M. Ho, S. Takayama, High-Throughput 3d Spheroid Culture And Drug Testing Using A 384 Hanging Drop Array, Analyst, 136 (2011) 473-478.

[65] S. Guven, P. Chen, F. Inci, S. Tasoglu, B. Erkmen, U. Demirci, Multiscale Assembly For Tissue Engineering And Regenerative Medicine, Trends In Biotechnology, 33 (2015) 269-279.

[66] A.Y. Hsiao, Y.C. Tung, X.G. Qu, L.R. Patel, K.J. Pienta, S. Takayama, 384 Hanging Drop Arrays Give Excellent Z-Factors And Allow Versatile Formation Of Co-Culture Spheroids, Biotechnology And Bioengineering, 109 (2012) 1293-1304.

[67] A.Y. Hsiao, Y.C. Tung, C.H. Kuo, B. Mosadegh, R. Bedenis, K.J. Pienta, S. Takayama, Micro-Ring Structures Stabilize Microdroplets To Enable Long Term Spheroid Culture In 384 Hanging Drop Array Plates, Biomedical Microdevices, 14 (2012) 313-323.

[68] S. Fox, S. Farr-Jones, M.A. Yund, High Throughput Screening For Drug Discovery: Continually Transitioning Into New Technology, Journal Of Biomolecular Screening, 4 (1999) 183-186.

[69] K.H. Bleicher, H.-J. Bohm, K. Muller, A.I. Alanine, Hit And Lead Generation: Beyond High-Throughput Screening, Nature Reviews Drug Discovery, 2 (2003) 369-378.

[70] Z. Wang, M.-C. Kim, M. Marquez, T. Thorsen, High-Density Microfluidic Arrays For Cell Cytotoxicity Analysis, Lab On A Chip, 7 (2007) 740-745.

[71] K.A. Mosiewicz, L. Kolb, A.J. Van Der Vlies, M.M. Martino, P.S. Lienemann, J.A. Hubbell, M. Ehrbar, M.P. Lutolf, In Situ Cell Manipulation Through Enzymatic Hydrogel Photopatterning, Nature Materials, 12 (2013) 1071-1077.

[72] M.J. Evans, A. Saghatelian, E.J. Sorensen, B.F. Cravatt, Target Discovery In Small-Molecule Cell-Based Screens By In Situ Proteome Reactivity Profiling, Nature Biotechnology, 23 (2005) 1303-1307.

[73] N.M. Alves, I. Pashkuleva, R.L. Reis, J.F. Mano, Controlling Cell Behavior Through The Design Of Polymer Surfaces, Small, 6 (2010) 2208-2220.

[74] P.-C. Chen, Y.-Y. Huang, J.-L. Juang, Mems Microwell And Microcolumn Arrays: Novel Methods For High-Throughput Cell-Based Assays, Lab On A Chip, 11 (2011) 3619-3625.

[75] J. Zhou, Y. Wu, S.-K. Lee, R. Fan, High-Content Single-Cell Analysis On-Chip Using A Laser Microarray Scanner, Lab On A Chip, 12 (2012) 5025-5033.

[76] O.I. Berthuy, L.J. Blum, C.A. Marquette, Cells On Chip For Multiplex Screening, Biosensors And Bioelectronics, 76 (2016) 29-37.

[77] T. Ueno, Y. Yamashita, M. Soda, K. Fukumura, M. Ando, A. Yamato, M. Kawazu, Y.L. Choi, H. Mano, High-Throughput Resequencing Of Target-Captured Cdna In Cancer Cells, Cancer Science, 103 (2012) 131-135.

[78] J. Ziauddin, D.M. Sabatini, Microarrays Of Cells Expressing Defined Cdnas, Nature, 411 (2001) 107-110.

[79] M. Schena, D. Shalon, R.W. Davis, P.O. Brown, Quantitative Monitoring Of Gene Expression Patterns With A Complementary Dna Microarray, Science, 270 (1995) 467-470.

[80] C. Shen, P. Xu, Z. Huang, D. Cai, S.-J. Liu, W. Du, Bacterial Chemotaxis On Slipchip, Lab On A Chip, 14 (2014) 3074-3080.

[81] F. Wunder, B. Kalthof, T. Mueller, J. Hueser, Functional Cell-Based Assays In Microliter Volumes For Ultra-High Throughput Screening, Combinatorial Chemistry & High Throughput Screening, 11 (2008) 495-504.

[82] A.M. Ghaemmaghami, M.J. Hancock, H. Harrington, H. Kaji, A. Khademhosseini, Biomimetic Tissues On A Chip For Drug Discovery, Drug Discovery Today, 17 (2012) 173-181.

[83] D. Huh, Y.-S. Torisawa, G.A. Hamilton, H.J. Kim, D.E. Ingber, Microengineered Physiological Biomimicry: Organs-On-Chips, Lab On A Chip, 12 (2012) 2156-2164.

[84] D. Huh, G.A. Hamilton, D.E. Ingber, From 3d Cell Culture To Organs-On-Chips, Trends In Cell Biology, 21 (2011) 745-754.

[85] G. Orive, E. Santos, D. Poncelet, R. Maria Hernandez, J. Luis Pedraz, L.U. Wahlberg, P. De Vos, D. Emerich, Cell Encapsulation: Technical And Clinical Advances, Trends In Pharmacological Sciences, 36 (2015) 537-546.

[86] D. Barata, C. Van Blitterswijk, P. Habibovic, High-Throughput Screening Approaches And Combinatorial Development Of Biomaterials Using Microfluidics, Acta Biomaterialia, 34 (2016) 1-20.

[87] S. Kobel, M.P. Lutolf, High-Throughput Methods To Define Complex Stem Cell Niches, Biotechniques, 48 (2010) Ix-Xxii.

[88] T. Hart, A. Zhao, A. Garg, S. Bolusani, E.M. Marcotte, Human Cell Chips: Adapting Dna Microarray Spotting Technology To Cell-Based Imaging Assays, Plos One, 4 (2009) E7088.

[89] D. Zahner, J. Abagat, F. Svec, J.M.J. Frechet, P.A. Levkin, A Facile Approach To Superhydrophilic-Superhydrophobic Patterns In Porous Polymer Films, Advanced Materials, 23 (2011) 3030-3034.

[90] H. Qi, Y.A. Du, L.Y. Wang, H. Kaji, H.J. Bae, A. Khademhosseini, Patterned Differentiation Of Individual Embryoid Bodies In Spatially Organized 3d Hybrid Microgels, Advanced Materials, 22 (2010) 5276-5281.

[91] L.Y. Wu, D. Di Carlo, L.P. Lee, Microfluidic Self-Assembly Of Tumor Spheroids For Anticancer Drug Discovery, Biomedical Microdevices, 10 (2008) 197-202.

[92] D. Huh, B.D. Matthews, A. Mammoto, M. Montoya-Zavala, H.Y. Hsin, D.E. Ingber, Reconstituting Organ-Level Lung Functions On A Chip, Science, 328 (2010) 1662-1668.

[93] J. Clausell-Tormos, D. Lieber, J.-C. Baret, A. El-Harrak, O.J. Miller, L. Frenz, J. Blouwolff, K.J. Humphry, S. Köster, H. Duan, C. Holtze, D.A. Weitz, A.D. Griffiths, C.A. Merten, Droplet-Based Microfluidic Platforms For The Encapsulation And Screening Of Mammalian Cells And Multicellular Organisms, Chemistry & Biology, 15 (2008) 427-437.

[94] W. Liu, D. Chen, W. Du, K.P. Nichols, R.F. Ismagilov, Slipchip For Immunoassays In Nanoliter Volumes, Analytical Chemistry, 82 (2010) 3276-3282.

[95] V. Lecault, M. Vaninsberghe, S. Sekulovic, D.J.H.F. Knapp, S. Wohrer, W. Bowden, F. Viel, T. Mclaughlin, A. Jarandehei, M. Miller, D. Falconnet, A.K. White, D.G. Kent, M.R. Copley, F. Taghipour, C.J. Eaves, R.K.

Humphries, J.M. Piret, C.L. Hansen, High-Throughput Analysis Of Single Hematopoietic Stem Cell Proliferation In Microfluidic Cell Culture Arrays, Nature Methods, 8 (2011) 581-586.

[96] J. Wu, I. Wheeldon, Y. Guo, T. Lu, Y. Du, B. Wang, J. He, Y. Hu, A. Khademhosseini, A Sandwiched Microarray Platform For Benchtop Cell-Based High Throughput Screening, Biomaterials, 32 (2011) 841-848.

[97] L. Ma, S.S. Datta, M.A. Karymov, Q.C. Pan, S. Begolo, R.F. Ismagilov, Individually Addressable Arrays Of Replica Microbial Cultures Enabled By Splitting Slipchips, Integrative Biology, 6 (2014) 796-805.

[98] D. Gao, H.X. Liu, Y.Y. Jiang, J.M. Lin, Recent Developments In Microfluidic Devices For In Vitro Cell Culture For Cell-Biology Research, Trac-Trends In Analytical Chemistry, 35 (2012) 150-164.

[99] S. Yamamura, H. Kishi, Y. Tokimitsu, S. Kondo, R. Honda, S.R. Rao, M. Omori, E. Tamiya, A. Muraguchi, Single-Cell Microarray For Analyzing Cellular Response, Analytical Chemistry, 77 (2005) 8050-8056.

[100] C. Moraes, G. Wang, Y. Sun, C.A. Simmons, A Microfabricated Platform For High-Throughput Unconfined Compression Of Micropatterned Biomaterial Arrays, Biomaterials, 31 (2010) 577-584.

[101] A.M. Kloxin, M.W. Tibbitt, K.S. Anseth, Synthesis Of Photodegradable Hydrogels As Dynamically Tunable Cell Culture Platforms, Nature Protocols, 5 (2010) 1867-1887.

[102] W.Q. Feng, L.X. Li, E. Ueda, J.S. Li, S. Heissler, A. Welle, O. Trapp, P.A. Levkin, Surface Patterning Via Thiol-Yne Click Chemistry: An Extremely Fast And Versatile Approach To Superhydrophilic-Superhydrophobic Micropatterns, Advanced Materials Interfaces, 1 (2014).

[103] F.L. Geyer, E. Ueda, U. Liebel, N. Grau, P.A. Levkin, Superhydrophobic-Superhydrophilic Micropatterning: Towards Genome-On-A-Chip Cell Microarrays, Angewandte Chemie-International Edition, 50 (2011) 8424-8427.

[104] A.N. Efremov, E. Stanganello, A. Welle, S. Scholpp, P.A. Levkin, Micropatterned Superhydrophobic Structures For The Simultaneous Culture Of Multiple Cell Types And The Study Of Cell-Cell Communication, Biomaterials, 34 (2013) 1757-1763.

[105] A.A. Popova, S.M. Schillo, K. Demir, E. Ueda, A. Nesterov-Mueller, P.A. Levkin, Droplet-Array (Da) Sandwich Chip: A Versatile Platform For High-Throughput Cell Screening Based On Superhydrophobic-Superhydrophilic Micropatterning, Advanced Materials, 27 (2015) 5217-5222.

[106] E. Figallo, C. Cannizzaro, S. Gerechi, J.A. Burdick, R. Langer, N. Elvassore, G. Vunjak-Novakovic, Micro-Bioreactor Array For Controlling Cellular Microenvironments, Lab On A Chip, 7 (2007) 710-719.

[107] A. Ranga, S. Gobaa, Y. Okawa, K. Mosiewicz, A. Negro, M.P. Lutolf, 3d Niche Microarrays For Systems-Level Analyses Of Cell Fate, Nature Communications, 5 (2014) 4324.

[108] P. Tayalia, C.R. Mendonca, T. Baldacchini, D.J. Mooney, E. Mazur, 3d Cell-Migration Studies Using Two-Photon Engineered Polymer Scaffolds, Advanced Materials, 20 (2008) 4494-4498.

[109] R. Gauvin, Y.C. Chen, J.W. Lee, P. Soman, P. Zorlutuna, J.W. Nichol, H. Bae, S.C. Chen, A. Khademhosseini, Microfabrication Of Complex Porous Tissue Engineering Scaffolds Using 3d Projection Stereolithography, Biomaterials, 33 (2012) 3824-3834.

[110] K. Nakazawa, Y. Izumi, J. Fukuda, T. Yasuda, Hepatocyte Spheroid Culture On A Polydimethylsiloxane Chip Having Microcavities, Journal Of Biomaterials Science-Polymer Edition, 17 (2006) 859-873.

[111] C. Hsiao, S.P. Palecek, Microwell Regulation Of Pluripotent Stem Cell Self-Renewal And Differentiation, Bionanoscience, 2 (2012) 266-276.

[112] K. Futrega, J.S. Palmer, M. Kinney, W.B. Lott, M.D. Ungrin, P.W. Zandstra, M.R. Doran, The Microwell-Mesh: A Novel Device And Protocol For The High Throughput Manufacturing Of Cartilage Microtissues, Biomaterials, 62 (2015) 1-12.

[113] U. Mirsaidov, J. Scrimgeour, W. Timp, K. Beck, M. Mir, P. Matsudaira, G. Timp, Live Cell Lithography: Using Optical Tweezers To Create Synthetic Tissue, Lab On A Chip, 8 (2008) 2174-2181.

[114] W.H. Tan, S. Takeuchi, Dynamic Microarray System With Gentle Retrieval Mechanism For Cell-Encapsulating Hydrogel Beads, Lab On A Chip, 8 (2008) 259-266.

[115] Y. Imura, K. Sato, E. Yoshimura, Micro Total Bioassay System For Ingested Substances: Assessment Of Intestinal Absorption, Hepatic Metabolism, And Bioactivity, Analytical Chemistry, 82 (2010) 9983-9988.

[116] J.M. Anderson, Biological Responses To Materials, Annual Review Of Materials Research, 31 (2001) 81-110.

[117] N. Verplanck, Y. Coffinier, V. Thomy, R. Boukherroub, Wettability Switching Techniques On Superhydrophobic Surfaces, Nanoscale Research Letters, 2 (2007) 577-596.

[118] G. Ciasca, M. Papi, L. Businaro, G. Campi, M. Ortolani, V. Palmieri, A. Cedola, A. De Ninno, A. Gerardino, G. Maulucci, M. De Spirito, Recent Advances In Superhydrophobic Surfaces And Their Relevance To Biology And Medicine, Bioinspiration & Biomimetics, 11 (2016) 011001-011001.

[119] L. Feng, Y. Zhang, J. Xi, Y. Zhu, N. Wang, F. Xia, L. Jiang, Petal Effect: A Superhydrophobic State With High Adhesive Force, Langmuir, 24 (2008) 4114-4119.

[120] R. Furstner, W. Barthlott, C. Neinhuis, P. Walzel, Wetting And Self-Cleaning Properties Of Artificial Superhydrophobic Surfaces, Langmuir, 21 (2005) 956-961.

[121] M. Ma, R.M. Hill, Superhydrophobic Surfaces, Current Opinion In Colloid & Interface Science, 11 (2006) 193-202.

[122] A. Marmur, The Lotus Effect: Superhydrophobicity And Metastability, Langmuir, 20 (2004) 3517-3519.

[123] X. Zhang, F. Shi, J. Niu, Y. Jiang, Z. Wang, Superhydrophobic Surfaces: From Structural Control To Functional Application, Journal Of Materials Chemistry, 18 (2008) 621-633.

[124] A.C. Lima, J.F. Mano, Micro/Nano-Structured Superhydrophobic Surfaces In The Biomedical Field: Part Ii: Applications Overview, Nanomedicine, 10 (2015) 271-297.

[125] Xiaoxue Zhang, L. Wang, E. Leva, Superhydrophobic Surfaces For The Reduction Of Bacterial Adhesion, Rsc Advances, 3 (2013) 12003-12020.

[126] Y. Lai, L. Lin, F. Pan, J. Huang, R. Song, Y. Huang, C. Lin, H. Fuchs, L. Chi, Bioinspired Patterning With Extreme Wettability Contrast On Tio2 Nanotube Array Surface: A Versatile Platform For Biomedical Applications, Small, 9 (2013) 2945-2953.

[127] W. Liang, Y. Zhang, B. Wang, Z. Guo, W. Liu, Biological Applications Of Biomimetic Superhydrophobic Surfaces, Acta Chimica Sinica, 70 (2012) 2393-2403.

[128] M.J. Hancock, K. Sekeroglu, M.C. Demirel, Bioinspired Directional Surfaces For Adhesion, Wetting, And Transport, Advanced Functional Materials, 22 (2012) 2223-2234.

[129] X. Yao, Y.L. Song, L. Jiang, Applications Of Bio-Inspired Special Wettable Surfaces, Advanced Materials, 23 (2011) 719-734.

[130] S.M. Oliveira, N.M. Alves, J.F. Mano, Cell Interactions With Superhydrophilic And Superhydrophobic Surfaces, Journal Of Adhesion Science And Technology, 28 (2014) 843-863.

[131] L. Feng, S. Li, Y. Li, H. Li, L. Zhang, J. Zhai, Y. Song, B. Liu, L. Jiang, D. Zhu, Super-Hydrophobic Surfaces: From Natural To Artificial, Advanced Materials, 14 (2002) 1857-1860.

[132] T. Onda, S. Shibuichi, N. Satoh, K. Tsujii, Super-Water-Repellent Fractal Surfaces, Langmuir, 12 (1996) 2125-2127.

[133] B.N. Lourenco, G. Marchioli, W.L. Song, R.L. Reis, C.A. Van Blitterswijk, M. Karperien, A. Van Apeldoorn, J.F. Mano, Wettability Influences Cell Behavior On Superhydrophobic Surfaces With Different Topographies, Biointerphases, 7 (2012) 46.

[134] P.A. Levkin, F. Svec, J.M.J. Frechet, Porous Polymer Coatings: A Versatile Approach To Superhydrophobic Surfaces, Advanced Functional Materials, 19 (2009) 1993-1998.

[135] T. Darmanin, E.T. De Givenchy, S. Amigoni, F. Guittard, Superhydrophobic Surfaces By Electrochemical Processes, Advanced Materials, 25 (2013) 1378-1394.

[136] X.Y. Lu, C.C. Zhang, Y.C. Han, Low-Density Polyethylene Superhydrophobic Surface By Control Of Its Crystallization Behavior, Macromolecular Rapid Communications, 25 (2004) 1606-1610.

[137] M.L. Ma, Y. Mao, M. Gupta, K.K. Gleason, G.C. Rutledge, Superhydrophobic Fabrics Produced By Electrospinning And Chemical Vapor Deposition, Macromolecules, 38 (2005) 9742-9748.

[138] Y.-C. Pang, Y. Zhao, J. Feng, Different Superhydrophobic Copper Surfaces Fabricated By Wet Chemical Oxidation Method And Their Anti-Condensation Property, Chemical Journal Of Chinese Universities-Chinese, 34 (2013) 919-924.

[139] R. Taurino, E. Fabbri, M. Messori, F. Pilati, D. Pospiech, A. Synytska, Facile Preparation Of Superhydrophobic Coatings By Sol-Gel Processes, Journal Of Colloid And Interface Science, 325 (2008) 149-156.

[140] S.M. Kang, I. You, W.K. Cho, H.K. Shon, T.G. Lee, I.S. Choi, J.M. Karp, H. Lee, One-Step Modification Of Superhydrophobic Surfaces By A Mussel-Inspired Polymer Coating, Angewandte Chemie-International Edition, 49 (2010) 9401-9404.

[141] Y.T. Cheng, D.E. Rodak, C.A. Wong, C.A. Hayden, Effects Of Micro- And Nano-Structures On The Self-Cleaning Behaviour Of Lotus Leaves, Nanotechnology, 17 (2006) 1359.

[142] T. Sun, G.J. Wang, H. Liu, L. Feng, L. Jiang, D.B. Zhu, Control Over The Wettability Of An Aligned Carbon Nanotube Film, Journal Of The American Chemical Society, 125 (2003) 14996-14997.

[143] Y. Zheng, H. Bai, Z. Huang, X. Tian, F.-Q. Nie, Y. Zhao, J. Zhai, L. Jiang, Directional Water Collection On Wetted Spider Silk, Nature, 463 (2010) 640-643.

[144] K. Koch, W. Barthlott, Superhydrophobic And Superhydrophilic Plant Surfaces: An Inspiration For Biomimetic Materials, Philosophical Transactions Of The Royal Society Of London A: Mathematical, Physical And Engineering Sciences, 367 (2009) 1487-1509.

[145] R.N. Wenzel, Resistance Of Solid Surfaces To Wetting By Water, Industrial & Engineering Chemistry, 28 (1936) 988-994.

[146] A.B.D. Cassie, S. Baxter, Wettability Of Porous Surfaces, Transactions Of The Faraday Society, 40 (1944) 546-551.

[147] T. Sun, L. Feng, X. Gao, L. Jiang, Bioinspired Surfaces With Special Wettability, Accounts Of Chemical Research, 38 (2005) 644-652.

[148] T.L. Sun, L. Feng, X.F. Gao, L. Jiang, Bioinspired Surfaces With Special Wettability, Accounts Of Chemical Research, 38 (2005) 644-652.

[149] B. Bhushan, Y.C. Jung, Natural And Biomimetic Artificial Surfaces For Superhydrophobicity, Self-Cleaning, Low Adhesion, And Drag Reduction, Progress In Materials Science, 56 (2011) 1-108.

[150] A.I. Neto, C.R. Correia, C.A. Custodio, J.F. Mano, Biomimetic Miniaturized Platform Able To Sustain Arrays Of Liquid Droplets For High-Throughput Combinatorial Tests, Advanced Functional Materials, 24 (2014) 5096-5103.

[151] A. Nakajima, K. Hashimoto, T. Watanabe, K. Takai, G. Yamauchi, A. Fujishima, Transparent Superhydrophobic Thin Films With Self-Cleaning Properties, Langmuir, 16 (2000) 7044-7047.

[152] X. Zhang, H. Kono, Z. Liu, S. Nishimoto, D.A. Tryk, T. Murakami, H. Sakai, M. Abe, A. Fujishima, A Transparent And Photo-Patternable Superhydrophobic Film, Chemical Communications, (2007) 4949-4951.

[153] J. Bravo, L. Zhai, Z. Wu, R.E. Cohen, M.F. Rubner, Transparent Superhydrophobic Films Based On Silica Nanoparticles, Langmuir, 23 (2007) 7293-7298.

[154] A.K. Sinha, M. Basu, M. Pradhan, S. Sarkar, T. Pal, Fabrication Of Large-Scale Hierarchical Zno Hollow Spheroids For Hydrophobicity And Photocatalysis, Chemistry-A European Journal, 16 (2010) 7865-7874.

[155] A.I. Neto, C.R. Correia, M.B. Oliveira, M.I. Rial-Hermida, C. Alvarez-Lorenzo, R.L. Reis, J.F. Mano, A Novel Hanging Spherical Drop System For The Generation Of Cellular Spheroids And High Throughput Combinatorial Drug Screening, Biomaterials Science, 3 (2015) 581-585.

[156] T. Liu, M. Winter, B. Thierry, Quasi-Spherical Microwells On Superhydrophobic Substrates For Long Term Culture Of Multicellular Spheroids And High Throughput Assays, Biomaterials, 35 (2014) 6060-6068.

[157] M. Lee, K. Yang, Y.H. Hwang, Y. Byun, D.Y. Lee, S.-W. Cho, H. Lee, Spheroform: Therapeutic Spheroid-Forming Nanotextured Surfaces Inspired By Desert Beetle Physosterna Cribripes, Advanced Healthcare Materials, 4 (2015) 511-515.

[158] J. Seo, J.S. Lee, K. Lee, D. Kim, K. Yang, S. Shin, C. Mahata, H.B. Jung, W. Lee, S.-W. Cho, T. Lee, Switchable Water-Adhesive, Superhydrophobic Palladium-Layered Silicon Nanowires Potentiate The Angiogenic Efficacy Of Human Stem Cell Spheroids, Advanced Materials, 26 (2014) 7043-7050.

[159] M.B. Oliveira, A.I. Neto, C.R. Correia, M. Isabel Rial-Hermida, C. Alvarez-Lorenzo, J.F. Mano, Superhydrophobic Chips For Cell Spheroids High-Throughput Generation And Drug Screening, Acs Applied Materials & Interfaces, 6 (2014) 9488-9495.

[160] K.M. Yamada, E. Cukierman, Modeling Tissue Morphogenesis And Cancer In 3d, Cell, 130 (2007) 601-610.

[161] J.M. Brown, W.R. Wilson, Exploiting Tumour Hypoxia In Cancer Treatment, Nature Reviews Cancer, 4 (2004) 437-447.

[162] F. Pampaloni, E.G. Reynaud, E.H. Stelzer, The Third Dimension Bridges The Gap Between Cell Culture And Live Tissue, Nature Reviews Molecular Cell Biology, 8 (2007) 839-845.

[163] H.K. Dhiman, A.R. Ray, A.K. Panda, Three-Dimensional Chitosan Scaffold-Based Mcf-7 Cell Culture For The Determination Of The Cytotoxicity Of Tamoxifen, Biomaterials, 26 (2005) 979-986.

[164] S. Breslin, L. O'driscoll, Three-Dimensional Cell Culture: The Missing Link In Drug Discovery, Drug Discovery Today, 18 (2013) 240-249.

[165] R.Z. Lin, H.Y. Chang, Recent Advances In Three-Dimensional Multicellular Spheroid Culture For Biomedical Research, Journal Of Biotechnology, 3 (2008) 1172-1184.

[166] E. Castro, J.F. Mano, Magnetic Force-Based Tissue Engineering And Regenerative Medicine, Journal Of Biomedical Nanotechnology, 9 (2013) 1129-1136.

[167] X. Gong, C. Lin, J. Cheng, J. Su, H. Zhao, T. Liu, X. Wen, P. Zhao, Generation Of Multicellular Tumor Spheroids With Microwell-Based Agarose Scaffolds For Drug Testing, Plos One, 10 (2015).

[168] M.B. Oliveira, A.I. Neto, C.R. Correia, M.I. Rial-Hermida, C. Alvarez-Lorenzo, J.F. Mano, Superhydrophobic Chips For Cell Spheroids High-Throughput Generation And Drug Screening, Acs Applied Materials & Interfaces, 6 (2014) 9488-9495.

[169] X. Li, X. Zhang, S. Zhao, J. Wang, G. Liu, Y. Du, Micro-Scaffold Array Chip For Upgrading Cell-Based High-Throughput Drug Testing To 3d Using Benchtop Equipment, Lab On A Chip, 14 (2014) 471-481.

[170] H.S. Lim, J.T. Han, D. Kwak, M. Jin, K. Cho, Photoreversibly Switchable Superhydrophobic Surface With Erasable And Rewritable Pattern, Journal Of The American Chemical Society, 128 (2006) 14458-14459.

[171] Q. Tan, S. Li, J. Ren, C. Chen, Fabrication Of Porous Scaffolds With A Controllable Microstructure And Mechanical Properties By Porogen Fusion Technique, International Journal Of Molecular Sciences, 12 (2011) 890-904.

[172] O. Oliviero, M. Ventre, P. Netti, Functional Porous Hydrogels To Study Angiogenesis Under The Effect Of Controlled Release Of Vascular Endothelial Growth Factor, Acta Biomaterialia, 8 (2012) 3294-3301.

[173] E. Tsuruga, H. Takita, H. Itoh, Y. Wakisaka, Y. Kuboki, Pore Size Of Porous Hydroxyapatite As The Cell-Substratum Controls Bmp-Induced Osteogenesis, Journal Of Biochemistry, 121 (1997) 317-324.

[174] J. Yeh, Y. Ling, J.M. Karp, J. Gantz, A. Chandawarkar, G. Eng, J. Blumling Iii, R. Langer, A. Khademhosseini, Micromolding Of Shape-Controlled, Harvestable Cell-Laden Hydrogels, Biomaterials, 27 (2006) 5391-5398.

[175] J. Ock, W. Li, Fabrication Of A Three-Dimensional Tissue Model Microarray Using Laser Foaming Of A Gas-Impregnated Biodegradable Polymer, Biofabrication, 6 (2014) 024110.

[176] M.B. Oliveira, C.L. Salgado, W.L. Song, J.F. Mano, Combinatorial On-Chip Study Of Miniaturized 3d Porous Scaffolds Using A Patterned Superhydrophobic Platform, Small, 9 (2013) 768-778.

[177] P. Agarwal, J.K. Choi, H. Huang, S. Zhao, J. Dumbleton, J. Li, X. He, A Biomimetic Core–Shell Platform For Miniaturized 3d Cell And Tissue Engineering, Particle & Particle Systems Characterization, 32 (2015) 809-816.

[178] A.S. Hoffman, Hydrogels For Biomedical Applications, Advanced Drug Delivery Reviews, 64 (2012) 18-23.

[179] N.A. Peppas, J.Z. Hilt, A. Khademhosseini, R. Langer, Hydrogels In Biology And Medicine: From Molecular Principles To Bionanotechnology, Advanced Materials, 18 (2006) 1345-1360.

[180] E. Tumarkin, L. Tzadu, E. Csaszar, M. Seo, H. Zhang, A. Lee, R. Peerani, K. Purpura, P.W. Zandstra, E. Kumacheva, High-Throughput Combinatorial Cell Co-Culture Using Microfluidics, Integrative Biology, 3 (2011) 653-662.

[181] M.J. Hancock, F. Piraino, G. Camci-Unal, M. Rasponi, A. Khademhosseini, Anisotropic Material Synthesis By Capillary Flow In A Fluid Stripe, Biomaterials, 32 (2011) 6493-6504.

[182] U.A. Gurkan, Y. Fan, F. Xu, B. Erkmen, E.S. Urkac, G. Parlakgul, J. Bernstein, W. Xing, E.S. Boyden, U. Demirci, Simple Precision Creation Of Digitally Specified, Spatially Heterogeneous, Engineered Tissue Architectures, Advanced Materials, 25 (2013) 1192-1198.

[183] M.J. Hancock, F. Yanagawa, Y.H. Jang, J. He, N.N. Kachouie, H. Kaji, A. Khademhosseini, Designer Hydrophilic Regions Regulate Droplet Shape For Controlled Surface Patterning And 3d Microgel Synthesis, Small, 8 (2012) 393-403.

[184] S.P. Kobaku, G. Kwon, A.K. Kota, R.G. Karunakaran, P. Wong, D.H. Lee, A. Tuteja, Wettability Engendered Templated Self-Assembly (Wets) For Fabricating Multiphasic Particles, Acs Applied Materials & Interfaces, 7 (2015) 4075-4080.

[185] Y. Li, P. Chen, Y. Wang, S. Yan, X. Feng, W. Du, S.A. Koehler, U. Demirci, B.F. Liu, Rapid Assembly Of Heterogeneous 3d Cell Microenvironments In A Microgel Array, Advanced Materials, (2016).

[186] Y. Du, M. Ghodousi, E. Lo, M.K. Vidula, O. Emiroglu, A. Khademhosseini, Surface-Directed Assembly Of Cell-Laden Microgels, Biotechnology And Bioengineering, 105 (2010) 655-662.

[187] J.W. Nichol, A. Khademhosseini, Modular Tissue Engineering: Engineering Biological Tissues From The Bottom Up, Soft Matter, 5 (2009) 1312-1319.

[188] D.R. Griffin, W.M. Weaver, P.O. Scumpia, D. Di Carlo, T. Segura, Accelerated Wound Healing By Injectable Microporous Gel Scaffolds Assembled From Annealed Building Blocks, Nature Materials, 14 (2015) 737-744.

[189] M. Oliveira, M. Ribeiro, S. Miguel, A.I. Neto, P. Coutinho, J.F. Mano, I.J. Correia, Biomimetic Superhydrophobic Surfaces Patterned With Wettable Spots As Implantable Chips For In Vivo High-Content 3d Biomaterials Response Assessment, Tissue Engineering Part A, 21 (2015) S140-S140.

SECTION II. MATERIALS AND METHODS

CHAPTER 2. MATERIALS AND METHODS

This Chapter aims to explaining in more detail and adding relevant information that is not present in the practical Chapters (3-8) of this thesis regarding materials and methods used during the development of such works. The detailed specifications of the suppliers can be found in the experimental subsections of each Chapter of Section III.

2.1 Materials

2.1.1 Superhydrophobic surfaces

Inspired by the water repellent behavior of micro/nanostructures surfaces found in the nature, superhydrophobic (SH) surfaces with water contact angles (WCA) higher than 150° have recently been focus of many research works [1-3]. To induce superhydrophobicity on polystyrene (PS) surfaces we followed the phase separation Protocol described by Oliveira et al. [4].

Protocol I

1. Dissolve commercial grade polystyrene (injection molding grade, Styrolution 158 k, UL Ides, Portugal) in anhydrous tetrahydrofuran (THF, containing 250 ppm butylated hydroxytoluene as inhibitor, ≥99.9%, Sigma,) solution to a yield final concentration of 70 mg.mL-1 for 24 hours under stirring at 300 rpm.
2. Add absolute ethanol (Panreac, Spain) to the pre-solution in a proportion of 2: 1.3 (polystyrene solution: absolute ethanol). Shake the mixture.
3. Cut small portions from commercially available smooth polystyrene (PS) sheets with 0.19 mm of thickness (Goodfellow, UK, ref. ST311190/1).
4. Dip the final mixture, with a transparent aspect, onto the smooth PS surfaces Remove the excess of the mixture solution and immerse the coated surface in a non-solvent for the polymer (absolute ethanol). (See Note 1)
5. Dry the surfaces under a gentle flow of nitrogen.

Phase separation is a simple and inexpensive method for the formation of rough and porous polymer films, leading to the fabrication of SH surfaces. In this method, a hardening process is adopted to produce porous materials that consist of a solid phase and a second phase that could be liquid or solid. After the second phase is removed, a porous rough surface is obtained. The PS precipitation on the surface leads to formation of a rough surface explained by the following mechanism: The mixture of the solvent and a non-solvent of polystyrene forms both poor and rich polystyrene phases. In the poor phase, polymer nuclei

[1] The mixture solution is removed from the surface after phase transitions started to occur, i.e., as soon as the surface started showing an opaque aspect. Polymer precipitation was then forced with the immersion of the coated surface in a non-solvent for the polymer (absolute ethanol).

are formed by precipitation. The rich phase aggregates around these nuclei in order to decrease surface tension. During polymer precipitation within the rich PS phase, a continuous deposition of spheres on the surface takes place [4]. Figure 2.1 shows the representative microstructure development onto a PS substrate using this methodology. It is possible to observe sub-micrometer spheres that are agglomerated in larger micrometer structures.

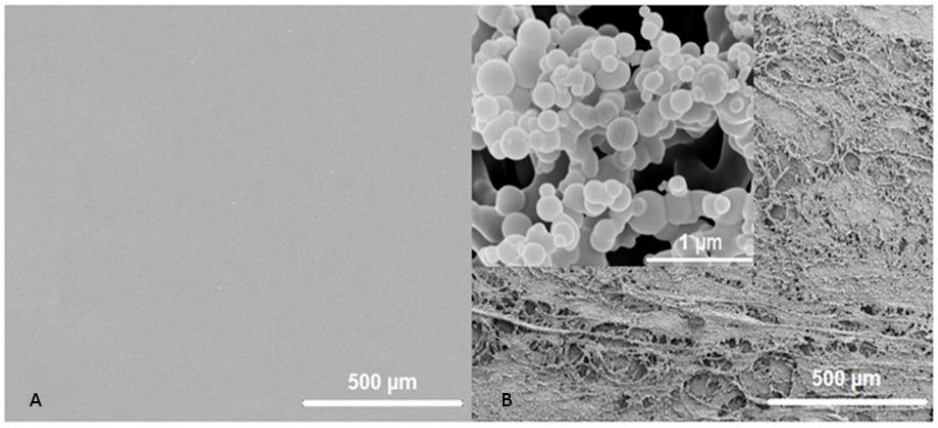

Figure 2.1 Representative scanning electron microscopy image of the A) original smooth PS substrate and B) superhydrophobic rough surface. The inset image depicts the topography of Sh surface using a higher magnification. Figure adapted from [5].

The *Protocol I* was applied using smooth PS sheets for Chapters 4, 5, 6 and 7. Using this surface treatment in Chapter 4, 6 and 7, a rough and porous surface resulted, thereby providing SH properties. In Chapter 5, phase separation methodology was used to produce SH surface patterned with transparent PS spots. In Chapter 8, a new SH platform developed by Levkin group was used [6]. Using phase separation principle, Feng and co-workers developed an extremely fast (<15 s), initiator-free surface modification method compatible with aqueous conditions for creating SH-superhydrophilic (SL) micropatterns using thiol-yne "click" chemistry, [6] based on *Protocol II*.

Protocol II

Activation:

1. Immerse glass slides in 1 M NaOH for 1 hr.
2. Wash with water and DI water.
3. Immerse glass slides in 1 M HCl for 30 min.
4. Wash with water and DI water.
5. Dry with nitrogen gun.

Fluorination:

6. Place activated glass slides in desiccator.
7. Pipet 30 µL tridecafluoro-(1,1,2,2)-tetrahydrooctyltrichlorosilane into Eppendorf tube and place in desiccator.

8. Slide on desiccator cover and ensure tight fit.
9. Pull vacuum to 50 mbar.
10. Leave glass slides overnight.
11. Modification: (See Note 2)
12. Pipette a few drops of modification mixture on activated glass slide and cover with another activated glass slide. Avoid/ remove bubbles and wait 30 min.
13. Repeat step before.
14. Wash with acetone and dry with nitrogen gun.

Polymerization:

15. Purify monomers (2-hydroxyethyl methacrylate (HEMA) and ethylene dimethacrylate (EDMA)) before usage by passing them through a short column packed with basic aluminum oxide to remove inhibitors.

a) Fill 5 mL syringe with Al2O3 up to 1 mL line.
b) Place syringe in 15 mL tube.
c) Pipet 3 mL monomer into syringe.
d) Pump syringe to pass monomer through the Al2O3 column.
e) Place the modified glass slide on top and allow the mixture to spread without forming air bubbles. Clamp the glass slides together.

16. Preform the polymerization by crosslinking a HEMA-EDMA polymer mixture via UV irradiation: place the glass slides with the fluorinated plate on bottom under the UV lamp and irradiate for 15 min with 12 mW/cm^2 intensity, 260 nm wavelength UV light.
17. Carefully separate glass slides using a scalpel.
18. Use adhesive film (Tesa) to remove smooth, nonporous layer that develops along fluorinated glass slide.
19. Tape down polymerized glass slide.
20. Uniformly place adhesive film (Tesa) without bubbles on surface.
21. Peel rapidly.
22. Rinse the polymer surface with ethanol and dried with an air gun.

Esterification:

23. Perform the esterification solution for two HEMA-EDMA surfaces. See Note 3.
24. Put a small magnetic stir bar in the 50 mL tube. Immerse two HEMA-EDMA surfaces back-to-back in the 50 ml tube. Seal the tube with Parafilm and cool at -20°C for 15 min.
25. Fix the tube over a magnetic stirrer. Add 180 µL of N,N'-Diisopropylcarbodiimide (DIC, Alfa Aesar, Cat. #A19292). Quickly seal the tube with parafilm to avoid water in the solution. Stir for 4 h. Alkyne groups (triple bonds) are formed on the surface.
26. Immerse the substrates in ethanol for 2 h to remove unreacted chemicals. See Note 4.

The patterning of SH polystyrene surfaces and SH glass slides are described in the following sub-sections.

---

[2] *The modification step allow functionalize glass slide surface with anchor group for methacrylates to covalently attach polymer layer.*

[3] *The solution can be reused at least 4 times by putting the solution in a new 50 mL tube and adding 20 mg of 4-Pentynoic acid each time.*

[4] *After esterification the glass slides can be store at RT or in ethanol. The static WCA of the surface should be around 90°.*

2.1.1.1 Patterned superhydrophobic surfaces with microindentations

After the production of SH surfaces following the *Protocol I,* multiple indentations were produced over the SH surfaces generating attachment points to produce arrays of droplets with any geometrical disposition and distance between them. In Chapter 6, the micro-indentations over the SH surfaces were produced using a microhardeness tester equipment (Leica VMHT 30) applying loads of 2942 mN, 4903 mN and 19610 mN with a dwell time of 10 s. A sharp rigid Vickers diamond pyramid indenter (included angle α = 136°) penetrated into the surface with a constant load during a complete loading–unloading cycle producing individual indentations. The surfaces patterned with adhesive micro-indentations were used as support for arrays of aqueous solution-based droplets, exhibiting a close spherical shape promoted by the extreme water repellency of the SH surface, but are fixed by the depression features. In Chapter 6, micro-indentations with different sizes were produced, while in Chapter 7, the micro-indentations over the SH surfaces were produced only applying loads of 2942 mN. In both Chapters 6 and 7, to produce the arrays to sustain droplets of cell culture medium, the micro-indentations were placed in the SH surface at a distance of 5 mm from each other, with a square configuration, in the total of 16 spots for each condition, mimicking the effect of rose petals [7] – See Figure 2.2.

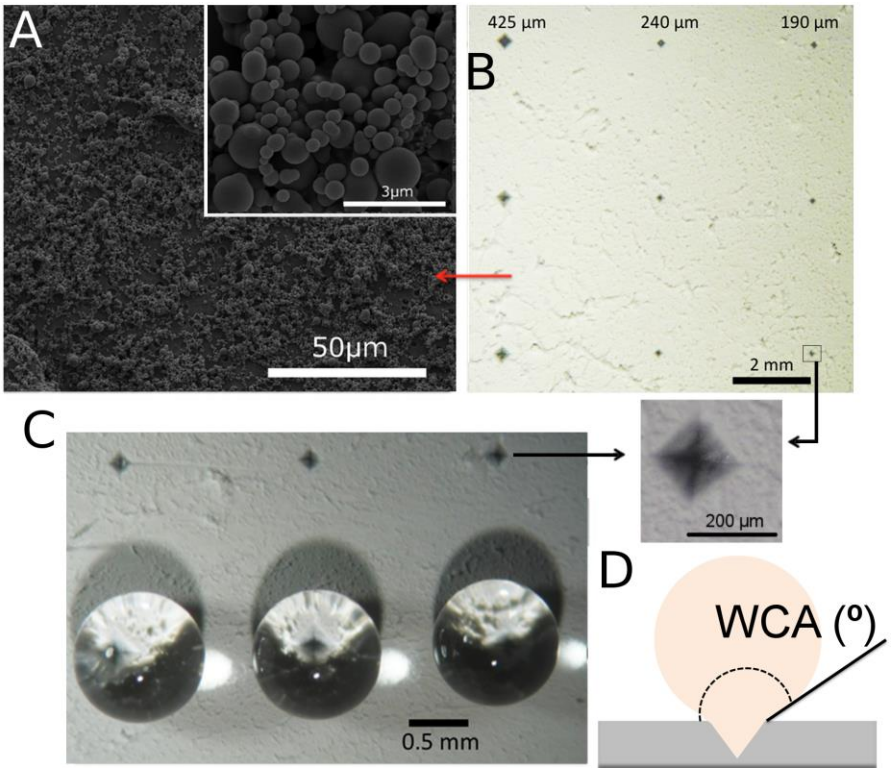

Figure 2.2 a) Microstructure of polystyrene SH surface observed by scanning electron microscope (SEM; two magnifications). b) Upper view of a SH platform patterned with micro-indentations to fix water droplets in the desired areas (c). d) Scheme of

the water droplet position in the micro-indentations magnifying the effect of the penetration of the liquid in the mark. Figure adapted from [8].

2.1.1.2 Polystyrene superhydrophobic surfaces with transparent spots

Using such polystyrene SH surface, a method to pattern with wettable spots was described by Neto et al. [5]. Exposure to UVO irradiation allowed the fast and simple patterning of SL regions with controlled wettability in SH flat surfaces. Such patterns were compatible with fluorescence microscopy analysis of cells attached to such SL regions. However, such method lacked transparency of the wettable spots (compatible with transmitted light microscopy).

We developed a new method that allows patterning transparent and permanent wettable regions in the superhydrophobic surfaces [9-11] - see Figure 2.3. This technique was applied in Chapter 5, following the *Protocol III*.

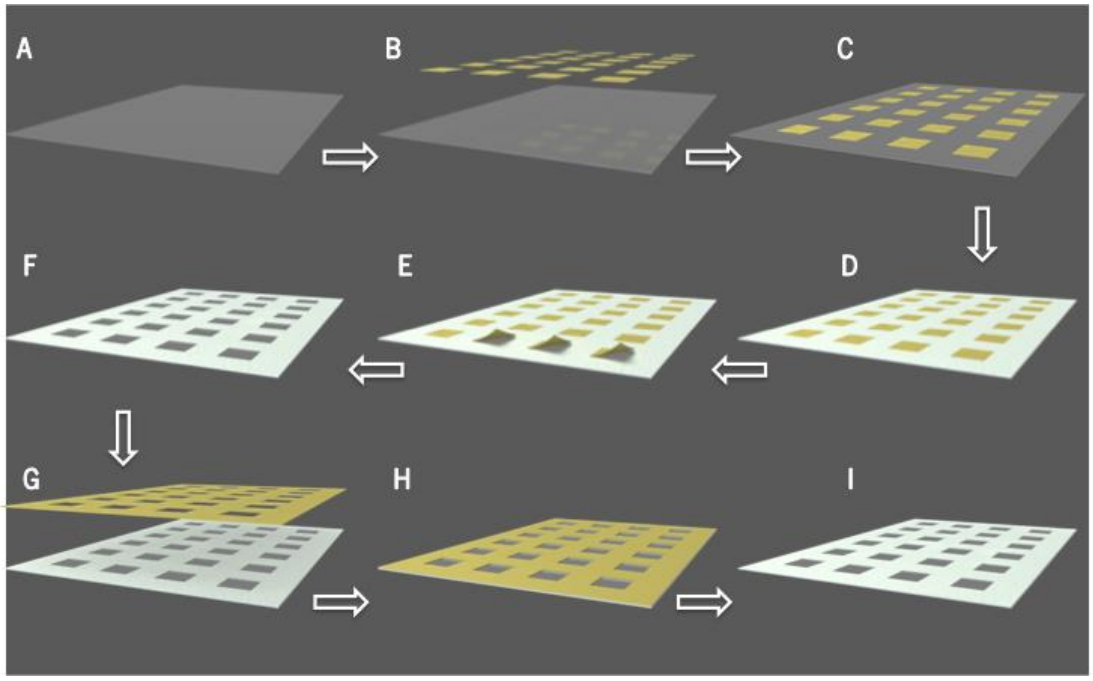

Figure 2.3 Schematic representation of the production of wettable patterns on polystyrene (PS) superhydrophobic surfaces using phase-separation technique.

Protocol III

1. Cut small portions from commercially available smooth polystyrene (PS) sheets (Figure 2.3 A).
2. Glue polyvinyl chloride (PVC) stickers (Oracal, USA) into smooth PS surface in the form of an array of 4 mm^2 squares separated by 2 mm (Figure 2.3 B-C). See Note 5.

[5] *In such applications, stickers of PVC were cut from an A4 sheet in a typography service using a computer numerical control laser-cutting machine in the shape of the wettable spot.*

3. Modify the PS surfaces containing square-shaped stickers according to Protocol I.

4. Dispense a necessary volume of the mixture solution to cover the clean PS substrate (Figure 2.3 D). After several seconds in air, immerse the substrate, containing with the mixture solution, in ethanol for 1 min in order to force the polymer precipitation, leading to the formation of a rough and porous topography at both the nano- and microscale levels. Dry the surfaces at ambient temperature.

5. Remove the stickers from the surfaces (Figure 2.3 E). The protected regions remain untreated and, consequently, wettable and transparent (Figure 2.3 F).

6. Prior material deposition, expose only the wettable polystyrene spots, using a mask with square holes (Figure 2.3 G-H)) to UV-ozone irradiation (procleaner 220, BioForce Nanoscience), in order to modify chemically the spots incorporating negative charged groups (Figure 2.3 I.)

The fact that the stickers allow having transparent spots after their removal improved the compatibility of the SH patterned chips the production of multilayer films, as observed in Chapter 5.

2.1.1.3 Superhydrophobic DropletMicroarray

DropletMicroarray (DMA) platform exploits the extreme contrast in wettability between SL and SH areas, which lead to a spontaneous formation of an array of separated micro-droplets when a water droplet is rolled on a SL-SH surface (Figure 2.4). Each microdroplet can serve as a reservoir for performing an individual experiment with biomaterials, drugs or cells. Using a rolling droplet method, the facile droplet formation does not require manual pipetting or a liquid handling device.

In this Chapter 8, we show the application of the DMA for the preparation of a high-density array of hydrogel particles encapsulating live cells, which can be used for high-throughput screening of cells in three dimensional (3D) microenvironments.

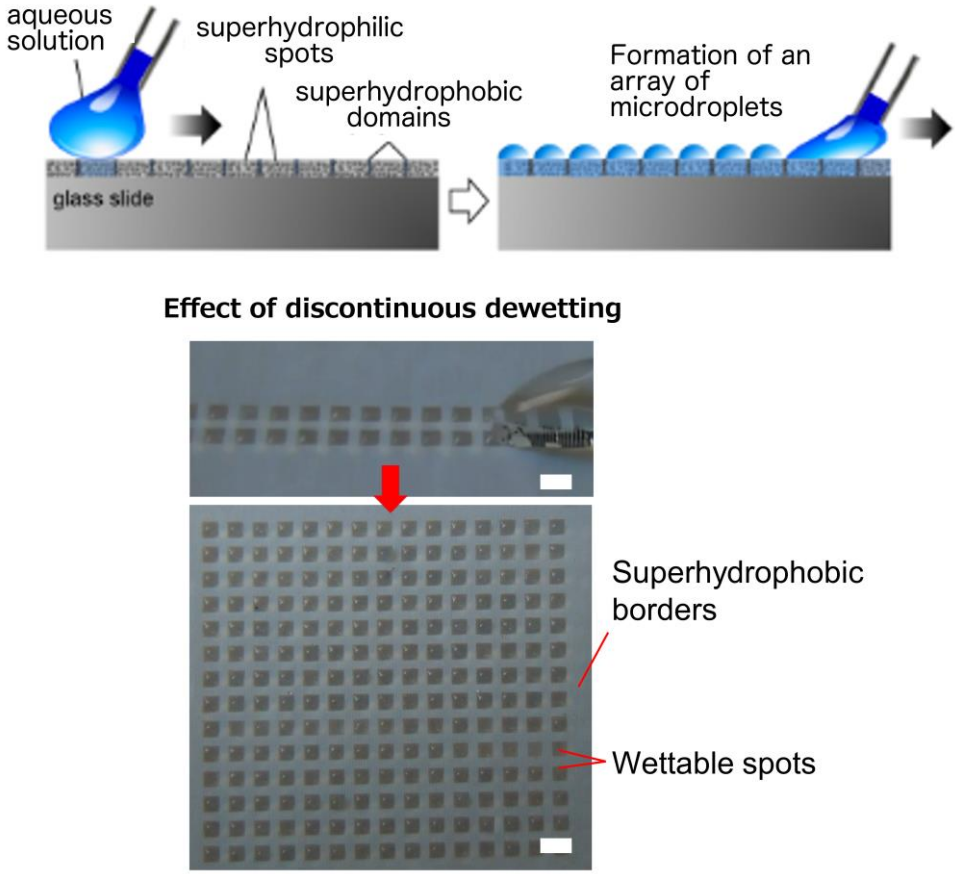

Figure 2.4 Formation of a DropletMicrorray (DMA) using the rolling droplet method. Schematic of a SL, nanoporous polymer layer grafted with SH moieties. When an aqueous solution is rolled along the surface, the extreme wettability contrast of SL spots on a SH background leads to the spontaneous formation of a high density array of completely separated microdroplets. Upper-view photographs of water being rolled along a SL-SH patterned surface with 1 mm square to form droplets only in the SL areas. Figure adapted from [12].

The patterned surfaces were prepared on a glass support by in situ UV-initiated free radical polymerization of HEMA-EDMA (*Protocol II*), followed by the generation of the SH-SL domains using the *Protocol IV*.

Protocol IV

Superhydrophobic pattern:

1. Dilute 1H,1H,2H,2H-Perfluorodecanethiol (Sigma-Aldrich, Cat. #660493) in acetone (5% v/v).
2. In a dark room, pipette 200 μL of the perfluorodecanethiol solution on the alkyne substrate, cover it with a photomask, and transfer everything under the UV lamp. Irradiate with 260 nm UV light at 12 mW/cm^2 for 1 min.
3. Before exposure to light, wash the substrate with acetone in the dark room and then wash the substrate again with acetone and dry it with an air gun.

Superhydrophilic spots:

1. Dissolve 10% v/v of 2-mercaptoethanol (Alfa Aesar, Cat. #A15890) in a 1:1 water:ethanol solution.

2. Pipette 200 µL of the hydrophilic thiol solution on the substrate and cover it with a fluorinated quartz slide. Irradiate with 260 nm UV light at 12 mW/cm^2 for 1 min. Wash the substrate with ethanol and dry it with an air gun.

Many of the materials used in this thesis – both polymeric constituents and reactives – were either purchased or obtained by biological processes. The detailed specifications of the suppliers can be found in the experimental subsections of each Chapter of Section III. Likewise, equipment suppliers are also discriminated in those subsections.

2.1.2 Polysaccharides

2.1.2.1 Chitosan

The use of marine resources is commonly considered inexpensive and abundant, with great interest to develop biological and biomedical applications. Chitosan (CHT) is derived from chitin, which is a natural polysaccharide composed of randomly distributed β-(1-4)-linked D-glucosamine (deacetylated unit) and N-acetyl-D-glucosamine (acetylated unit), abundantly occurring in shrimp´s shells. CHT is obtained by removing sufficient acetyl groups (CH_3-CO-) for the molecule (chitin) to be soluble in most diluted acids (Figure 2.5). This process, called deacetylation, releases amine groups (NH_2) and gives the CHT a cationic characteristic at lower pH. Conventionally, the compound is called "CHT" when the degree of deacetylation of chitin reaches about 50% [13]. CHT undergoes a conformational transition in solution around a pH value of 6. Its amine groups, as is characteristic of polybases, are protonated at pH below the pKa and deprotonated at higher pH values [14]. CHT is non-toxic, biodegradable and has an excellent biocompatibility. So, CHT is a great candidate for a series of biomedical applications [15-17].

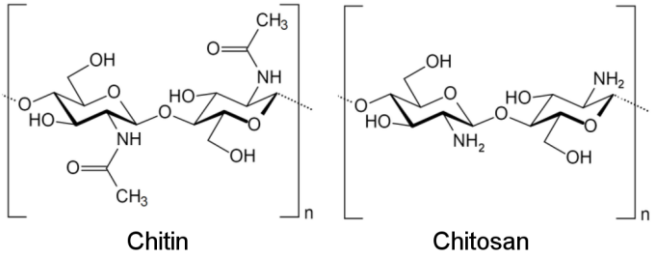

Figure 2.5 Chemical structures of CHTtin and Chitosan. Figure adapted from [18].

In Chapters 3 and 5, CHT with N-deacetylation degree of 80% and a molecular weight obtained by viscosimetry of 770 kDa was purchased from Sigma, and purified afterwards. The solution was filtered using Whatman® ashless filters, with a cutoff of 20-25 µm, so the insoluble materials remained in the

filter. Multilayer films were produced using CHT in the form of a cationic polymer, by dissolution of CHT in 1% acetic acid, with a pH 5.5 to yield a final concentration of 0.5 $mg.mL^{-1}$.

In Chapter 6, the formation of CHT hydrogels were developed on SH platforms following the crosslinking reaction of CHT with genipin, a natural crosslinking agent of CHT. Water-soluble highly purified Chitosan, CHT (Protasan UP CL 213, viscosity 107 mPa.s, molecular weight Mw = 2.7x105 $g.mol^{-1}$, 83% degree of deacetylation) was purchased from NovaMatrix. CHT was dissolved in distilled water at concentrations of 0.1 $mg.mL^{-1}$, 1 $mg.mL^{-1}$, 5 $mg.mL^{-1}$, 7.5 $mg.mL^{-1}$ and 10 $mg.mL^{-1}$. After the addition of distinct concentrations of genipin, a dark-blue coloration appeared in the formed hydrogels due to the reaction between the amino groups of CHT and genipin [19].

2.1.2.2 Alginate

Alginate (ALG) is a natural polysaccharide extracted from brown seaweed [20]. ALG is a linear anionic copolymer composed of two monomers: β-D-mannuronic acid, α-L-guluronic. It can be obtained from the cellular wall, accounting for up to 45% of the dry weight of these seaweeds. ALG has stimuli-responsiveness toward pH. The carboxylic acid groups from the guluronate and mannuronate monomers can be deprotonated above pH values of 3.2 and 4, respectively. Thus, alginate behaves as polyacid and exhibits polyanionic behavior above these pKa values [21]. ALG and also CHT, which share a marine origin, both show biocompatibility, adhesiveness, non-toxicity. These properties make of these polysaccharides suitable constituents for multilayer formulations that resort to natural materials [22]. ALG was used as a multilayer constituent, in Chapter 5. Alginic acid sodium salt from brown algae was purchased from Fluka (ref. 71238, molecular weight 100-200 kDa). ALG was dissolved in in 0.15M of NaCl solution, with a pH 5.5 to yield a final concentration of 0.5 mg.mL-1.

ALG also become an extremely important because of their utility in preparing hydrogels at mild pH and temperature conditions, suitable for sensitive biomolecules like proteins and nucleic acids, and even for living cells such as islets of Langerhans [23]. In Chapter 8, ALG was processed as an ionic hydrogel, crosslinked with calcium chloride. Hydrogels are hydrophilic polymer networks, which may absorb from 10 – 20% (an arbitrary lower limit) up to thousands of times their dry weight in water [24, 25]. Hydrogels may be chemically stable or they may degrade and eventually disintegrate and dissolve. Calcium alginate is an example of this type of hydrogel. Thus, when polyelectrolytes of opposite charges are mixed, they may gel or precipitate depending on their concentrations, the ionic strength, and pH of the solution [20].

2.1.2.3 Hyaluronic acid

HA is a polysaccharide that can be found in tissues and body fluids of vertebrates and also in some bacteria [26]. It is a linear polymer and a naturally occurring non-sulfated glucosaminoglycan composed of D-N-acetylglucosamine and D-glucuronic acid [27, 28]. As an integral component of extracellular matrix [29], HA is an attractive building block for new biocompatible and biodegradable materials that can be used for drug delivery and tissue engineering [30, 31].

In Chapters 3 and 5, HA-hyaluronic acid sodium salt from Streptococcus equi - was purchased from Sigma (ref. 53747, molecular weight of 595 kDa), and was used as a multilayer constituent and to produce two conjugated biopolymers- see next sub-section. For multilayer films construction, HA was dissolved in in 0.15M of NaCl solution, with a pH 5.5 to yield a final concentration of 0.5 $mg.mL^{-1}$.

2.1.3 Synthesis of dopamine-modified hyaluronic acid

Dopamine-modified hyaluronic acid (HA-DN) is a synthetic catecholamine polymer inspired by mussel adhesive proteins (MAPs). It is known that MAPs found in marine mussels form outstandingly moisture-resistant adhesive bonds capable of surviving to the destructive conditions of the ocean. Such proteins provide contain considerable concentrations of an unusual amino acid, 3,4-dihydroxy-L-phenylalanine (DOPA), which is formed by postranslational modification of tyrosine. A key aspect of DOPA and its analog dopamine (DN) is the ortho-dihydroxyphenyl (catechol) functional group, which forms strong bonds with various inorganic/organic surfaces [32-34]. For the purpose of constructing LbL-based systems in Chapters 3 and 6, HA-DN was synthesized, according to Protocol V, based on the procedure proposed by Lee and co-workers [35]- see Figure 2.6.

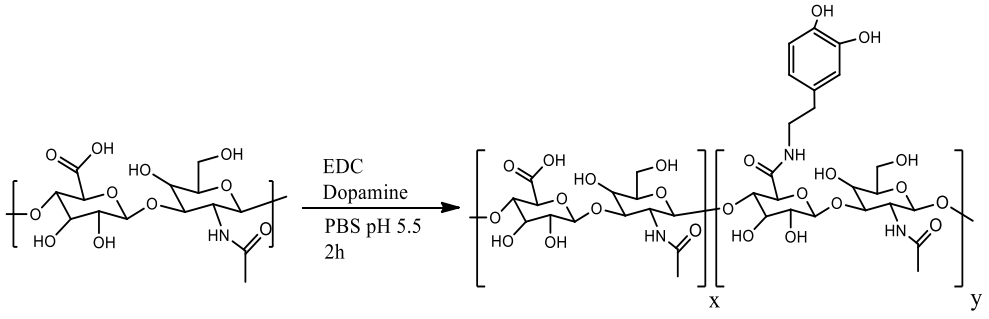

Figure 2.6 Synthesis and chemical structure of HA-DN

Protocol V

1. HA solution (transparent): 1 g of HA (Hyaluronic acid sodium salt from Streptococcus equi (HA), molecular weight (MW) of 595 kDa, Sigma) in 100 mL of phosphate buffered saline (PBS, sterile) solution. Adjusted pH to 5.5 of HA solution with hydrochloric acid (HCl) aqueous solution.
2. Purge HA solution with nitrogen for 30 minutes, using low pressure. (See Note 6)
3. HA-DN solution (transparent): 338 mg of EDC (N-(3-Dimethylaminopropyl)-N'-ethylcarbodiimide hydrochloride, MW of 191.70 $g.mol^{-1}$, Sigma-Aldrich) and 474 mg of DN (Dopamine hydrochloride, Light sensitive, MW of 189.64 $g.mol^{-1}$, Sigma-Aldrich) in HA solution during 2 hours. Maintain the pH at 5.5. (See Note 7)
4. Remove the unreacted chemicals and urea byproducts by extensive dialysis (during 3-4 days), and afterwards, freeze-dry the conjugate (usually one week). For the storage see Note 8.
5. Calculate the degree of substitution of dopamine in the conjugate using three different techniques: Ultraviolet (UV) spectrophotometry and proton nuclear magnetic resonance (H-NMR) and carbon-13 nuclear magnetic resonance (C-NMR).
6. For the UV analysis, prepare different concentrations of DN solution, ranging 0.05 mM to 1 mM in distillated water.
7. For ^{1}H-NMR and ^{13}C-NMR analyses, dissolve DN in deuterated water (D2O) for 24 hours at final concentrations of 1 $mg.mL^{-1}$ and 10 $mg.mL^{-1}$. The final spectra are obtained at 298 K and 300 MHz for ^{1}H-NMR analysis and 333 K and 75.4 MHz for 13C-NMR analysis.

In Chapter 5, to bring more insights upon catechol substitution, two conjugated biopolymers based on DN-modified hyaluronic acid (HA-DN and HA-4DN), that differ in the amount of DN conjugated, the later having a fourfold excess of the dopamine used in the reaction. Thus, 338 of EDC and 1896 mg of DN were dissolved in HA solution during 2 hours. The pH was maintained at 5.5.

2.2 Characterization of the materials

2.2.1 Degree of substitution of dopamine

After the synthesis of HA-DN, which was used in the experimental work of Chapters 3 and 5, it was necessary to determine the precise degree of substitution dopamine in conjugate solution. For that

---

[6] *Controlling oxygen in a viscous solution can be achieved by bubbling nitrogen gas through it. HA solution should be placed inside a flasks or tube (falcon tube) that can be closed with a lid. This can be performed using a nitrogen supply, and a flask containing a rubber stopper with a hole in it and an open-ended pasteur pipette enabling a bubble nitrogen goes into the solution to purge oxygen.*

[7] *It is important to prepare the conjugate solutions protected from the light and at 4°C chamber/room in order to avoid dopamine oxidation. During the preparation, the DN and EDC should be added and stirred in HA solution using a very slow rotation.*

[8] *After the freeze-dryer, the white-color conjugated is obtained, and should be store in the freezer (-20 °C) protected for the light, in order to avoid dopamine oxidation.*

purpose, hydrogen-1 nuclear magnetic resonance and carbon-13 nuclear magnetic resonance (^{1}H-NMR and ^{13}C-NMR) spectra were recorded for a sample of HA-DN. NMR is a common technique used to determine the structure of unknown organic structures, by applying a nuclear magnetic resonance with respect to hydrogen-1 nuclei within the molecules of a substance. Among other things, it allows determining the number of protons in a molecule, different types of hydrogen atoms (e.g., protons bonded to carbon atoms that are attached to different functional groups), and the number of "neighbor" hydrogen atoms a proton has [36]. Thus, dopamine and un-modified hyaluronic acid and the produced conjugate were dissolved in deuterated water (D_2O) for 24 hours at final concentrations of 1 mg.mL^{-1} and 10 mg.mL^{-1}. An aliquot of this solution was placed in a 5 mm NMR tube and the spectrum recorded at 60 °C. The final spectra of ^{1}H-NMR analysis was obtained at 298 K and 300 MHz. It is known that the new N-H linkage formed in the conjugate could not be detected by 1H-NMR as this conjugate is only soluble in water and in this solvent the NH linkage interchange with water so no new signal appears. In order to overcome this limitation, the conjugate was also analyzed by ^{13}C-NMR and the final spectra were obtained at 333 K and 75.4 MHz.

Ultraviolet visible spectrophotometry was also used to confirm if the modification of hyaluronic acid with catechol groups was successful, measuring the absorbance between 200 and 400 nm. UV-Visible spectrophotometry involves measuring the amount of ultraviolet or visible radiation absorbed by a substance in solution.

In Chapters 3 and 5, with the purpose to calculate the degree of dopamine substitution, the absorbance of distinct solutions of dopamine (ranging concentrations of 0.05 mM to 1 mM) was measured. It was noticed that an excitation band appears at approximately 280 nm. The real degree of dopamine substitution in each case was obtained by following the UV excitation band centered at 280 nm and upon comparison with a standard curve obtained for distinct concentrations of free dopamine in solution (Figure 2.7).

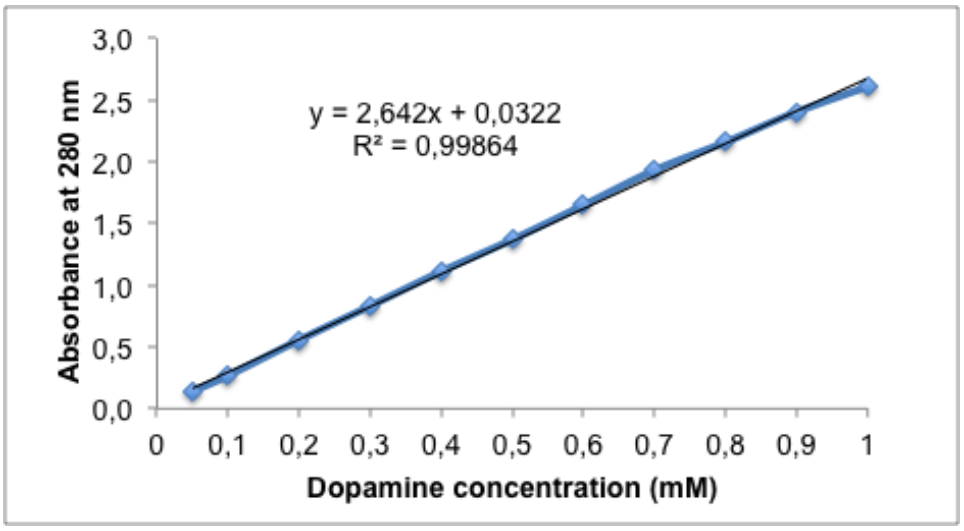

Figure 2.7 Calibration curve obtained from different concentrations of dopamine at 280 nm.

The "R^2" obtained from the trend line of the calibration curve, known as the coefficient of determination (in multiple linear regression) is explained by the relationship with one or more predictor variables. R^2 is always between 0 and 100%.

Using the measured absorbance of the conjugates and the equation obtained from the standard curve, the concentration of dopamine units in both conjugates was 11% and 15% for HA-DN and HA-4DN, respectively.

2.2.2 Assessment of LbL films growth

2.2.2.1 In situ monitoring

In order to determine if a set of ingredients can be used to construct multilayer films and coatings, a quartz-crystal microbalance with dissipation monitoring (QCM-D, Q-Sense, E4 system) was used in Chapters 3 and 5, a technique that is able to detect adsorbed surface density changes in the order of ng.cm^{-2} and measure the viscoelastic properties of the resulting surface in real time. QCM allows the in situ formation of the multilayers films and the measurement of the changes in the resonant frequency and in the viscoelastic properties (dissipation) when a film is adsorbed at the crystal surface. In this technique, a sensor is composed of a thin AT-cut quartz disk sandwiched between a pair of electrodes. Quartz allows exploiting the piezoelectric which makes it possible to convert an electric AC voltage across its electrodes into mechanical motion, exciting the quartz to oscillation at a fundamental frequency of 5 MHz. Therefore, the use of quartz sensors for QCM requires the use of gold sensor crystals (most frequently used) that are coated by the electrode material. An AT-cut quartz crystal can be excited at its fundamental frequency (5 MHz) and at several overtones: 1, 3, 5, 7, 9, 11 and 13, corresponding

respectively to 5, 15, 25, 35, 45, 55 and 65 MHz, although different overtones can be monitored, depending on the equipment's supplier. When a thin film is deposited onto the sensor crystal the frequency decreases. If the film is thin and rigid, the decrease in frequency (Δf) is proportional to the mass of the film. However, when using polymers, the adsorbed film is not rigid and this relation is not valid. At the same time, monitoring of dissipation (ΔD) gives an indirect indication of the film's viscoelastic properties. An increase in ΔD represents a shift towards a film with a higher viscous component and damping properties typical of "soft" polymeric LbL films. The dissipation values for a soft film are higher due to increased energy loss from the crystal, whereas smaller dissipation values are obtained for a rigid film [37-40]. The adsorption of polymeric layers was studied onto gold-coated quartz crystals, cleaned with acetone, absolute ethanol and 2-propanol prior to the experiments. The quartz crystals were excited at multiple overtones: 1, 3, 5, 7, 9, 11 and 13. For all monitoring experiments, adsorption took place at 25 °C. Once the selection of functional polymers was done, the progress of LbL assembly was monitored by QCM-D, as shown in Table 2.1.

Table 2. 1 Polyelectrolytes used on the build-up of multilayer films using QCM

Polycation	Chitosan (CHT)
Polyanions	Dopamine-modified hyaluronic acid (HA-DN)
	Dopamine-modified hyaluronic acid (HA-4DN)
	Hyaluronic acid (HA) - negative control
	Alginate (ALG) – negative control

In situ formation of LbL films containing 10 layers of CHT/HA-DN and CHT/HA was investigated in Chapter 3, and CHT/HA-4DN, CHT/HA-DN, CHT/HA CHT/ALG was investigated in Chapter 5, following the Protocol VI.

Protocol VI

1. Prepare fresh polyelectrolyte solutions of HA-4DN, HA-DN, HA, and ALG in 0.15 M of NaCl solution and CHT in 1% acetic acid, with a pH 5.5 to yield a final concentration of 0.5 mg.mL^{-1}. See Note 9.

[9] *Since layer-by-layer development is based on the adsorption of polyelectrolytes with oppositely charged macromolecules, it is important to ensure that the selected polymers retain their positive or negative charge. HA is a negatively charged polyelctrolyte above its pKa (≈ 2.9). CHT is a positively charged polyelectrolyte in acidic medium, with a pKa ≈ 6.24. However, at pH 7 the amine groups on CHT deprotonate since its pKa is approx. 6.2 preventing the interaction of Chitosan with anionic components. In order to construct multilayer films, the pH of the polyelectrolyte solutions should be adjusted to 5.5.*

2. Start the experiment with a washing solution (NaCl) baseline, to ensure that the crystals are perfectly clean and therefore show a null frequency.

3. Inject polyelectrolyte solutions into the cell during 10 minutes at a flow rate of 100 μL.min^{-1} using a peristaltic pump, beginning with a polycation, CHT.

4. Include a rinsing step of 10 minutes with the solvent between the adsorptions of each polyelectrolyte.

5. During the entire process, the normalized frequency ($\Delta f/\upsilon$) and dissipation (ΔD) shifts are continuously recorded as a function of time.

6. Produce films with 10 layers. (See Note 10)

2.2.2.2 Estimation of films´ thickness

The Voigt-based viscoelastic model, which is integrated into the QTools software from Q-Sense (supplier of the equipment) was used to estimate the thickness of the films from the QCM-D monitoring data. The changes in the resonant frequency (equation 1) and in the dissipation factor (equation 2) according to Voinova and co-workers [41] are:

$$\Delta f \approx -\frac{1}{2\pi\rho_0 h_0}\left\{\frac{\eta_B}{\delta_B} + h_L\rho_L\omega - 2h_L\left(\frac{\eta_B}{\delta_B}\right)^2\frac{\eta_L\omega^2}{\mu_L^2+\omega^2\eta_L^2}\right\} \quad (1)$$

$$\Delta D \approx -\frac{1}{\pi_f\rho_0 h_0}\left\{\frac{\eta_B}{\delta_B} + 2h_L\left(\frac{\eta_B}{\delta_B}\right)^2\frac{\eta_L\omega}{\mu_L^2+\omega^2\eta_L^2}\right\} \quad (2)$$

The angular frequency of the oscillation is represented by ω and ρ0 and h0 are the density and thickness of the crystal, respectively. The viscosity of the bulk liquid is ηB, δB (= 2 (ηB / ρB ω)1/2) is the viscous penetration depth of the shear wave in the bulk liquid and ρB is the liquid´s density. The thickness, density, viscosity and elastic shear modulus of the adsorbed layer are represented by hL, ρL, ηL and μL respectively. Iterations of the model were performed using at least three overtones. The model requires three parameters, namely solvent density, solvent viscosity and film density, to be fixed. The solvent viscosity repeat as desired was therefore fixed at 0.001 Pa·s (same as water) and the film density at 1200 kg.m^{-3} (often assumed to return the lowest calculation error). The area density, a rough approximation of the mass adsorbed on top of a gold-coated quartz sensor was calculated by multiplying the thickness by the films density (1200 kg.m^{-3}).

[10] *In cell studies it is highly recommended that all the solutions used are non-cytotoxic to ensure cell viability. Since CHT is soluble in diluted acid solutions, the last solution added on the build-up of the multilayer films is always the polyanion solution (HA-DN), in order to produce surfaces with improved adhesive properties and an enhanced biological performance. CHT-HA and CHT-ALG multilayer films were used as negative control.*

2.2.3 Assembly of the multilayer films

After determining if a set of constituents provided a favorable multilayer construction, they were reproduced outside of the QCM-D. Multilayer films based on the diverse polymeric materials used herein were constructed by dipping alternately glass substrates (Chapter 3) or into patterned superhydrophobic chips (Chapter 5).

2.2.3.1 In planar surface

In similarity to most metallic alloys, glass is negatively charged, and thus provided support for the formation of a multilayer coating by adsorbing CHT as a polycation primer layer [42]. Films consisting of CHT/HA-DN and CHT/ HA (negative control) were produced in parallel under the same experimental conditions. Commercial glass from a local store were acquired and cut into 100×20 mm^2 slides with 3 mm of thickness and cleaned using absolute ethanol. The construction was assisted by an in-house developed dipping robot that allowed the automated assembly of each layer in a programmed manner. The construction proceeded until 20 layers (10 bilayers) were adsorbed, as the following Protocol:

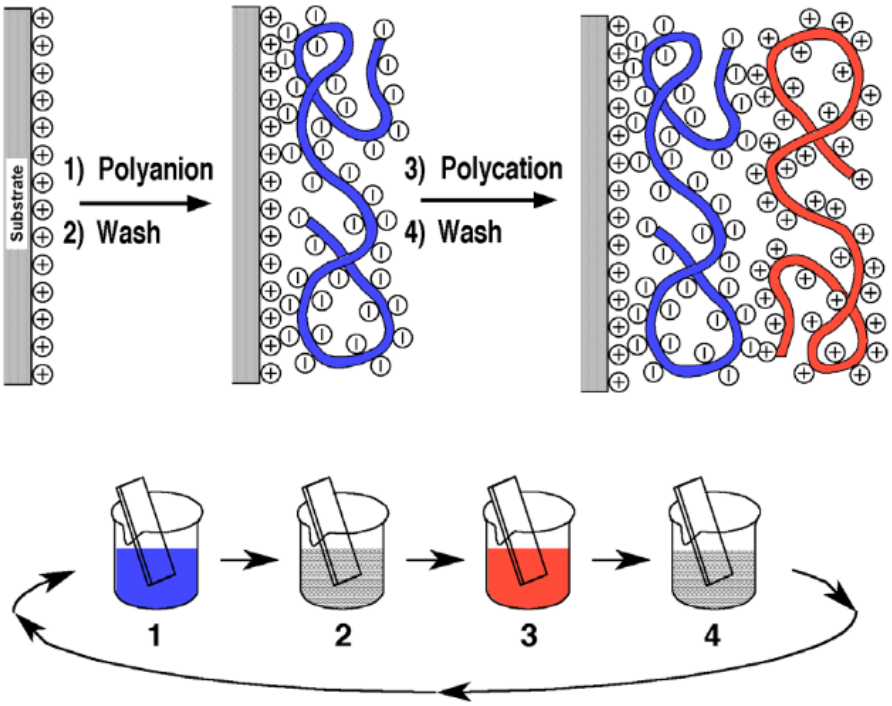

Figure 2.8 Schematic representation of LbL adsorption on the top glass slides. Figure adapted from [43].

Protocol VII

1. Prepare fresh polyelectrolyte solutions of HA-DN and HA in 0.15 M of NaCl solution and CHT in 1% acetic acid, with a pH 5.5 to yield a final concentration of 0.5 $mg.mL^{-1}$.

2. Adjust the pH of the solutions to 5.5, using HCl or NaOH solutions.

3. Immerse the glass slide in polycation solution, CHT, and subsequently, in polyanion solutions, HA-DN and HA. Set the time of immersion for 10 min at room temperature. (See scheme of the Figure 2.8)

4. Between each polyelectrolyte immersion; wash the glass slide with the washing solution (0.15 M NaCl solution) for 5 min to remove excess non-absorbed macromolecules.

5. Repeat this process ten times to obtain a film with 10 bi-layered.

6. Washed the films until a neutral pH was achieved, in order to perform the mechanical tests at the same pH as the biological tests.

7. Sodium periodate ($NaIO_4$) Solution: 5mM of NaIO4 (Sodium periodate Sigma-Aldrich, ref. 311448)) in distillated water to yield concentration of 5nM.

8. Coat glass plaques with oxidized films. Immerse the glass slides in a 5 mM sodium periodate solution during 2 hours, after the procedure previously described.

9. Polydopamine solution: DN in 10 mM tris-HCl (Tris (hydroxymethyl) aminomethane, Sigma-Aldrich, ref. 252859) with pH 8.5 to a yield final concentration of 2 $mg.mL^{-1}$.

10. Polydopamine coating: Immerse the glass slides into a dopamine solution (2 $mg.mL^{-1}$ in 10 mM tris-HCl, pH 8.5) at 25 °C, overnight. (See Note 11)

11. Rinse the coated surfaces with ultrapure water and dried at room temperature.

2.2.3.2 In patterned microarray substrate

In Chapter 5, distinct combinations of nanostructured films were produced using LbL methodology in a single microarray chip. Flat biomimetic superhydrophobic patterned chips produced by a bench-top methodology were used for the build- up of arrays of multilayer films – see *Protocol III*. The extreme wettability contrasts imprinted onto the chips allow the production of individual, position controlled, and multilayer films in the wettable regions. In each SL spot, sequentially deposition of droplets with different polyelectrolytes, combined with washing solutions, were performed to assemble the multilayers (Figure 2.9). Using the experiment set-up described in *Protocol VIII*, an array of 48 spots, combining 5, 10, or 15 bilayers prepared from a library of five polyelectrolytes (four distinct pairs), was designed with four replicates per combination to obtain statistical information.

Protocol VIII

1. Prepare patterned SH surfaces, according to the Protocol III.

2. Prepare fresh polyelectrolyte solutions of HA-4DN, HA-DN, HA, and ALG in 0.15 M of NaCl solution and CHT in 1% acetic acid, with a pH 5.5 to yield a final concentration of 0.5 mg.mL-1.

[11] *Increasing the pH of dopamine solution to 8.5, the oxidation is induced, and the solution color changes to dark brown.*

3. Construct the multilayer films in the wettable spots of the patterned SH surfaces:

4. Pipette, alternately, droplets of 5 µL of the polyelectrolyte solutions during 10 min, beginning with CHT (Figure 2.9 A-B).

5. Remove the droplets using a pipette, and then, rinse the spots with droplets of 0.15 M NaCl solution during 5 min. A rising step should be included between the adsorptions of each polyelectrolyte.

6. Produce films with 5, 10, and 15 bilayers onto the wettable spots of the SH surface (Figure 2.9 C).

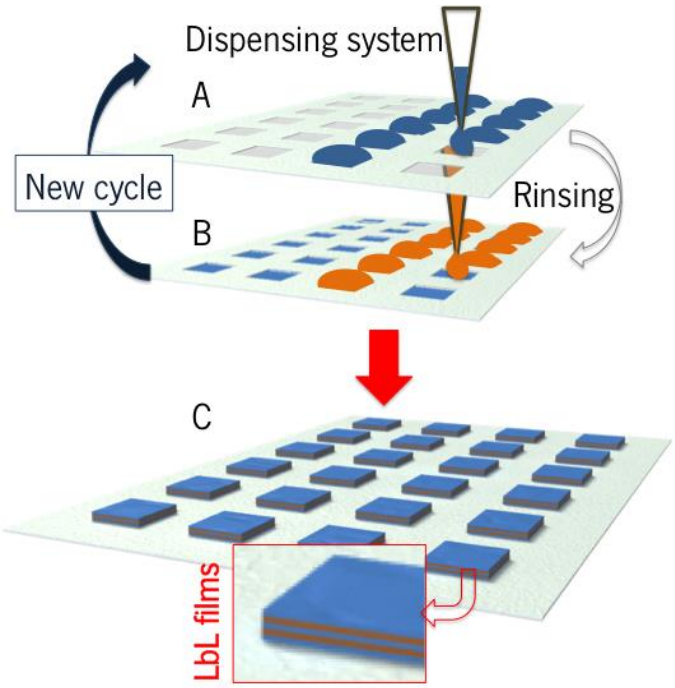

Figure 2.9 Schematic dispensing of A) polycation solution and B) polyanion solution in the wettable spots surrounded by SH domains. C) Build-up of layer-by-layer films using different cycles of polyelectrolytes solutions.

2.2.4 Surface characterization

Many characterization techniques were specific for each of the materials used: superhydrophobic surfaces and multilayer films.

2.2.4.1 Surface topography

Atomic force microscopy (AFM) is an excellent tool to study morphology and texture of diverse surfaces. The versatility of this technique allows meticulous observations and evaluations of the textural and morphological characteristics of the films, showing better facilities than other microscopic methods.

AFM measurements were performed in LbL-coated glass slides cut into pieces of 1×1 cm^2, in Chapter 3, and directly on patterned SH platform in Chapter 5. This technique is a synthesis of the mechanical profilometer, using mechanical springs to sense forces, and the scanning tunneling microscopy (STM),

using piezoelectric transducers for scanning. In force microscopy, a probing tip is attached to a cantilever-type spring. In response to the force between tip and sample, the cantilever is deflected. This deflection is then translated into a visual image [36]

The amplitude parameters of a sample are described by parameters, which give information about statistical average values, shape of the histogram heights and other extreme properties. In Chapters 3 and 5, the surface topography of the dried multilayer films were analyzed by AFM and the root mean square (Rq) and average roughness (Ra) were measured. Ra is the mean height as calculated over the entire measured length/area. Ra is typically used to describe the roughness of maCHTned surfaces. It is useful for detecting general variations in overall profile height characteristics and for monitoring an established manufacturing process. Rq is a function that takes the square of the measures. The Rq roughness of a surface is similar to the Ra, with the only difference being the mean squared absolute values of surface roughness profile. The function Rq is defined as:

$$Rq = \sqrt{\frac{1}{L}\int_0^L |Z^2(x)|dx} \qquad (3)$$

The Rq is more sensitive to peaks and valleys than the average roughness due to the squaring of the amplitude in its calculation [44].

AFM measurements were performed in a MultiMode STM microscope controlled by the NanoScope III from Digital Instruments system, operating in tapping mode at a frequency of 1 Hz. At least five measurements were performed in the different sample, which had been previously air-dried. When a multilayer film is rough, viscous and/or thick, AFM may not be appropriate technique to scan its topography. In these cases, scanning electron microscopy (SEM), a technique that allows observing the surface of an object by bombarding it with an electron beam, presents itself as a viable alternative.

2.2.4.2 Surface morphology

Scanning electron microscopy (SEM) is a type of electron microscope that produces images of a sample by scanning it with a focused beam of electrons. The electrons interact with atoms in the sample, producing various signals that can be detected and that contain information about the sample's surface topography and composition. When accelerated electrons enter a solid, they are scattered both elastically (by electrostatic interaction with atomic nuclei) and inelastically (by interaction with atomic electrons). Most of this interaction is “forward” scattering, which implies deflection angles of less than 90°. But a small fraction of the primaries are elastically backscattered ($\theta > 90°$) with only small fractional loss of energy. Due to their high kinetic energy, these backscattered electrons have a reasonable probability of

leaving the specimen and re-entering the surrounding vacuum, in which case they can be collected as a backscattered-electron signal. Inelastic scattering involves relatively small scattering angles and so contributes little to the backscattered signal. However, it reduces the kinetic energy of the primary electrons until they are eventually brought to rest and absorbed into the solid; in a metal specimen they could become conduction electrons. The depth (below the surface) at which this occurs is called the penetration depth or the electron range [39].

SEM was used in Chapters 3,4,5,6 and 7 of this thesis to evaluate the topography of different surfaces. Before each analysis, the surfaces were gradually dehydrated using solutions with increasing amounts of ethanol (50%, 70%, 80%, 95% and 100%), immersing the surfaces for 10 minutes in each solution - See Note 12. Due to their non-conductive behavior, the surfaces were coated with a thin, electrically deposited gold palladium layer, to minimize charge accumulation using a sputter coater (JEOL JFC-1100). The surface morphology of the multilayer films (Chapters 3 and 5), polystyrene SH surface (Chapters 4, 6 and 7) and cells spheroid arrangement (Chapter 7) was observed using a Leica Cambridge S-360 scanning electron microscope. The SEM micrographs were taken at an accelerating voltage of 15 kV and at different magnifications.

2.2.4.3 Water contact angle measurements

Material characteristics, such as roughness and chemistry define the wettability of the surfaces. In terms of topography, the existence of micro/nano-roughness significantly affects the wettability properties of the materials, since they increase the water contact angle (WCA) in low-energy surfaces and decrease it in high-energy surfaces. The contact angle of a liquid drop on a solid surface is the angle at which a liquid/vapor interface meets a solid surface. Surfaces with high energy typically exhibit a low contact angle, whereas hydrophobic surfaces exhibit low surface energy [37]. It is defined by the mechanical equilibrium of the drop under the action of three interfacial tensions and allows quantifying the wettability of a solid surface by a liquid via the Young equation:

$$\cos\theta_y = \frac{\gamma sv - \gamma sl}{\gamma lv} \qquad (4)$$

where θ is the contact angle in the Young's mode, and γsv (liquid-vapor), γsl (solid-vapor) and γlv (solid-liquid) are the different surface tensions involved in the system. The Young model (Figure 2.10 A)

[12] *In Chapter 7 after the spheroid formation, 5 μL of 10% formalin was dispensed to the droplets.to fix the cells for 2 hours and subsequent washing with PBS. Then, the spheroids were dehydrated with a series of increasing ethanol concentrations.*

describes the contact between a sessile drop onto rigid, homogeneous, flat and inert surfaces – ideal smooth surfaces.

of

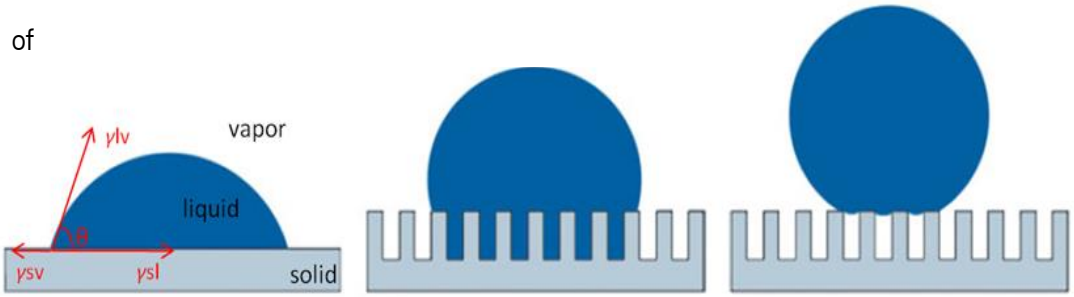

Figure 2.10 Typical wetting behavior of a droplet on rough solid substrates. Developed mathematical models could explain the droplet-surface interaction: A) the Young's model relates the contact angle to interfacial tensions (energies, γ) in an ideal smooth surface; B) Wenzel´s models and C) Cassie-Baxter, have in consideration the effect of surface roughness. Figure adapted from [45].

SH surfaces present imperfections related to physical defects such as roughness. The static contact angle lies between two values: advanced angle (θ_A) and receding angle (θ_R). The difference advanced and receding angles ($\theta_A - \theta_R$) is called hysteresis. In this case, the force is opposed to droplet motion and the contact angle hysteresis (CAH) is smaller enabling a better move of liquid droplet. Empirical models, known as, Wenzel [46] and Cassie-Baxter [47] models, have been proposed in order to rationalize the effect of roughness and surface energy.

There are two types of non-wettable surfaces differing in their adhesive properties. If the CAH is higher than 10°, the water droplet stay preferentially adhered onto the surface - Figure 2.10 B. Otherwise, if the CAH is less than 10°, the surface is non-adhesive, and the water droplet rolls off the surface at a minimum inclination- Figure 2.10 C. In high-adhesive surfaces (Wenzel state), present a larger pitch leading the liquid to impregnate partially within the nanostructures [48]. Wenzel's model proposed an equation for predicting the influence of the surface roughness or morphology on the WCA. The area of the drops of solid-liquid interface is enlarged by a factor r (surface roughness factor), and the apparent WCA on the rough surface (θ_w).

$$\cos\theta_w = r\cos\theta_y \qquad (5)$$

The surface roughness factor is defined as the relationship between real surface and apparent surface (r >1 for rough surface and r=1 for smooth surface). From equation 5, it can be found that if the WCA of a liquid on a smooth surface is less than 90°, the apparent angle on a rough surface will be smaller; while for a WCA higher than 90°, the angle on a rough surface will be larger and the hydrophobic surface will become more hydrophobic with increasing degree of roughness. The energy of liquid droplet is minimized

when remaining on the top of a rough surface and not when penetrates in the asperities and therefore the Wenzel law is valid only for one certain scale of roughness and for apparent angles lower than 180°. The drop sticks to the surface and the Wenzel state contrasts the superhydrophobicity idea, i.e. the rolling ball effect, proposed by the equation of Cassie –Baxter model:

$$\cos\theta_{CB} = rf\cos\theta_0 + f - 1 \qquad (6)$$

In the case of non-adhesive SH surfaces (Cassie-Baxter state) the existence of a hierarchical morphology from the nano- to the micro-scale leads to minimal contact between the liquid and the surface. The water dispensed onto this type of surfaces acquires an almost spherical shape in order to minimize the energy, being suspended on the top of the micro- and nano-structures that compose the surface, and at minimal inclinations the droplets roll off [49].

The wettability of the multilayer films (Chapters 3 and 5) and polystyrene SH surface (Chapters 4, 6 and 7) was assessed by contact angle measurements. Static WCA measurements were carried out using an OCA15+ goniometer (DataPhysics, Germany) using the sessile drop method. Distilled or ultra pure water (3 μL) was dropped on the surfaces and pictures were taken after stabilization of the water drop. At least five measurements were carried out. In Chapter 5, for each multilayer film construction, an array of 15 combinations, containing 5, 10, and 15 bilayers of the same biomaterials is designed (five replicates per combination were used). During the WCA experiment, ultrapure water droplets are used with volume of 3 μL. This volume was small enough so that the droplets could occupy an area lower than the area of the multilayers in the spots. At least five measurements were carried out for each sample. In Chapter 6 the adhesion of droplets with different volumes in the micro-indentations with different sizes of the SH surfaces were also studied: the sliding WCA of droplets with different volumes was analyzed in each micro-indentations by sloping SH surfaces until 90°.

2.2.4.4 Adhesiveness of the multilayer films

The adhesion properties of the multilayer films using glass slide and patterned SH platform were evaluated using a universal mechanical testing machine (Instron model 5540, USA), following the ASTM D1002 standard.

In planar surfaces

In Chapter 3, the adhesiveness of CHT/HA-DN multilayer films and respective control CHT/HA was studied measuring the lap shear adhesive strength between two individual films. This technique

determines the force that causes an adhesive to slide on a surface in the direction parallel to the plan of contact, as depicted in Figure 2.11.

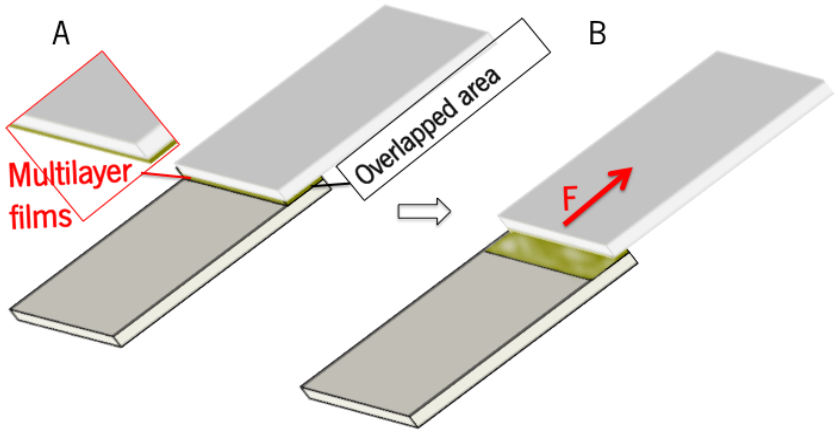

Figure 2.11 Experimental set-up for the measurement of the lap shear adhesive strength of the overlapped multilayer films.

As soon as the construction of the multilayer films was concluded, the adhesion test was performed using the next *Protocol.*

Protocol X

1. Prepare fresh polyelectrolyte solutions of HA-DN, and HA in 0.15 M of NaCl solution and CHT in 1% acetic acid, with a pH 5.5 to yield a final concentration of 0.5 $mg.mL^{-1}$.
2. Prepare glass plaques coated with oxidized films, immersing the glass plaques containing the multilayer films (previously prepared) in 5 mM sodium periodate solution during 2 hours.
3. Prepare glass plaques with a polydopamine coating, according to the procedure described by Lee H. et al. [50], immersing the glass slides into a dopamine solution overnight- see Note 13. Then, rinse the coated surfaces with ultrapure water and dried at room temperature.
4. As soon as the construction of the films is concluded, put in contact a pair of coated glass slides and superimpose covered areas with 10 x 20 mm^2 at 40 °C, overnight (Figure 2.11 A) - see Note 14.
5. Place the bonded glass slides in testing machine fixed by one binder grip in each extremity, and employ a crosshead speed of 5 mm/min. Apply the enough stress until trigger their detachment and pull the glass slides apart. Determine the lap shear bonding strength from the maximum of the force–deformation curve (Figure 2.11 B). Perform the test at least using five samples.

In patterned microarray substrate

[13] *Increasing the pH of dopamine solution to 8.5, the oxidation is induced, and the solution color changes to dark brown.*

[14] *To promote better adhesion, a weight of 6 kg was applied perpendicularly to the joint area and after a curing time of 24 of, the weight was removed.*

Methods for screening adhesiveness rely on the measurement of either tensile or shear strengths. The first test usually uses perpendicular forces necessary to separate two surfaces in contact, while the second determines the force that causes an adhesive to slide on a surface in direction parallel to the plane of contact (described in the sub-section before). In Chapter 5, tensile strengths were chosen and measured for multilayer films with 5, 10, and 15 bilayers built-up in the wettable spots of the SH chip. The flat configuration of the CHT allows to perform a series of non-destructive and non-conventional measurements directly on the individual spots. In situ adhesion properties were directly measured in each spot. For this, an innovative method described in *Protocol XI* was developed using iron pillars. The surface base of the pillars containing the same size and shape of the spots, were put in contact with the top of the multilayer films - see Figure 2.12.

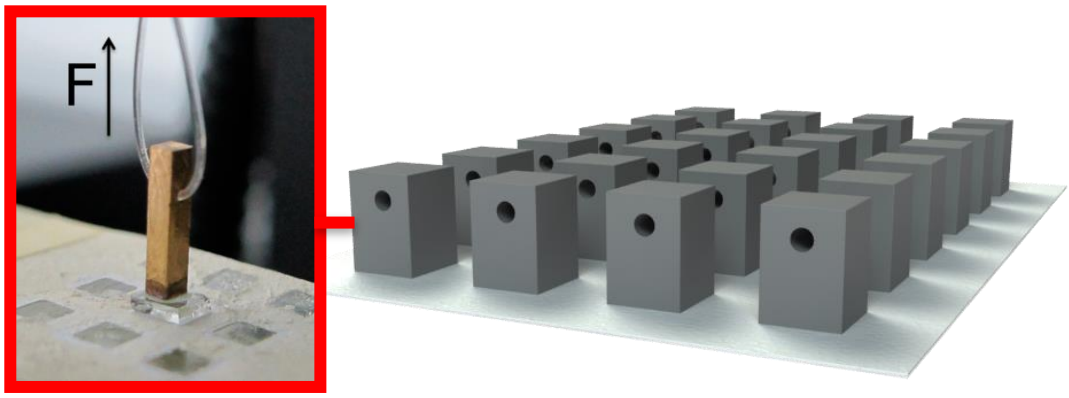

Figure 2.12 Experimental set-up of the on-chip measurement of the adhesive strength between the multilayer films produced over the wettable regions of the SH microarray and the iron pillars.

Protocol XI

1. Prepare fresh polyelectrolyte solutions of HA-4DN, HA-DN, HA, and ALG in 0.15 M of NaCl solution and CHT in 1% acetic acid, with a pH 5.5 to yield a final concentration of 0.5 $mg.mL^{-1}$.
2. Prepare patterned SH surfaces, according to the Protocol III.
3. Construct the multilayer films with 5, 10, and 15 bi-layers onto the wettable spots of the SH chip according to Protocol VIII. For each multilayer film construction, prepare an array of 15 combinations, containing 5, 10, and 15 bi-layers of the same biomaterials (use five replicates per combination).
4. Glue small glasses (3 mm square-size) on the surface base of the iron pillars. (See Note 15)
5. Put the iron pillars in contact with the multilayer films and superimpose and maintain at 40 °C overnight.

[15] *The small glasses glued on the iron pillars are used to guarantee that the whole nanofilm created is in contact and adhered in the smooth glass surface. All iron pillars had a hole on the top, where a "fishing wire" was passed by, in order to pull the pillars. The pillar could be made of other materials or the base could be from any other substance.*

6. Place the bonded multilayer films and the pillars on the testing machine and perform the tensile tests individually using a crosshead speed of 5 $mm.min^{-1}$ until the total detachment from the base of the chip is achieved - see scheme in Figure 2.12.

7. Determine the lap shear bonding strength from the maximum of the force-deformation curve obtained, as well as the average and standard deviations using the results from five samples.

2.3 On-chip alginate hydrogel particles production

In Chapter 8, DropletMicroarray platform was used for high-throughput fabrication of free-standing hydrogel particles with defined geometry and size for 3D cell culture, cell screenings and modular tissue engineering. The extreme wettability contrast of SL spots on a SH background allowed spontaneous separation of an aqueous solution, leading to the formation of arrays of droplets of pre-hydrogel solutions on SL patterns using the process of discontinuous dewetting, followed by their gelation via the parallel addition of $CaCl_2$ to the individual droplets via the sandwching method. This rapid and facile droplet formation does not require manual pipetting or a liquid handling device. The preparation of a high density array of hydrogel microparticles is described in the following *Protocol.*

Protocol XII

1. Dissolve 2% w/v of ALG in 0.15 M of NaCl. Adjust the pH of the ALG solution to 7.
2. Produce hydrogel particles using patterned DMA by a sandwich method.
3. Prepare Slide 1 using rolling droplet method: Rolling a drop of 1M $CaCl_2$, in which liquid solution fills only the DMA slide's wettable areas.
4. Prepare Slide 2 using the standing droplet technique: Place a droplet of 1 mL of ALG solution on the top of a patterned array followed by slightly tilting the slide, thus enabling droplets to from spontaneously.

Sandwich method

1. Place the Slide 1 on a manual x,y linear stage PKT 130 (Owis GmbH, Staufen, Germany) mounted on a bottom plate.

2. Place Slide 2 on the top place, so that its pre-printed pattern matched the geometry of the CaCl2 slide.

3. Use a goniometer TP 65 (Owis GmbH, Staufen, Germany) to co-planar the surfaces to enable the droplets' homogeneous diffusion.

4. Use a UI-5490-SE camera (IDS Imaging Development Systems GmbH, Obersulm, Germany), to monitor the sandwiching process in real time and align both patterned slides.

5. After few seconds in contact, separate the patterned slides from each other and an array of hydrogel particles is obtained on the bottom glass slide. (See Note 16)

Hydrogels on-chip

6. Use the described procedure to produce immediately an array of hydrogel particles that remain fixed within the DMA even when the slide is immersed in liquid solution (Figure 2.13 A)

Free-standing hydrogel particles

7. Move the Slide 1 slide to the top of the device (Figure 2.13 B) and use the same sandwich method procedure. Immerse the array of hydrogel particles in liquid solution (buffer or cell culture medium) to detach the hydrogels from the DMA platform.

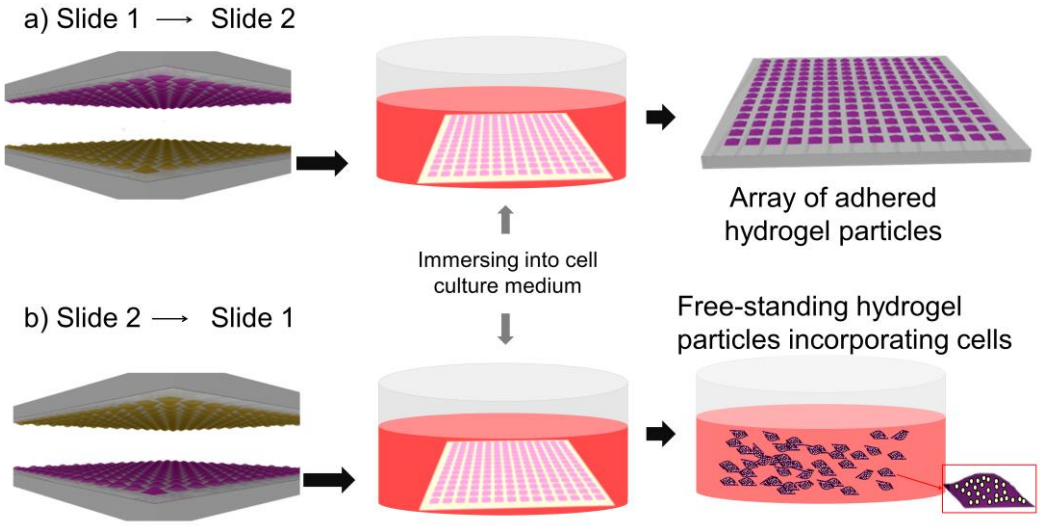

Figure 2.13 Schematic representation of the DMA platform and workflow for the high-throughput fabrication of hydrogel particles via the sandwiching method.

For the precise alignment and sandwiching of $CaCl_2$ and alginate slides, mount both surfaces on a vacuum clamping system to ensure proper handling.

2.4 *In vitro* studies on patterned superhydrophobic surfaces

Many of strategies to study combinatorial biomaterial interactions as well as cell-materials and cell-cell interactions represented an advance in the development of devices for high-throughput screening. However, some needs for the Tissue Engineering field remained still to accomplish. With the use of polystyrene SH surfaces patterned with micro-indentations, a series of works in which a method that does not involve complicated processing or expensive equipments or materials is proposed in Chapter 4. In

[16] *The vacuum clamping system enabled fast and reproducible handling, allowing for highly coplanar removal of the upper glass slide and preventing the* risk of cross contamination between droplets.

order to show the suitability of the developed platform distinct in vitro experiments were performed using such patterned SH surfaces, including:

a) The efficacy of the mechanical agitation tested in a simple physical process, namely, the dissolution of salt crystals inside the droplets;

b) The monitoring of a chemical reaction, namely the crosslinking of CHT with genipin with different concentrations of reagents;

c) The evaluation of cell viability, in this case tested when cells are in contact with culture media at different pHs, and;

d) The evaluation of the cytotoxicity of an antitumor drug at different concentrations in cell spheroids.

For the last example, in Chapter 7, taking advantage of the high positional stability and adhesiveness of the quasi-spherical droplets even when the platform is inverted 180°, the production of 3D cell spheroids was explored. The applicability of this hanging droplet approach is described in the following sub-sections of 3D cell culture.

2.4.1 Preparation of microreactor based on patterned SH surfaces

In Chapter 4, the ability to fix with high stability arrays of controlled volumes of droplets, with minimum contact with the SH surfaces, was shown to be useful in the design of innovative robust droplet-based micro-reactors. Droplets were fixed in defined positions by the action of micro-indentations patterned with an array arrangement on polystyrene SH surfaces. A droplet-based micro-reactor was proposed using magnetic microspheres, enabling to create mechanical stresses inside the microliter-size droplets.

Thus, droplets with and without magnetic microparticles were firstly deposited on a patterned SH surface. Cooper sulphate crystal ($CuSO_4$) crystals were introduced inside the individual droplets, at time 0, and the platform was placed over a magnetic stirrer. The dissolution of the crystal was monitored by following with time the size of the crystal (h) comparing with its initial size (h_0). The agitation power was easily controlled in the magnetic stirrer open the applicability in many high throughput biochemical and biological studies at a lab-on-chip scale. Further details are described in *Protocol XIII.*

Protocol XIII

1. Produce micro-indentations with 190 μm of size in the SH surface using an indentation force of 2942 mN- see Figure 2.2.
2. Pipette 10 μL of water droplet containing magnetic microspheres over a micro-indented SH surface using a micro-dispenser.

3. Apply to the droplet suspension a magnetic field by placing a magnetic stirrer (Fisher Scientific) with variable speed below the SH surface.

4. Start the experience with an increasing speed until 100 rpm allowing that the magnetic microspheres form chain-like structure under the influence of the imposed magnetic field.

5. Incorporate a CuSO4 into the droplet.

6. Imaging: Use a Stereo Microscope + Lamp Schott KL 200 (model Stemi 1000 PG-HITEC, Zeiss) with 2.5X magnification, equipped with a digital camera with 5X optical zoom.

2.4.2 Chemically Crosslinked Hydrogels

Genipin is known as natural crosslinking agent with low cytotoxicity. Genipin reacts promptly with Chitosan, as well as with proteins or amines in general, as a bi-functional crosslinking compound, thus producing blue-colored fluorescent hydrogels. On the right side of the Figure 2.14, two Chitosan chains (represented by their structural units) react covalently with one mole of genipin to yield two newly formed chemical functions.

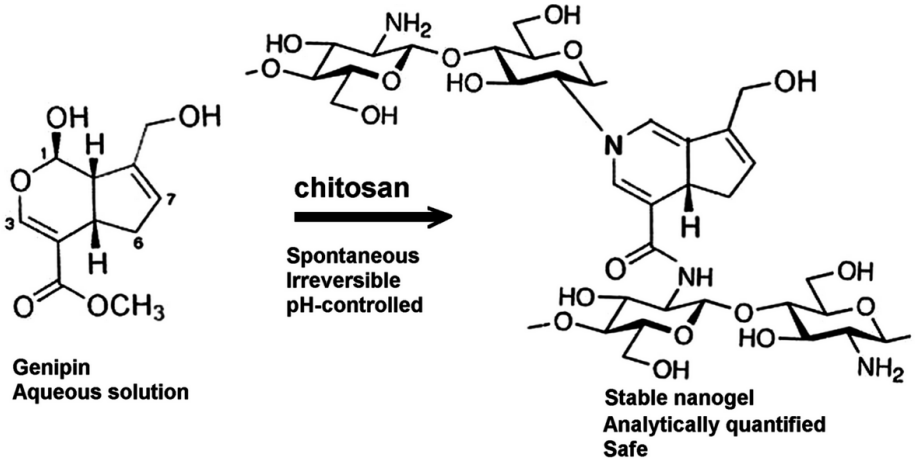

Figure 2.14 Crosslinking reaction mechanism between Chitosan and genipin. Figure adapted from [51].

The reaction between Chitosan and genipin is well understood for a variety of experimental conditions with no cytotoxicity for human and animal cells [52], with vast applicability on the preparation of hydrogels for cartilage substitutes, delivery systems and the encapsulation of biological products [19, 53-55].

In Chapter 6, the crosslinking reaction of CHT with genipin was analyzed, using a combinatorial approach. For this purpose, in situ formation of hydrogels on microarray platform was evaluated starting with the deposition of combinations of liquid precursors in the form of droplets. Different droplet solutions containing different relative amounts of CHT and genipin were deposited in the micro-indentations of the

SH surface. The experiment was performed at 40°C under saturated humidity to avoid droplets evaporation. CHT decomposition during heating has been widely established and the rate and degree of the polymer damage was found to accelerate with rising temperature and duration of heating [56]. The dark-blue coloration that appears in the hydrogels is associated with the oxygen radical-induced polymerization of genipin as well as its reaction with amino groups. Independent calibration experiments by reacting known amounts of glycine and genipin permitted to produce standard curves relating the intensity of the blue-color of the droplets and the extent of the reaction of the amine groups. The experiment was based on *Protocol XIV.*

Protocol XIV

1. Produce micro-indentations with 190 μm of size in the SH surface using an indentation force of 2942 mN.
2. CHT Solutions: Dissolve CHT in 1% v/v of acetic acid at concentrations of 0.1 $mg.mL^{-1}$, 1 $mg.mL^{-1}$, 5 $mg.mL^{-1}$, 7.5 $mg.mL^{-1}$ and 10 $mg.mL^{-1}$.
3. Genipin solution: Genipin (Wako chemical, ref. 078-03021) in pure water (0.15 NaCl, pH 5.5) mixture to a final concentration of 1 $mg.mL^{-1}$, 5 $mg.mL^{-1}$, 7.5 $mg.mL^{-1}$and 10 $mg.mL^{-1}$.
4. Dispense 10 μL of each polymeric solution over the micro-indentations with 190 μm size in a drop-by-drop logic. Each droplet separated by 5 mm, represents a different combination of CHT and genipin. (See Note 17)
5. Place the SH chips in a desiccator with saturated humidity at 40 °C.
6. Each 30 minutes, capture images of the chip until one of the conditions being completely crosslinked, confirmed by the unchanging of the color intensity (dark-blue coloration).
7. Calibration curve: Prepare different quantities of soluble glycine, ranging 0.2 to 2 $mg.mL^{-1}$, including genipin at a concentration of 10 $mg.mL^{-1}$.
8. Analysis: Measure the pixel intensity from each glycine concentration over a total of 6 samples. Use the intensity of the pixels, grey scale 0-255, in which 0 correspond to dark color and 255 white color, to associate the color intensity of the solutions. Correlate the intensity color of the droplets of CHT with genipin with the pixels intensity of the standard curve. Calculate the percentage of reacted amine groups in each droplet dividing the number of reacted amino molecules of the repeating unit of CHT obtained by the calibration curve by the initial number of amine molecules.

2.4.3 Combinatorial analysis of fibroblasts-like cells on patterned SH surfaces

The variations of the pH of cell microenvironment can denature proteins or activate enzymes that normally are inactive around neutral pH. In Chapter 6, a combinatorial analysis of fibroblasts-like cells on patterned

[17] *Chitosan and genipin were mixed using the same quantity of the different concentrations leading to 20 different combinations. CHT solutions with the same concentrations without genipin were used as control.*

SH surfaces was performed when cells are in contact with culture media at different pHs. Thus, cells were re-suspended in culture medium with different pHs (pH ranging from 1-14) adjusted with HCl and NaOH solutions. Droplets of 5 μL with $1x10^3$ cells were seeded in the micro-indentations of patterned SH surfaces. Specimens were incubated at different times (5, 30, 60, 90 and 120 minutes) at 37°C in a humidified 5% CO_2 atmosphere.

2.4.3.1 Drug screening tests

Doxorubicin is an anti-cancer agent, widely used in human cancer chemotherapy that inhibits RNA and DNA synthesis [57]. This drug induces an alternative cell death mechanism to apoptosis. Doxorubicin intercalates between base pairs in the DNA helix, thereby preventing DNA replication and ultimately inhibiting protein synthesis. Additionally, doxorubicin inhibits topoisomerase II that results in an increased and stabilized cleavable enzyme-DNA linked complex during DNA replication and subsequently prevents the ligation of the nucleotide strand after double-strand breakage. Doxorubicin also forms oxygen free radicals resulting in cytotoxicity secondary to lipid peroxidation of cell membrane lipids; the formation of oxygen free radicals also contributes to the toxicity of the anthracycline antibiotics, namely the cardiac and cutaneous vascular effects [58].

In Chapter 6 and 7, different amounts of doxorubicin were introduced in the droplets to assess the dose-dependent response of the formed tumour spheroids to this anticancer drug. After 48 hours of cell culture for spheroid formation, a volume of 2 μL of doxorubicin (Doxorubicin hydrochloride, Sigma-Aldrich) with different concentrations (0.1 $mg.mL^{-1}$, 0.01 $mg.mL^{-1}$ and 0.001 $mg.mL^{-1}$) was dispensed in the different droplets. After 24h of incubation time at 37°C in a humidified 5% CO2 atmosphere, live/dead images from fluorescence microscopy showed a high resistance from L929 cells to these drug concentrations. The same procedure was performed to 2D cell culture.

2.5 In vitro studies on 3D hydrogels produced using superhydrophobic surfaces

2.5.1 Magnetic hydrogel particles (cell co-culture)

Using the *Protocol IV* to produce droplet microarray platform, free-standing hydrogels can be loaded with functional magnetic or other nanoparticles to enable the use of magnetic field for the remote manipulation of the hydrogels. In Chapter 8, magnetic hydrogel particles were produced following the *Protocol XII.* This method allowed the culturing of different types of cells inside hydrogel particles with different shapes. HeLa cells expressing GFP cells (green) were immobilized in circle-shaped free-standing hydrogels and

MLIy-mCherry cells (expressing fluorescent red) were immobilized in squared-shaped free-standing hydrogels, following *Protocol XIV.*

Protocol XIV

1. Prepare magnetic bead solution to a final concentration of 10 mg.mL^{-1} and then centrifuged at 4000 rpm and 25°C for 10 minutes.
2. Remove the liquid and add 2% w/v alginate solution.
3. Prepare two different solutions of magnetic beads containing alginate: in the first solution, add red fluorescent rat mammary carcinoma MLIy-CMV-mCherry-neo, and for the second solution add green fluorescent HeLa-GFP.
4. Encapsulate green fluorescent cells inside alginate hydrogel particles prepared in 3 x 3 mm circular DMA, using Protocol IV.
5. Encapsulate red fluorescent cells were encapsulated inside alginate hydrogel particles prepared in 3 x 3 square-sized DMA, using Protocol IV.
6. Immerse hydrogels of different geometries with distinct cell types in the same culture medium.

2.5.2 Drug uptake on hydrogel particles

Dexamethasone, a synthetic glucocorticoid, is a potent steroid that is used to treat a variety of disorders. The ability of this agent to reduce the edema associated with the spread of malignant tumors form other organs to the brain led to therapeutic trials for high-altitude cerebral edema [56]. The rate of drug release by diffusion through the polymer matrix normally decreases with time, since the agent has a progressively longer distance to travel and therefore requires a longer diffusion time to release. The correct drug administration is often dependent on tailored delivery mechanisms from hydrogel or other polymeric matrices. The standard methods for the in vitro monitoring of molecules release are resource spending and laborious. As a simplifying alternative to these methods, in Chapter 8 is shown the ability to remotely compress hydrogel particle assemblies and the stimuli-responsive release of a small molecule drug incorporated inside the hydrogel using an external magnetic field as the stimulus.

The dexamethasone uptake study on alginate free-standing hydrogel particles was evaluated using *Protocol XV*.

Protocol XV

1. Prepare magnetic bead solution to a final concentration of 10 mg.mL^{-1} and then centrifuged at 4000 rpm and 25°C for 10 minutes.
2. Remove the liquid and add 2% w/v alginate added.

3. Add 10 µL of dexamethasone solution with 1 mL of prepared alginate solution with a final drug concentration of 25 µg/mL.

4. Prepare magnetic hydrogel particles containing dexamethasone (n=40, 5 µL of each hydrogel particles) in 3 x 3 mm circular DMA slide.

5. Prepare bulk alginate hydrogels (negative control) in falcon tube using 100 µL of 1M of CaCl2 solution and 100 µL of 2 % w/v alginate solution containing magnetic beads and dexamethasone solution.

6. Immerse magnetic hydrogel particles and bulk hydrogel in 10 mL of pure water solution up to 240 minutes at room temperature.

7. Read the absorbance of both formulations at 241 nm over time, with and without the application of external magnetic field.

2.5.2 Modular building blocks

An increase attention has been devoted to modular tissue engineering. This approach aim to address the challenge of recreating biomimetic structures by designing structural features on the microscale to build modular tissues that can be used as building blocks to create larger tissues. In Chapter 8, DMA platform was also used to form magnetic hydrogel particles incorporating live cells. These particles can be employed for the modular tissue engineering due to the possibility to manipulate both single particles and particles assemblies using external magnetic field. The ability to easily create and manipulate hydrogel particles of controlled size and geometry is essential for 3D cell studies and modular tissue engineering. Thus, magnetic hydrogel particles with 3 mm of diameter (n=250) were placed in glass vial (5 mL) and the assembly of hydrogels was carried out using a stereo microscope. By applying 50 times an external magnetic field, the length of the modular tissue assembly was further measured using ImageJ program.

2.6 In vitro biological studies

2.6.1 Cell expansion and culture conditions

The biological response of cells to biomaterials in vitro is critical to estimate if a harmful reaction is triggered upon contact of a newly developed system with a living organism, common when biomedical applications are envisaged. Herein, cells were either seeded onto a substrate modified with multilayers, or as 3D cell spheroid or even seeded onto a cell culture support and incubated in the culture medium.

In Chapters 3 and 5, mouse lung fibroblastic cell line (L929) and human primary osteosarcoma cell line (SaOs-2), from European Collection of cell Cultures (ECA CC, UK) were used to study the adhesion, viability and proliferation of the cells on the multilayer films.

In Chapters 6 and 7, the viability of L929 fibroblasts spheroids was evaluated.

In Chapter 8, human cervical tumor cell line (HeLa expressing GFP) was used to evaluate the viability of the cells encapsulated in hydrogel particles. Red fluorescent rat mammary carcinoma MLIy-CMV-mCherry-neo was used for cell co-culture.

All cell types were expanded and culture using the *Protocol XVI.*

Protocol XVI

1. Supplemented DMEM cell culture medium: Dubelcco's Modified Eagle Medium (DMEM) (Gibco, UK) supplemented with 10% heat- inactivated fetal bovine serum (BiochromAG, Germany) and 1% antibiotic/antimycotic solution (penicillin 100 units.mL^{-1} and streptomycin 100 mg.mL^{-1}; Gibco, UK).
2. Culture the cells with low glucose supplemented DMEM cell culture medium.
3. For cell expansion, at 90% of confluence, wash the cells grown in tissue culture flasks with sterile PBS.
4. Detach the cells by a chemical procedure with 0.05% trypsin-EDTA solution at 37 °C in a humidified air atmosphere of 5% CO_2.
5. After 5 min of incubation, add cell culture medium to inactivate the trypsin effect, and centrifuged at 1200 rpm for 5 min.
6. Discard the supernatant.

2.6.2 Cell culture on biomaterials or as cell spheroids

2.6.2.1 Cell seeding on multilayer films

In Chapter 3, samples containing multilayer films were sterilized by UV radiation for 1h. Afterwards, 30 µL of supplemented DMEM containing a cell suspension with 5×103 cells was added to a 10 bi-layered CHT/HA-DN film, the respective negative control CHT/HA, the positive control (cover glasses) and polydopamine coated cover glasses, also used as a control (in triplicate). The polydopamine coating was performed as previously described *Protocol VII.* The samples were further incubated at 37 °C in a humidified air atmosphere of 5% CO2. After 4 hours supplemented DMEM was added.

In Chapter 5 all biological characterization of the multilayer films was performed using image-based analysis directly on the chip, taking advantage of the transparency of the spots.

The biological response was evaluated on multilayer films containing distinct features, including:

a) Films ending with the negatively charged polymer without any further modification;
b) Films ended with the negatively charged polymers followed by fibronectin adsorption;
c) Positively charged CHT-ended films followed by fibronectin adsorption;
d) Positively charged CHT-ended films crosslinked with genipin.

Multilayer films consisting of CHT/HA-4DN, CHT/HA-DN, CHT/HA and CHT/ALG were composed by 5, 10 and 15 bi-layers and were built on the transparent spots of patterned SH surfaces (see *Protocol VIII*). After the multilayer films being dried, droplets of genipin and fibronectin were dispensed atop of the created films. An array of 48 combinations of biomaterials based in an initial library of five polyelectrolytes was created. The design of the patterned chip is based on the construction of four parameters of each multilayer film, containing 6 replicates of the wettable spots with the same number of multilayers deposited. Since two cell types were studied in the same chip, a total of 48 distinct conditions for the same number film layers were used (see Figure 2.15).

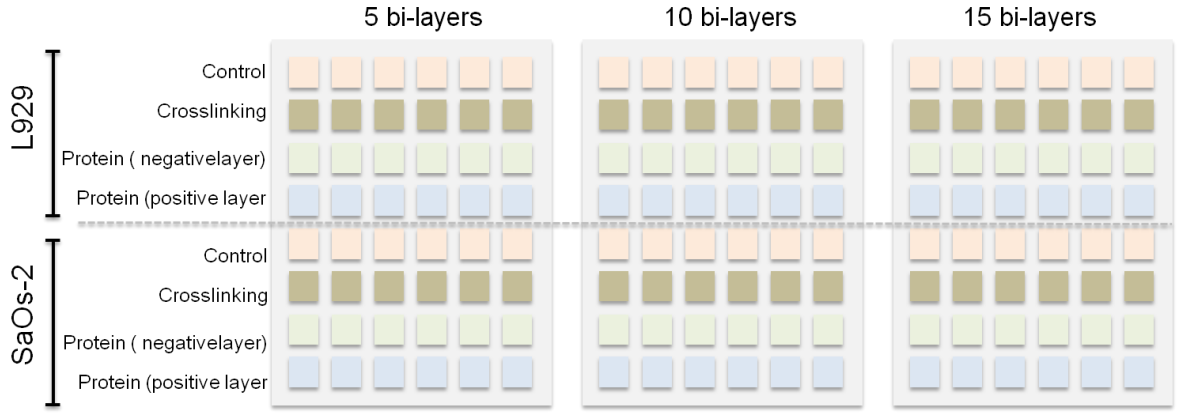

Figure 2.15 Experiment set-up for combinatorial analysis of the biological response on distinct multilayer films.

Based on previous works, genipin was used in the concentration of 1 $mg.mL^{-1}$, and the patterned slide was slide was incubated for 24 hours, in the incubator at 37°C. After 23 hours of incubation, droplets of fibronectin with a concentration of 50 µg /mL [59] were added to other spots of the same patterned chip. Afterwards the chip was again incubated for 1 hour. The coated films with 5, 10 and 15 bilayers were carefully washed, and sterilized by UV radiation for 30 minutes. Droplets of 5 µL of supplemented DMEM containing a cell suspension with 5×10^3 cells was added on the top of the coated multilayer films. Then, the samples were incubated at 37 °C in a humidified air atmosphere of 5% CO_2.

2.6.2.2 3D Hanging Droplet System

The micro-indentations produced on the SH surfaces promote the fixation of the droplets over the highly water-repellent surfaces, even when the surface and cell suspension droplets are turned upside down. Therefore, it is possible to produce an array of spheroids on SH surfaces patterned with adhesive micro-indentations using hanging droplet method- see Figure 2.16.

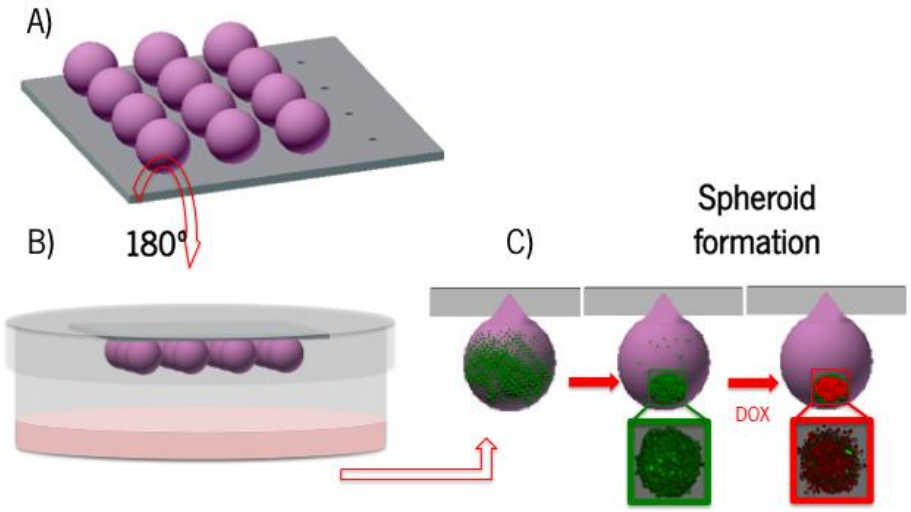

Figure 2.16 Experiment set-up of the spheroid formation. (A) Upper view scheme of the SH platform patterned with micro-indentations able to suspend arrays of droplets containing cells. (B) Turning the platform 180°, the cell suspension inside the droplet (C) leads to the formation of spheroids due to the gravitational force applied to the cells. Drug-screening tests by adding the anti-cancer drug, doxorubicin, in the droplets containing cell spheroids.

In Chapters 6 and 7, a SH platform containing droplets of cell suspension was fixed into the lids of polystyrene petri dishes (commercially available), and the bottom part was filled with cell culture media, in order to create a saturated environment and avoid the evaporation of the droplets. A volume of 5 µL of L929 cell suspension was dispensed by manual pipetting in each microindentation of the chip. The gravitational force applied on the cells in the hanged droplets induced its sedimentation and the formation of fibroblasts-like cell spheroids after 48h of seeding time. Each droplet in the chip formed a singular spheroid with a consistent cell population that is generated without the need of any scaffold or adhesive substances. In Chapter 7, the cell behavior of 3D spheroids was compared to monolayer cell culture upon being subjected to the effect of various concentrations of doxorubicin. For 2D cell culture, 1 mL of supplemented DMEM containing different cell suspensions was placed in a non-treated surface of 48-well cell plate (in triplicate). The plates were incubated at 37 °C in a humidified air atmosphere of 5% CO_2 at different incubation days.

2.6.2.3 Cell encapsulation in biomaterials

In Chapter 8 both live human cervical tumor cell line expressing GFP (HeLa-GFP) and MLTy-CMV-mCherry-neo cells expressing cherry fluorescent protein were encapsulated in hydrogels particles (crosslinking with calcium chloride, $CaCl_2$). Both cell types were mixed with 2% w/v alginate solution that was dispensed in wettable spots of the DMA platform, in a concentration of 6 x 10^5 cells per mL of alginate. This solution was then used to produce alginate hydrogels particles with the sandwich method previously described- see *Protocol XII*. Fixed and detached alginate hydrogel particles prepared in 1 x 1 mm size DMA with

HeLa expressing GFP encapsulated cells were immersed in culture medium. The detached alginate hydrogels particles prepared in 3 x 3 mm circle-sized DMA containing HeLa-GFP encapsulated cells were immersed in cell culture medium, with and without supplementation of $CaCl_2$. Bulk alginate hydrogels (negative control) with HeLa-GFP cells were prepared in 24 well-plate using 1 M of CaCl2 solution and 2 % w/v alginate solution with cells in a ratio of 1:1 and cell culture medium. Briefly, 200 µL of alginate solution containing cells was added into individual well (in triplicate) and further 200 µL CaCl2 solution was added in order to crosslink the polymer solution. Afterwards, 500 µL of cell culture medium was added on the top of bulk hydrogel. During the incubation time, the culture medium was exchanged every 2 to 3 days.

2.6.3 Cellular characterization

2.6.3.1 Cell Viability

LIVE/DEAD® assay

Cell viability was evaluated by a non-destructive live/dead assay. Live/dead Kit (LifeTechnologies, USA) is a quick and easy two-color assay to determine viability of cells in a population based on plasma membrane integrity and esterase activity. Calcein AM is a cell-permeable and non-fluorescent compound. It is hydrolyzed in live cells, and the fluorescence intensity is proportional to the amount of live cells, as it becomes fluorescent after hydrolysis of AM group. Propidium iodide (PI) stains dead cells as it enters cells with damaged membrane.

In Chapters 6 and 7, live/dead assay was assessed. Thus, 2 µL of PBS containing calcein-AM and PI was added to each spheroid at a ratio of 1:1000 and 1:500. Respectively.

In Chapter 8, hydrogel particles (n = 3 per well in triplicate) and controls (n = 3 of cells suspensions and bulk hydrogels) were incubated for 1, 3, 5 and 7 days at 37°C and in a humidified 5% of CO2 atmosphere. PI staining was performed during each time culture period. HeLa-expressing GFP cells contain a green fluorescent cell marker retained in the cytoplasm. The unviable cells lose their green fluorescence. At each time point, PI was added to each well at a ratio of 1:1000. Samples were incubated at 37°C for 10 minutes protected from the light.

2.6.3.2 Cell Metabolic activity

AlamarBlue colorimetric assay

The alamarBlue cell viability reagent is widely used to assess cell viability by simply adding the 10X, ready-to-use solution to cells in culture media. The assay incorporates a fluorometric/colorimetric growth indicator based on detection of metabolic activity. An oxidation-reduction (REDOX) indicates that both fluoresces and changes color in response to chemical reduction of growth medium resulting from cell growth. In Chapters 3 and 7, cell metabolic activity was evaluated on multilayer films and monolayer cell culture, respectively. For both experiments, alamarBlue was used using the *Protocol XVII.*

Protocol XVII

1. Multilayer films: place the samples with adhered cells in a non-treated surface 24-well cell culture plate (in triplicate) and incubated at 37 °C and 5% CO_2. Perform the assay using different time points, at 1, 3, 7, 14 and 21 days of culture, protected from light.
2. 2D cell culture: place different cells density in a treated surface 48-well cell culture plate (in triplicate) and incubated at 37 °C and 5% CO_2. After 48 hours, perform the assay protected from light.
3. Remove the culture medium of each well and add 500 µL of supplemented DMEM containing alamarBlue solution with a dilution ratio of 1:10 to each well.
4. Incubate the samples, protected from the light, at 37 °C and 5% CO_2.
5. After 3 h, transfer 100 µL of each well (in triplicate) to a 96-well plate.
6. Read the absorbance at 570 nm and 600 nm using a microplate reader (Synergy HT, Bio-TEK).

MTT viability assay

MTT assay is based on the bioreductive ability of mitochondrial dehydrogenase enzymes present in viable cells to convert the (3-(4,5-dimethylthiazol-2-yl)-2,5-diphenyltetrazolium bromide) tetrazolium (MTT) compound into a cell culture-soluble purple formazan product.

In Chapter 8, alginate hydrogel particles were tested for cytotoxicity and suitability for live cell encapsulation using a MTT colorimetric assay, according to *Protocol XVIII.*

Protocol XVIII

1. Prepare alginate hydrogel particles (circular 3 x 3 mm size DMA) encapsulating HeLa expressing GFP cells.
2. Place the hydrogel particles in a non-treated surface 24-well cell culture plate (n = 3 per well, in triplicate) and incubate at 37°C and 5% CO2.
3. Perform the assay using different time points, at 1, 3, 5 and 7 days of culture, protected from the light.

4. Remove the culture medium of each well and add 500 µL of serum-free DMEM containing MTT solution with a dilution ratio of 1:10 added to each well.

5. Re-suspend the wells containing hydrogel participles using a pipette in order to release the cells encapsulated.

6. Incubate the samples, protected from the light, at 37 °C and 5% CO_2.

7. After 3h, transfer 100 µL of each well (in triplicate) to a 96-well plate.

8. Add 100 µL of dimethyl sulfoxide (DMSO) to each well to dissolve formazan crystals, and incubated for 1h at 37°C and 5% CO_2.

9. Measure the amount of formazan product by absorbance at a wavelength of 570 nm using a multiwell spectrophotometer. (See Note 18)

2.6.3.3 Cell number quantification

DNA quantification

Quantitative double-stranded DNA is a very accurate method to assess number of cells, since these two parameters are directly correlated. Use this method to assess cell-seeding efficiency into biomaterials, as well as to determine cell proliferation. For Chapter 3, DNA quantification was performed according to *Protocol XIX*.

Protocol XIX

1. Perform DNA quantification in order to evaluate cell proliferation in the samples using the Quant-iTTM Pico-Green double-stranded DNA Assay Kit (InvitrogenTM, Molecular ProbesTM, Oregon, USA), according to the instructions of the manufacturer.

2. For each culture time, use PBS to wash the wells of the plate and then add to each well 1 mL of ultrapure sterile water. (See Note 19)

3. After transfer each solution to a 96-well white opaque plate (in triplicates), incubate the plate at room temperature protected from light.

4. Generate the standard curve for DNA analysis with provided DNA from the assay kit.

5. Read the fluorescence at excitation of 485/20 nm and emission of 528/20 nm using a microplate reader (Synergy HT, BioTek, U.S.A.).

---

[18] *The background was corrected by subtracting MTT blank solution. In Chapter 8, all these procedures took place for hydrogel particles cultured in culture medium with and without supplementation of CaCl2, bulk hydrogels, cells suspended in culture medium with and without CaCl2 supplementation, hydrogel particles with and without incorporation of magnetic beads, and cells suspended in culture medium with and without the supplementation of magnetic beads.*

[19] *In order to use the same conditions of the viability assay, and save reagent and material costs on the preparation of new multilayer films, the same samples used alamarBlue assay, can also be used for DNA quantification, if cautions during the washing with PBS are taken.*

Cell nuclei staining

Cells' nuclei were stained with 4',6-diamidino-2-phenylindole (DAPI, Sigma). DAPI is a fluorescent stain that binds strongly to A-T rich regions in DNA. DAPI stains preferentially double-stranded DNA by delineating cells nuclei in blue. DAPI has an absorption maximum at a wavelength of 358 nm and its emission maximum is at 461 nm. In Chapter 3, at each defined time culture the multilayer films seeded with L929 and SaOs-2 cells were prepared for DAPI fluorescence assay.

Protocol XX

1. Prior to staining, at each time point, remove the culture medium and add 10 % formalin to each well (in triplicate).
2. After 1 hour at room temperature, remove formalin and wash the samples with phosphate buffer saline (PBS).
3. Add 1 mL of PBS containing 1 μL of DAPI to each well.
4. After 1 hour at room temperature and protected from light, wash the samples and visualize cells´ nuclei using an Imager Z1 fluorescence microscope (Zeiss) and photographed using an Axio Cam MRm (Zeiss).

In Chapter 5, after one day in culture, the entire patterned multilayer chip seeded with L929 and SaOs-2 cells was rinsed thrice with sterile PBS and fixed with formalin. Samples were incubated in the dark with DAPI for 10 minutes (1:1000). After rinsing the samples, the nuclei were observed the same fluorescence microscope of the described protocol.

In Chapter 7, prior to staining, the culture medium was removed and 5 μL of 10% formalin was dispensed to the droplets containing spheroids. Then, 2 μL of PBS containing DAPI (1:1000) was added to each droplet.

2.6.3.4 Cell image analysis

Quantification of Chitosan crosslinking

In Chapter 6, the percentage of reacted amine groups of CHT for each combination with genipin was assessed by colorimetric assay using the WCIF Image J software. Images of the chip were captured in each 30 minutes until one of the conditions being completely crosslinked, confirmed by the unchanging of the color intensity. A standard calibration curve (logarithmic curve, r^2=0.98) of pixel color intensity vs. glycine concentration was made. Different quantities of soluble glycine, ranging 0.2 to 2 $mg.mL^{-1}$ were prepared including genipin at a concentration of 10 $mg.mL^{-1}$. The measurements of the pixel intensity from each glycine concentration were performed over a total of 6 samples. The intensity of the pixels, grey scale 0-255, in which 0 correspond to dark color and 255 white color, was used to associate the

color intensity of the solutions. The intensity color of the droplets of CHT with genipin was correlated with the pixels intensity of the standard curve. The percentage of reacted amine groups in each droplet was determined: the number of reacted amino molecules of the repeating unit of CHT obtained by the calibration curve was divided by the initial number of amine molecules.

Cell area quantification

Fluorescent images of the cell nuclei and cytoskeleton were obtained after performing DAPI-Phalloidin TRITC (tetramethylrhodamine B isothiocyanate, Sigma-Aldrich) fluorescent assay at each time culture period. Phalloidin binds F-actin with high selectivity while TRITC provides red-orange fluorescence of unparalleled brightness and photostability. Demonstrating very little nonspecific staining, Rhodamine phalloidin allows high-contrast discrimination of actin staining.

In Chapters 3, 5 and 7, cells' nuclei were stained with DAPI and in Chapters 5 and 7, F-actin was stained with phalloidin-tetramethyl rhodamine isothiocyanate, according to *Protocol XXI.* Cell number was quantified through cell nuclei counting using particle analysis of ImageJ software (NIH, USA). Cell area was calculated by particle analysis of the F-actin staining images, using ImageJ software (NIH, USA) –see Figure 2.17. Each fluorescent image was divided in red and blue channels and transformed in a gray scale (grey scale intensity 0 - 255, in which 0 correspond to black colour and 255 white colour). The total cell number was achieved counting the cells of the blue channel. The area occupied by the cytoskeleton was determined processing to binary the grey figure of the red channel. The same threshold criterion was used in all images. The histogram of the each image was analyzed, and % of the area covered by the cells was determined dividing the total number of while pixels covered by the cells with the total area analyzed.

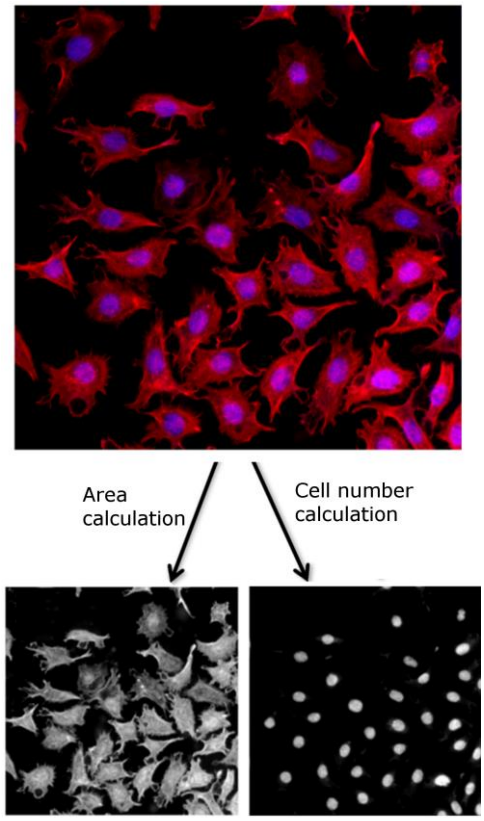

Figure 2.17 Example of an original image, where the number of cells (stained with DAPI) and cell density (% of the area covered by the cells) were quantified by ImageJ analysis.

Protocol XXI

1. Prior to cell staining, rinse the entire patterned chip thrice with sterile PBS and fix with formalin 2.5% (v/v).
2. Incubate the samples in the dark with Phalloidin-TRITC solution in PBS (ratio 1:100) for 30 min, then with DAPI in PBS for 10 min (ratio 1:1000).
3. Wash the samples (at least 3 times) with PBS and visualized in the dark using fluorescence microscopy.
4. Visualize, in the dark, the cytoskeleton and nuclei of the cells using an Imager Z1 fluorescence microscope (Zeiss) and photographed using an Axio Cam MRm (Zeiss).
5. Use WCIF ImageJ software (NIH, USA) to calculate the percentage of the area covered by the cells adhered on the multilayer films.

2.6.3.5 Cell viability and cell quantification

In Chapters 3, 5 and 7 cell quantification was performed by staining the cells nuclei with DAPI. In Chapters 3, 5 cells´ nuclei were observed using an Imager Z1 fluorescence microscope (Zeiss) and photographed using an Axio Cam MRm (Zeiss). In Chapter 7, the cells' nuclei were observed using an inverted confocal microscopy (Leica, TCS SP8). WCIF ImageJ software (NIH, USA) software was used to quantify the cells

adhered on the multilayer films (Chapters 3 and 5) and to observe total number of cells of the formed spheroids (Chapter 7).

In Chapters 6 and 7, cells stained with Calcein AM or PI in each sample were quantified using transmitted light microscopy (Axio Imager Z1m, Zeiss) and inverted confocal microscopy (Leica, TCS SP8). ImageJ was used to evaluate the percentage of live/dead cells of each droplet condition. Each image of stained spheroids obtained from confocal microscope was divided in green and red channels and transformed in a gray scale. The number in each channel (grey scale intensity 0 - 255, in which 0 correspond to black colour and 255 white colour) was counted and divided for the number of total analysed area. The same threshold criterion was used in all images.

In Chapter 8, cell mortality of ALG hydrogel particles (n = 3 per well in triplicate) and controls (n = 3 of cells suspensions and bulk hydrogels) was evaluated using PI staining. PI was added to each well at a ratio of 1:1000. Samples were incubated at 37°C for 10 minutes protected from the light. Images of the formed hydrogels were taken with the fluorescent microscope BZ-9000 Keyence (Japan) to enable accurate quantification. Double staining was obtained in Z-stack mode with a resolution of 90 µm between the slides for the hydrogel particles.

2.6.3.6 Statistical analysis

The statistical analysis analyzes significant differences between formulations. Perform using two-way analysis of variance (ANOVA) with Bonferroni post-test using GraphPad Prism 5.0 software. Adopt the follow nomenclature: statistical differences in grouped by time point analysis mark with (*), (**) and (***), which stand for p-value < 0.05; $p < 0.01$ and $p < 0.001$, respectively. All results should be presented as mean ± standard deviation.

In Chapter 3, data were grouped by formulation, namely, Control (positive control), polydopa, CHT/HA-DN, and CHT/HA (negative control), to assess time-course significant differences of each formulation. The statistical differences relating to the time point before was evaluating using symbols as # and § to represent CHT/HA and CHT/HA-DN groups respectively. Single symbol (# and §) represent $p< 0.05$; double symbols (## and§§) $p < 0.01$ and triple symbols (### and §§§) $p < 0.001$.

In Chapter 5 data were grouped by formulation, namely CHT/HA-4DN, CHT/HA-DN, CHT/HA, and CHT/ALG multilayer films containing 5, 10 and 15 bilayers. The statistical differences relating to the time point before was evaluating using symbol # to represent the statistical differences relating to the control

(CHT/HA) films with the same number of bilayers, namely double symbols (##, $p < 0.01$) and triple symbols (###, $p < 0.001$).

In Chapter 7, data were grouped by formulation, namely 2D cell culture and 3D spheroid culture to assess time-course significant differences of each formulation. The statistical differences relating to the time point before was evaluating using symbol # to represent 3D spheroid. Double symbols (##) represent $p < 0.01$ and triple symbols (###) represent $p < 0.001$. All results were presented as mean ± standard deviation.

In Chapter 8, MTT and fluorescent assay data were grouped by time point, namely 1, 3, 5 and 7 days to analyze significant differences between formulations. The statistical differences relating to the time point before was evaluating using symbol #. Single symbol (#) represent $p < 0.05$, double symbols (##) $p < 0.01$ and triple symbols (###) $p < 0.001$. All the results were presented as mean ± standard deviation.

2.7 References

[1] M. Ma, R.M. Hill, Superhydrophobic Surfaces, Current Opinion In Colloid & Interface Science, 11 (2006) 193-202.

[2] X. Zhang, F. Shi, J. Niu, Y. Jiang, Z. Wang, Superhydrophobic Surfaces: From Structural Control To Functional Application, Journal Of Materials Chemistry, 18 (2008) 621-633.

[3] R. Furstner, W. Barthlott, C. Neinhuis, P. Walzel, Wetting And Self-Cleaning Properties Of Artificial Superhydrophobic Surfaces, Langmuir, 21 (2005) 956-961.

[4] N.M. Oliveira, A.I. Neto, W. Song, J.F. Mano, Two-Dimensional Open Microfluidic Devices By Tuning The Wettability On Patterned Superhydrophobic Polymeric Surface, Applied Physics Express, 3 (2010) 085205.

[5] A.I. Neto, C.A. Custodio, W.L. Song, J.F. Mano, High-Throughput Evaluation Of Interactions Between Biomaterials, Proteins And Cells Using Patterned Superhydrophobic Substrates, Soft Matter, 7 (2011) 4147-4151.

[6] W. Feng, L. Li, E. Ueda, J. Li, S. Heißler, A. Welle, O. Trapp, P.A. Levkin, Surface Patterning Via Thiol-Yne Click Chemistry: An Extremely Fast And Versatile Approach To Superhydrophilic-Superhydrophobic Micropatterns, Advanced Materials Interfaces, 1 (2014) 1400269.

[7] L. Feng, Y. Zhang, J. Xi, Y. Zhu, N. Wang, F. Xia, L. Jiang, Petal Effect: A Superhydrophobic State With High Adhesive Force, Langmuir, 24 (2008) 4114-4119.

[8] A.I. Neto, C.R. Correia, C.A. Custodio, J.F. Mano, Biomimetic Miniaturized Platform Able To Sustain Arrays Of Liquid Droplets For High-Throughput Combinatorial Tests, Advanced Functional Materials, 24 (2014) 5096-5103.

[9] M.B. Oliveira, A.I. Neto, C.R. Correia, M. Isabel Rial-Hermida, C. Alvarez-Lorenzo, J.F. Mano, Superhydrophobic Chips For Cell Spheroids High-Throughput Generation And Drug Screening, Acs Applied Materials & Interfaces, 6 (2014) 9488-9495.

[10] M. Oliveira, M. Ribeiro, S. Miguel, A.I. Neto, P. Coutinho, J.F. Mano, I.J. Correia, Biomimetic Superhydrophobic Surfaces Patterned With Wettable Spots As Implantable Chips For In Vivo High-Content 3d Biomaterials Response Assessment, Tissue Engineering Part A, 21 (2015) S140-S140.

[11] A.I. Neto, N.L. Vasconcelos, S.M. Oliveira, D. Ruiz-Molina, J.F. Mano, High-Throughput Topographic, Mechanical, And Biological Screening Of Multilayer Films Containing Mussel-Inspired Biopolymers, Advanced Functional Materials, (2016).

[12] E. Ueda, F.L. Geyer, V. Nedashkivska, P.A. Levkin, Droplet Microarray: Facile Formation Of Arrays Of Microdroplets And Hydrogel Micropads For Cell Screening Applications, Lab On A Chip, 12 (2012) 5218-5224.

[13] M. Rinaudo, Chitin And Chitosan: Properties And Applications, Progress In Polymer Science, 31 (2006) 603-632.

[14] S. Brittain, K. Paul, X.M. Zhao, G. Whitesides, Soft Lithography And Microfabrication, Physics World, 11 (1998) 31-36.

[15] M. Rinaudo, M. Milas, P. Ledung, Characterization Of Chitosan - Influence Of Ionic-Strength And Degree Of Acetylation On Chain Expansion, International Journal Of Biological Macromolecules, 15 (1993) 281-285.

[16] L.L. Hench, Biomaterials: A Forecast For The Future, Biomaterials, 19 (1998) 1419-1423.

[17] R. Jayakumar, M. Prabaharan, R.L. Reis, J.F. Mano, Graft Copolymerized Chitosan—Present Status And Applications, Carbohydrate Polymers, 62 (2005) 142-158.

[18] I. Younes, M. Rinaudo, Chitin And Chitosan Preparation From Marine Sources. Structure, Properties And Applications, Marine Drugs, 13 (2015) 1133-1174.

[19] L.P. Yan, Y.J. Wang, L. Ren, G. Wu, S.G. Caridade, J.B. Fan, L.Y. Wang, P.H. Ji, J.M. Oliveira, J.T. Oliveira, J.F. Mano, R.L. Reis, Genipin-Cross-Linked Collagen/Chitosan Biomimetic Scaffolds For Articular Cartilage Tissue Engineering Applications, Journal Of Biomedical Materials Research, Part A, 95a (2010) 465-475.

[20] K.Y. Lee, D.J. Mooney, Alginate: Properties And Biomedical Applications, Progress In Polymer Science, 37 (2012) 106-126.

[21] M.L. Ma, Y. Mao, M. Gupta, K.K. Gleason, G.C. Rutledge, Superhydrophobic Fabrics Produced By Electrospinning And Chemical Vapor Deposition, Macromolecules, 38 (2005) 9742-9748.

[22] S.G. Caridade, C. Monge, F. Gilde, T. Boudou, J.F. Mano, C. Picart, Free-Standing Polyelectrolyte Membranes Made Of Chitosan And Alginate, Biomacromolecules, 14 (2013) 1653-1660.

[23] S.N. Pawar, K.J. Edgar, Alginate Derivatization: A Review Of Chemistry, Properties And Applications, Biomaterials, 33 (2012) 3279-3305.

[24] A.S. Hoffman, Hydrogels For Biomedical Applications, Advanced Drug Delivery Reviews, 64 (2012) 18-23.

[25] K.Y. Lee, D.J. Mooney, Hydrogels For Tissue Engineering, Chemical Reviews, 101 (2001) 1869-1879.

[26] J.R.E. Fraser, T.C. Laurent, U.B.G. Laurent, Hyaluronan: Its Nature, Distribution, Functions And Turnover, Journal Of Internal Medicine, 242 (1997) 27-33.

[27] W.G. Pitt, R.N. Morris, M.L. Mason, M.W. Hall, Y. Luo, G.D. Prestwich, Attachment Of Hyaluronan To Metallic Surfaces, Journal Of Biomedical Materials Research Part A, 68a (2004) 95-106.

[28] Y. Lee, H.J. Chung, S. Yeo, C.H. Ahn, H. Lee, P.B. Messersmith, T.G. Park, Thermo-Sensitive, Injectable, And Tissue Adhesive Sol-Gel Transition Hyaluronic Acid/Pluronic Composite Hydrogels Prepared From Bio-Inspired Catechol-Thiol Reaction, Soft Matter, 6 (2010) 977-983.

[29] J. Mullegger, G. Lepperdinger, Hyaluronan Is An Abundant Constituent Of The Extracellular Matrix Of Xenopus Embryos, Molecular Reproduction And Development, 61 (2002) 312-316.

[30] Y. Luo, K.R. Kirker, G.D. Prestwich, Cross-Linked Hyaluronic Acid Hydrogel Films: New Biomaterials For Drug Delivery, Journal Of Controlled Release, 69 (2000) 169-184.

[31] D. Jiang, J. Liang, P.W. Noble, Hyaluronan In Tissue Injury And Repair, Annual Review Of Cell And Developmental Biology, 23 (2007) 435-461.

[32] J.H. Waite, M.L. Tanzer, Polyphenolic Substance Of Mytilus-Edulis - Novel Adhesive Containing L-Dopa And Hydroxyproline, Science, 212 (1981) 1038-1040.

[33] Y. Lee, H. Lee, Y.B. Kim, J. Kim, T. Hyeon, H. Park, P.B. Messersmith, T.G. Park, Bioinspired Surface Immobilization Of Hyaluronic Acid On Monodisperse Magnetite Nanocrystals For Targeted Cancer Imaging, Adv Mater, 20 (2008) 4154-4157.

[34] A.I. Neto, H.J. Meredith, C.L. Jenkins, J.J. Wilker, J.F. Mano, Combining Biomimetic Principles From The Lotus Leaf And Mussel Adhesive: Polystyrene Films With Superhydrophobic And Adhesive Layers, Rsc Advances, 3 (2013) 9352-9356.

[35] H. Lee, Y. Lee, A.R. Statz, J. Rho, T.G. Park, P.B. Messersmith, Substrate-Independent Layer-By-Layer Assembly By Using Mussel-Adhesive-Inspired Polymers, Advanced Materials, 20 (2008) 1619-1623.

[36] P. Lavalle, C. Gergely, F. Cuisinier, G. Decher, P. Schaaf, J. Voegel, C. Picart, Comparison Of The Structure Of Polyelectrolyte Multilayer Films Exhibiting A Linear And An Exponential Growth Regime: An In Situ Atomic Force Microscopy Study, Macromolecules, 35 (2002) 4458-4465.

[37] D.Y. Kwok, A.W. Neumann, Contact Angle Measurement And Contact Angle Interpretation, Advances In Colloid And Interface Science, 81 (1999) 167-249.

[38] J.S. Barbosa, R.R. Costa, A.M. Testera, M. Alonso, J.C. Rodriguez-Cabello, J.F. Mano, Multi-Layered Films Containing A Biomimetic Stimuli-Responsive Recombinant Protein, Nanoscale Research Letters, 4 (2009) 1247-1253.

[39] J. Goldstein, D.E. Newbury, P. Echlin, D.C. Joy, A.D. Romig Jr, C.E. Lyman, C. Fiori, E. Lifshin, Scanning Electron Microscopy And X-Ray Microanalysis: A Text For Biologists, Materials Scientists, And Geologists, Springer Science & Business Media, 2012.

[40] R.R. Costa, C.A. Custodio, F.J. Arias, J.C. Rodriguez-Cabello, J.F. Mano, Layer-By-Layer Assembly Of Chitosan And Recombinant Biopolymers Into Biomimetic Coatings With Multiple Stimuli-Responsive Properties, Small, 7 (2011) 2640-2649.

[41] M.V. Voinova, M. Rodahl, M. Jonson, B. Kasemo, Viscoelastic Acoustic Response Of Layered Polymer Films At Fluid-Solid Interfaces: Continuum Mechanics Approach, Physica Scripta, 59 (1999) 391-396.

[42] R.A. Muzzarelli, Genipin-Crosslinked Chitosan Hydrogels As Biomedical And Pharmaceutical Aids, Carbohydrate Polymers, 77 (2009) 1-9.

[43] G. Decher, Fuzzy Nanoassemblies: Toward Layered Polymeric Multicomposites, Science, 277 (1997) 1232-1237.

[44] H.-J. Butt, B. Cappella, M. Kappl, Force Measurements With The Atomic Force Microscope: Technique, Interpretation And Applications, Surface Science Reports, 59 (2005) 1-152.

[45] L. Zhu, Y. Feng, X. Ye, Z. Zhou, Tuning Wettability And Getting Superhydrophobic Surface By Controlling Surface Roughness With Well-Designed Microstructures, Sensors And Actuators A-Physical, 130 (2006) 595-600.

[46] R.N. Wenzel, Resistance Of Solid Surfaces To Wetting By Water, Industrial And Engineering Chemistry, 28 (1936) 988-994.

[47] A.B.D. Cassie, S. Baxter, Wettability Of Porous Surfaces, Transactions Of The Faraday Society, 40 (1944) 0546-0550.

[48] R.N. Wenzel, Resistance Of Solid Surfaces To Wetting By Water, Industrial & Engineering Chemistry, 28 (1936) 988-994.

[49] A.B.D. Cassie, S. Baxter, Wettability Of Porous Surfaces, Transactions Of The Faraday Society, 40 (1944) 546-551.

[50] H. Lee, S.M. Dellatore, W.M. Miller, P.B. Messersmith, Mussel-Inspired Surface Chemistry For Multifunctional Coatings, Science, 318 (2007) 426-430.

[51] R.A. Muzzarelli, M. El Mehtedi, C. Bottegoni, A. Aquili, A. Gigante, Genipin-Crosslinked Chitosan Gels And Scaffolds For Tissue Engineering And Regeneration Of Cartilage And Bone, Marine Drugs, 13 (2015) 7314-7338.

[52] F.-L. Mi, Y.-C. Tan, H.-F. Liang, H.-W. Sung, In Vivo Biocompatibility And Degradability Of A Novel Injectable-Chitosan-Based Implant, Biomaterials, 23 (2002) 181-191.

[53] S.S. Silva, A. Motta, M.T. Rodrigues, A.F.M. Pinheiro, M.E. Gomes, J.F. Mano, R.L. Reis, C. Migliaresi, Novel Genipin-Cross-Linked Chitosan/Silk Fibroin Sponges For Cartilage Engineering Strategies, Biomacromolecules, 9 (2008) 2764-2774.

[54] R.A.A. Muzzarelli, Genipin-Crosslinked Chitosan Hydrogels As Biomedical And Pharmaceutical Aids, Carbohydrate Polymers, 77 (2009) 1-9.

[55] M. Arteche Pujana, L. Perez-Alvarez, L.C. Cesteros Iturbe, I. Katime, Biodegradable Chitosan Nanogels Crosslinked With Genipin, Carbohydrate Polymers, 94 (2013) 836-842.

[56] A. Toffey, G. Samaranayake, C.E. Frazier, W.G. Glasser, Chitin Derivatives. I. Kinetics Of The Heat-Induced Conversion Of Chitosan To Chitin, Journal Of Applied Polymer Science, 60 (1996) 75-85.

[57] G. Aubelsadron, D. Londosgagliardi, Daunorubicin And Doxorubicin, Anthracycline Antibiotics, A Physicochemical And Biological Review, Biochimie, 66 (1984) 333-352.

[58] F. Arcamone, Doxorubicin: Anticancer Antibiotics, Elsevier, 2012.

[59] A.I. Neto, C.A. Custodio, W. Song, J.F. Mano, High-Throughput Evaluation Of Interactions Between Biomaterials, Proteins And Cells Using Patterned Superhydrophobic Substrates, Soft Matter, 7 (2011) 4147-4151.

SECTION III. OPTIMIZATION OF MULTILAYER FILMS AND SUPERHYDROPHOBIC MICROARRAYS FOR HIGH-THROUGHPUT TISSUE ENGINEERING STUDIES

CHAPTER 3. NANOSTRUCTURED POLYMERIC COATINGS BASED ON CHITOSAN AND DOPAMINE-MODIFIED HYALURONIC ACID FOR BIOMEDICAL APPLICATIONS *

3.1 Abstract

In a marine environment, specific proteins are secreted by mussels and used as a bioglue to stick to a surface. These mussel proteins present an unusual amino acid 3,4-dihydroxyphenylalanine (known as DOPA). The outstanding adhesive properties of these materials in the sea harsh conditions have been attributed to the presence of the catechol groups present in DOPA. Inspired by the structure and composition of these adhesive proteins, we used dopamine-modified hyaluronic acid (HA-DN) prepared by carbodiimide chemistry to form thin and surface-adherent dopamine films. This conjugate was characterized by distinct techniques, such as nuclear magnetic resonance (NMR) and ultra-violet spectrophotometry (UV). Multilayer films were developed based on chitosan (CHT) and HA-DN to form polymeric coatings using the Layer-by-Layer (LbL) methodology. The nanostructured films formation was monitored by quartz crystal microbalance (QCM-D). The film surface was characterized by atomic force microscopy (AFM) and scanning electron microscopy (SEM). Water contact angle measurements were also conducted. The adhesion properties were analyzed showing that the nanostructured films with DN promote an improved adhesion. In vitro tests showed an enhanced cell adhesion, proliferation and viability for the biomimetic films with catechol groups, demonstrating their potential to be used in distinct biomedical applications.

** This chapter is based on the publication: Neto A. I., Cibrão A. C., Correia C. R., Carvalho R. R., Luz G. M., Ferrer G. G., Botelho G., Picart C., Alves N. M., and Mano J. F. Nanostructured Polymeric Coatings Based on Chitosan and Dopamine-Modified Hyaluronic Acid for Biomedical Applications. **Small**, 12, 2459–2469, 2014.*

3.2 Introduction

It is well known that biomaterials interact with cells and tissues through their interfaces, so surface properties are determinant on cell behavior [1, 2]. In some situations it is also important that biomaterials adhere to tissues and organs [3]. The development of adhesive substrates that would enhance cell attachment and proliferation and could also adhere to tissues would constitute a substantial breakthrough for tissue engineering and other biomedical applications. Mussel adhesive proteins (MAPs) found in marine mussels form outstandingly moisture- resistant adhesive bonds capable of surviving to the destructive conditions of the ocean. Such proteins provide the role of cement, which upon secretion become quickly solidified in wet environments via chemical crosslinking into an insoluble plaque, binding the animal to surfaces [4]. It is known that MAPs contain considerable concentrations of an amino acid, 3,4-dihydroxy-L-phenylalanine (DOPA), which is formed by postranslational modification of tyrosine. A key aspect of DOPA and its analog dopamine (DN) is the ortho-dihydroxyphenyl (catechol) functional group, which forms strong bonds with various inorganic/organic surfaces [5-7]. Several authors have developed new adhesives trying to mimic the adhesion properties found in marine mussels [8-12]. For example, Deming and co-workers synthesized simple co-polypeptides of L-lysine and DOPA with different compositions [9]. Yu et al. synthesized copolymers of DOPA and L-lysine that form moisture-resistant adhesive bonds with a variety of substrates (aluminum, steel, glass and plastics) when suitably oxidized [8]. Anderson et al. also showed that the adhesion of DOPA/N5- (2-hydroxyethyl)-L-glutamine films to mica and TiO_2 surfaces increases with DOPA concentration [12]. Lee et al [11] developed new thermo-sensitive and injectable DOPA modified hyaluronic acid (HA)/Pluronic hydrogels and showed that these hydrogels exhibited excellent tissue-adhesion properties with superior in vivo gel stability.

MAPs are in fact a source of inspiration for the development of nanostructured materials. Some techniques, such as layer-by-layer (LbL) have been used in the production of such functional materials. LbL is a simple methodology that allows the possibility to coat surfaces through multiple deposition steps, with an ability to control the build-up of complex geometries at the nanometer length scale. This constitutes a great advantage in comparison to other thin film assembly techniques. Multilayer films were produced by LbL using chitosan (CHT) and dopamine modified hyaluronic acid (HA-DN) in the present work, in order to try to combine the adhesion properties found in marine mussels with a simple film production method and with the known advantages of CHT and HA for biomedical applications.

In fact, HA and CHT are very popular biomaterials that have been often to form nanostructured coatings [13-20]. HA is a polysaccharide that can be found in tissues and body fluids of vertebrates and also in

some bacteria [21]. It is a linear polymer and a naturally occurring non-sulfated glucosaminoglycan composed of D-N-acetylglucosamine and D-glucuronic acid [11, 22]. HA is a negatively charged polyelctrolyte above its pKa (≈ 2.9) [23]. Because of its excellent lubricity and bacterial inhibitory effect, HA is suitable for tissue engineering applications [22, 24]. CHT, due to the primary amines present in its structure, is a positively charged polyelectrolyte in acidic medium, with a pKa ≈ 6.24 It is non toxic, biodegradable and has an excellent biocompatibility. So, CHT is a great candidate for a series of biomedical applications [25-27].

Several works have demonstrated the advantages of using the materials chosen in the present work in the biomedical field. For example, the surface of titanium, a common implant material for orthopaedic applications, has been modified with HA and CHT coatings, allowing to promote osteoblast functions [24]. Also, Lee et al.[4] have incorporated catechol groups (which are present in DN) into coatings of distinct substrates and induced the reduction of silver ions to metallic silver when immersed in an aqueous metal salt solution, providing antibacterial properties to the coated surfaces.

There are only a few studies where LbL films inspired by MAPs were studied [4, 28, 29]. A recent work of Zhang et al. [29], showed that multilayer films of dopamine-modified hyaluronic acid/chitosan (DHA/CHI) built on the surface of Ti–24Nb–2Zr (TNZ) alloy can improve osteoblast proliferation and biocompatibility for orthopedics applications, when compared with to original ones.

In this work, we hypothesize that the formation of multilayers films of conjugate HA-DN and CHT can produce surfaces with distinct properties, when compared with the conventional CHT/HA ones. The greatest advantage that the current approach presents over other reported methods is that we try to combine an enhanced cell response with a significantly improved adhesive strength, whereas the other reported methods have only showed improvements on cell behaviour. The combination of this particular system could be extremely advantageous regarding biomedical applications.

The formation of CHT and HA-DN multilayer films by the LbL technique was investigated using quartz crystal microbalance with dissipation monitoring (QCM-D). The film surface was characterized by atomic force microscopy (AFM) and scanning electron microscopy (SEM). The wettability was analyzed by water contact angle measurements. The mechanical adhesive properties and the in vitro cell behavior were evaluated on such nanostructured films inspired on mussel adhesive proteins.

3.3 Results and Discussion

3.3.1 HA-DN Conjugate synthesis and characterization

In order to know if the synthesis of the conjugate was successful the product of the synthesis was analyzed by two techniques: NMR and UV spectroscopy.

The ^{1}H-NMR spectrum of the unmodified hyaluronic acid is shown in Figure 3.1 A and is consistent with the one found in literature [30-32], where the multiplets located at δ = 2.028 ppm are associated with the protons of N-COCH3 groups. Figure 3.1 B shows the ^{1}H-NMR spectrum of dopamine. The multiplets centered at δ = 2.876 ppm and δ = 3.227 ppm that can be observed in this figure are associated with the protons of the aliphatic group, according to the literature [33]. The region between δ = 6.7 ppm and δ = 7.0 ppm corresponds to the protons in orto and meta coupling position of the ring.

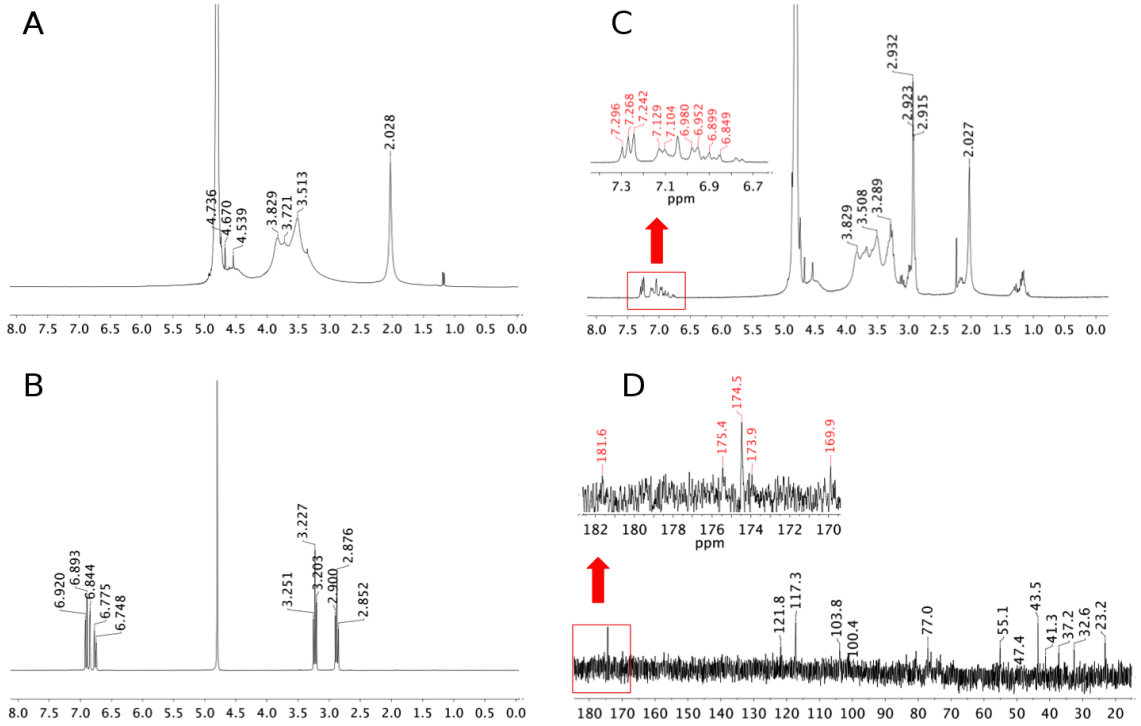

Figure 3.1 ^{1}H-NMR spectra of A) hyaluronic acid (HA), B) dopamine and C) the synthesized conjugate (HA-DN) with an expanded view. ^{13}C-NMR spectra of the conjugate with expanded view.

By using the experimental conditions previously described, the conjugate was obtained and characterized by ^{1}H-NMR spectrum - see Figure 3.1C. It is known that the new N-H linkage formed in the conjugate could not be detected by ^{1}H-NMR as this conjugate is only soluble in water and in this solvent the NH linkage interchange with water so no new signal appears. In order to overcome this limitation and using the conditions described in the experimental section, the conjugate was obtained and characterized by

^{13}C-NMR. The ^{13}C-NMR spectrum of the unmodified hyaluronic acid is consistent with published results [34]. According to the literature [35, 36], the carbonyl chemical shift of HA should be between 173 and 174 ppm. The ^{13}C-NMR new signal of around 175 ppm shown in Figure 3.1 D confirms that the HA-DN conjugate was successfully synthesized.

The results obtained by UV-Vis spectroscopy are presented in Figure 3.2. It can be seen that, at approximately 280 nm, one band appears for the HA-DN conjugate, being not observed in HA - see Figure 3.2 A.

In fact, dopamine presents a band in the UV spectrum at this wavelength [37]. These results indicate the presence of dopamine in the synthesized product in agreement with the NMR results. Several spectra of solutions with different concentrations of dopamine can be seen in Figure 3.2 B; they all have an excitation band at approximately 280 nm, similar to the conjugate band. Using the measured absorbance of the conjugate, obtained at 280 nm, it was determined that the concentration of DN units in the HA-DN solution was 2.86x10^{-4} M. Therefore, the degree of dopamine substitution in the synthesized conjugate is 11%, being different than the ones found in other works [4, 6, 11]. However some conditions, such as the relative proportions of the reagents used and/or the time of the reaction, employed in the synthesis of HA-DN differ from the ones used in these studies.

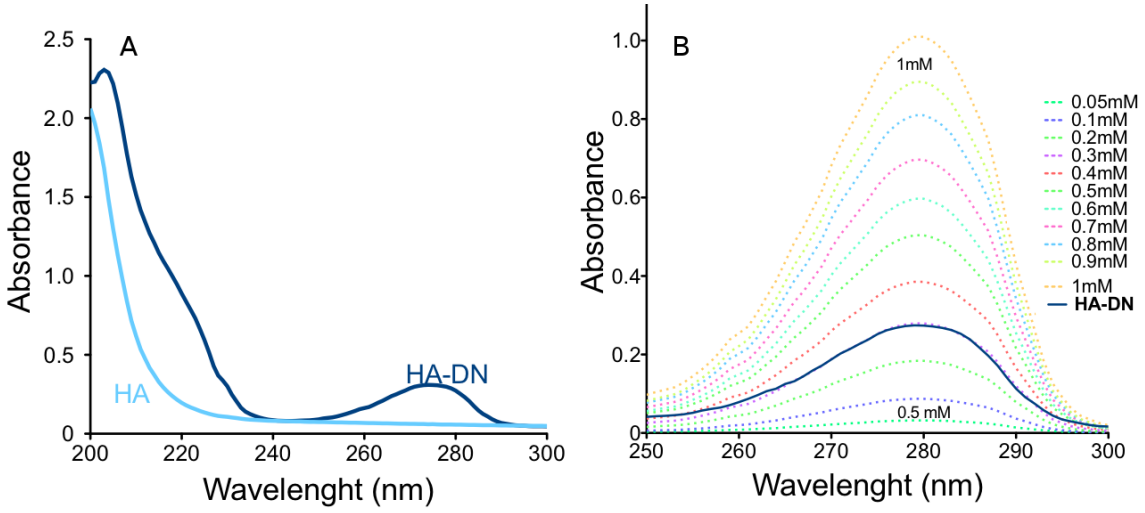

Figure 3.2 A) UV-Vis spectra of the conjugate (HA-DN) and the control (HA). B) Spectra of dopamine solutions with different concentrations; the spectrum of the conjugate is also shown for comparison.

3.3.2 Build-up of CHT/ HA-DN multilayer films and surface characterization

The development of LbL films containing materials inspired by MAPs is still very scarce. Lee et al. [4] were the first to propose this kind of films and successfully assembled HA-DN with poly(ethylenimine).

The composition, structure and the crosslinking methodology lead to the development of LbL films with high strength. Charlot et al. [28] prepared robust antimicrobial films on stainless steel based on the LbL deposition of polyelectrolytes that contained DOPA. A polycationic copolymer (N-methacrylated DOPA) with (2-(methacryloxy) ethyl trimethylammonium chloride) known as P(DOPA)-co-P(DMAEMA+), was synthesized and co-deposited with precursors of silver nanoparticles as the first layer. Multilayer films obtained by alternating this nanoparticle-loaded polycationic copolymer with polystyrene sulfonate, a commercial polyanion, resulted in stainless steel with high antibacterial activity against Gram-negative E. coli bacteria [28].

In the present work the formation of LbL films of CHT/HA-DN and CHT/HA was investigated in situ using QCM-D- see Figure 3.3 A. For graphical simplification, the results in this figure present $\Delta f/\upsilon$ and ΔD as a function of time for the 7th harmonic. It can be seen that the normalized frequency $\Delta f/\upsilon$ decreases with each CHT, HA-DN or HA injection, indicating that mass is added during each deposition step. When rising with NaCl solution after CHT, HA-DN or HA adsorption, an increase in $\Delta f/\upsilon$ is observed due to the desorption of a small fraction of free polyelectrolyte. Regarding ΔD, an increase is observed after each CHT, HA-DN or HA injection due to the viscoelastic nature of the adsorbed layers, typical of polymeric systems.

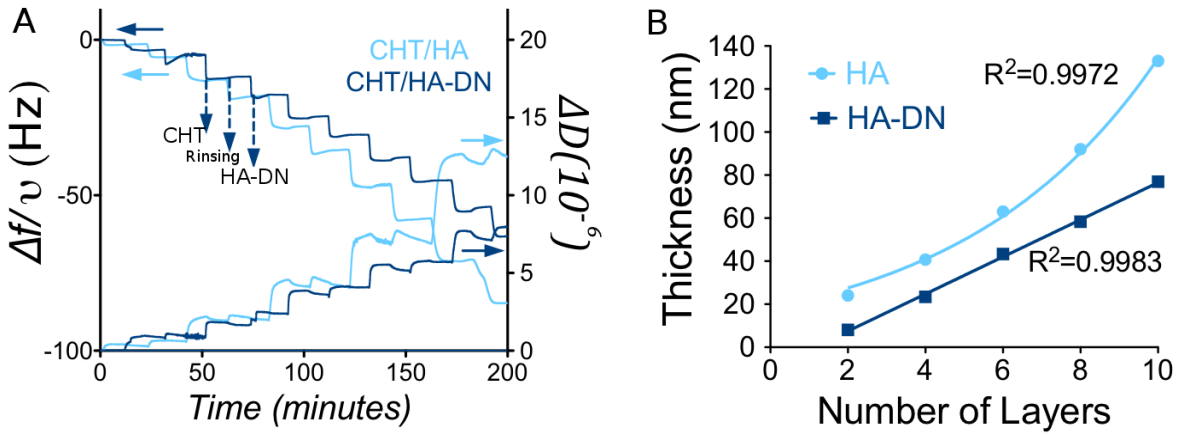

Figure 3.3 Build-up assemblies of chitosan (CHT), conjugate (HA-DN and hyaluronic acid (HA) up to 10 deposition layers in 0.15 M of NaCl at pH 5.5. A) Quartz-crystal microbalance with dissipation monitoring (QCM-D) with normalized frequency ($\Delta f/\upsilon$) and dissipation (ΔD) variations at the 7th overtone as a function of the time. B) Cumulative thickness evolution of CHT/HA-DN and CHT/HA polymeric films as a function of the number of deposition layers. Thickness measurements were estimated using a Voigt viscoelastic model.

Figure 3.3 A also shows that $\Delta f/\upsilon$ and ΔD variations are higher for the CHT/HA film than for the CHT/HA-DN film. The lower ΔD variation of CHT/HA-DN (Figure 3.3 A) indicates the formation of a thinner, more

rigid and less water-rich film. Figure 3.3 B shows that the CHT/HA film presents an exponential film growth, which could explain the higher *f/υ* variation for this system, whereas the CHT/HA-DN film represents a linear trend line. Other authors have reported an exponential growth of polyelectrolyte films containing chitosan and hyaluronic acid [38, 39], in agreement with our results for the control films. Two explanations for an exponential growth mechanism have been proposed in literature: one relies on the diffusion of polyelectrolyte "in" and "out" of the film during each bilayer step [38, 39] whereas the second one relies on the increase in film surface roughness as the film builds up [40, 41].In order to clarify the mechanism of the exponential growth, the surface roughness of the developed and control films was analysed by AFM- see Figure 3.4. In fact, it was found that the roughness of the CHT/HA films is higher than the one of the CHT/HA-DN films, suggesting that the CHT/HA interface is getting rougher and the surface area is increasing so that more CHT or HA can absorb. Figure 3.4 also shows the results of an additional characterization of the film surface by SEM and water contact angle measurements. The results for the control (glass slide) are also shown for the sake of comparison.

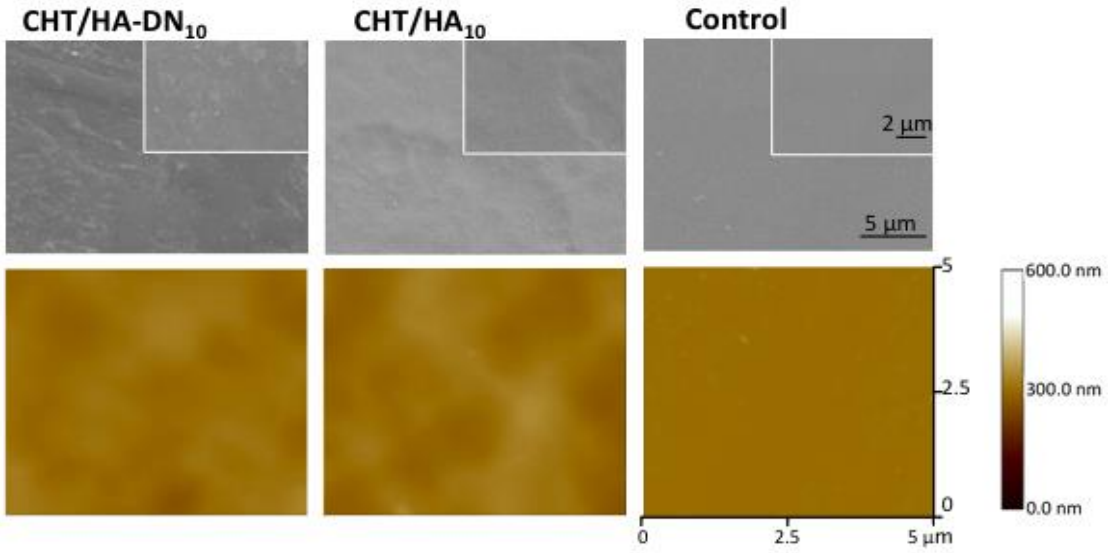

	CHT/HA-DN$_{10}$	CHT/HA$_{10}$	Control
Rq (nm)	10.22 ± 0.72	13.01 ± 0.90	3.27 ± 1.15
Ra (nm)	7.94 ± 0.55	10.35 ± 0.86	1.98 ± 0.48
WCA (°)	73.34 ± 1.82	77.36 ± 1.44	43.42 ± 1.38

Figure 3.4 Representative images of scanning electron microscopy (SEM) and atomic force microscopy (AFM) of CHT/HA-DN and CHT/HA films with 10 bilayers. The images of the control (glass slide) are also shown for the sake of comparison. The

root mean Square (R_q), average roughness (R_a) of the studied surfaces (n=3) and corresponding water contact angle (WCA, n=5, 3 μL drop volume) are indicated below the images.

The changes in the water contact angle and topography of the glass control provided evidence of the presence of the coatings. SEM and AFM results also showed the rougher surface of the coatings when compared with the control surface. Moreover, it was found that the water contact angle values of the CHT/HA-DN and CHT/HA films are similar, although the CHT/HA-DN value is slightly lower (around 73°) than the one of the CHT/HA films (around 77°). Water contact angles of nearly 50° were reported for polydopamine coated glass substrates [42], which are significantly lower than the ones measured for the developed CHT/HA-DN coatings. In our case, as the dopamine fraction in the films is small, the corresponding contact angle is also small.

Further information on the viscoelastic properties of the formed films were obtained by applying a Voigt based model [43]. The data of Figure 3.3 B were fitted according to this model. By assuming a fluid density of 1000 $kg.m^{-3}$, a fluid viscosity of 1m.Pa.s and a layer density of 1100$kg.m^{-3}$ it was possible to estimate the thickness as a function of the number of layers during the build-up of the film - see Figure 3.3 B. Lee and co-workers, measured the thickness of LbL films based on poly(ethylenimine) and HA-DN with 20 bilayers and they obtained a thickness of approximately 45 nm [4]. We found that the thickness of the CHT/HA-DN film with 10 layers is approximately 75 nm and for CHT/HA is 130 nm at pH 5.5. It can also be seen that the thickness of the HA-DN film is lower than the one of HA film, as expected taking into account the ΔD variation and the different growth, as already discussed earlier. It must be noted that the estimated values of thickness are based on the assumption that the adsorbed layer has an uniform thickness, a necessary requirement for the used viscoelastic model [44-46]. The thickness values estimated by fitting of the QCM-D data were further confirmed by ellipsometry measurements. Films built in the same conditions as the ones used in the QCM-D experiments were analysed by ellipsometry. The thickness values were 94.06 ± 4.42 nm and 124.42 ± 2.50 nm for the CHT/HA-DN and the CHT/HA films, respectively, which are in agreement with the QCM-D results.

It should be pointed that the conjugation of dopamine to the COOH groups of HA should affect its pKa. However, as the degree of DOPA substitution in the prepared conjugate was just 11% as measured by UV-spectrophotometry, and given the neutral nature of the molecule, this change should not be so significant. In fact, the QCM data showed that is possible to build the films by LbL at pH 5.5, meaning that HA-DN is still negatively charged.

3.3.3 Adhesion properties of the CHT/HA-DN films

The adhesion strength of multilayer and nanostructured films using the LbL technology was studied for the first time. The adhesion of CHT/HA-DN and CHT/HA (negative control) films to a glass substrate was evaluated using a universal mechanical testing machine, according to the standard procedure ASTM D1002. Figure 3.5 A presents representative load-extension curves of both coatings, showing that the final displacement of CHT/HA-DN is higher, which indicates a higher adhesive strength compared with the control, CHT/HA. The adhesive strength results of the multilayer films are shown in Figure 5B. In fact, it can be seen in Figure 3.5 B that the adhesive strength of CHT/HA-DN is 2.32 ± 2.20 MPa and for CHT/HA is 0.75 ± 0.14 MPa. It is most likely that the increase in the adhesion force is due to the strong adhesion force of the catechol moieties in the modified HA. It should be mentioned that adhesion tests were also performed with films stained with eosin, which specifically stains the CHT component of the films. It was observed that, after plate detachment, both plates were stained, as shown in the representative image of the glass plates at the rupture point that is included in Figure 3.5. This is an indication that break occurred somewhere between the layers of the film.

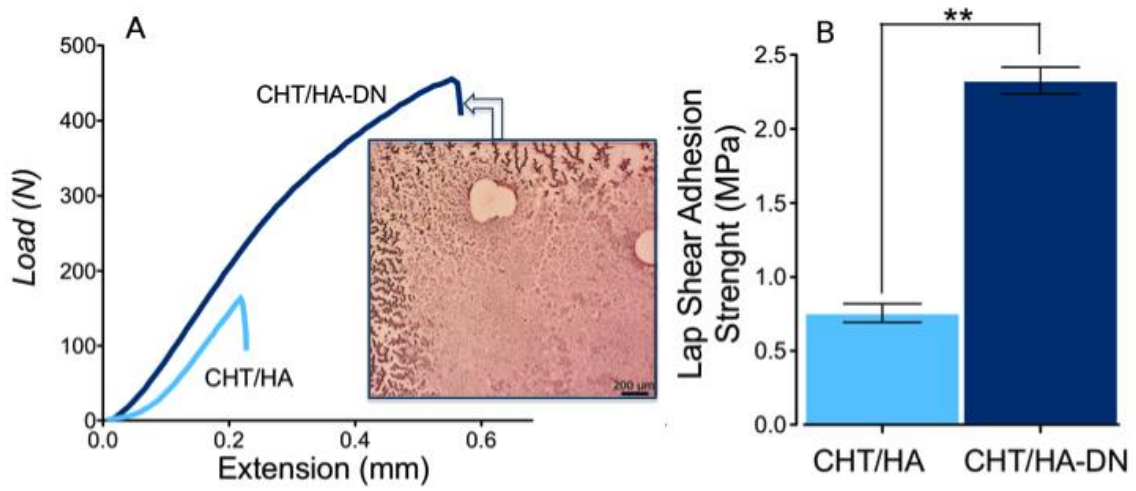

Figure 3.5 A) Force vs Displacement curves of CHT/HA and CHT/HA-DN films. B) Adhesive strength of CHT/HA and CHT/HA-DN films between glass slides. Data are means SD (n=5; **= p<0.01). Representative image of the glass slides at rupture point.

Yamada et al. used the tyrosinase-catalyzed reactions of dopamine to try to confer adhesive properties to semidilute solutions of CHT and analysed their adhesive strength using glass as the substrate [47]. Adhesive shear strengths of over 0.4 MPa were observed for these modified CHT samples, while control CHT solutions conferred no adhesive strength. These values are about one order of magnitude lower than the results of this work.

Yu et al. measured the adhesive strength of DOPA and L-lysine copolymers using the same mechanical testing protocol adopted in this work and found that they formed moisture-resistant adhesive bonds with a variety of substrates (aluminum, steel, glass and plastics) [8]. They obtained values of adhesive strength were between 0.5 and 4 MPa, depending on the substrate and the oxidation conditions. Distinct oxidizing agents, air (O_2), $NaIO_4$, H_2O_2 and mushroom tyrosinase were used in that work [8]. The authors found that successful adhesiveness was dependent on oxidation conditions and that the choice of oxidant was partially substrate-specific. In our case, the measured adhesive properties presented in Figure 3.5 correspond to un-oxidized films, and high adhesion strength was found for the films containing dopamine without the need of using oxidizing agents. Nevertheless, mechanical adhesion tests were also performed using sodium periodate as the oxidizing agent, which was found in literature to be an effective oxidizing agent of the catechol groups [48]. For the used sodium periodate concentration (5 mM, based on the typical concentration values used by other authors to oxidize the catechol groups) no significant changes were found on the adhesion of these films: an adhesive strength of 2.34 ± 0.13MPa was obtained for the oxidized film.

Additional mechanical tests were performed in order to measure the adhesion strength of polydopamine coatings typically reported in literature [42, 49] under the same conditions used for the developed LbL coatings. It was found that the polydopamine coatings presented a practically null adhesive strength, i.e., the glass plaques coated with polydopamine detached immediately after the beginning of the mechanical tests.

3.3.4 Evaluation of cell behavior

Saos-2 and L929 cells were used for the analysis of cell behavior of the developed films. These two cell lines were chosen because these are standard cell lines typically used in the biomedical field. Moreover, it is well known that cell response is quite dependent on the cell type [2]. Hence, it was intended to analyse the cell behaviour of the developed coatings with cells that present distinct phenotypes, in this case Saos-2 cells as a model for human osteoblastic cells and L929 cells to analyse fibroblasts response. The use of these cell lines allowed to analyse if the observed trends on cell response were the same or were independent of cell type.

Saos-2 and L929 cells (Figure 3.6 A and B, respectively) were seeded on the top of CHT/HA-DN and CHT/HA 10-bilayered films. Subsequently, the biological performance of the nanostructured multilayers films was evaluated up to 21 days of culture. At predetermined time intervals, namely, 1, 3, 7, 14, and 21 days, the samples were compared concerning cell adhesion, viability, and proliferation. The cell

response results for the glass-only control were included in Figure 3.6, for the sake of comparison, and they showed a good cell response as typically observed for mammalian cells when the substrate is glass. To evaluate cell adhesion, a DAPI fluorescence assay was performed on the surfaces seeded with Saos-2 or L929 cells (Figures 3.6 A.i-iii and 3.6 B.i-iii, respectively). DAPI assay images show that the incorporation of DN on the multilayers led to an improved cell attachment by comparing CHT/HA to CHT/HA-DN in both cell types. These differences are evidenced by the quantification results of the percentage of adhered cells per area presented in Figures 3.6 A.iii and 3.6 B.iii. The good adhesion on CHT/HA-DN films suggests that this system could have potential applicability in the development of adhesive coatings for a variety of implants requiring improved cell response. As the fabrication of these multilayered films is based on a dipping process, it would be possible to process coatings on substrates with complex geometry.

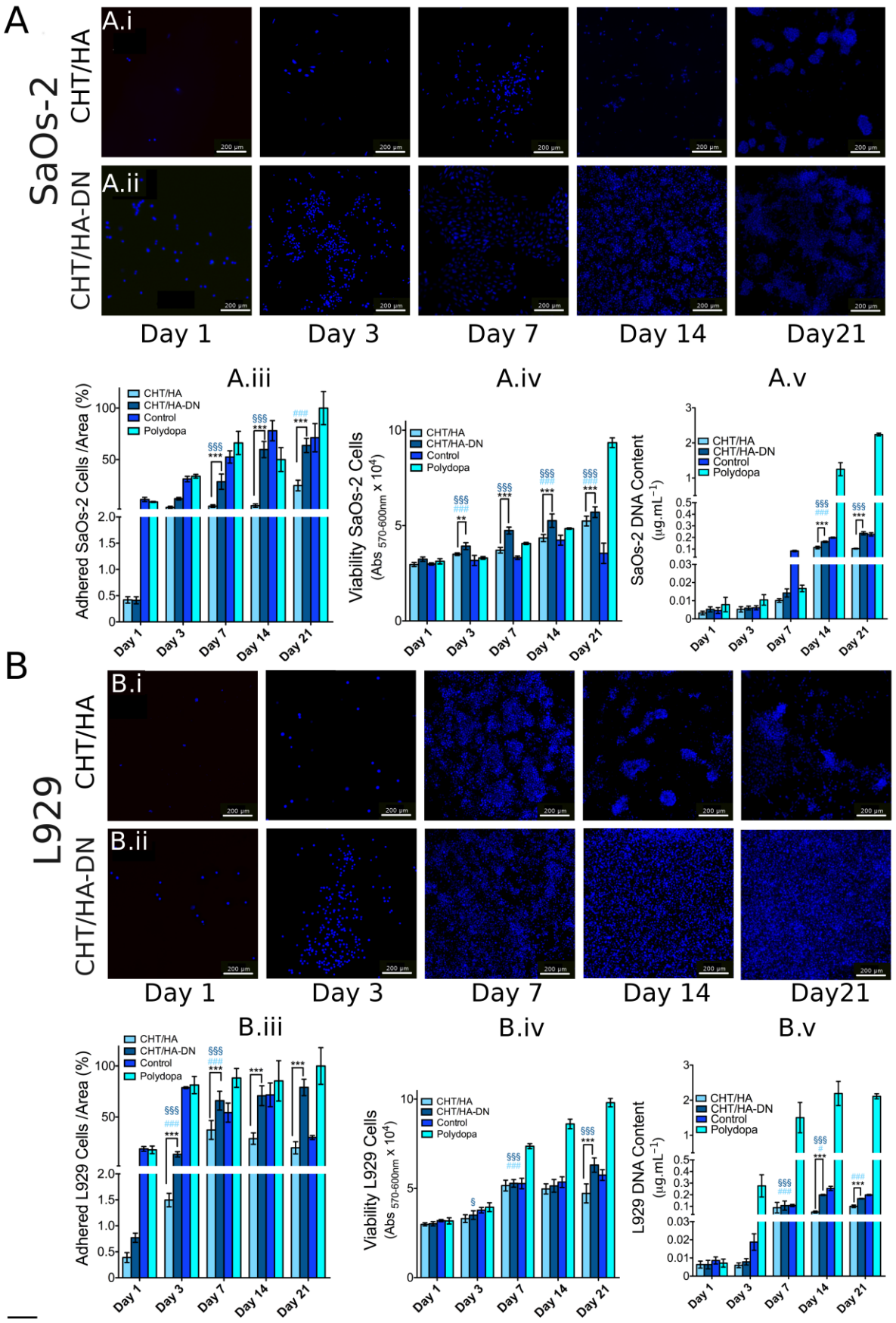

Figure 3.6 A) Fluorescence images of cells stained with DAPI for A) SaOs-2 and B) L929 at 1, 3, 7, 14 and 21 days of culture. Multilayer films of CHT/HA-DN and CHT/HA (negative control), cover glasses (positive control) and polydopamine coatings

were tested. Cellular density quantification was measured in the multilayer films for SaOs-2 (A.iii) and L929 (B.iii) cells. Viability of all formulations was tested for SaOs-2 (A.iv) and L929 (B.iv) cells by alamar blue. Absorbance was read at wavelength of 570 nm and 600 nm. DNA quantification of all formulations was tested for SaOs-2 (A.v) and L929 (B.v) cells. Statistical differences in grouped by time point analysis were marked with (*), (**) and (***), which stand for p-value < 0.05; p < 0.01 and p < 0.001, respectively. For evaluate the statistical differences relating to the time point before, single symbol (# and §) represent p< 0.05; double symbols (## and§§) p < 0.01 and triple symbols (### and §§§) p < 0.001. All results were presented as mean ± standard deviation.

Cell viability was evaluated by alamar blue colorimetric assay. Despite of all formulations presented a good amount of well spread cells, CHT/HA-DN films also presented enhanced cell viability for L929 and SaOs-2 cells when compared to the negative and positive controls. Specifically, for films with SaOs-2 cells, from day 3, CHT/HA-DN films present significant differences compared to CHT/HA films (Figure 3.6 A.iv). Additionally, only the viability of CHT/HA-DN films significantly increases with time. These results are an indicator factor that the materials employed to construct the multilayers did not jeopardize the viability of the films. Moreover, for films with L929 cells (Figure 3.6 B.iv) besides the higher amount of cells adhered, only on day 21 were detected differences statistically significant between both multilayer films, due the lack of adhesion in the case of CHT/HA films. Ultimately, a DNA quantification assay was performed to evaluate cell proliferation. Results showed that CHT/HA-DN films had the highest proliferation for both cell types (Figure 3.6 A.v and 3.6 B.v). Additionally, these films had a continuous proliferation increase up to 14 days of culture for both cells type. Significant differences between the two multilayer films could be noticed at days 14 and 21 for both cells.

Other recent works have showed that the use of mussel adhesive proteins may contribute for a higher cell adhesion to the substrate [11, 42, 49]. An HA-DN/Pluronic hydrogel, developed by Lee and co-workers [11] was subcutaneously injected into a 6-week-old mice. Both inflammatory response and fibrosis were barely visible after 21 days. This suggests that the HA-DN/Pluronic hydrogel is biocompatible and non-immunogenic. Also, the hydrogel mass was adhered onto the nearby serous tissue of parietal peritoneum, which implied that the HA-DN/Pluronic hydrogel was adhesive to the tissue surface due to the adhesive function of unreacted catechol moieties remaining in the hydrogel structure. Ku et al. coated different substrates with polydopamine [42]. They investigated mouse osteoblast MC3T-E1 cells adhesion on the coated substrates. When the osteoblasts were seeded onto non-adhesive polyethylene (PE), poly(tetrafluoroethylene) (PTFE), silicon rubber and poly(dimethyl-siloxane) (PDMS) substrates, the cells barely adhered and spread. On the other hand, the substrates coated with polydopamine exhibited normal adhesion. Ku and Park coated PCL nanofibers with polydopamine and when compared to unmodified and gelatin-coated nanofibers, human umbilical vein endothelial cells (HUVECs) exhibited highly enhanced adhesion and viability on the polydopamine coated fibers [49].

The cell response results for polydopamine-only controls, i.e. coatings using glass as the substrate and prepared using the typical conditions adopted for these coatings [42, 49] (see experimental section), were also included in Figure 3.6 for the sake of comparison. As expected, these controls showed an enhanced cell response in agreement with the results of the above mentioned works [42, 49]. Therefore, the greatest advantage that the developed LbL coatings present over the typical polydopamine coatings is that they combine an enhanced cell adhesion, proliferation and viability (Figure 3.6) with a significantly improved adhesive strength (Figure 3.5), whereas the polydopamine coatings have only revealed improvements on cell response. In fact, as mentioned before, it was found that the polydopamine coatings present a practically null adhesive strength. The enhanced adhesive strength of the developed films is particularly important in specific applications, for example they can be used as coatings of a variety of implants to improve both cell response and adhesion strength in a simple and versatile way.

The increase of cell adhesion on polydopamine coated PCL fibers was attributed to the adsorption/immobilization of serum proteins on the poly-dopamine ad-layer [49]. This layer can react with amine- or thiol-functionalized molecules via Shiff- base or Michael addition chemistry; thus, serum proteins, some of them supporting cell adhesion, can strongly attach to polydopamine coatings. Since the proteins adsorbed on polydopamine coating maintained their native structure and activity [50], the serum proteins attached to polydopamine layer serve as cell adhesion sites. However, as in our case the culture medium was not supplemented with serum, this is not the explanation for the enhanced cell adhesion on our dopamine containing LbL films. Furthermore, the mechanism behind enhanced cellular adhesion might be explained by potentially enhanced surface roughness, which could follow deposition of the polysaccharide-based films or by differences in the wettability of the surfaces. However, as discussed before, the results of Figure 3.4 revealed that the mechanism behind the enhanced cellular adhesion of the CHT/HA-DN films may not be explained by potentially enhanced surface roughness or by the slight difference in hydrophilicity. Ku et al. [42] also found that cells adhere on polydopamine - modified PTFE surfaces exhibiting well-stretched actin bundles similar to those shown in cells that adhered on normal glass substrate. The cells on polydopamine ad-layers indicate that underwent the general adhesion processes, i.e., substrate attachment /spreading/ cytoskeleton development. Moreover, it should be referred that the presence of polydopamine in the coatings proposed by other authors and in the films developed in the present work could even act as a strong anchor between cells and substrates without any covalent grafting [10]. In fact the presence of the characteristic groups of DOPA and dopamine enable the formation of both covalent and non-covalent interaction [10, 51].

3.4 Conclusion

HA-DN conjugates with a substitution degree of 11% were synthesized. Moreover, it was possible to successfully prepare LbL films of HA-DN and CHT. QCM-D data showed that it is possible to assemble CHT/HA-DN films. The thickness of a 10 layer film could reach nearly 75 nm. The adhesive strength of the CHT/HA-DN films to a glass substrate was found to be significantly higher than the one of the control film. The evaluation of cell behavior demonstrated that the CHT/HA-DN films present enhanced cell adhesion, proliferation and viability. These films could be potentially used as adhesive coatings of distinct implants in order to improve both cell response and adhesion strength in a simple and versatile way.

3.5 Experimental Section

Materials: Chitosan (CHT) with a N-deacetylation degree of 80% and a molecular weight obtained by viscosimetry of 770 kDa was purchased from Sigma, and purified afterwards. Hyaluronic acid (HA) with a molecular weight of 595 kDa was purchased from Sigma (ref. 53747) as hyaluronic acid sodium salt from Streptococcus equi. Dopamine hydrochloride (DN) (ref. H8502) and N-(3-Dimethylaminopropyl)-N'-ethylcarbodiimide hydrochloride (EDC) (ref. 03450, purum, ≥ 98.0% (AT)) were purchased from Sigma and used without any further purification. Sodium periodate ($NaIO_4$) was purchased from Sigma (ref. 311448). Tris- HCl solution was purchased from Sigma (ref. 252859) as Tris (hydroxymethyl) aminomethane.

Synthesis of HA-DN: HA-DN conjugates were synthesized using EDC as an activation agent of the carboxyl groups on HA chains, based on the procedure proposed by Lee and co-workers [4] Briefly, 1g of HA was dissolved in 100 mL of phosphate buffered saline (PBS) solution and the pH was adjusted to 5.5 with an hydrochloric acid (HCl) aqueous solution. The solution was purged with nitrogen for 30 minutes. Then, 338 mg of EDC and 474 mg of DN were added and the pH of the reaction solution was maintained at 5.5 for 2 hours. Unreacted chemicals and urea byproducts were removed by extensive dialysis, and afterwards, the conjugate was lyophilized. In order to avoid oxidation, the conjugate was stored at 4°C in a desiccator under vacuum and protected from the light.

Ultraviolet (UV) spectrophotometry and nuclear magnetic resonance (NMR) analysis of HA-DN: The degree of substitution of dopamine in the conjugate was determined using a UV-vis spectrophotometer (Shimadzu UV-2501 PC) and 1cm quartz cells. A solution of 1mg.mL^{-1} in 0.15M sodium chloride (NaCl) was prepared for the UV analysis. The samples were dissolved in deuterated water (D_2O) for 24 hours at concentrations of 1mg.mL^{-1} and 10 mg.mL^{-1}, for ^{1}H-NMR and ^{13}C-NMR analyses respectively. The results were obtained

using a spectrometer Varian Unity plus 300 and tetramethylsilane (TMS) as the internal standard. The spectra were recorded at 298 K and 300 MHz for ^{1}H-NMR analysis and 333 K and 75.4 MHz for ^{13}C-NMR analysis.

Quartz crystal microbalance (QCM-D): The formation of the multilayers of CHT and HA-DN was followed in situ by QCM-D (Q-Sense, E4 system). The mass change results from the variation of the normalized resonant frequency ($\Delta f/\upsilon$) of an oscillating quartz crystal when adsorption occurs on the surface and the dissipation factor (ΔD) provides a measure of the energy loss in the system. If a rigid mass is adsorbed onto the surface of the piezoelectric crystal there will be a decrease in the oscillation frequency.

For viscoelastic materials the adsorbed mass does not fully couple to the oscillation of the crystal and dampens the oscillation. QCM-D allows simultaneously measuring the changes in the resonant frequency and in the viscoelastic properties (dissipation) when a film is adsorbed at the crystal surface. The measurements can be conducted at the fundamental frequency and at several overtones number (υ = 1,3,5,...).

CHT was used as the polycation while HA-DN acted as the polyanion. Fresh polyelectrolyte solutions were prepared by dissolution of HA-DN and CHT in 0.15 M of NaCl to yield a final concentration of 0.5 mg.mL^{-1}.

The sensor crystals used were AT-cut quartz (Q-Sense) with gold plated polished electrodes. These crystals were excited at 5 MHz as well as at 15, 25, 35, 45 and 55 MHz corresponding to the 3rd, 5th, 7th, 9th and 11th overtones. The crystals were previously cleaned with sequential sonication for 3 minutes in acetone, ethanol and isopropanol and then dried with flowing nitrogen gas avoiding contamination prior to use. In order to ensure that the crystals are perfectly clean and therefore show a null frequency, all the experiments started with a NaCl baseline. Then, the polyelectrolyte solutions were injected into the cell during 10 minutes at a flow rate of 100 μL.min^{-1} using a peristaltic pump, beginning with CHT. A rinsing step of 10 minutes with the solvent was included between the adsorptions of each polyelectrolyte. The multilayer systems were assembled at pH 5.5. The pH was adjusted with HCl or NaOH. CHT/HA films were also prepared for comparison. Films with 10 layers were produced. All experiments were conducted at 25 °C. During the entire process $\Delta f/\upsilon$ and ΔD shifts were continuously recorded as a function of time.

The QCM-D response of a viscoelastic film, such as the films produced in this work, can be modeled using a Voigt based model [43] defined as a spring and dashpot in parallel under no slip conditions. The changes in the resonant frequency (equation 1) and in the dissipation factor (equation 2) according to Voinova and co-workers [43] are:

$$\Delta f \approx -\frac{1}{2\pi\rho_0 h_0}\left\{\frac{\eta_B}{\delta_B} + h_L\rho_L\omega - 2h_L\left(\frac{\eta_B}{\delta_B}\right)^2\frac{\eta_L\omega^2}{\mu_L^2+\omega^2\eta_L^2}\right\} \quad (1)$$

$$\Delta D \approx -\frac{1}{\pi_f\rho_0 h_0}\left\{\frac{\eta_B}{\delta_B} + 2h_L\left(\frac{\eta_B}{\delta_B}\right)^2\frac{\eta_L\omega}{\mu_L^2+\omega^2\eta_L^2}\right\} \quad (2)$$

where ω is the angular frequency of the oscillation and ρ_0 and h_0 are the density and thickness of the crystal, respectively. The viscosity of the bulk liquid is η_B, δ_B (= 2 $(\eta_B/\ \rho_B\ \omega)^{1/2}$) is the viscous penetration depth of the shear wave in the bulk liquid and ρ_B is the liquid´s density. The thickness, density, viscosity and elastic shear modulus of the adsorbed layer are represented by h_L, ρ_L, η_L and μ_L respectively.

Thickness measurements were performed using the Voigt viscoelastic model implemented in the QTools software from Q-Sense and also using an Ellipsometer equipment (SpecEl-2000-vis, Mikropack). Changes in resonant frequency and dissipation of the 7th overtone were fitted.

Surface characterization: The surface morphology of the samples was observed using a Leica Cambridge S-360 scanning electron microscope (SEM). All samples were coated with a conductive layer of sputtered gold. The SEM micrographs were taken at an accelerating voltage of 15 kV and at different magnifications.

The surface roughness of the samples was analyzed by atomic force microscope (AFM). AFM measurements were performed in a MultiMode STM microscope controlled by the NanoScope III from Digital Instruments system, operating in tapping mode at a frequency of 1 Hz. At least five measurements were performed in the different sample, which had been previously air-dried.

Water contact angle measurements were also performed at room temperature using an OCA 15 plus goniometer (DataPhysics Instruments). The values were obtained by the sessile drop method. The used liquid was ultrapure water and the drop volume was 3 μL. At least five measurements were carried out for each sample.

Adhesion tests: The adhesion properties of the multilayer films using glass as the substrate were evaluated using a universal mechanical testing machine (Instron model 5540, USA), following the ASTM D1002 standard. Fresh polyelectrolyte solutions were prepared by dissolution of HA and HA-DN in 0.15M of NaCl solution and CHT in 1% acetic acid, with a pH 5.5 to yield a final concentration of 0.5 mg.mL^{-1}.

Glass plaques with 3 mm of thickness were dipped alternately in the polyelectrolyte solutions during 10 minutes, beginning with CHT. A rinsing step of 5 minutes with 0.15 M NaCl solution was included between the adsorptions of each polyelectrolyte. Films with 10 bilayers were produced onto the surface of each glass plaque. Then, these films were washed until a neutral pH was achieved, in order to perform the mechanical tests at the same pH as the biological tests. Additionally, glass plaques coated with oxidized

films were prepared by immersion in a 5 mM sodium periodate solution during 2 hours, after the procedure previously described. The oxidized agent and oxidation time were chosen based on literature [48]. In fact, sodium periodate is an effective oxidizing agent of the catechol groups.

Glass plaques with a polydopamine coating were also prepared using the procedure described by Lee H. et al. [10]. Briefly, the glass slides were immersed into a dopamine solution (2 $mg.mL^{-1}$ in 10 mM tris-HCl, pH 8.5) at 25 °C. pH-induced oxidation changes the solution color to dark brown. The substrates were immersed in the polydopamine solution overnight. Then, the coated surfaces were rinsed with ultrapure water and dried at room temperature.

All the adhesion experiments were conducted at 25 °C. A pair of plates was put in contact and covered areas with 10 x 20 mm^2 were superimposed and maintained at 40 °C overnight. Then, the bonded glass slides were placed on the testing machine and a crosshead speed of 5 $mm.min^{-1}$ was employed. The samples were stressed until enough force was applied to trigger their detachment and pull them apart. The lap shear bonding strength was then determined from the maximum of the force–deformation curve obtained. The average and standard deviations were determined using the results from five samples.

Evaluation of cell behavior: Two cell lines, namely, a mouse lung fibroblastic cell line (L929) and a human primary osteosarcoma cell line (SaOs-2), were obtained from European Collection of cell Cultures (ECA CC, UK). The cells were cultured with low glucose DMEM supplemented with 3.7 $mg.mL^{-1}$ sodium bicarbonate, 10% FBS, and 1% penicillin–streptomycin at pH 7.4. The cells were grown in 75 cm^2 tissue culture flasks and incubated at 37 °C in a humidified air atmosphere of 5% CO_2. The medium was changed every 3–4 days. At 90% of confluence, cells grown in tissue culture flasks were washed with PBS and subsequently detached by a chemical procedure with 0.05% trypsin-EDTA solution for 5 min at 37 °C in a humidified air atmosphere of 5% CO_2. To inactivate the trypsin effect, cell culture medium was added. The cells were then centrifuged at 300 g and 25 °C for 5 min and the medium was decanted.

Prior to cell seeding, the samples were sterilized by UV radiation for 1h. 30 µL of supplemented DMEM containing a cell suspension with 5×10^3 cells was added to a 10 bilayered CHT/HA-DN film, the respective negative control CHT/HA, the positive control (cover glasses) and polydopamine coated cover glasses, also used as a control (in triplicate). The polydopamine coating was performed adopting the same conditions used for the mechanical adhesion tests. Then, the samples were incubated at 37 °C in a humidified air atmosphere of 5% CO_2. After 4 hours supplemented DMEM was added.

To obtain fluorescent images, DAPI fluorescent assay was performed at each time culture period. DAPI stains preferentially double-stranded DNA by delineating cells nuclei in blue. Prior to staining, at each

time point, the culture medium was removed and 10% formalin was added to each well (in triplicate). After 1 hour at room temperature, formalin was removed and the samples were washed with phosphate buffer saline (PBS). 1 mL of PBS containing 1 µL of DAPI was added to each well. After 1 hour at room temperature protected from light, samples were washed three times with PBS and immediately visualized in the dark by fluorescence microscopy. ImageJ software was used to quantify the cells adhered on the multilayer films.

The samples were tested for cytotoxicity using alamarBlue colorimetric assay. Briefly, the samples with adhered cells were placed in a non-treated surface 24-well cell culture plate (in triplicate) and incubated at 37 °C and 5% CO_2. At 1, 3, 7, 14 and 21 days of culture, the assay was performed, protected from light. The culture medium was removed and 500 µL of supplemented DMEM containing alamarBlue solution with a dilution ratio of 1:10 was added to each well. The samples were then incubated in the dark at 37 °C and 5% CO_2. After 3 h, 100 µL of each well (in triplicate) was transferred to a 96-well plate. The absorbance was monitored at 570 nm and 600 nm using a microplate reader (Synergy HT, Bio-TEK).

A DNA quantification assay was also performed in order to evaluate cell proliferation in the samples. For each culture time, the wells of the plate (the same samples used in viability assay) were extensively washed with PBS, and then, 1 mL of ultrapure sterile water was added to each well. The well plate was placed in a shaking water bath at 37 °C for 1 hour. Ultimately, the plates were immediately stored at −80 °C until use. The quantification of total DNA was determined after cell lysis, according to the manufacturer's description. After transferring each solution to a 96-well white opaque plate (in triplicates), the plate was incubated at room temperature protected from light for 10 minutes. The standard curve for DNA analysis was generated with provided DNA from the assay kit. Fluorescence was read at excitation of 485/20 nm and emission of 528/20 nm using a microplate reader (Synergy HT, BioTek, U.S.A.).

Statistical Analysis was performed to analyze significant differences between formulations. Data of viability and DNA were grouped by formulation, namely, Control (positive control), polydopa, CHT/HA-DN, and CHT/HA (negative control), to assess time-course significant differences of each formulation. Statistical analysis of both data cases was performed using two-way analysis of variance (ANOVA) with Bonferroni post-test using GraphPad Prism 5.0 software. The adopted nomenclature was the following: statistical differences in grouped by time point analysis were marked with (*), (**) and (***), which stand for p-value < 0.05; $p < 0.01$ and $p < 0.001$, respectively. For evaluate the statistical differences relating to the time point before, symbols as # and § were used to represent CHT/HA and CHT/HA-DN groups respectively.

Single symbol (# and §) represent $p < 0.05$; double symbols (## and§§) $p < 0.01$ and triple symbols (### and §§§) $p < 0.001$. All results were presented as mean ± standard deviation.

3.6 Acknowledgements

The authors want to acknowledge the COST Action TD0906 - Biological adhesives: from biology to biomimetics. The authors also acknowledge the financial support from the Fundação para a Ciência e para a Tecnologia through the Ph.D. grants with the references SFRH/BD/73119/2010 and SFRH/BD/69529/2010. G.G. Ferrer acknowledges the support of the Spanish Ministry of Science and Innovation for the mobility grant JC2008-00135. G. Botelho acknowledges the NMR portuguese network (PTNMR, Bruker Avance III 400-Univ. Minho).

3.7 References

[1] Z. Ma, Z. Mao, C. Gao, Surface Modification And Property Analysis Of Biomedical Polymers Used For Tissue Engineering, Colloids Surface B Biointerfaces, 60 (2007) 137-157.

[2] N.M. Alves, I. Pashkuleva, R.L. Reis, J.F. Mano, Controlling Cell Behavior Through The Design Of Polymer Surfaces, Small, 6 (2010) 2208-2220.

[3] H. Shin, S. Jo, A.G. Mikos, Biomimetic Materials For Tissue Engineering, Biomaterials, 24 (2003) 4353-4364.

[4] H. Lee, Y. Lee, A.R. Statz, J. Rho, T.G. Park, P.B. Messersmith, Substrate-Independent Layer-By-Layer Assembly By Using Mussel-Adhesive-Inspired Polymers, Advanced Materials, 20 (2008) 1619-1623.

[5] J.H. Waite, M.L. Tanzer, Polyphenolic Substance Of Mytilus-Edulis - Novel Adhesive Containing L-Dopa And Hydroxyproline, Science, 212 (1981) 1038-1040.

[6] Y. Lee, H. Lee, Y.B. Kim, J. Kim, T. Hyeon, H. Park, P.B. Messersmith, T.G. Park, Bioinspired Surface Immobilization Of Hyaluronic Acid On Monodisperse Magnetite Nanocrystals For Targeted Cancer Imaging, Advanced Materials, 20 (2008) 4154-4157.

[7] A.I. Neto, H.J. Meredith, C.L. Jenkins, J.J. Wilker, J.F. Mano, Combining Biomimetic Principles From The Lotus Leaf And Mussel Adhesive: Polystyrene Films With Superhydrophobic And Adhesive Layers, Rsc Advances, 3 (2013) 9352-9356.

[8] M.E. Yu, T.J. Deming, Synthetic Polypeptide Mimics Of Marine Adhesives, Macromolecules, 31 (1998) 4739-4745.

[9] T.J. Deming, Mussel Byssus And Biomolecular Materials, Current Opinion In Chemical Biology, 3 (1999) 100-105.

[10] H. Lee, S.M. Dellatore, W.M. Miller, P.B. Messersmith, Mussel-Inspired Surface Chemistry For Multifunctional Coatings, Science, 318 (2007) 426-430.

[11] Y. Lee, H.J. Chung, S. Yeo, C.H. Ahn, H. Lee, P.B. Messersmith, T.G. Park, Thermo-Sensitive, Injectable, And Tissue Adhesive Sol-Gel Transition Hyaluronic Acid/Pluronic Composite Hydrogels Prepared From Bio-Inspired Catechol-Thiol Reaction, Soft Matter, 6 (2010) 977-983.

[12] T.H. Anderson, J. Yu, A. Estrada, M.U. Hammer, J.H. Waite, J.N. Israelachvili, The Contribution Of Dopa To Substrate-Peptide Adhesion And Internal Cohesion Of Mussel-Inspired Synthetic Peptide Films, Advanced Functional Materials, 20 (2010) 4196-4205.

[13] T. Serizawa, M. Yamaguchi, T. Matsuyama, M. Akashi, Alternating Bioactivity Of Polymeric Layer-By-Layer Assemblies: Anti- Vs Procoagulation Of Human Blood On Chitosan And Dextran Sulfate Layers, Biomacromolecules, 1 (2000) 306-309.

[14] C. Picart, P. Lavalle, P. Hubert, F.J.G. Cuisinier, G. Decher, P. Schaaf, J.C. Voegel, Buildup Mechanism For Poly(L-Lysine)/Hyaluronic Acid Films Onto A Solid Surface, Langmuir, 17 (2001) 7414-7424.

[15] X. Qiu, S. Leporatti, E. Donath, H. Möhwald, Studies On The Drug Release Properties Of Polysaccharide Multilayers Encapsulated Ibuprofen Microparticles, Langmuir, 17 (2001) 5375-5380.

[16] J. Zhang, B. Senger, D. Vautier, C. Picart, P. Schaaf, J.C. Voegel, P. Lavalle, Natural Polyelectrolyte Films Based On Layer-By Layer Deposition Of Collagen And Hyaluronic Acid, Biomaterials, 26 (2005) 3353-3361.

[17] Y. Liu, T. He, C. Gao, Surface Modification Of Poly(Ethylene Terephthalate) Via Hydrolysis And Layer-By-Layer Assembly Of Chitosan And Chondroitin Sulfate To Construct Cytocompatible Layer For Human Endothelial Cells, Colloids And Surf B Biointerfaces, 46 (2005) 117-126.

[18] A. Schneider, C. Vodouhe, L. Richert, G. Francius, E. Le Guen, P. Schaaf, J.C. Voegel, B. Frisch, C. Picart, Multifunctional Polyelectrolyte Multilayer Films: Combining Mechanical Resistance, Biodegradability, And Bioactivity, Biomacromolecules, 8 (2007) 139-145.

[19] Z.R. Wu, J. Ma, B.F. Liu, Q.Y. Xu, F.Z. Cui, Layer-By-Layer Assembly Of Polyelectrolyte Films Improving Cytocompatibility To Neural Cells, Journal Of Biomedical Materials Research Part A, 81a (2007) 355-362.

[20] C.R. Wittmer, J.A. Phelps, W.M. Saltzman, P.R. Van Tassel, Fibronectin Terminated Multilayer Films: Protein Adsorption And Cell Attachment Studies, Biomaterials, 28 (2007) 851-860.

[21] J.R.E. Fraser, T.C. Laurent, U.B.G. Laurent, Hyaluronan: Its Nature, Distribution, Functions And Turnover, Journal Of Internal Medicine, 242 (1997) 27-33.

[22] W.G. Pitt, R.N. Morris, M.L. Mason, M.W. Hall, Y. Luo, G.D. Prestwich, Attachment Of Hyaluronan To Metallic Surfaces, Journal Of Biomedical Materials Research Part A, 68a (2004) 95-106.

[23] L. Lapcik, L. Lapcik, S. De Smedt, J. Demeester, P. Chabrecek, Hyaluronan: Preparation, Structure, Properties, And Applications, Chemical Reviews, 98 (1998) 2663-2684.

[24] P.H. Chua, K.G. Neoh, E.T. Kang, W. Wang, Surface Functionalization Of Titanium With Hyaluronic Acid/Chitosan Polyelectrolyte Multilayers And Rgd For Promoting Osteoblast Functions And Inhibiting Bacterial Adhesion, Biomaterials, 29 (2008) 1412-1421.

[25] M. Rinaudo, M. Milas, P. Ledung, Characterization Of Chitosan - Influence Of Ionic-Strength And Degree Of Acetylation On Chain Expansion, International Journal Of Biological Macromolecules, 15 (1993) 281-285.

[26] L.L. Hench, Biomaterials: A Forecast For The Future, Biomaterials, 19 (1998) 1419-1423.

[27] R. Jayakumar, M. Prabaharan, R.L. Reis, J.F. Mano, Graft Copolymerized Chitosan—Present Status And Applications, Carbohydrate Polymers, 62 (2005) 142-158.

[28] A. Charlot, V. Sciannaméa, S. Lenoir, E. Faure, R. Jérôme, C. Jérôme, C. Van De Weerdt, J. Martial, C. Archambeau, N. Willet, A.-S. Duwez, C.-A. Fustin, C. Detrembleur, All-In-One Strategy For The Fabrication Of Antimicrobial Biomimetic Films On Stainless Steel, Journal Of Materials Chemistry, 19 (2009) 4117.

[29] X.M. Zhang, Z.Y. Li, X.B. Yuan, Z.D. Cui, X.J. Yang, Fabrication Of Dopamine-Modified Hyaluronic Acid/Chitosan Multilayers On Titanium Alloy By Layer-By-Layer Self-Assembly For Promoting Osteoblast Growth, Applied Surface Science, 284 (2013) 732-737.

[30] T. Segura, B.C. Anderson, P.H. Chung, R.E. Webber, K.R. Shull, L.D. Shea, Crosslinked Hyaluronic Acid Hydrogels: A Strategy To Functionalize And Pattern, Biomaterials, 26 (2005) 359-371.

[31] J. Baier Leach, K.A. Bivens, C.W. Patrick, Jr., C.E. Schmidt, Photocrosslinked Hyaluronic Acid Hydrogels: Natural, Biodegradable Tissue Engineering Scaffolds, Biotechnology And Bioengineering, 82 (2003) 578-589.

[32] Z. Bezáková, M. Hermannová, E. Dřímalová, A. Malovíková, A. Ebringerová, V. Velebný, Effect Of Microwave Irradiation On The Molecular And Structural Properties Of Hyaluronan, Carbohydrate Polymers, 73 (2008) 640-646.

[33] D.D. Mueller, T.D. Morgan, J.D. Wassenberg, T.L. Hopkins, K.J. Kramer, H-1 And C-13 Nmr Of 3-O And 4-O Conjugates Of Dopamine And Other Catecholamines, Bioconjugate Chemistry, 4 (1993) 47-53.

[34] Y. Tokita, A. Okamoto, Hydrolytic Degradation Of Hyaluronic-Acid, Polymer Degradation And Stability, 48 (1995) 269-273.

[35] B.J. Kvam, M. Atzori, R. Toffanin, S. Paoletti, F. Biviano, H-1-Nmr And C-13-Nmr Studies Of Solutions Of Hyaluronic-Acid Esters And Salts In Methyl Sulfoxide - Comparison Of Hydrogen-Bond Patterns And Conformational Behavior, Carbohydrate Research, 230 (1992) 1-13.

[36] A.J. Metta-Magana, R. Reyes-Martinez, H. Tlahuext, Crystal Structure And Nmr Spectroscopy Of Aldonamides Derived From D-Glycero-D-Gulo-Heptono-1,4-Lactone, Carbohydrate Research, 342 (2007) 243-253.

[37] S.-M. Chen, K.-T. Peng, The Electrochemical Properties Of Dopamine, Epinephrine, Norepinephrine, And Their Electrocatalytic Reactions On Cobalt(Ii) Hexacyanoferrate Films, Journal Of Electroanalytical Chemistry, 547 (2003) 179-189.

[38] L. Richert, P. Lavalle, E. Payan, X.Z. Shu, G.D. Prestwich, J.F. Stoltz, P. Schaaf, J.C. Voegel, C. Picart, Layer By Layer Buildup Of Polysaccharide Films: Physical Chemistry And Cellular Adhesion Aspects, Langmuir, 20 (2004) 448-458.

[39] O. Etienne, A. Schneider, C. Taddei, L. Richert, P. Schaaf, J.C. Voegel, C. Egles, C. Picart, Degradability Of Polysaccharides Multilayer Films In The Oral Environment: An In Vitro And In Vivo Study, Biomacromolecules, 6 (2005) 726-733.

[40] R.A. Mcaloney, M. Sinyor, V. Dudnik, M.C. Goh, Atomic Force Microscopy Studies Of Salt Effects On Polyelectrolyte Multilayer Film Morphology, Langmuir, 17 (2001) 6655-6663.

[41] J. Ruths, F. Essler, G. Decher, H. Riegler, Polyelectrolytes I: Polyanion/Polycation Multilayers At The Air/Monolayer/Water Interface As Elements For Quantitative Polymer Adsorption Studies And Preparation Of Hetero-Superlattices On Solid Surfaces, Langmuir, 16 (2000) 8871-8878.

[42] S.H. Ku, J. Ryu, S.K. Hong, H. Lee, C.B. Park, General Functionalization Route For Cell Adhesion On Non-Wetting Surfaces, Biomaterials, 31 (2010) 2535-2541.

[43] M.V. Voinova, M. Rodahl, M. Jonson, B. Kasemo, Viscoelastic Acoustic Response Of Layered Polymer Films At Fluid-Solid Interfaces: Continuum Mechanics Approach, Physica Scripta, 59 (1999) 391-396.

[44] M. Edvardsson, S. Svedhem, G. Wang, R. Richter, M. Rodahl, B. Kasemo, Qcm-D And Reflectometry Instrument: Applications To Supported Lipid Structures And Their Biomolecular Interactions, Analytical Chemistry, 81 (2009) 349-361.

[45] G.V. Martins, J.F. Mano, N.M. Alves, Nanostructured Self-Assembled Films Containing Chitosan Fabricated At Neutral Ph, Carbohydrate Polymers, 80 (2010) 570-573.

[46] G.V. Martins, E.G. Merino, J.F. Mano, N.M. Alves, Crosslink Effect And Albumin Adsorption Onto Chitosan/Alginate Multilayered Systems: An In Situ Qcm-D Study, Macromolecular Bioscience, 10 (2010) 1444-1455.

[47] K. Yamada, T.H. Chen, G. Kumar, O. Vesnovsky, L.D.T. Topoleski, G.F. Payne, Chitosan Based Water-Resistant Adhesive. Analogy To Mussel Glue, Biomacromolecules, 1 (2000) 252-258.

[48] B.P. Lee, J.L. Dalsin, P.B. Messersmith, Synthesis And Gelation Of Dopa-Modified Poly(Ethylene Glycol) Hydrogels, Biomacromolecules, 3 (2002) 1038-1047.

[49] S.H. Ku, C.B. Park, Human Endothelial Cell Growth On Mussel-Inspired Nanofiber Scaffold For Vascular Tissue Engineering, Biomaterials, 31 (2010) 9431-9437.

[50] H. Lee, J. Rho, P.B. Messersmith, Facile Conjugation Of Biomolecules Onto Surfaces Via Mussel Adhesive Protein Inspired Coatings, Advanced Materials, 21 (2009) 431-434.

[51] H. Lee, N.F. Scherer, P.B. Messersmith, Single-Molecule Mechanics Of Mussel Adhesion, Proceedings Of The National Academy Of Sciences Of The United States Of America, 103 (2006) 12999-13003.

CHAPTER 4. COMBINING BIOMIMETIC PRINCIPLES FROM THE LOTUS LEAF AND MUSSEL ADHESIVE: POLYSTYRENE FILMS WITH SUPERHYDROPHOBIC AND ADHESIVE LAYERS *

4.1 Abstract

Lotus leaves are well known for their extremely water repellent surfaces. Marine mussels are also a popular research topic when considering biological adhesives. Both organisms have inspired the development of several biomimetic materials. Herein we describe a two-sided film made almost entirely from polystyrene onto which the properties of both lotus leaves and mussel adhesive are incorporated. On one side of the film, imparting micrometer and nanometer scale hierarchical roughness yields superhydrophobicity and water repellency, which facilitates rapid fluid flow. The other side of the film is modified with a copolymer mimic of 3,4-dihydroxyphenylalanine (DOPA)-containing mussel adhesive proteins. This copolymer incorporates 3,4-dihydroxystyrene, to represent DOPA, randomly into a polystyrene host polymer. The flexibility of the polystyrene backing film enabled rolling of the assembly into a tubular shape. Inside the polystyrene tube was the superhydrophobic lotus mimic. The mussel adhesive mimic, on the outer layer, was used to glue the tube to itself, thus maintaining the tubular shape. The film was also successfully glued to a variety of flat substrates. These two-dimensional and three-dimensional assemblies can be used to direct and localize the flow of fluids, with partitioning between superhydrophobic and relatively hydrophilic regions. Such assemblies may facilitate the design of liquid transport for industrial and biomedical devices.

* *Neto A. I., Meredith H. J., Jenkins C. L., Wilker J. J., and Mano J. F. Combining Biomimetic Principles from the Lotus Leaf and Mussel Adhesive: Polystyrene Films with Superhydrophobic and Adhesive Layers.* ***RSC Advances****, 3, 9352-9356, 2013.*

4.2 Introduction

Nature has inspired the development of several novel materials for single applications [1, 2]. Examples include bioinspired robots for neuroscience [3], self-cleaning surfaces modeled after plants and insects [4], shape memory polymers similar to spider silk [5], high strength adhesives analogous to geckos and mussels [6, 7], self-healing polymer composites based on vascular networks [8], and scaffolds for tissue engineering much like the extracellular matrix [9]. Incorporation of multiple biomimetic principles into one system is less common [10-16]. By integrating properties from multiple organisms we are able to create an evolved system that broadens the scope of materials as well as the potential applications. Here we present two-dimensional and three-dimensional assemblies that simultaneously display superhydrophobic surfaces similar to the lotus leaf and the bonding properties of mussel adhesive proteins (Figure 4.1).

4.2.1 Lotus leaf

The extreme water repellent behavior displayed by lotus leaves is an example of design elegance in nature. This superhydrophobic effect is a result of both the low surface energy of a waxy coating and a hierarchical roughness at the micrometer and nanometer scales [1, 4]. Several other plant species also exhibit superhydrophobicity, including banana tree leaves, rice leaves, and red rose petals (Figure 4.1A) [1, 17]. These properties have inspired the fabrication of several synthetic superhydrophobic surfaces [18-21]. Phase-separation methodologies and UV/Ozone (UVO) irradiation are both methods that are able to alter surface wettability, thus give rise to superhydrophobic and superhydrophilic properties, respectively [22, 23].

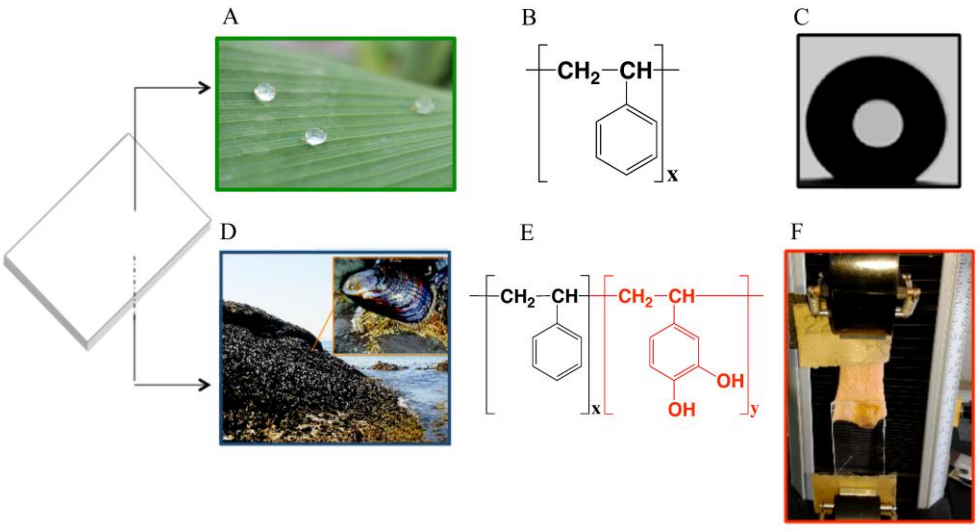

Figure 4.1 Schematic representation of the sequential steps used to create asymmetric polystyrene films exhibiting: (i) the natural superhydrophobic surface (A) with extreme water-based liquids repellency (C) in one region and (ii) mussel-inspired

(D) macromolecules (E) with high strength adhesive features (F) in another region. Films were modified to produce superhydrophobic surfaces made of roughened polystyrene (B) and adhesive surfaces using a biomimetic polystyrene-based copolymer (E).

While substrates displaying the superhydrophobic effect are present in various fields, applications in medicine are scarce. Within a biomedical context, this superhydrophobic concept may be useful when constructing artificial blood vessels and urethral implants. In such vascular applications, superhydrophobic surfaces may prevent cellular and platelet adsorption [24-26]. These superhydrophobic surface modifications can improve the *in vivo* performance of expanded poly(tetrafluoroethylene) (ePTFE) vascular grafts [27]. Prior reports state that water repellency prevented the adhesion and proliferation of stem cells when compared with smoother surfaces [28]. We can envision that biomimetic superhydrophobicity may also be of use for *ex vivo* devices such as plastics for storage or mixture of liquids and plastics for micropipettes within which sample adhesion is not desired.

4.2.2 Mussel adhesive

Proteins secreted by mussels are cross-linked to generate an impressive adhesive that can bond strongly to virtually all inorganic and organic surfaces, even in wet environments (Figure 4.1 D) [29]. These unique proteins contain the unusual amino acid 3,4-dihydroxyphenylalanine (DOPA), which is formed by posttranslational modification of tyrosine [30]. Cross-linking of DOPA by oxidation [31, 32], metal binding with redox reactions [33-35], or enzymatic mechanisms [31, 32, 36], couples the proteins to cure the glue and provide high strength adhesion.

There is an expanding class of synthetic polymers that incorporate mussel adhesion chemistry [37]. The use of different DOPA-modified polymers allows the development of new antifouling coatings [38-41], hydrogels [42, 43], loaded nanocapsules [44, 45], and free radical scavengers [46], among several other applications [47-50]. Here we are using a simple polystyrene-based copolymer mimic of mussel adhesive proteins (Figure 4.1 E). This biomimetic polymer, poly(3,4-dihydroxystyrene-*co*-styrene), exhibits significant bulk adhesion [51, 52]. The styrene and 3,4- dihydroxystyrene monomers are distributed randomly throughout the polystyrene host [51], which is analogous to how DOPA residues are located within mussel adhesive proteins [53]. By working with a mussel adhesive mimic built from polystyrene, we are then able to combine technologies with other polystyrene-based materials.

4.2.3 Combining biomimetic materials

One way to alter the function of materials is by constructing specific patterns. This approach has been demonstrated using soft lithography to create superhydro*philic* patterns on a superhydro*phobic* surface [13]. Another design strategy is to bring two biomimetic concepts together into one material. This field, however, is less well developed, with only a limited selection of examples presented so far [10-16].
Herein, we demonstrate that two biomimetic concepts can be used together for developing devices with multifunctional capabilities. The superhydrophobic properties of a lotus leaf (Figure 4.1 C) is joined with the adhesive bonding of marine mussels (Figure 4.1 F). Polystyrene provides the starting point for both systems (Figure 4.1 B). Derivatization of the polystyrene / film to exhibit superhydrophobicity yields materials that restrict the flow of liquids to within specific regions and facilitates transport through others. These polystyrene membranes with both superhydrophobic and adhesive domains can also be fashioned into three-dimensional tube structures by employing the adhesion to provide bonding for construction. Such materials may provide the basis for microfluidic devices as well as synthetic blood or fluid flow vessels.

4.3 Experimental section

Commercial polystyrene sheets of 0.19 mm thickness were purchased from Goodfellow, UK. These sheets provided the film templates. A one step phase separation methodology was used to modify one of the smooth sides of the polymeric film to exhibit superhydrophobicity by incorporating hierarchical roughness [23]. This topology was achieved by first creating a pre-solution of 70% v/v polystyrene (injection molding grade) in tetrahydrofuran (Fluka). Then 1.4 mL of ethanol (Panreac) was stirred into 2 mL
of the polystyrene pre-solution. One side of the polystyrene sheet was then coated with this mixture. Following deposition, the modified sheet was immersed in ethanol for 1 min to induce polymer precipitation. A rough and porous surface resulted, thereby providing superhydrophobic properties. The assembly was dried at ambient temperature.
Surface morphology of the superhydrophobic samples was analysed by scanning electron microscopy (Leica Cambridge, UK). Surface wettability was assessed with contact angle measurements using an OCA 15+ goniometer (DataPhysics, Germany). Static water contact angle (WCA) measurements were carried out with the sessile drop method.

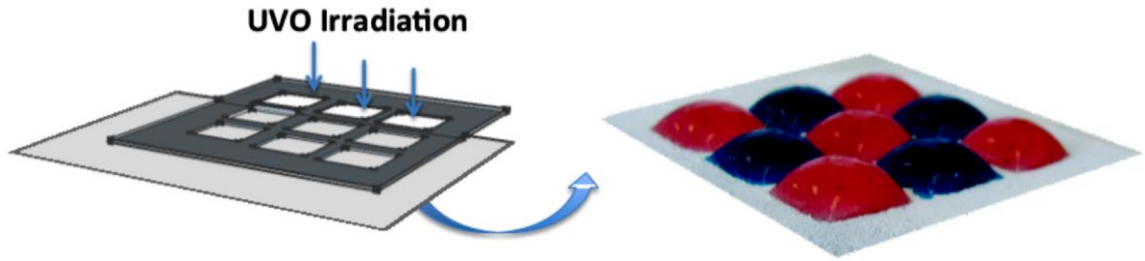

Figure 4.2 Patterns of superhydrophobic polystyrene surround UVO-modified polystyrene, which is hydrophilic, relatively speaking. This pattern confines water to only the regions surrounded by superhydrophobicity. In this particular example, volumes of colored water are completely restrained within squared-shaped zones.

Patterned superhydrophobic surfaces with hydrophilic regions were prepared using a mask with open areas of 1 x 1 cm^2 (Figure 4.2). The superhydrophobic substrates were covered with the mask and exposed to 10 min of UVO irradiation (Bioforce, Nanoscience) using a high intensity mercury vapour lamp (254 nm). The surface modification occurred only at the open mask regions. The resulting surface contained lines of superhydrophobic polystyrene surrounding the 1 x 1 cm^2 regions of UVO-modified polystyrene that was more hydrophilic.

An adhesive copolymer, poly(3,4-dihydroxystyrene-*co*-styrene), containing 75 mole percent styrene and 25 mole percent of 3,4-dihydroxystyrene monomers was synthesized according to methods reported previously [51]. This copolymer was dissolved in a 1:1 volume ratio of acetone:dichloromethane by adding 0.30 g of polymer per 1 mL of solvent. The tetrabutylammonium periodate, $(N(C_4H_9)_4)(IO_4)$, cross-linker was prepared according to a literature procedure [54]. The same solvent (1 mL) was used to dissolve 0.29 g of $(N(C_4H_9)_4)(IO_4)$. This cross-linker was added to the adhesive polymer in a 3:1 ratio of 3,4-dihydroxystyrene: $(IO_4)^-$. The polymer solution (21 μL) was placed on the opposite side of the superhydrophobic substrate. The cross-linker (7 μL) was then added dropwise to the polymer solution to induce cross-linking.

Adhesion strength for the biomimetic copolymer was determined using a universal mechanical testing system (Instron 5540, USA). Smooth polystyrene was bonded to steel, glass, Teflon (polytetrafluoroethylene) and pig skin in a lap shear configuration using the copolymer (Figure 4.4 A). Each assembly, with an overlap area of 2.5 x 1.0 cm^2, was cured at room temperature for 24 hours. The samples were pulled apart in shear until failure at a crosshead speed of 1.3 mm/min following the ASTM D1002-05 standard [55]. The average force to break and standard deviations were determined using five bonded substrates of each type.

4.4 Results and discussion

4.4.1 Superhydrophobic and hydrophilic patterning

Microfluidic systems have been reported previously, taking advantage of superhydrophobic surfaces to form channels of low friction fluid flow [23]. In one recent example, hydrophilic polydopamine was patterned atop a superhydrophobic sheet in order to direct the flow of water droplets [13]. Consequently, we were inspired to form patterns in which the localization of aqueous solutions could be controlled by judicious placement of the superhydrophobic and hydrophilic regions. This enabled us to form an arrangement of these properties on one surface, controlled within XY space. Figure 4.2 shows how UVO patterning was used to create a surface upon which hydrophilic features were surrounded by superhydrophobic areas. The resulting surfaces control liquid deposition into the patterned spaces. These regions can sustain significant volumes of liquids relative to the footprint size, and are well confined by superhydrophobic regions.

4.4.2 Combining lotus leaves and mussel adhesive

In addition to patterning, asymmetric surfaces could be deposited onto a polystyrene film. One side of the film was modified structurally to contain the superhydrophobic features similar to the lotus leaf. A mussel mimetic adhesive copolymer was deposited onto the other side. In doing so, two unique biomimetic polystyrene-based materials were combined onto one flexible membrane.

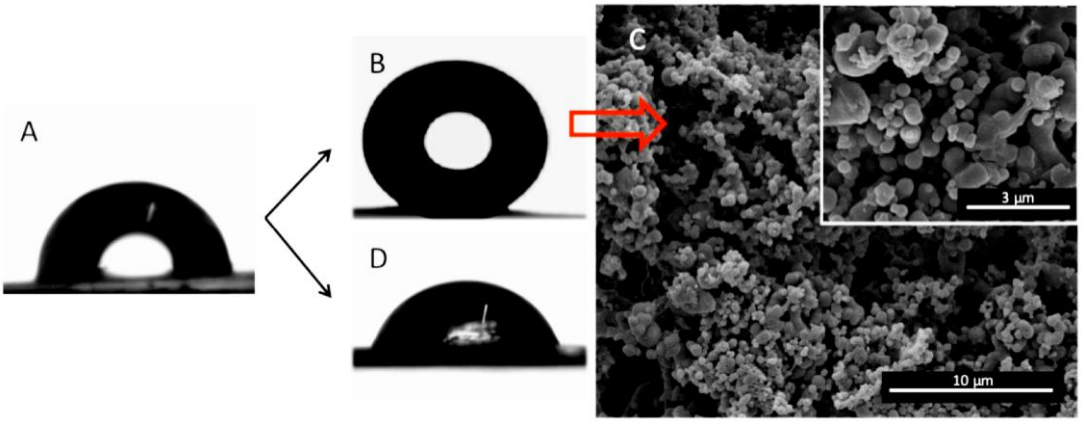

Figure 4.3 (A) Water droplet on smooth polystyrene; (B) water droplet on superhydrophobic polystyrene surface with (C) rough morphology at both micro and nano scales; (D) water droplet on a polystyrene surface coated with the biomimetic adhesive copolymer.

A water contact angle of 98.9° ± 1.1° was found for the unmodified polystyrene surface (Figure 4.3 A). When the solution of adhesive poly(3,4-dihydroxystyrene-*co*-styrene) was placed onto the polystyrene film,

the water contact angle decreased to 73.8° ± 1.05° (Figure 4.3 D). The presence of pendant catechol groups in the copolymer is the likely source of this increase in hydrophilicity. After modifying the polystyrene surface to introduce superhydrophobicity, the water contact angle increased to 156.2° ± 0.3° (Figure 4.3 B). Scanning electron microscopy shows that this surface is made up of nanometer-sized spheres (50 – 200 nm), agglomerated to form larger structures on the micrometer scale (Figure 4.3 C). Qualitatively, we observed that with such surfaces water droplets roll easily off, perhaps a result of both this hierarchical roughness and the low surface energy of the underlying polystyrene

4.4.3 Adhesive bonding

Lap shear adhesion testing was conducted to evaluate the bonding performance of modified polystyrene films when attached to a variety of substrates.

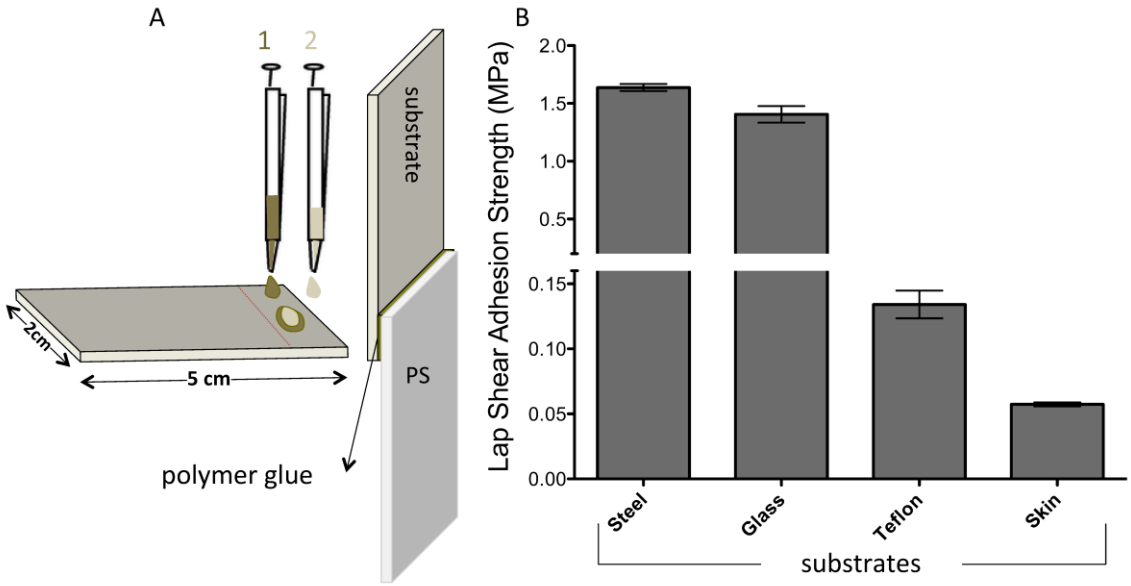

Figure 4.4 Adhesion tests of the polystyrene film coated with poly(3,4-dihydroxystyrene-*co*-styrene) on distinct substrates. A) Drops of (1) copolymer and (2) cross-linker solutions were placed onto smooth polystyrene surfaces in a lap shear configuration. B) Adhesion strength performance of different substrates (steel, glass, Teflon and pig skin) glued to polystyrene membrane backings.

Lap shear adhesion testing was conducted to evaluate the bonding performance of modified polystyrene films when attached to a variety of substrates. High adhesion strength for the copolymer alone, without the polystyrene backings, was recently reported on several surfaces and shown to be comparable to commercial products such as cyanoacrylate Krazy Glue [52]. Addition of periodate $(IO_4)^-$ induces crosslinking of poly(3,4-dihydroxystyrene-*co*-styrene), further enhancing the adhesion properties of the copolymer [52]. Mechanical testing here revealed that the polystyrene film modified with poly(3,4-

dihydroxystyrene-*co*-styrene) was able to adhere to all surfaces (Figure 4.4 B). The film adhered most strongly to steel and glass substrates, which present somewhat similar strengths of 1.64 ± 0.05 MPa and 1.40 ± 0.12 MPa, respectively (Figure 4.4 B). The bond strengths for Teflon (0.13 ± 0.01 MPa) and pig skin (0.05 ± 0.002 MPa) were lower. The low surface energy of Teflon and the wet nature of pig skin makes bonding to these substrates difficult.

4.4.4 Constructing three-dimensional assemblies

Taking into account flexibility of the starting polystyrene backing, we were able to change the film geometry and form three-dimensional shapes using bonding from the mussel mimic. Changing thickness of the initial polystyrene films also offered control over flexibility. A tube was constructed containing the superhydrophobic inner wall. The assembly was made by rolling the film over itself, with the superhydrophobic surface on the inside and the adhesive layer on the outside. The adhesive layer was overlapped with itself, thus holding the assembly together. No tape or external bracing was needed to maintain this shape. The superhydrophobic inner layer allowed water-based liquid to flow easily, with very little drag. Figure 4.5 shows colored drops of water rolling rapidly through the tube interior, without wetting the superhydrophobic surface.

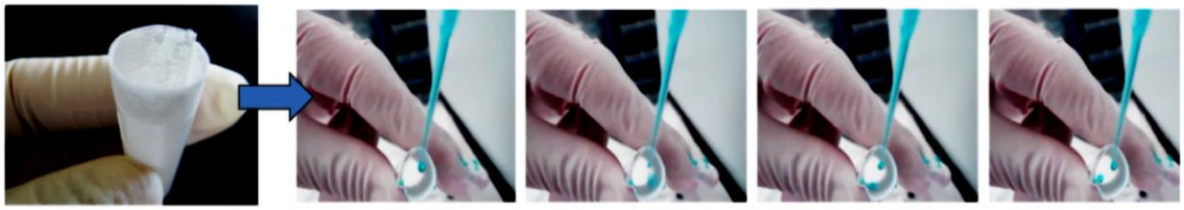

Figure 4.5 Bioinspired asymmetric films with superhydrophobic features in one region and adhesive properties in another region. A tubular structure was formed by curling of the superhydrophobic inner membrane surface until joining of the outside adhesive region. Colored drops show rapid, non-wetting water rolling over the superhydrophobic area.

4.5 Conclusions

Polystyrene has been derivatized in two ways to mimic the properties of both a superhydrophobic lotus leaf and a strongly adhering mussel. These characteristics were combined into a three-dimensional tube system allowing fluid flow much like a low resistance blood vessel. Superhydrophobic and hydrophilic features could also be patterned onto one surface, thereby constraining the localization of water. We hope that these efforts will contribute to future advances in materials development, especially the biomedical management of fluid flow, by showing that multiple bioinspired approaches can be combined into one system.

4.6 Acknowledgements

We thank the United States Office of Naval Research for support of this work. We would also like to thank Debra Lubelski and Kevin Chaput for their assistance with images.

4.7 References

[1] K. Liu, L. Jiang, Multifunctional Integration: From Biological To Bio-Inspired Materials, Acs Nano, 5 (2011) 6786-6790.

[2] J.F. Mano, Biomimetic Approaches For Biomaterials Development, John Wiley & Sons, 2013.

[3] R. Pfeifer, M. Lungarella, F. Iida, Self-Organization, Embodiment, And Biologically Inspired Robotics, Science, 318 (2007) 1088-1093.

[4] S. Nishimoto, B. Bhushan, Bioinspired Self-Cleaning Surfaces With Superhydrophobicity, Superoleophobicity, And Superhydrophilicity, Rsc Advances, 3 (2013) 671-690.

[5] O. Emile, A. Le Floch, F. Vollrath, Biopolymers: Shape Memory In Spider Draglines, Nature, 440 (2006) 621-621.

[6] A.K. Geim, S. Dubonos, I. Grigorieva, K. Novoselov, A. Zhukov, S.Y. Shapoval, Microfabricated Adhesive Mimicking Gecko Foot-Hair, Nature Materials, 2 (2003) 461-463.

[7] A. Stepuk, J.G. Halter, A. Schaetz, R.N. Grass, W.J. Stark, Mussel-Inspired Load Bearing Metal–Polymer Glues, Chem. Commun., 48 (2012) 6238-6240.

[8] R. Trask, H. Williams, I. Bond, Self-Healing Polymer Composites: Mimicking Nature To Enhance Performance, Bioinspiration & Biomimetics, 2 (2007) P1.

[9] T.G. Kim, H. Shin, D.W. Lim, Biomimetic Scaffolds For Tissue Engineering, Advanced Functional Materials, 22 (2012) 2446-2468.

[10] H. Lee, B.P. Lee, P.B. Messersmith, A Reversible Wet/Dry Adhesive Inspired By Mussels And Geckos, Nature, 448 (2007) 338-341.

[11] F. Xia, L. Jiang, Bio-Inspired, Smart, Multiscale Interfacial Materials, Advanced Materials, 20 (2008) 2842-2858.

[12] W.L. Min, B. Jiang, P. Jiang, Bioinspired Self-Cleaning Antireflection Coatings, Advanced Materials, 20 (2008) 3914-3918.

[13] S.M. Kang, I. You, W.K. Cho, H.K. Shon, T.G. Lee, I.S. Choi, J.M. Karp, H. Lee, One-Step Modification Of Superhydrophobic Surfaces By A Mussel-Inspired Polymer Coating, Angewandte Chemie International Edition, 49 (2010) 9401-9404.

[14] Y. Zhao, H. Gu, Z. Xie, H.C. Shum, B. Wang, Z. Gu, Bioinspired Multifunctional Janus Particles For Droplet Manipulation, Journal Of The American Chemical Society, 135 (2012) 54-57.

[15] L. Zhang, J. Wu, Y. Wang, Y. Long, N. Zhao, J. Xu, Combination Of Bioinspiration: A General Route To Superhydrophobic Particles, Journal Of The American Chemical Society, 134 (2012) 9879-9881.

[16] X. Zhang, Z. Li, K. Liu, L. Jiang, Bioinspired Multifunctional Foam With Self-Cleaning And Oil/Water Separation, Advanced Functional Materials, 23 (2013) 2881-2886.

[17] S. Sepeur, Nanotechnology: Technical Basics And Applications, Vincentz Network Gmbh & Co Kg, 2008.

[18] K. Liu, L. Jiang, Bio-Inspired Design Of Multiscale Structures For Function Integration, Nano Today, 6 (2011) 155-175.

[19] T. Sun, L. Feng, X. Gao, L. Jiang, Bioinspired Surfaces With Special Wettability, Accounts Of Chemical Research, 38 (2005) 644-652.

[20] X. Zhang, N. Zhao, S. Liang, X. Lu, X. Li, Q. Xie, X. Zhang, J. Xu, Facile Creation Of Biomimetic Systems At The Interface And In Bulk, Advanced Materials, 20 (2008) 2938-2946.

[21] D. Zahner, J. Abagat, F. Svec, J.M. Fréchet, P.A. Levkin, A Facile Approach To Superhydrophilic–Superhydrophobic Patterns In Porous Polymer Films, Advanced Materials, 23 (2011) 3030-3034.

[22] A.I. Neto, C.A. Custódio, W. Song, J.F. Mano, High-Throughput Evaluation Of Interactions Between Biomaterials, Proteins And Cells Using Patterned Superhydrophobic Substrates, Soft Matter, 7 (2011) 4147-4151.

[23] N.M. Oliveira, A.I. Neto, W. Song, J.F. Mano, Two-Dimensional Open Microfluidic Devices By Tuning The Wettability On Patterned Superhydrophobic Polymeric Surface, Applied Physics Express, 3 (2010) 085205.

[24] B.N. Lourenço, G. Marchioli, W. Song, R.L. Reis, C.A. Van Blitterswijk, M. Karperien, A. Van Apeldoorn, J.F. Mano, Wettability Influences Cell Behavior On Superhydrophobic Surfaces With Different Topographies, Biointerphases, 7 (2012) 46.

[25] T. Sun, H. Tan, D. Han, Q. Fu, L. Jiang, No Platelet Can Adhere—Largely Improved Blood Compatibility On Nanostructured Superhydrophobic Surfaces, Small, 1 (2005) 959-963.

[26] J. Ballester-Beltrán, P. Rico, D. Moratal, W. Song, J.F. Mano, M. Salmerón-Sánchez, Role Of Superhydrophobicity In The Biological Activity Of Fibronectin At The Cell–Material Interface, Soft Matter, 7 (2011) 10803-10811.

[27] G. Toes, K. Van Muiswinkel, W. Van Oeveren, A. Suurmeijer, W. Timens, I. Stokroos, J. Van Den Dungen, Superhydrophobic Modification Fails To Improve The Performance Of Small Diameter Expanded Polytetrafluoroethylene Vascular Grafts, Biomaterials, 23 (2002) 255-262.

[28] N.M. Alves, J. Shi, E. Oramas, J.L. Santos, H. Tomás, J.F. Mano, Bioinspired Superhydrophobic Poly (L-Lactic Acid) Surfaces Control Bone Marrow Derived Cells Adhesion And Proliferation, Journal Of Biomedical Materials Research Part A, 91 (2009) 480-488.

[29] J.H. Waite, N.H. Andersen, S. Jewhurst, C. Sun, Mussel Adhesion: Finding The Tricks Worth Mimicking, The Journal Of Adhesion, 81 (2005) 297-317.

[30] J.H. Waite, X. Qin, Polyphosphoprotein From The Adhesive Pads Of Mytilus Edulis, Biochemistry, 40 (2001) 2887-2893.

[31] C. Fant, K. Sott, H. Elwing, F. Hook, Adsorption Behavior And Enzymatically Or Chemically Induced Cross-Linking Of A Mussel Adhesive Protein, Biofouling, 16 (2000) 119-132.

[32] P.A. Suci, G.G. Geesey, Influence Of Sodium Periodate And Tyrosinase On Binding Of Alginate To Adlayers Of Mytilus Edulis Foot Protein 1, Journal Of Colloid And Interface Science, 230 (2000) 340-348.

[33] J.J. Wilker, Marine Bioinorganic Materials: Mussels Pumping Iron, Current Opinion In Chemical Biology, 14 (2010) 276-283.

[34] M.J. Sever, J.T. Weisser, J. Monahan, S. Srinivasan, J.J. Wilker, Metal-Mediated Cross-Linking In The Generation Of A Marine-Mussel Adhesive, Angewandte Chemie, 116 (2004) 454-456.

[35] J.J. Wilker, The Iron-Fortified Adhesive System Of Marine Mussels, Angewandte Chemie International Edition, 49 (2010) 8076-8078.

[36] L.A. Burzio, J.H. Waite, Cross-Linking In Adhesive Quinoproteins: Studies With Model Decapeptides, Biochemistry, 39 (2000) 11147-11153.

[37] J. Sedó, J. Saiz-Poseu, F. Busqué, D. Ruiz-Molina, Catechol-Based Biomimetic Functional Materials, Advanced Materials, 25 (2013) 653-701.

[38] A. Statz, J. Finlay, J. Dalsin, M. Callow, J.A. Callow, P.B. Messersmith, Algal Antifouling And Fouling-Release Properties Of Metal Surfaces Coated With A Polymer Inspired By Marine Mussels, Biofouling, 22 (2006) 391-399.

[39] C. Gao, G. Li, H. Xue, W. Yang, F. Zhang, S. Jiang, Functionalizable And Ultra-Low Fouling Zwitterionic Surfaces Via Adhesive Mussel Mimetic Linkages, Biomaterials, 31 (2010) 1486-1492.

[40] S. Yuan, D. Wan, B. Liang, S. Pehkonen, Y. Ting, K. Neoh, E. Kang, Lysozyme-Coupled Poly (Poly (Ethylene Glycol) Methacrylate)− Stainless Steel Hybrids And Their Antifouling And Antibacterial Surfaces, Langmuir, 27 (2011) 2761-2774.

[41] H. Lee, K.D. Lee, K.B. Pyo, S.Y. Park, H. Lee, Catechol-Grafted Poly (Ethylene Glycol) For Pegylation On Versatile Substrates, Langmuir, 26 (2010) 3790-3793.

[42] N. Holten-Andersen, M.J. Harrington, H. Birkedal, B.P. Lee, P.B. Messersmith, K.Y.C. Lee, J.H. Waite, Ph-Induced Metal-Ligand Cross-Links Inspired By Mussel Yield Self-Healing Polymer Networks With Near-Covalent Elastic Moduli, Proceedings Of The National Academy Of Sciences, 108 (2011) 2651-2655.

[43] J.H. Ryu, Y. Lee, W.H. Kong, T.G. Kim, T.G. Park, H. Lee, Catechol-Functionalized Chitosan/Pluronic Hydrogels For Tissue Adhesives And Hemostatic Materials, Biomacromolecules, 12 (2011) 2653-2659.

[44] A. Postma, Y. Yan, Y. Wang, A.N. Zelikin, E. Tjipto, F. Caruso, Self-Polymerization Of Dopamine As A Versatile And Robust Technique To Prepare Polymer Capsules, Chemistry Of Materials, 21 (2009) 3042-3044.

[45] B. Yu, D.A. Wang, Q. Ye, F. Zhou, W. Liu, Robust Polydopamine Nano/Microcapsules And Their Loading And Release Behavior, Chemical Communications, (2009) 6789-6791.

[46] K.-Y. Ju, Y. Lee, S. Lee, S.B. Park, J.-K. Lee, Bioinspired Polymerization Of Dopamine To Generate Melanin-Like Nanoparticles Having An Excellent Free-Radical-Scavenging Property, Biomacromolecules, 12 (2011) 625-632.

[47] H. Shao, K.N. Bachus, R.J. Stewart, A Water-Borne Adhesive Modeled After The Sandcastle Glue Of P. Californica, Macromolecular Bioscience, 9 (2009) 464-471.

[48] K.H. Bae, Y.B. Kim, Y. Lee, J. Hwang, H. Park, T.G. Park, Bioinspired Synthesis And Characterization Of Gadolinium-Labeled Magnetite Nanoparticles For Dual Contrast T 1-And T 2-Weighted Magnetic Resonance Imaging, Bioconjugate Chemistry, 21 (2010) 505-512.

[49] S. Saxer, C. Portmann, S. Tosatti, K. Gademann, S. Zurcher, M. Textor, Surface Assembly Of Catechol-Functionalized Poly (L-Lysine)-Graft-Poly (Ethylene Glycol) Copolymer On Titanium Exploiting Combined Electrostatically Driven Self-Organization And Biomimetic Strong Adhesion, Macromolecules, 43 (2009) 1050-1060.

[50] P. Glass, H. Chung, N.R. Washburn, M. Sitti, Enhanced Reversible Adhesion Of Dopamine Methacrylamide-Coated Elastomer Microfibrillar Structures Under Wet Conditions, Langmuir, 25 (2009) 6607-6612.

[51] G. Westwood, T.N. Horton, J.J. Wilker, Simplified Polymer Mimics Of Cross-Linking Adhesive Proteins, Macromolecules, 40 (2007) 3960-3964.

[52] C.R. Matos-PéRez, J.D. White, J.J. Wilker, Polymer Composition And Substrate Influences On The Adhesive Bonding Of A Biomimetic, Cross-Linking Polymer, Journal Of The American Chemical Society, 134 (2012) 9498-9505.

[53] B.P. Lee, P.B. Messersmith, J.N. Israelachvili, J.H. Waite, Mussel-Inspired Adhesives And Coatings, Annual Review Of Materials Research, 41 (2011) 99.

[54] E. Santaniello, A. Manzocchi, C. Farachi, Tetrabutylammonium Periodate; A Selective And Versatile Oxidant For Organic Substrates, Synthesis, 1980 (1980) 563-565.

[55] A. Internation, Standard Test Method For Apparent Shear Strength Of Single-Lap-Joint Adhesively Bonded Metal Specimens By Tension Loading (Metal-To-Metal), Astm D1002-10, Astm International, West Conshohocken, Pa, Usa, (2010).

CHAPTER 5. HIGH-THROUGHPUT TOPOGRAPHIC, MECHANICAL AND BIOLOGICAL SCREENING OF MULTILAYER FILMS CONTAINING MUSSEL-INSPIRED BIOPOLYMERS *

5.1 Abstract

We report a high-content screening method to characterize multifunctional multilayer films that combine mechanical adhesion and favorable biological response. Distinct combinations of nanostructured films were produced using layer-by-layer methodology and their morphological, physicochemical and biological properties were analyzed in a single microarray chip. Inspired by the composition of the adhesive proteins in mussels, we studied thin films containing dopamine-modified hyaluronic acid. Flat biomimetic superhydrophobic patterned chips produced by a bench-top methodology were used for the build-up of arrays of multilayer films. The wettability contrasts imprinted onto the chips allowed to produce individual, position controlled, multilayer films in the wettable regions. The flat configuration of the chip permits to perform a series of non-destructive measurements directly on the individual spots. *In situ* adhesion properties were directly measured in each spot, showing that nanostructured films richer in dopamine promote the adhesion. In vitro tests showed an enhanced cell adhesion for the films with more catechol groups. The advantages presented by this platform includes: ability to control the uniformity and size of the multilayers films; it's suitability to be used as a new low cost toolbox and for high-content cellular screening; and capability for monitoring *in situ* a variety of distinct material properties.

---

* *Neto A. I., Vasconcelos N. L., Oliveira S.M., Ruiz-Molina D. and Mano J. F. High-throughput topographic, mechanical and biological screening of multilayer films containing mussel-inspired biopolymers.* ***Advanced Functional Materials****, 26, 2745-2755, 2016.*

5.2 Introduction

In the field of nanotechnology many efforts have been made to control shape, size distribution and surface chemistry of nanostructures [1]. Specifically, adsorption of biopolymers in defined spatial surface arrangements offers a promising skill for the generation of innovative nanostructures, suitable for a broad range of applications in the fields of biomedical materials, tissue engineering, and diagnosis. So, development of novel tailored simple and versatile strategies for throughput biopolymer surface modification and its corresponding characterization have become a challenging area of continuous research over the years [2, 3]. Among the different approaches so far reported, the layer-by-layer (LbL) deposition technique as popularized by Decher et al. [4], represents an effective and reproducible method, with a wide range of advantages, particularly in the biomedical field, as detailed next: (i) this technique can be performed in virtually any kind of substrate (planar, porous, colloidal, among others) and different surface chemistries, (ii) the film organization can be spatio-temporal controlled and (iii) the assembly can be performed under "mild" conditions with a large variety of inexpensive materials compatible with physiological media, permitting also the integration of large amounts of bioactive molecules and extra-cellular matrix components in the films [5, 6]. Moreover, the final biological, physicochemical and mechanical properties of the multilayered films can be finely tuned by controlling multiple factors, such as the nature of the inserted components, their distribution along the thickness of the film (e.g. the nature of the top layer), the number of layers, the introduction of any additional molecules, or the post-treatment of the film (e.g. crosslinking). However, even successful as previously described, this technique most often requires expensive and time-consuming methodologies that represent a great shortcoming limiting its applicability. Hence, novel experimental approaches that allow for a rapid, simple and accurate screening of multilayer arrays obtained from the large portfolio of available biopolymers, processing conditions and combinations of them, are needed.

High-throughput screening (HTS) technologies represent an excellent tool with this aim [7-11]. Distinct HTS procedures have already been used for the production of LbL constructs based on: selective deposition [12], microfluidics [13, 14], disruption of hydrogen-bonded multilayers [15, 16] and photoreactive multilayers [17]. For instance, Barret et al. reported a combinatorial analysis of 5000 individual synthetic polyelectrolyte multilayers with modulated two-dimensional physical properties and thicknesses gradients simply by rotating the substrate along the deposition process [18]. Hammond and co-workers [19], used a capillary flow technique to produce gradients, based on patterned isolated spots of a microfluidic chip with LbL thin film constructs. However, in spite of these pioneering examples, the

preparation of discrete and nanostructured multilayered LbL films on a single substrate that allow for a fast HTS screening has not yet being reported.

Herein we fill this gap with the use of a superhydrophobic, flexible and flat platform decorated with patterned arrays of wettable regions acting as liquid reservoirs, where several combinations of nanostructured multilayer films can be obtained with a full control in space and time. A schematic representation of the patterned chip along with the fabrication procedure and the corresponding characterization of the arrays is shown in Figure 5.1. This new setup can allow for the first time to individually analyze several distinct small-sized multilayer films within a single chip, where the number of layers, crosslinking, protein adsorption and nature of terminal layers are systematically tuned. As a proof-of-concept to demonstrate the feasibility of our approach, we have studied how the functionalization of polyelectrolytes with different amounts of dopamine (DN) affect the surface properties (morphology and wettability), the mechanical behavior and cell adhesion performance of the resulting LbL films through a combinatorial analysis of different experiments. The conjugation of polymers with DN, inspired by the structure and composition of an unusual amino acid presented in mussels protein (3,4-dihydroxyphenylalanine, DOPA) [20], has already been shown to improve the adhesive properties of the coatings [21-24]. For instance, multilayered films of hyaluronic acid (HA) and DN showed applicability for tissue engineering and biomedical applications [25]. However, and in spite of its clear interest, there was a lack of detailed and systematic studies that allow for a proper understanding, and therefore optimization, of films containing DN. This fact has been achieved here thanks to our new high-throughput chip where several different combinations of HA-DN and chitosan (CHT) are studied and compared between them (CHT and alginate (ALG) are also studied for comparison purposes).

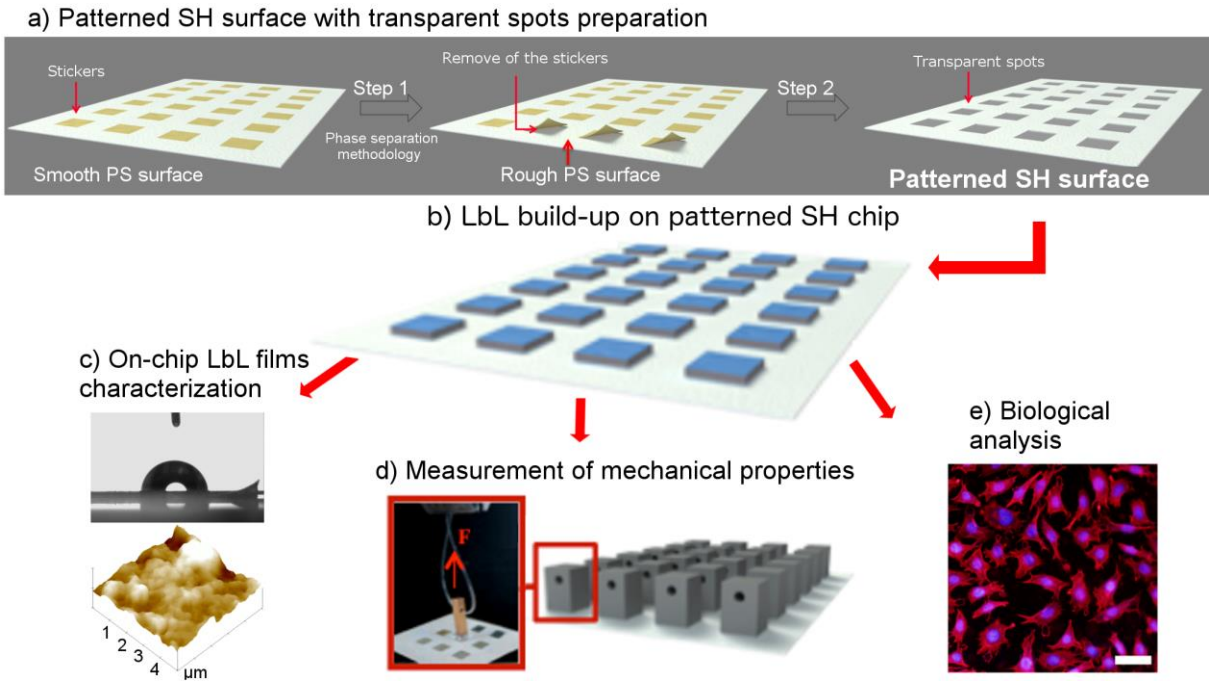

Figure 5.1 a) Preparation of superhydrophobic (SH) chips patterned with arrays of wettable regions prepared as detailed next: Initially an array of stickers in a polystyrene untreated film is formed; step 1 refers to the same array upon inducing a roughness increase with an additional *in situ* deposition of polystyrene, and therefore inducing an increase of the SH character at the macroscopic level. In step 2 wettable areas are obtained by removing the stickers; b) Build-up of layer-by-layer films using different combinations of polyelectrolytes solutions in the wettable spots surrounded by SH domains. Afterwards, surface characterization (c), mechanical adhesion properties (d) and biological response of the multilayer films (e) are assessed directly on the different spots. Scale bar: 50 µm.

5.3 Results and Discussion

5.3.1 Study of the LbL multilayer films formation

Initially, LbL films containing the targeted polymeric combinations to be deposited on the chip were first obtained as bulk surfaces and the film growth studied to get more insight into their formation. The choice of polycationic polysaccharides is very limited and among them, chitosan (CHT) the de-acetylated form of chitin, was selected because being far the most widespread biopolymer used in polyelectrolyte multilayer films due to its numerous interesting properties [26], including biodegradability, biocompatibility, and antibacterial properties. As a negatively charged polymer we have used HA. This is a polysaccharide containing alternating N-acetyl-d-glucosamine and d-glucuronic acid monosaccharide units. As an integral component of extracellular matrix [27], HA is an attractive building block for new biocompatible and biodegradable materials that can be used for drug delivery and tissue engineering [28, 29]. Moreover, HA is well known to complex with CHT; for instance, LbL deposition of a combination of both polymers has already been used to repair damaged blood vessels [30]. Finally, to bring more insights upon catechol substitution, two conjugated biopolymers based on DN-modified hyaluronic acid (HA-DN

and HA-4DN), that differ in the amount of DN conjugated, the later having a four-fold excess of the dopamine used in the reaction, have also been studied. The real degree of dopamine substitution in each case was obtained by following the UV excitation band centered at 280 nm and upon comparison with a standard curve obtained for distinct concentrations of free dopamine in solution (for more details see Experimental Section) [31]. UV-Vis spectra of the different polymers used in this work are shown in Figure 5.2. Using the measured absorbance, the obtained concentration of dopamine units in both conjugates was 11% and 15% for HA-DN and HA-4DN, respectively. Once the selection of functional polymers was done, the progress of LbL assembly was monitored by quartz crystal microbalance with dissipation (QCM-D), as shown in Figure 5.2b. This technique is able to detect mass changes in the order of nanograms per square centimeter while it measures the viscoelastic properties of the surface [32]. During QCM-D measurements, a favorable and successful construction is identified by a decrease in Δf caused by a mass adsorption at the top of the sensor. The $\Delta f/\upsilon$ (where υ is the overtone) decreased upon flushing the substrate with the sequence of polyelectrolytes, due to the deposition of the new polymer layer on the surface of the crystal. At the same time, monitoring of ΔD gives an indication of the film viscoelastic properties. An increase in ΔD represents a shift towards a film with a higher viscous component and damping properties that characterize a softer and hydrated film that is deposited over the metallic sensor. Figure 5.2b shows the normalized frequency, $\Delta f/\upsilon$ and dissipation variation, ΔD, for the 5th overtone (25 MHz) of the three targeted polymeric multilayers (5 layers) grown on gold-coated quartz sensors: $(CHT/HA\text{-}DN)_5$, $(CHT/HA\text{-}4DN)_5$ and $(CHT/HA)_5$. In addition to the different CHT/HA mixtures, a negatively charged polymer such as ALG was also used for comparison purposes [33-35]. Each solution adsorption step corresponds to a decrease of Δf with each CHT, HA-4DN, HA-DN, HA or ALG injection and a subsequent increase in $\Delta f/\upsilon$ due to desorption of a small fraction of free polyelectrolyte during the rising step. In parallel, an increase of ΔD is found, meaning that the materials deposited onto the crystal surface exhibit viscoelastic properties. Typically, a lower ΔD variation indicates that the film layer becomes denser and a strong asymmetric growth occurs, displaying a linear growth law. Parameters, such as the chemical nature of the polymer pair or the concentration of salt added to solutions used for deposition and/or rinsing have also a strong influence on the nature of the film formed [36].

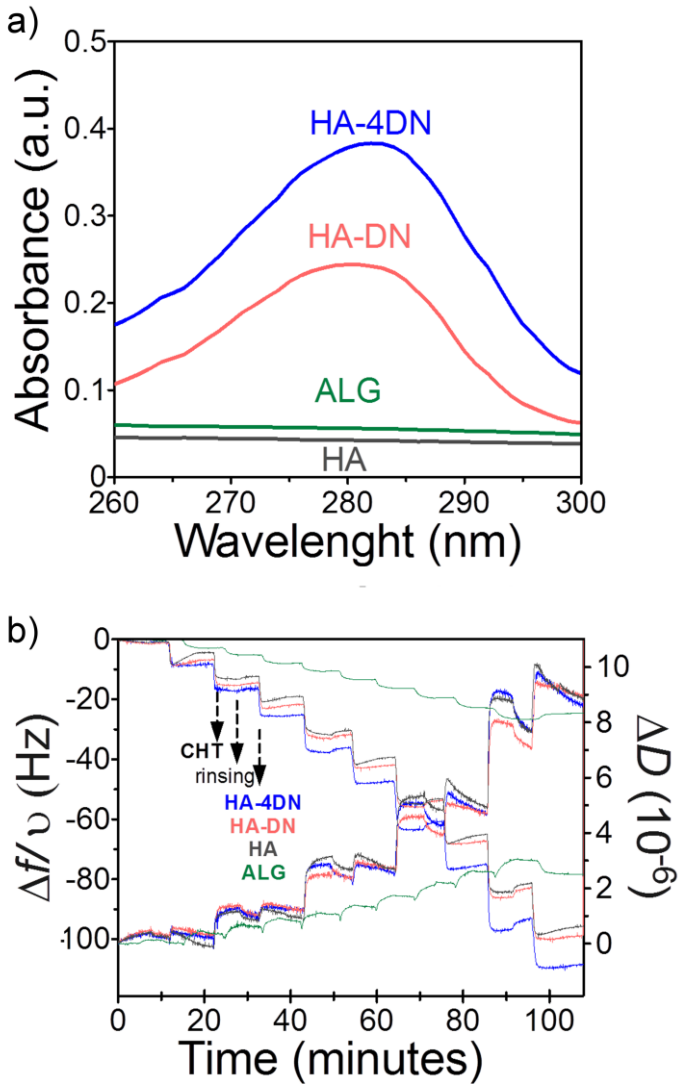

Figure 5.2 a) UV-Vis spectra of the conjugates (HA-DN and HA-4DN) and the controls (HA and ALG), b) QCM-D monitoring of the LbL construction of CHT with the conjugates (HA-DN, HA-4DN) and CHT with the controls (HA and ALG) up to 5 deposition bi-layers in 0.15M of NaCl, maintaining the pH at 5.5.

We also revealed that multilayer films containing catechol groups exhibit a linear film growth, thus giving rise to more rigid thin films. The results evidence the assembly of chitosan with the conjugates within the microarrays as those used as control as already reported [37-41]. Build-up of the multilayer film using the new conjugate (HA-4DN) has never been reported before.

5.3.2 Multichip fabrication and topographic characterization

The working principle behind the platform developed in this work consists of a polystyrene (PS) superhydrophobic (SH) surface patterned with wettable regions produced by a bench-top methodology. Briefly, square-shaped stickers were attached to polystyrene film, and afterwards the resulting surface treated and coated with rough polystyrene by a phase-separation method [42]. Afterwards, the stickers

were totally removed and the whole surface washed with pure ethanol in order to avoid possible traces of the adhesive (Figure 5.1a). While the dots obtained upon removal of the stickers exhibit a proper wettability, macroscopically the film still retains its SH behavior thanks to the peculiar lotus-like features including micro- and nano- roughness and low surface energy [43]. By using such wettability contrast, in each spot, sequentially deposition of droplets with different polyelectrolytes, combined with washing solutions, were performed to assemble the multilayers (Figure 5.1b). An array of 48 spots, combining 5, 10 or 15 bilayers prepared from a library of five polyelectrolytes (4 distinct pairs), was designed with 4 replicates per combination to obtain statistical information.

Representative scanning electron microscopy (SEM) images shown in Figure 5.3 revealed the final surface topography of the polymeric arrays obtained directly from the developed substrate. A more quantitative analysis was done by atomic force microscopy (AFM) (see also Figure 5.3). The root mean square (R_q) and average roughness (R_a) obtained by AFM topographical studies are summarized in Table 1. As can be seen there, all the surfaces exhibit a roughness that increases upon increasing the number of deposited layers, in agreement with the work reported by Lee and co-workers [44].

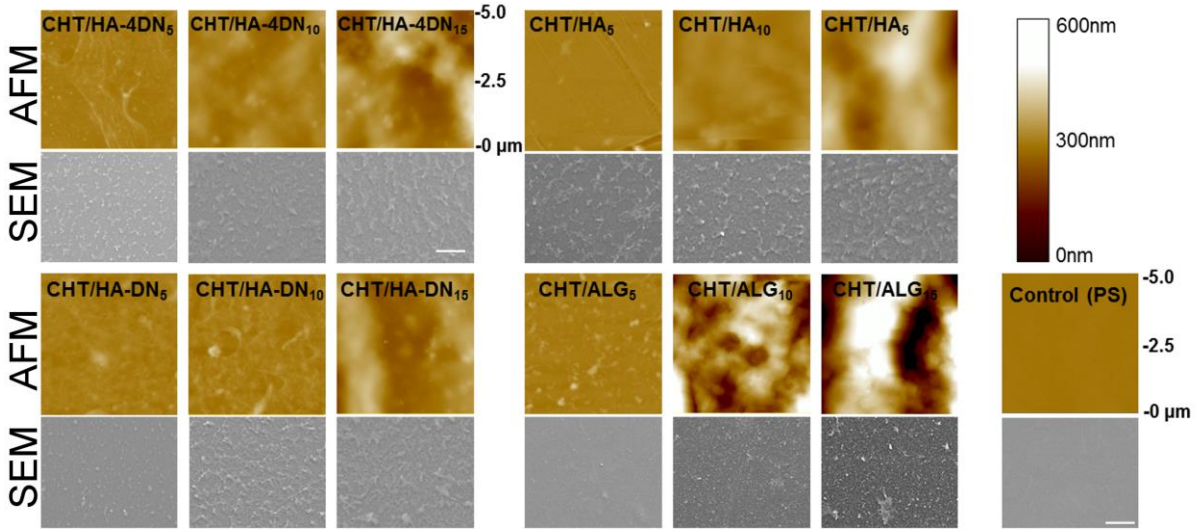

Figure 5.3 a) Representative AFM and SEM images of CHT/HA-DN, CHT/HA-4DN, CHT/HA and CHT/ALG films with 5, 10 and 15 bilayers, assembled in the wettable spots of the patterned SH surface. The images of the control (polystyrene surface) are also shown for comparison purposes. Scale bar of SEM images: 5 µm.

Table 5. 1 Root mean square (Rq), average roughness (Ra) and water contact angle (WCA, 3 µL drop volume) of the studied multilayered surfaces (n=5) taken directly from the developed chips.

	CHT/HA-DN			CHT/HA-4DN		
N° of layers	*5*	*10*	*15*	*5*	*10*	*15*
Rq (nm)	10.2 ± 0.7	10.8 ± 1.7	41.2 ± 5.6	9.1 ± 0.4	11.2 ± 2.2	47.9 ± 6.1
Ra (nm)	7.9 ± 0.6	7.6 ± 1.1	32.9 ± 4.6	6.9 ± 0.7	7.1 ± 0.2	39.9 ± 4.0
WCA (°)	66.9 ± 3.7	78.7 ± 4.1	84.9 ± 2.1	71.4 ± 4.9	79.5 ± 2.5	89.2 ± 3.7

	CHT/HA			CHT/ALG			Control
N° of layers	5	10	15	5	10	15	No Layers
Rq (nm)	6.4 ± 1.2	13 ± 0.9	65.9 ± 1.8	13.6 ± 3.8	87.8 ± 21.2	156.5 ± 13.3	1.7 ± 0.2
Ra (nm)	3.7 ± 0.2	10.4 ± 0.9	52.9 ± 2.4	7.9 ± 1.8	69.6 ± 15.9	122.6 ± 19.4	1.4 ± 0.1
WCA (°)	61.7 ± 1.3	77.6 ± 1.6	82 ± 3.4	66.4 ± 4.1	53.5 ± 0.7	18.1 ± 1.6	92.2 ± 4.1

Diffusion processes take place during the assembly of the CHT/HA and CHT/ALG systems, which growth in an exponential regime. So, the final thickness of these films is mainly related to the ability of CHT to diffuse "in" and "out" in the whole film during each deposition step and also to the non-desorption of the CHT/HA and CHT/ALG layers during the rinsing steps. The results suggest that the interface of CHT/HA and CHT/ALG is getting rougher and the surface area is increasing due to the fact that the surface becomes hydrated. Hydration is a critical parameter in polyelectrolyte multilayer films, impacting film thickness, mechanical/ viscoelastic properties, swelling ability, transport properties and molecular mobility [45].

Related with the surface topography, the wettability of the films was also evaluated *in situ* by water contact angle (WCA) measurements and the results included in Table 5.1. The volume of the water droplets was small enough so that the WCA measurements could be performed in the individual spots. The changes in the water contact angle and topography of the glass control provided additional evidence of the presence of the coatings. As a main tendency, except for the CHT/ALG combination, it was found that the WCA values increase upon increasing the number of deposited layers. Moreover, a gradual increase of the catechol content is translated into a small increase of the WCA; for instance, the CHT/HA-4DN value for 15 layers is around 89°, which is slightly larger than CHT/HA-DN films for the same number of layers (around 85°) and CHT/HA (around 82°).

5.3.3 In situ mechanical test

Methods for screening adhesiveness rely on the measurement of either tensile or shear strengths; according to Thirawong et al. [46]. The first test usually uses perpendicular forces necessary to separate

two surfaces in contact, while the second determines the force that causes an adhesive to slide on a surface in direction parallel to the plane of contact. In the present study tensile strengths were chosen and measured for multilayer films with 5, 10, and 15 bilayers built-up in the wettable spots of the SH chip. For this, iron pillars containing the surface base with the same size and shape of the spots, were put in contact with the top of the films. The mechanical properties of the films were then assessed after 24 hours of contact using the lap adhesive strength test according to the standard protocol ASTM D1002. For these measurements, the pillars were pulled until the total detachment from the base of the chip is achieved. Representative load-extension curves for the detachment of the pillars from the coatings are presented in Figure 5.4a.

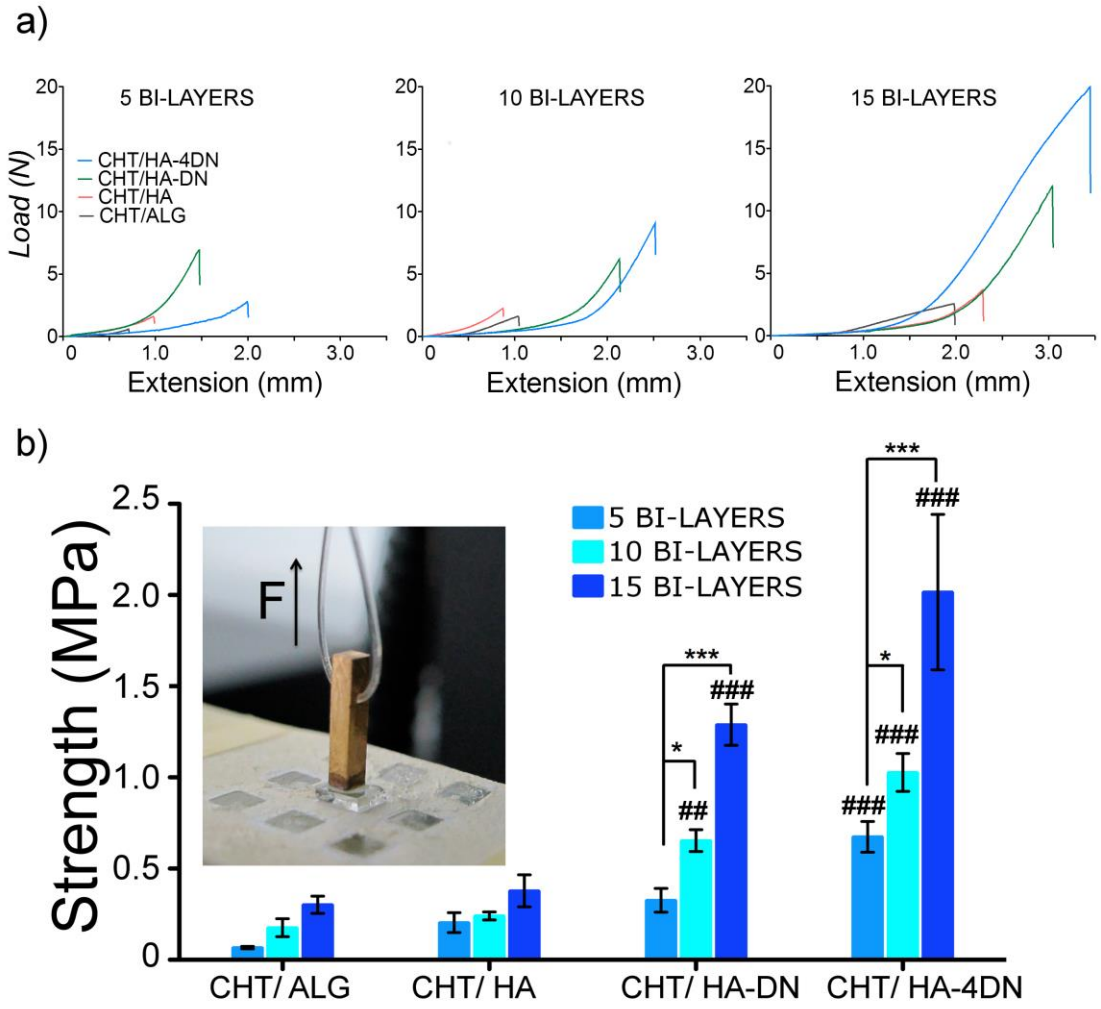

Figure 5.4 a) Representative Force vs Displacement curves for the pull-out experiments over CHT/ HA-4DN, CHT/ HA-DN, CHT/ HA, CHT/ ALG multilayer films. b) Adhesive strength between the multilayer films produced over the wettable regions of the SH microarray and the iron pillars. Data are means SD (n=5; *= p<0.1 and ***= p<0.001). The statistical differences relating to CHT/HA films with the same number of bilayers are represented by doubles symbols (##, p<0.01) and triple

symbols (###, $p<0.001$). Representative image of an adhesion measurement in a single spot where an iron pillar is pulled out with a constant strain rate.

As can be seen there, the elongation modulus of the distinct multilayer films is similar, but the final displacement of the films containing DOPA is higher, due to its larger adhesive strength. The lap shear strength of the different multilayer films is shown in Figure 5.4 b. It is clear, that upon increasing the number of multilayered films, the adhesion force increases. In addition, multilayer films containing higher amount of catechol group present higher strength. Worth to mention, the obtained adhesion values for the experiments performed using small-sized surfaces are in agreement with results already reported using cm-scale surfaces and conventional tests [25]. For instance, spots with 10 bilayers and a contact area of 4 mm^2, achieved values varying between 0.65 ± 0.06 MPa and 0.24 ± 0.02 MPa, for CHT/HA-DN and CHT/HA, respectively, in agreement with those previously reported for the same systems using larger surfaces [25].

5.3.4 *In vitro* cell studies

The biological performance of the multilayers was assessed using two cell types (L929 – murine fibroblasts, and SaOs-2 – human osteoblast-like cells), both relevant and standard cell lines commonly used in biomedical studies. All biological characterization was performed using image-based analysis directly on the chip, taking advantage of the transparency of the spots. Chips were prepared with spots containing multilayer films composed by 5, 10 and 15 bilayers and featuring the following characteristics: I) films ending with the negatively charged polymer without any further modification; II) films ended with the negatively charged polymers followed by fibronectin adsorption; III) positively charged CHT-ended films followed by fibronectin adsorption and; (IV) positively charged CHT-ended films crosslinked with genipin. As can be immediately deduced, two new components (fibronectin and genipin) have been added for these studies since both tested cells are dependent on the presence of proteins for anchorage and extracellular instructions, which turns the composition of the absorbed layer a key point to modulate cell behavior [47]. Fibronectin is an extracellular matrix glycoprotein that plays crucial role in many cell functions such as adhesion. It contains the tripeptide arginine-glycine-aspartic acid (RGD) which is an integrin cell recognition site and that turns it a good candidate to promote cell adhesion onto biomaterials [48, 49]. Genipin is a natural product derived from geniposides and has been extensively investigated in the crosslinking of amine-containing polymers (e.g. chitosan, collagen or gelatin) as well as in multilayered films [41, 50].

In a typical experiment first multilayer films were locally coated with the crosslinking solution or the protein solution (except in the case of the control substrates). Both L929 and SaOs-2 were then seeded on the above-mentioned multilayer films by simple confined deposition of cells suspension droplets in the different spots. Thus, independently on the nature of the multilayer film any desired combination of cells or cell densities can be tested on individual basis. Cell adhesion was assessed by on-spot image-based analysis after 24 hours in culture. Figure 5.5 shows representative images of the cells nuclei and stained cytoskeleton revealing their attachment and spreading on the LbL films.

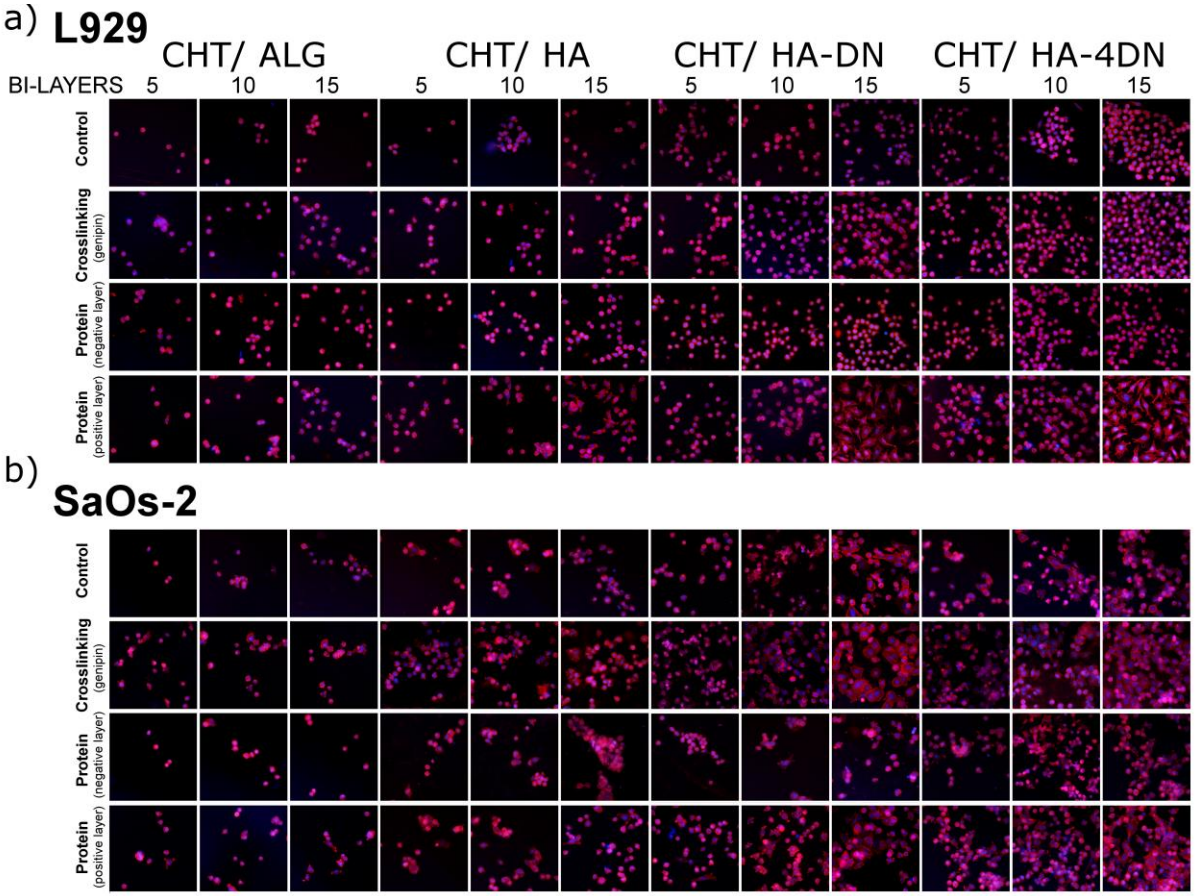

Figure 5.5 Representative fluorescence microscope images of the coated spots with L929 and SaOs-2 cells stained with DAPI/ phalloidin after being cultured for 24h. Multilayer films of CHT/ALG, CHT/HA, CHT/HA-DM and CHT/HA-4DN with 5, 10 and 15 bilayers were tested over the patterned chip. Cells attachment was also evaluated in the multilayer patterns coated with fibronectin (over positively or negatively terminating multilayers) or crosslinked with genipin. Scale bar: 50 μm

Having a quick look to Figure 5.5 one can immediately determine that, from a qualitative point of view, there are noticeable differences between the different arrays: I) cells adhered mostly onto surfaces containing DOPA in their composition; II) cells tended to adhere more in films with higher number of layers; and III) crosslinking also revealed potential to improve cell attachment. The quantitative percentage of area covered by the adhered cells, obtained from image analysis, is represented in Figure 5.6. Typically,

cells assume distinct morphologies depending on the physicochemical and architectural features of the substrate [51]. The cells seeded on the CHT/HA and CHT/ALG multilayer films presented lower adhesion accompanied by round morphology. The higher surface hydration-level and softness, compared with the crosslinked films, may justify such performance decay [41, 45]. The presence of DOPA in the films, besides enhancing cell attachment [22], allowed a cell spreading enhancement along the multilayer films, showing a higher percentage of area covered. The individual cell morphology was also analyzed upon culturing the cells on different multilayer films (Figure 5.6b). An image-based tool (ImageJ) was used to evaluate both the area covered by each cell and the number of cells adhered in the films. Each fluorescence image was divided into grey scale, and the area occupied by the cytoskeleton was determined. The analysis permitted also to count the total number of cell nuclei per spot. Figure 5.6c shows the correlation between cell number and the fraction of the area covered by the cells. All formulations have presented suitable cells attachment, but the positive effect of the incorporation of DOPA is evident. Cells are more elongated, and thus, with higher area occupied, and the morphology became more spread and trapezoidal-like shape for DOPA multilayer films covered by genipin and fibronectin. Multilayer films with CHT-ended layers and with pre-adsorption of fibronectin show higher cell attachment compared with the multilayer films ended with negative charged biopolymers. This could be explained due to the fact that fibronectin has an acidic isoelectric point, presenting a negative net charge above pH 5-6, which would enhance their electrostatic binding to the positive terminal multilayers rather than to the negative ones. Some studies have suggested surfaces containing positively charged functional groups to enhance cell attachment and spreading [52]. The physicochemical properties of the multilayer films are also reported to influence the cell attachment process [41, 53-56]. Both cell types have shown similar behavior on the crosslinked multilayers, relatively to the controls (unmodified multilayers). The crosslinking process decreases water content and increases stiffness in multilayers [41, 55]. Consequently, L929 and SaOs-2 attachment tended to increase for the multilayers crosslinked with genipin. This observation corroborates previous studies where a similar trend was reported with different cell types [21, 40, 41, 57-59]. Previously, we evidenced the suitability of such platform for micro-tissues formation and drug screening [60, 61], as well as, high-content *in vivo* studies [62]. This work clearly demonstrated that the technology could be extended to the screening of more complex biomaterials (in this case nanostructured multilayers) and to other physico-chemical analysis, such as topography, wettability and adhesion.

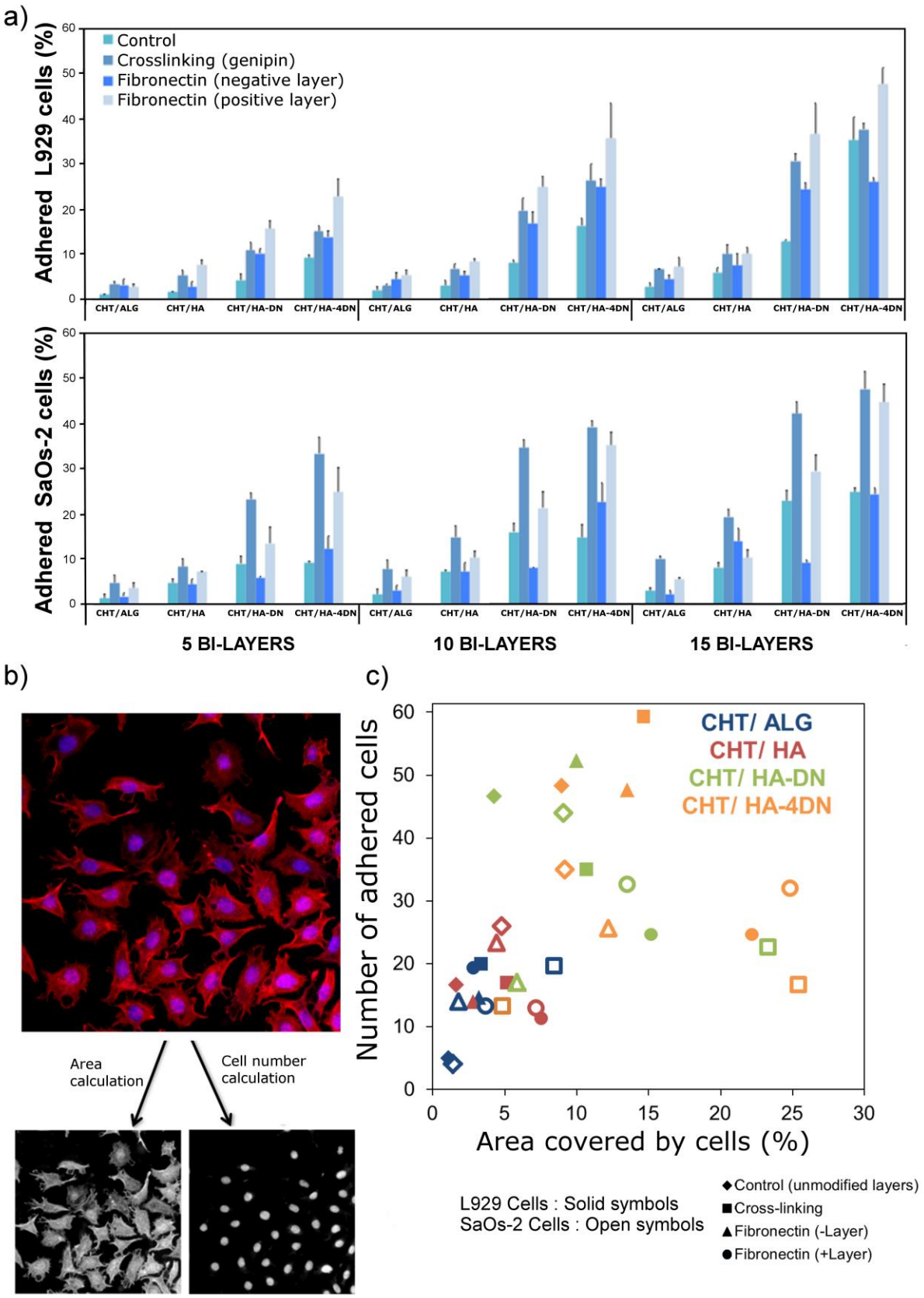

Figure 5.6 a) L929 and SaOs-2 cellular density (% of the area covered by the cells) quantified using image analysis in the studied multilayer films for (n=3). b) Example of an original image, where the number of cells and cell density (% of the area covered by the cells) were quantified by image analysis; this procedure was performed in all studied multilayer films for L929 and SaOs-2 cells. c) Correlation between the number of cells adhered per spot and density (percentage of the area covered)

of L929 cells (solid symbols) and SaOs-2 cells (open symbols). Cells attachment was studied over 5 bilayer films of CHT/ALG (blue color), CHT/HA (red color), CHT/HA-DN (green color) and CHT/HA-4DN (orange color), also coated with fibronectin and crosslinked with genipin. Scale bar: 50 μm

5.4 Conclusions

The preparation of discrete and structured multilayered regions deposited on a single chip that allow for a fast HTS screening has been reported. The platform presents several advantages in comparison with other microarrays already described: I) The size and composition of the platform, as well as, the geometry of the wettable spots, can be easily controlled in an individual form, and the assays in the liquid state occur only in the desired wettable area without cross-talking between spots, II) the SH platform is solely physically modified polystyrene which guarantees the lack of cytotoxicity and the chemical stability of the platform; III) the use of micro-size droplets for the production of nanostructure films and biological assays allows a drastic reduction of the volume in which the cells are grown; cell culture media can be changed easily without destroying the multilayer films; IV) drugs or other molecules can be added at any time, and if precautions are taken the mechanical impact in the cells is reduced; V) the platform is compatible with or easily adapted to many characterization can be performed using image-based analysis directly on the chip taking the benefit of the transparency of the spots and VI) high-throughput combinatorial analysis may be performed in situ using different cell types.

As a proof-of-concept for the feasibility of this new approach we have demonstrated the influence of doping biopolymers such as HA with functional dopamine molecules on three specific LbL properties of interest: (1) final roughness, wettability, and morphology; (2) discrete measurement of adhesion properties of the films and (3) in situ examination of cells adhesion. Overall, multilayer films containing catechol groups presented higher mechanical adhesion strength and enhanced cell adhesion, showing potential to be used as a new generation of wound healing bandages or surgical sealants, or even, as surface coatings for optimized cell-substrate interaction.

According with the results obtained, we do believe that this versatile and cost-effective platform for enabling high throughput screening may also have potential in several other biomedical areas, including tissue engineering, regenerative medicine and drug discovery, among others. Moreover, this method can be operated as a single lab bench-top apparatus or combined with liquid–handling robotics to extend the library size, allowing this user-friendly platform to achieve considerable advances for miniaturized bio-analytical and biomedical analysis in the near future.

5.5 Experimental Section

Materials: Medium molecular weight chitosan (CHT) was purchased from Sigma-Aldrich (ref 448877, Brookshield viscosity 200-800 cP, molecular weight 190-310 kDa) and purified by a series of filtering steps and precipitation in water and ethanol, followed by freeze-drying. Hyaluronic acid (HA) - hyaluronic acid sodium salt from Streptococcus equi - was purchased from Sigma (ref. 53747, molecular weight of 595 kDa). Dopamine hydrochloride (DN) (ref. H8502) and N-(3-Dimethylaminopropyl)-N'-ethylcarbodiimide hydrochloride (EDC) (ref. 03450, purum, ≥ 98.0% (AT)) were purchased from Sigma and used without any further purification. Alginate (ALG) -alginic acid sodium salt from brown algae – was purchased from Fluka (ref. 71238, molecular weight 100-200 kDa). Genipin was purchased from Wako chemical (ref. 078-03021). Human plasma fibronectin (HFN) was purchased from Sigma- Aldrich (95% pure, 0.1%). Tetrahydrofuran (THF) was from Fluka (p.a.>99.5%) and ethanol absolute from Panreac. *Smooth polystyrene (PS) sheets were purchased from Goodfellow, UK, with 0.19 mm of thickness, ref. ST311190/1.*

Synthesis of HA-DN: HA-DN conjugates were synthesized using EDC as an activation agent of the carboxyl groups on HA chains, based on the procedure proposed by Lee and co-workers [44]. Briefly, 1g of HA was dissolved in 100 mL of phosphate buffered saline (PBS) solution and the pH was adjusted to 5.5 with an hydrochloric acid (HCl) aqueous solution. The solution was purged with nitrogen for 30 minutes. Then, 338 mg of EDC and 474 mg of DN were added and the pH of the reaction solution was maintained at 5.5 for 2 hours. Unreacted chemicals and urea byproducts were removed by extensive dialysis, and afterwards the conjugate was lyophilized. In order to avoid oxidation, the conjugate was stored at 4°C in a desiccator under vacuum and protected from the light.

Ultraviolet (UV) spectrophotometry and Quartz crystal microbalance (QCM-D): The degree of substitution of dopamine in the conjugate was determined using a UV-vis spectrophotometer (Shimadzu UV-2501 PC) and 1cm quartz cells. A solution of 1mg.mL^{-1} in 0.15M sodium chloride (NaCl) was prepared for the UV analysis. A Q-sense E4 quartz-crystal microbalance (Q-sense AB, Sweden) with a dissipation monitoring system was used to monitor the adsorption of CHT-DN, CHT-4DN, CHT-HA and CHT-ALG, onto gold coated quartz crystal in situ. The crystals were previously cleaned with sequential sonication for 3 minutes in acetone, ethanol and isopropanol and then dried with flowing nitrogen gas avoiding contamination prior to use. In order to ensure that the crystals are perfectly clean and therefore show a null frequency, all the experiments started with a NaCl baseline. The quartz crystal was excited at multiple overtones: 1, 3, 5, 7, 9, 11 and 13, corresponding respectively to 5, 15, 25, 35, 45, 55, 65 MHz. Adsorption took place at 25 °C using solutions at 0.5 mg.mL^{-1}, 0.15M NaCl and at a constant flow rate of 100 mL.min-1, with an

adsorption time of 10 min (starting with CHT) and an intermediate rinsing step of 10 min. The frequency of each overtone was normalized to the fundamental resonant frequency of the quartz crystal, by dividing it by ν (where ν is the number of the overtone, ν = 1, 3, 5,...). If a rigid mass is adsorbed onto the surface of the piezoelectric crystal there will be a decrease in the oscillation frequency. For viscoelastic materials the adsorption of mass does not fully couple to the oscillation of the crystal and dampens the oscillation. QCM-D allows simultaneously measuring the changes in the resonant frequency and in the viscoelastic properties (dissipation) when a film is adsorbed at the crystal surface. CHT was used as the polycation (always the first deposited layer) while HA-DN, HA-4DN, HA and ALG acted as the polyanion (used as ended-polymer layer). The multilayer systems were assembled at pH 5.5. The pH was adjusted with HCl or NaOH. Films with 10 layers were produced.

Fabrication of Patterned SH Surfaces: Small portions of polystyrene (PS) were cut from commercially available smooth PS sheets. Polyvinyl chloride (PVC) stickers (Oracal, USA) were glued into PS surface in the form of an array of 2x2 mm^2 squares separated by 2 mm. The PS surfaces containing square-shaped stickers were modified according to a phase separation protocol described elsewhere [42]. Briefly, superhydrophobic surfaces were produced by dissolving 70% v/v solution of PS (Styrolution PS 158 K) in tetrahydrofuran solvent for approx. 2 hours to form a pre-solution. Then, 1.4 mL of ethanol was added into 2 mL of PS pre-solution and the mixed solution was stirred. A necessary volume to cover the PS substrate with this mixture was dipped onto a cleaned PS smooth surface. After several seconds in air, the substrate with the mixture was immersed in ethanol for 1 min in order to force the polymer precipitation, leading to the formation of a rough and porous topography at both the nano- and microscale levels. Afterwards the surface was dried at ambient temperature. The stickers were then removed from the surface and the protected regions remained untreated and, consequently, were kept wettable and transparent – see Figure 5.1a. Prior material deposition, the wettable polystyrene spots were exposed to UV-ozone irradiation (procleaner 220, BioForce Nanoscience), in order to modify chemically the spots incorporating negative charged-groups.

Preparation of the multilayer films: Multilayer films were constructed manually in the wettable spots of the patterned superhydrophobic surfaces, by pipetting alternately droplets of 5 µL of the polyelectrolyte solutions during 10 minutes, beginning with CHT. The droplets were removed using a pipette, and then, a rinsing step of 5 minutes with droplets of 0.15 M NaCl solution was included between the adsorptions of each polyelectrolyte.

On-chip surface characterization: The surface morphology of the multilayered film on the chip was observed using a Leica Cambridge S-360 scanning electron microscope (SEM). All samples were coated

with a conductive layer of sputtered gold. The SEM micrographs were taken at an accelerating voltage of 15 kV and at different magnifications.

The surface roughness of the samples was analyzed by atomic force microscope (AFM). AFM measurements were performed in a MultiMode STM microscope controlled by the NanoScope III from Digital Instruments system, operating in tapping mode at a frequency of 1 Hz. At least five measurements were performed in the different sample, which had been previously air-dried.

Water contact angle measurements were also performed at room temperature using an OCA 15plus goniometer (DataPhysics Instruments, Germany). The values were obtained by the sessile drop method. The used liquid was ultrapure water and the drop volume was 3 μL. This volume was small enough so that the droplets could occupy an area lower than the area of the multilayers in the spots. At least five measurements were carried out for each sample. Films with 5, 10 and 15 bilayers were produced onto the wettable spots of the SH chip. For each multilayer film construction, an array of 15 combinations, containing 5, 10 and 15 bilayers of the same biomaterials was designed (5 replicates per combination were used).

Adhesion tests: The adhesion properties of the multilayer films was evaluated using a universal mechanical testing machine (Instron model 5540, USA), following the ASTM D1002 standard. Fresh polyelectrolyte solutions were prepared by dissolution of HA-4DN, HA-DN, HA and ALG in 0.15M of NaCl solution and CHT in 1% acetic acid, with a pH 5.5 to yield a final concentration of 0.5 $mg.mL^{-1}$.

Films with 5, 10 and 15 bilayers were produced onto the wettable spots of the SH chip. For each multilayer film construction, an array of 15 combinations, containing 5, 10 and 15 bilayers of the same biomaterials was designed (5 replicates per combination were used).

All the adhesion experiments were conducted at 25 °C. Iron pillars (base of 2 x 2 mm^2 and height of 10 mm) with a small square piece of glass (base of 3 x 3 mm^2) glued on the bottom surface of each pillar, were put in contact with the multilayer films and were superimposed and maintained at 40 °C overnight - see scheme in Figure 5.1. The small glasses were used o guarantee that the whole nanofilm created is in contact and adhered in the smooth glass surface. Then, the bonded multilayer films and the pillars were placed on the testing machine and tensile tests were individually performed using a crosshead speed of 5 $mm.min^{-1}$ until detachment. All iron pillars had a hole on the top, where a “fishing wire” was passed by, in order to pull the pillars. The pillar could be made of other materials or the base could be from any other substance. The lap shear bonding strength was then determined from the maximum of the force–deformation curve obtained. The average and standard deviations were determined using the results from five samples.

Statistical analysis was performed to analyze significant differences between formulations, using two-way analysis of variance (ANOVA) with Bonferroni post-test using GraphPad Prism 5.0 software. The adopted nomenclature was the following: statistical differences in grouped by time point analysis were marked with (*), and (***), which stand for p-value < 0.05 and p < 0.001, respectively, and the statistical differences relating to CHT/HA films with the same number of bilayers were marked by doubles symbols (##, p<0.01) and triple symbols (###, p<0.001).

Evaluation of cell behavior: Two cell lines, namely, a mouse lung fibroblastic cell line (L929) and a human primary osteosarcoma cell line (SaOs-2), were obtained from European Collection of cell Cultures (ECA CC, UK). The cells were cultured with low glucose DMEM supplemented with 3.7 $mg.mL^{-1}$ sodium bicarbonate, 10% FBS, and 1% penicillin–streptomycin at pH 7.4. The cells were grown in 75 cm^2 tissue culture flasks and incubated at 37 °C in a humidified air atmosphere of 5% CO_2. The medium was changed every 3–4 days. At 90% of confluence, cells grown in tissue culture flasks were washed with PBS and subsequently detached by a chemical procedure with 0.05% trypsin-EDTA solution for 5 min at 37 °C in a humidified air atmosphere of 5% CO_2. To inactivate the trypsin effect, cell culture medium was added. The cells were then centrifuged at 300 g and 25 °C for 5 min and the medium was decanted.

Prior to cell seeding, the multilayer films with 5, 10 and 15 bilayers were built on the patterned superhydrophobic surface. After drying, droplets of genipin and fibronectin were dispensed atop of the created films. An array of 48 combinations of biomaterials based in an initial library of five polyelectrolytes was created. The design of the patterned chip is based on the construction of four parameters of each multilayer film, containing 6 replicates of the wettable spots with the same number of multilayers deposited. Since two cell types were studied in the same chip, a total of 48 distinct conditions for the same number film layers were used. Based on previous works, genipin was used in the concentration of 1 $mg.mL^{-1}$,[41] and the patterned slide was slide was incubated for 24 hours, in the incubator at 37°C. After 23 hours of incubation, droplets of fibronectin with a concentration of 50 $\mu g.mL^{-1}$ [8] were added to other spots of the same patterned chip. Afterwards the chip was again incubated for 1 hour. The coated films with 5, 10 and 15 bilayers were carefully washed, and sterilized by UV radiation for 30 minutes. Droplets of 5 µL of supplemented DMEM containing a cell suspension with 5×10^3 cells was added on the top of the coated multilayer films. Then, the samples were incubated at 37 °C in a humidified air atmosphere of 5% CO_2.

After one day in culture, and prior to cell staining, the entire patterned chip was rinsed thrice with sterile PBS and fixed with formalin 2.5% (v/v) for cytoskeleton and nuclei staining with phalloidin–tetramethylrhodamine B isothiocyanate (Phalloidin- TRITC, Sigma-Aldrich) and 4,6-diamino-2-phenyindole

dilactate (DAPI, Sigma-Aldrich). Samples were incubated in the dark with Phalloidin-TRITC solutions (1:100) for 30 minutes, then with DAPI for 10 minutes (1:1000). After rinsing the samples, the cytoskeleton and nuclei were observed using an Imager Z1 fluorescence microscope (Zeiss) and photographed using an Axio Cam MRm (Zeiss). ImageJ software was used to calculate the percentage of the area covered by the cells adhered on the multilayer films.

5.6 Acknowledgements

The authors acknowledge the financial support from the FCT- Fundação para a Ciência e para a Tecnologia through the Ph.D. grants with the references SFRH/BD/73119/2010 and SFRH / BD / 70107 / 2010. The research was also funded by FEDER through the Competitive Factors Operation Program - COMPETE and by National Funds through FCT in the scope of the project PTDC/CTM-BIO/1814/2012.

5.7 References

[1] Figure5. Dzenis, Materials Science - Structural Nanocomposites, Science, 319 (2008) 419-420.

[2] Figure5. Huang, X.F. Duan, Q.Q. Wei, C.M. Lieber, Directed Assembly Of One-Dimensional Nanostructures Into Functional Networks, Science, 291 (2001) 630-633.

[3] B.D. Gates, Q.B. Xu, M. Stewart, D. Ryan, C.G. Willson, G.M. Whitesides, New Approaches To Nanofabrication: Molding, Printing, And Other Techniques, Chemical Reviews, 105 (2005) 1171-1196.

[4] R.R. Costa, J.F. Mano, Polyelectrolyte Multilayered Assemblies In Biomedical Technologies, Chemical Society Reviwes, 43 (2014) 3453-3479.

[5] J.F. Quinn, A.P.R. Johnston, G.K. Such, A.N. Zelikin, F. Caruso, Next Generation, Sequentially Assembled Ultrathin Films: Beyond Electrostatics, Chemical Society Reviews, 36 (2007) 707-718.

[6] K. Ariga, J.P. Hill, M.V. Lee, A. Vinu, R. Charvet, S. Acharya, Challenges And Breakthroughs In Recent Research On Self-Assembly, Science And Technology Of Advanced Materials, 9 (2008).

[7] A.L. Hook, D.G. Anderson, R. Langer, P. Williams, M.C. Davies, M.R. Alexander, High Throughput Methods Applied In Biomaterial Development And Discovery, Biomaterials, 31 (2010) 187-198.

[8] A.I. Neto, C.A. Custodio, Figure5. Song, J.F. Mano, High-Throughput Evaluation Of Interactions Between Biomaterials, Proteins And Cells Using Patterned Superhydrophobic Substrates, Soft Matter, 7 (2011) 4147-4151.

[9] R. Potyrailo, K. Rajan, K. Stoewe, I. Takeuchi, B. Chisholm, Figure5. Lam, Combinatorial And High-Throughput Screening Of Materials Libraries: Review Of State Of The Art, Acs Combinatorial Science, 13 (2011) 579-633.

[10] C.G. Simon, Jr., S. Lin-Gibson, Combinatorial And High-Throughput Screening Of Biomaterials, Advanced Materials, 23 (2011) 369-387.

[11] M.B. Oliveira, J.F. Mano, High-Throughput Screening For Integrative Biomaterials Design: Exploring Advances And New Trends, Trends In Biotechnology, 32 (2014) 627-636.

[12] J. Park, P.T. Hammond, Multilayer Transfer Printing For Polyelectrolyte Multilayer Patterning: Direct Transfer Of Layer-By-Layer Assembled Micropatterned Thin Films, Advanced Materials, 16 (2004) 520-525.

[13] C. Kantak, S. Beyer, L. Yobas, T. Bansal, D. Trau, A 'Microfluidic Pinball' For On-Chip Generation Of Layer-By-Layer Polyelectrolyte Microcapsules, Lab On A Chip, 11 (2011) 1030-1035.

[14] Figure5. Wang, Figure5. Liu, Figure5. Cheng, E. Kim, G.Figure5. Rubloff, Figure5.E. Bentley, G.F. Payne, Coupling Electrodeposition With Layer-By-Layer Assembly To Address Proteins Within Microfluidic Channels, Advanced Materials, 23 (2011) 5817-5821.

[15] S.A. Sukhishvili, S. Granick, Layered, Erasable Polymer Multilayers Formed By Hydrogen-Bonded Sequential Self-Assembly, Macromolecules, 35 (2002) 301-310.

[16] G.K. Such, A.P.R. Johnston, F. Caruso, Engineered Hydrogen-Bonded Polymer Multilayers: From Assembly To Biomedical Applications, Chemical Society Reviews, 40 (2011) 19-29.

[17] M. Marchl, M. Edler, A. Haase, A. Fian, G. Trimmel, T. Griesser, B. Stadlober, E. Zojer, Tuning The Threshold Voltage In Organic Thin-Film Transistors By Local Channel Doping Using Photoreactive Interfacial Layers, Advanced Materials, 22 (2010) 5361-5365.

[18] M. Sailer, C.J. Barrett, Fabrication Of Two-Dimensional Gradient Layer-By-Layer Films For Combinatorial Biosurface Studies, Macromolecules, 45 (2012) 5704-5711.

[19] S.A. Castleberry, Figure5. Li, D. Deng, S. Mayner, P.T. Hammond, Capillary Flow Layer-By-Layer: A Microfluidic Platform For The High-Throughput Assembly And Screening Of Nano Layered Film Libraries, Acs Nano, 8 (2014) 6580-6589.

[20] Josep Sedó, Javier Saiz-Poseu, Felix Busqué, D. Ruiz-Molina, Catechol-Based Biomimetic Functional Materials, Advanced Materials, 25 (2012) 653-701.

[21] L. Zhang, Figure5.-B. Yin, J.-J. Luo, P.-Figure5. Yang, J.-Figure5. Cai, Construction Of Electrochemical Sensor Based On Poly Dopamine-Hyaluronic Acid Composite Membrane For Detection Of Hydrogen Peroxide, Chinese Journal Of Analytical Chemistry, 41 (2013) 534-539.

[22] X. Zhang, Z. Li, X. Yuan, Z. Cui, X. Yang, Fabrication Of Dopamine-Modified Hyaluronic Acid/Chitosan Multilayers On Titanium Alloy By Layer-By-Layer Self-Assembly For Promoting Osteoblast Growth, Applied Surface Science, 284 (2013) 732-737.

[23] Figure5.Figure5. Kim, J.B. Park, M.J. Kang, Figure5.Figure5. Park, Surface-Modified Silk Hydrogel Containing Hydroxyapatite Nanoparticle With Hyaluronic Acid-Dopamine Conjugate, International Journal Of Biological Macromolecules, 70 (2014) 516-522.

[24] S. Yuan, Z. Li, J. Zhao, S. Luan, J. Ma, L. Song, Figure5. Shi, J. Jin, J. Yin, Enhanced Biocompatibility Of Biostable Poly(Styrene-B-Isobutylene-B-Styrene) Elastomer Via Poly(Dopamine)-Assisted Chitosan/Hyaluronic Acid Immobilization, Rsc Advances, 4 (2014) 31481-31488.

[25] A.I. Neto, A.C. Cibrao, C.R. Correia, R.R. Carvalho, G.M. Luz, G.G. Ferrer, G. Botelho, C. Picart, N.M. Alves, J.F. Mano, Nanostructured Polymeric Coatings Based On Chitosan And Dopamine-Modified Hyaluronic Acid For Biomedical Applications, Small, 10 (2014) 2459-2469.

[26] C.J. Detzel, A.L. Larkin, P. Rajagopalan, Polyelectrolyte Multilayers In Tissue Engineering, Tissue Engineering Part B-Reviews, 17 (2011) 101-113.

[27] J. Mullegger, G. Lepperdinger, Hyaluronan Is An Abundant Constituent Of The Extracellular Matrix Of Xenopus Embryos, Molecular Reproduction And Development, 61 (2002) 312-316.

[28] Figure5. Luo, K.R. Kirker, G.D. Prestwich, Cross-Linked Hyaluronic Acid Hydrogel Films: New Biomaterials For Drug Delivery, Journal Of Controlled Release, 69 (2000) 169-184.

[29] D. Jiang, J. Liang, P.Figure5. Noble, Hyaluronan In Tissue Injury And Repair, Annual Review Of Cell And Developmental Biology, 23 (2007) 435-461.

[30] B. Thierry, F.M. Winnik, Figure5. Merhi, M. Tabrizian, Nanocoatings Onto Arteries Via Layer-By-Layer Deposition: Toward The In Vivo Repair Of Damaged Blood Vessels, Journal Of The American Chemical Society, 125 (2003) 7494-7495.

[31] Figure5.Figure5. Wang, Figure5. Sun, B. Tang, Study On Fluorescence Property Of Dopamine And Determination Of Dopamine By Fluorimetry, Talanta, 57 (2002) 899-907.

[32] K.A. Marx, Quartz Crystal Microbalance: A Useful Tool For Studying Thin Polymer Films And Complex Biomolecular Systems At The Solution-Surface Interface, Biomacromolecules, 4 (2003) 1099-1120.

[33] Figure5.Figure5. Tonnesen, J. Karlsen, Alginate In Drug Delivery Systems, Drug Development And Industrial Pharmacy, 28 (2002) 621-630.

[34] J.F. Mano, G.A. Silva, Figure5.S. Azevedo, P.B. Malafaya, R.A. Sousa, S.S. Silva, L.F. Boesel, J.M. Oliveira, T.C. Santos, A.P. Marques, N.M. Neves, R.L. Reis, Natural Origin Biodegradable Systems In Tissue Engineering And Regenerative Medicine: Present Status And Some Moving Trends, Journal Of The Royal Society Interface, 4 (2007) 999-1030.

[35] K.Figure5. Lee, D.J. Mooney, Alginate: Properties And Biomedical Applications, Progress In Polymer Science, 37 (2012) 106-126.

[36] P. Bieker, M. Schoenhoff, Linear And Exponential Growth Regimes Of Multi Layers Of Weak Polyelectrolytes In Dependence On Ph, Macromolecules, 43 (2010) 5052-5059.

[37] N.M. Alves, C. Picart, J.F. Mano, Self Assembling And Crosslinking Of Polyelectrolyte Multilayer Films Of Chitosan And Alginate Studied By Qcm And Ir Spectroscopy, Macromolecular Bioscience, 9 (2009) 776-785.

[38] G.V. Martins, E.G. Merino, J.F. Mano, N.M. Alves, Crosslink Effect And Albumin Adsorption Onto Chitosan/Alginate Multilayered Systems: An In Situ Qcm-D Study, Macromolecular Bioscience, 10 (2010) 1444-1455.

[39] G.V. Martins, J.F. Mano, N.M. Alves, Nanostructured Self-Assembled Films Containing Chitosan Fabricated At Neutral Ph, Carbohydrate Polymers, 80 (2010) 570-573.

[40] S.G. Caridade, C. Monge, F. Gilde, T. Boudou, J.F. Mano, C. Picart, Free-Standing Polyelectrolyte Membranes Made Of Chitosan And Alginate, Biomacromolecules, 14 (2013) 1653-1660.

[41] J.M. Silva, A.R.C. Duarte, S.G. Caridade, C. Picart, R.L. Reis, J.F. Mano, Tailored Freestanding Multi Layered Membranes Based On Chitosan And Alginate, Biomacromolecules, 15 (2014) 3817-3826.

[42] N.M. Oliveira, A.I. Neto, Figure5. Song, J.F. Mano, Two-Dimensional Open Microfluidic Devices By Tuning The Wettability On Patterned Superhydrophobic Polymeric Surface, Applied Physics Express, 3 (2010) 085205.

[43] A.I. Neto, Figure5.J. Meredith, C.L. Jenkins, J.J. Wilker, J.F. Mano, Combining Biomimetic Principles From The Lotus Leaf And Mussel Adhesive: Polystyrene Films With Superhydrophobic And Adhesive Layers, Rsc Advances, 3 (2013) 9352-9356.

[44] Figure5. Lee, Figure5. Lee, A.R. Statz, J. Rho, T.G. Park, P.B. Messersmith, Substrate-Independent Layer-By-Layer Assembly By Using Mussel-Adhesive-Inspired Polymers, Advanced Materials, 20 (2008) 1619-+.

[45] J. Borges, S.G. Caridade, J.M. Silva, J.F. Mano, Unraveling The Effect Of The Hydration Level On The Molecular Mobility Of Nanolayered Polymeric Systems, Macromolecular Rapid Communications, 36 (2015) 405-412.

[46] N. Thirawong, J. Nunthanid, S. Puttipipatkhachorn, P. Sriamornsak, Mucoadhesive Properties Of Various Pectins On Gastrointestinal Mucosa: An In Vitro Evaluation Using Texture Analyzer, European Journal Of Pharmaceutics And Biopharmaceutics, 67 (2007) 132-140.

[47] S.M. Oliveira, V.E. Santo, M.E. Gomes, R.L. Reis, J.F. Mano, Layer-By-Layer Assembled Cell Instructive Nanocoatings Containing Platelet Lysate, Biomaterials, 48 (2015) 56-65.

[48] E. Ruoslahti, M. Pierschbacher, New Perspectives In Cell Adhesion: Rgd And Integrins, Science, 238 (1987) 491-497.

[49] C.R. Wittmer, J.A. Phelps, C.M. Lepus, Figure5.M. Saltzman, M.J. Harding, P.R. Van Tassel, Multilayer Nanofilms As Substrates For Hepatocellular Applications, Biomaterials, 29 (2008) 4082-4090.

[50] J.M. Silva, A.R.C. Duarte, C.A. Custódio, P. Sher, A.I. Neto, A.C.M. Pinho, J. Fonseca, R.L. Reis, J.F. Mano, Nanostructured Hollow Tubes Based On Chitosan And Alginate Multilayers, Advanced Healthcare Materials, 3 (2014) 433-440.

[51] Natália M. Alves, Iva Pashkuleva, Rui L. Reis, J.F. Mano, Controlling Cell Behavior Through The Design Of Polymer Surfaces, Small, 6 (2010) 2208–2220.

[52] K. Webb, V. Hlady, P.A. Tresco, Relationships Among Cell Attachment, Spreading, Cytoskeletal Organization, And Migration Rate For Anchorage-Dependent Cells On Model Surfaces, Journal Of Biomedical Materials Research, 49 (2000) 362-368.

[53] A. Schneider, G. Francius, R. Obeid, P. Schwinte, J. Hemmerle, B. Frisch, P. Schaaf, J.C. Voegel, B. Senger, C. Picart, Polyelectrolyte Multilayers With A Tunable Young's Modulus: Influence Of Film Stiffness On Cell Adhesion, Langmuir, 22 (2006) 1193-1200.

[54] C. Picart, Polyelectrolyte Multilayer Films: From Physico-Chemical Properties To The Control Of Cellular Processes, Current Medicinal Chemistry, 15 (2008) 685-697.

[55] K. Ren, T. Crouzier, C. Roy, C. Picart, Polyelectrolyte Multilayer Films Of Controlled Stiffness Modulate Myoblast Cell Differentiation, Advanced Functional Materials, 18 (2008) 1378-1389.

[56] S.M. Oliveira, T.Figure5. Silva, R.L. Reis, J.F. Mano, Nanocoatings Containing Sulfated Polysaccharides Prepared By Layer-By-Layer Assembly As Models To Study Cell-Material Interactions, Journal Of Materials Chemistry B, 1 (2013) 4406-4418.

[57] S. Yamanlar, S. Sant, T. Boudou, C. Picart, A. Khademhosseini, Surface Functionalization Of Hyaluronic Acid Hydrogels By Polyelectrolyte Multilayer Films, Biomaterials, 32 (2011) 5590-5599.

[58] V. Gribova, R. Auzely-Velty, C. Picart, Polyelectrolyte Multilayer Assemblies On Materials Surfaces: From Cell Adhesion To Tissue Engineering, Chemistry Of Materials, 24 (2012) 854-869.

[59] S.G. Caridade, C. Monge, J. Almodovar, R. Guillot, J. Lavaud, V. Josserand, J.-L. Coll, J.F. Mano, C. Picart, Myoconductive And Osteoinductive Free-Standing Polysaccharide Membranes, Acta Biomaterialia, 15 (2015) 139-149.

[60] M.B. Oliveira, A.I. Neto, C.R. Correia, M. Isabel Rial-Hermida, C. Alvarez-Lorenzo, J.F. Mano, Superhydrophobic Chips For Cell Spheroids High-Throughput Generation And Drug Screening, Acs Applied Materials & Interfaces, 6 (2014) 9488-9495.

[61] A.I. Neto, C.R. Correia, M.B. Oliveira, M.I. Rial-Hermida, C. Alvarez-Lorenzo, R.L. Reis, J.F. Mano, A Novel Hanging Spherical Drop System For The Generation Of Cellular Spheroids And High Throughput Combinatorial Drug Screening, Biomaterials Science, 3 (2015) 581-585.

[62] M.B. Oliveira, M.P. Ribeiro, S.P. Miguel, A.I. Neto, P. Coutinho, I.J. Correia, J.F. Mano, In Vivo High-Content Evaluation Of Three-Dimensional Scaffolds Biocompatibility, Tissue Engineering Part C-Methods, 20 (2014) 851-864.

CHAPTER 6. BIOMIMETIC MINIATURIZED PLATFORM ABLE TO SUSTAIN ARRAYS OF LIQUID DROPLETS FOR HIGH-THROUGHPUT COMBINATORIAL TESTS *

6.1 Abstract

The development of high-throughput and combinatorial technologies is helping to speed up research that is applicable in many areas of chemistry, engineering and biology. We propose a new model of flat devices for high-throughput screening of accelerated evaluations of multiplexed processes and reactions taking place in aqueous-based environments. Superhydrophobic (SH) biomimetic surface based on so-called lotus effect were produced onto which array of micro-indentations to fix liquid droplets, based on the rose petals effect. The developed platforms were able to sustain arrays of quasi-spherical micro droplets allowing to isolate and confine different combinations of substances and living cells. We showed that distinct compartmentalized physical, chemical and biological processes may take place and be monitored in each droplet. The devices permit the addition/removal of liquid and mechanical stirring by adding the magnetic microparticles in each droplet. By facing down the chip, it was possible to produce arrays of cells spheroids developed by gravity in the suspended droplets, with potential to be used as micro-tissues in drug screening tests.

* *Neto A. I., Correia C. R., Custódio C. A., and Mano J. F. Biomimetic Miniaturized Platform Able to Sustain Arrays of Liquid Droplets for High-Throughput Combinatorial Tests.* ***Advanced Functional Materials****, 24, 5096–5103, 2014.*

6.2 Introduction

The development of combinatorial methods can accelerate the scientific outcome, and thus the expansion of new materials and processes, when the effect of multiple variables is required [1]. For example, high-throughput screening have been employed in the study of interactions between biomaterials, cells and soluble factors, helping to identify the optimal conditions for particular biomedical applications [2-4]. Microarrays enable to assemble numerous cell-material or cell-cell combinations to analyze different parameters, including cell adhesion, proliferation, differentiation and gene expression that can be monitored on a single microarray chip [5-7]. Array-based technologies have broad applications in drug discovery, microbiology, cell biology and in many other non-biomedical fields. The high content and small scale of the micro arrays provide parallel processing and monitoring of chemical and biological assays using low amounts of liquids. The conventional microtiter plate-based assays have moved away from the conventional 96-well format to the 384 well system, or even the 1536-well platform or high dense microfluidic devices [8]. Tung et al. [9] report a new technology enable to culture 384 spheroids in a hanging drop approach and in the same platform. However, the developed platform presents a single pattern and is fabricated by the injection molding technology. The cost associated to the production of such innovative platforms requires high precision and expertise equipment, which can be extremely expensive. Current developments in microfluidic, microarrays systems and micro-reactors devices are directed towards further reductions in sample volumes, increasing analytical throughput and to integrate the pre- and post assay processing. Microarrays, such as DNA and protein quantification, have showed indispensable roles in genomic and proteomic research [10]. However, in chemical microarrays, the evaluation of a large number of chemical structures and biological targets [11], has been a longstanding process. The problem is associated with the fact that such microarrays do not allow to perform individual analysis. In our group, we made advances in this field, by creating an innovative platform for the individually dispense of miniaturized biomaterials, cells and culture medium, based on the use superhydrophobic (SH) surfaces patterned with wettable regions [12-16]. The topography of these SH surfaces exhibit peculiar features like micro- and nano- hierarchical roughness, leading to low surface energy, mimicking SH surfaces found in the nature, such as the Lotus leaf. We hypothesize that such SH substrates could be used to work with individual liquid volumes for a series of tests. Our main motivation is the handling of small amount of liquid volumes, which is an important task in miniaturized bio-analytical and biomedical systems, since decreasing the size of the samples can reduce significantly the required time for the analysis and associated costs.

In this work we propose the use of SH platforms to arrange quasi-spherical aqueous-based droplets with the capability to support and monitor a series of chemical and biological reactions on a lab-on-chip scale. Such platforms could have several advantages in comparison with the microarrays presented in the literature. The size and composition can be easily controlled in an individual form, and the processes in the liquid state occur with minimum contact with the solid substrate. Furthermore, the SH platform is solely physically modified polystyrene (PS) [17-19], which guarantees the lack of cytotoxicity and the chemical stability of the platform.

We demonstrated that it is possible to add agitation capability in the developed droplet-based micro-reactor using magnetic microspheres, enabling to create mechanical stresses inside the microliter-size droplets. The droplets are fixed in defined positions by the action of micro-indentations patterned with an array arrangement on polystyrene SH surfaces. Different experiments were performed to demonstrate the suitability of the developed platform, including: (i) the efficacy of the mechanical agitation tested in a simple physical process, namely the dissolution of salt crystals inside the droplets; (ii) the monitoring of a chemical reaction, namely the crosslinking of chitosan (CHT) with genipin with different concentrations of reagents; (iii) the evaluation of cell viability, in this case tested when cells are in contact with culture media at different pHs; and (iv) the evaluation of the cytotoxicity of an antitumor drug at different concentrations in cells spheroids. For the last example, we took advantage of the high positional stability and adhesiveness of the droplets that allowed to invert 180° the SH platform. Therefore, cells initially suspended in the droplets give rise to spheroids, formed by gravity. The developed cell spheroids were used as micro-tissues for a drug delivery assay. The viability of the cells in the spheroids was assessed using image-based analysis tools upon adding doxorubicin, a drug used in cancer chemotherapy, in different concentrations.

6.3 Results and Discussion

6.3.1 Preparation and wettability characterization of SH patterned chips

Polystyrene SH surfaces were prepared by phase-separation methodology, mimicking the extreme water repellency of lotus leave by presenting a water contact angle (WCA) higher than 150°. This feature was achieved by the introduction of micro- and nano- roughness (Figure 6.1a), without further chemical modification of the polymeric structure. Such substrates presented a similar topography previously observed in polystyrene SH substrates [19]. The developed surfaces patterned with adhesive micro-indentations (Figure 6.1b) were used as support for arrays of aqueous solutions-based droplets. Micro-

indentations with different sizes were produced on the rough surface in order to fix liquid droplets, mimicking the effect of rose petals. In these surfaces, water droplets show spherical shape, but they cannot roll off the surface even when the surface is turned upside down [20-22], because of the peculiar morphology characterized by micro papillae with cuticular folds on top. In contrast to the lotus surface where the air pockets formed between cell papilla provide low adhesion to droplets, the rose petal surface prevent air pocket formation and droplets penetrate into the cuticular folds by capillary forces [23, 24]. The micro- and nanostructures of the surface of rose petals are larger than those found on the lotus leaves, allowing droplets to penetrate into the larger grooves of the petals, causing the Cassie impregnating wetting state [23].

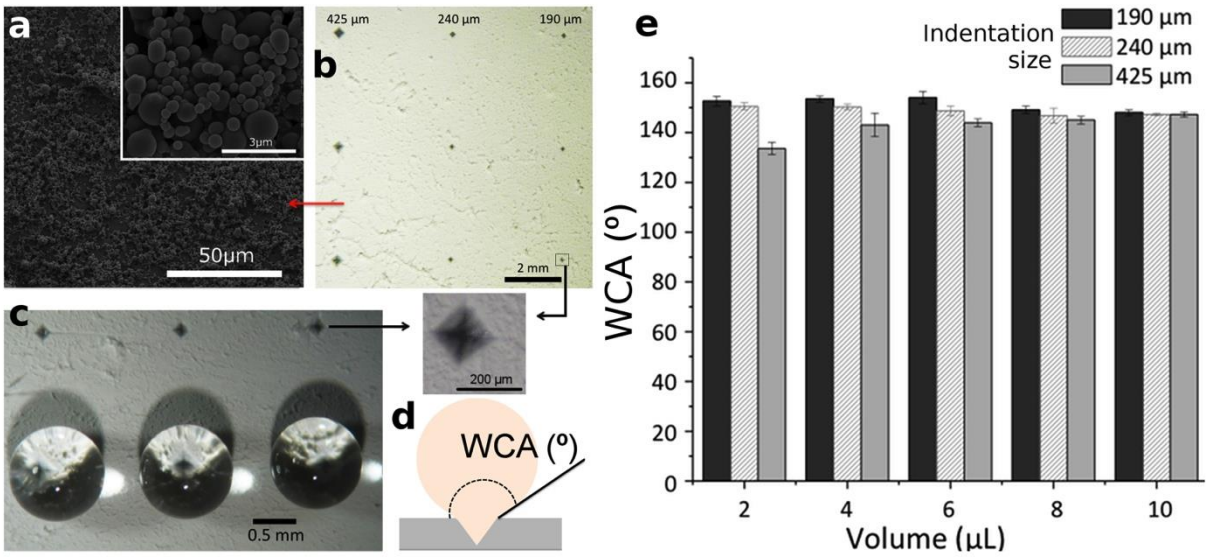

Figure 6.1 a) Microstructure of polystyrene SH surface observed by SEM (two magnifications). b) Upper view of a SH platform patterned with micro-indentations to fix water droplets in the desired areas (c). d) Scheme of the water droplet position in the micro-indentations magnifying the effect of the penetration of the liquid in the mark. e) Water contact angle (WCA) measurement of water droplets with different volumes dispensed in the micro-indentations with different sizes.

Water droplets placed on the micro-indentations exhibit a close spherical shape promoted by the extreme water repellent of the SH surface but are fixed by the depression features. By producing multiple indentations over the SH surfaces one can generate attachment points to produce arrays of droplets with any geometrical disposition and distances between them (Figure 6.1c). The indentations created on low surface-energy SH surfaces present some advantages when compared with high adhesive SH surfaces, due to the possibility to confine and stabilize droplets only on the desired places with minimum contact area between the droplet and the SH surface (Figure 6.1d).

The WCA was measured for droplets with distinct volumes placed over indentations of different sizes (Figure 6.1e). Small volumes of droplets in the micro-indentations present WCA higher than 150°,

showing that the smallest indentations on the SH surface are able to fix the droplets on the surface, without compromising the water repellency of the surface.

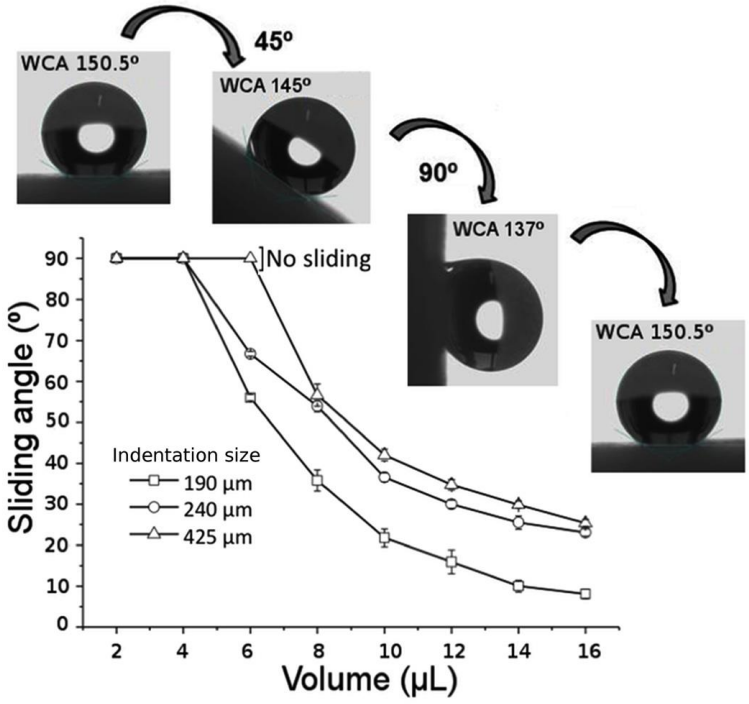

Figure 6.2 Sliding angle of droplets with different water volumes on patterned SH surfaces with different micro-indentation sizes (see legend). Representative images are shown of water droplets with 4 µL deposited in micro-indentations with 190 µm of size in the surfaces with different tilt levels.

To assess the adhesive behavior of the indented points, the sliding angle was measured at different conditions of indentation sizes and droplet volumes - see Figure 6.2. The sliding angle is defined as the critical angle where a water droplet of certain volume and weight begins to slide down the sloping surface. The results show that when the liquid volume is lower than 4 µL, the water droplet cannot roll on neither be fixed on the surface for all micro-indentations sizes analyzed, even when the tilt of the surface is 90°. As expected, increasing the volume deposited in the micro-indentation decreases the sliding angles, since the capillary forces exert a less adhesion effect onto bigger droplets. Furthermore, the stability of the smallest droplets in the surfaces allows the WCA remaining inalterable, even after returning form a tilt of 90° (Figure 6.2 - representative images).

We hypothesized that the ability to fix with high stability arrays of controlled volumes of droplets, with minimum contact with the SH surfaces, could be useful in the design of innovative robust droplet-based microreactors.

6.3.2 Microdroplets based microreactor built on patterned SH surfaces

Droplet-based microreactor technology, such as microemulsions, array-based microreactors or microfluidic systems has attracted a great interest since it enables the miniaturization of reactions [25-28]. These systems permitted significant advances in protein crystallization, enzymatic kinetics, cell encapsulation, drug delivery or in other biochemical reactions [25] using several methods such as electrowetting [29], dielectrophoresis and magnetism [30, 31]. Shikida et al. [32] developed a magnetic bead-cluster handling system in which the droplets are driving from one well to the next, through a narrow connection by requiring the displacement of an external magnet. Based on this technology, SH surfaces have been used to manipulate the movement of magnetic droplets with a permanent magnet underneath [29, 33], with applicability in biotechnology and biomedicine, e.g. for high throughput biochemical analysis and microassays [34, 35]. In this work, we present an alternative possibility for create motion by activating the mobility of magnetic microparticles in fixed droplets to induce internal mechanical agitations. Water droplets with and without magnetic microparticles were firstly deposited on a patterned SH surface. $CuSO_4$ crystals were introduced inside the droplets, at time 0, and the platform was placed over a magnetic stirrer. The dissolution of the crystal was monitored by following with time the size of the crystal (h) comparing with its initial size (h_0) (Figure 6.3).

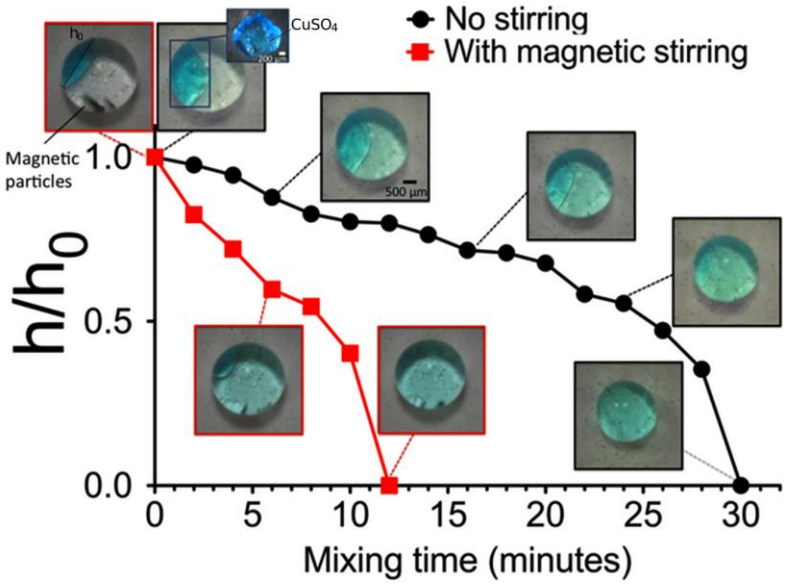

Figure 6.3 Miniaturized droplet based-reactor using water droplets with and without magnetic microparticles on patterned SH surface. Crystals of cooper sulphate were introduced inside the droplets, at time 0, and the platform, which contains droplets

with magnetic particles inside, was placed over a magnetic stirrer. The dissolution of the crystal was monitored by following the size of the crystal (h) comparing with its initial size (h_0).

The droplets that contained magnetic beads, the crystal with h_0 of about 2 mm was completely dissolved after 12 minutes (Figure 6.3). On the other hand, without mechanical agitation the dissolution time was the double. Obviously, the agitation power may be easily controlled in the magnetic stirrer. This result shows that the usual agitation and mixing processes performed in many chemical and engineering processes may be miniaturized in microliter volumes over the proposed platforms. Such example of controlled agitation can be essential in many biochemical and biological processes allowing the high throughput and effective study of complex processes at a lab-on-chip scale.

6.3.3 Monitoring of a crosslinking reaction through combinatorial chemical analysis

One current problem on the development of chemical microarrays is that compounds with different structures and properties are traditionally screened in a solution phase, and individual reactions need to be isolated in wells plates or tubes. There are several reasons to use droplets rather than well plates, namely smaller volumes, higher speeds and the isolation of the droplet content from the solid surface. Small volumes conserve expensive reagents and reduce the time required to assay extremely large libraries. Hydrogels have attracted a great interest in many fields, including biomedicine due to their general high biocompatibility, ability to encapsulate cells, mechanical and structural properties similar to soft tissues and their ability to be injected as a liquid in which gels *in situ* using minimally invasive procedures [36-38]. We have proposed SH-based chips to assess how cells interact with hydrogels in combinatorial studies [14].

Herein, we propose to analyze the formation of hydrogels on the developed platforms, starting with the deposition of combinations of liquid precursors in the form of droplets. We designed a combinatorial analysis to follow the crosslinking reaction of chitosan (CHT) with genipin, a natural crosslinking agent with low cytotoxicity. CHT hydrogels have been widely used in different biomedical applications [39-41]. In particular, crosslinked CHT with genipin have been used on the preparation of elastic and hydrogels for cartilage substitutes, drug delivery systems and the encapsulation of biological products [42-45]. Results show that the resulting crosslinked complexes are not cytotoxic [46]. The deposition of different droplet solutions containing different relative amounts of CHT and genipin was carried out in the developed microarray: distinct concentrations of 0.1, 1, 5, 7.5 and 10 $mg.mL^{-1}$ of CHT and genipin were analysed. The prepared solutions were dispensed in each spot with individual volumes of 10 μL. The same CHT solutions without genipin were used as control. The experiment was performed at 40°C under

saturated humidity to avoid droplets evaporation. Figure 6.4a shows the time evolution of the droplets in the array during the reaction. The dark-blue coloration that appears in the formed hydrogels is associated with the reaction between the amino groups of CHT and genipin [44]. Independent calibration experiments by reacting known amounts of glycine and genipin permitted to produce standard curves relating the intensity of the blue-color of the droplets and the extent of the reaction of the amine groups. An intensity map is shown in Figure 6.4b for the array analyzed, where the evolution of the extent of reaction of the amine group of CHT is represented as function of the time for each combinations analyzed.

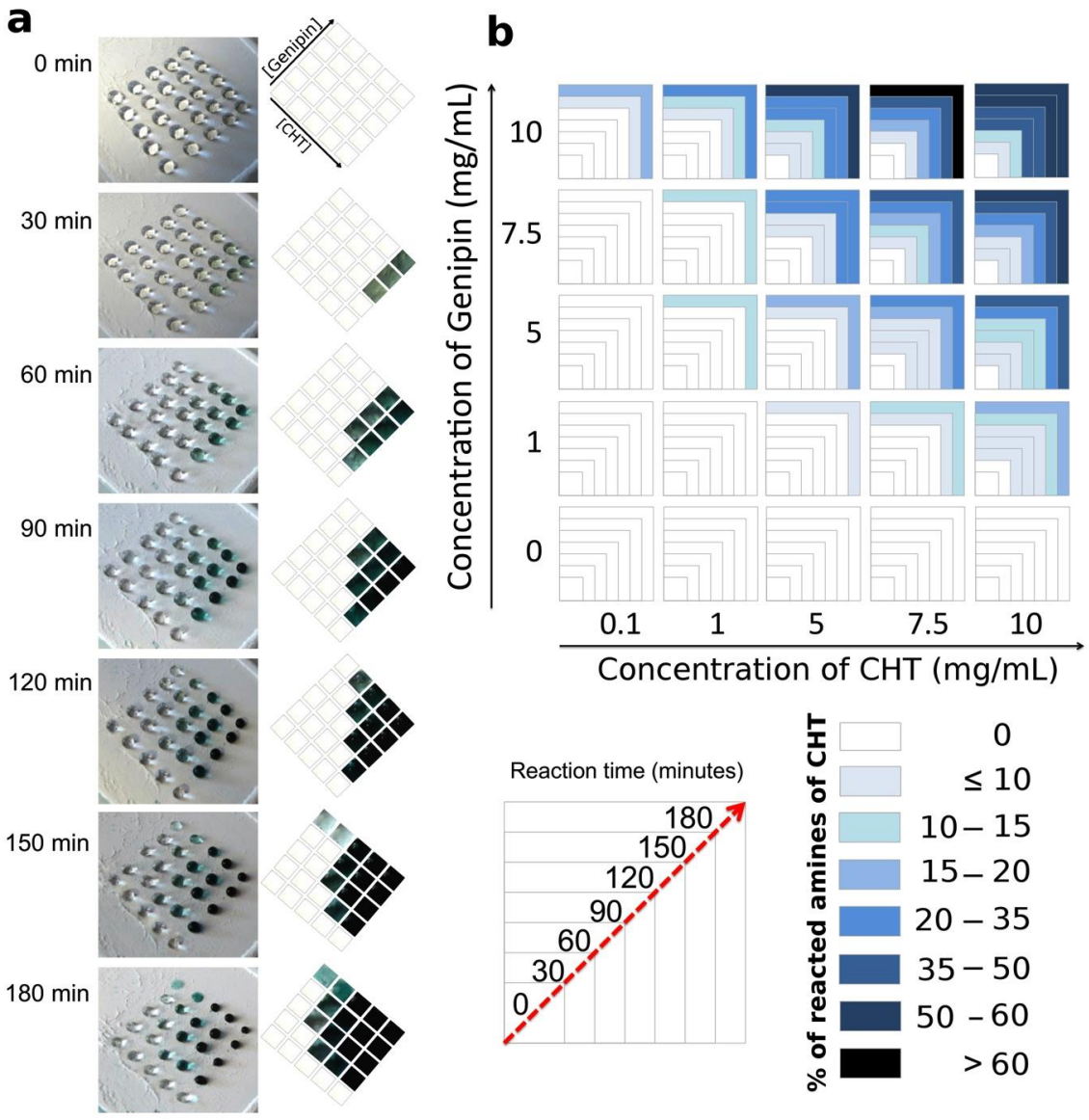

Figure 6.4 Combinatorial analysis following the reaction between CHT and genipin in arrays of droplets microreactors. a) Droplets with different concentrations of CHT and genipin were dispensed on a patterned SH surface. b) The intensity map

display the evolution of the crosslinking reaction between CHT and genipin for each concentration of reagents analysed. The increase of blue intensity is correlated to the percentage of reacted amine groups of CHT at different time points.

When the concentration of CHT and genipin increased, faster and more amino groups reacted, reaching values above 60% after 3 hours of incubation. The system used could be extended to more complex combinations, for example, by including mixtures of different polymers able to react with genipin. For example, Silva et al. [42] studied the crosslinking of the mixture of CHT and silk fibroin. The primary structure of fibroin chains contains a low percentage of amine-containing aminoacids, such as lysine and arginine that contributes for crosslinking sites upon reaction with genipin. We envisage the possibility to monitoring many other reactions occurring in aqueous media, provided that changes of color (even outside the visible spectrum) take place, such as addition or substitution reactions or redox processes.

6.3.4 High-throughput screening of cell-based assays

Microarrays platforms can address *in vitro* problems by creating distinct combinations of chemical/ biochemical microenvironment to study cellular behavior [47]. The advantage of the method proposed is that different biomaterials or even different types of cells can be easily deposited in each liquid spot with a minimum contact with the supporting solid material. As a simple demonstration of such hypothesis, we evaluated the influence of the pH in the cellular medium on the viability of fibroblasts-like cells.

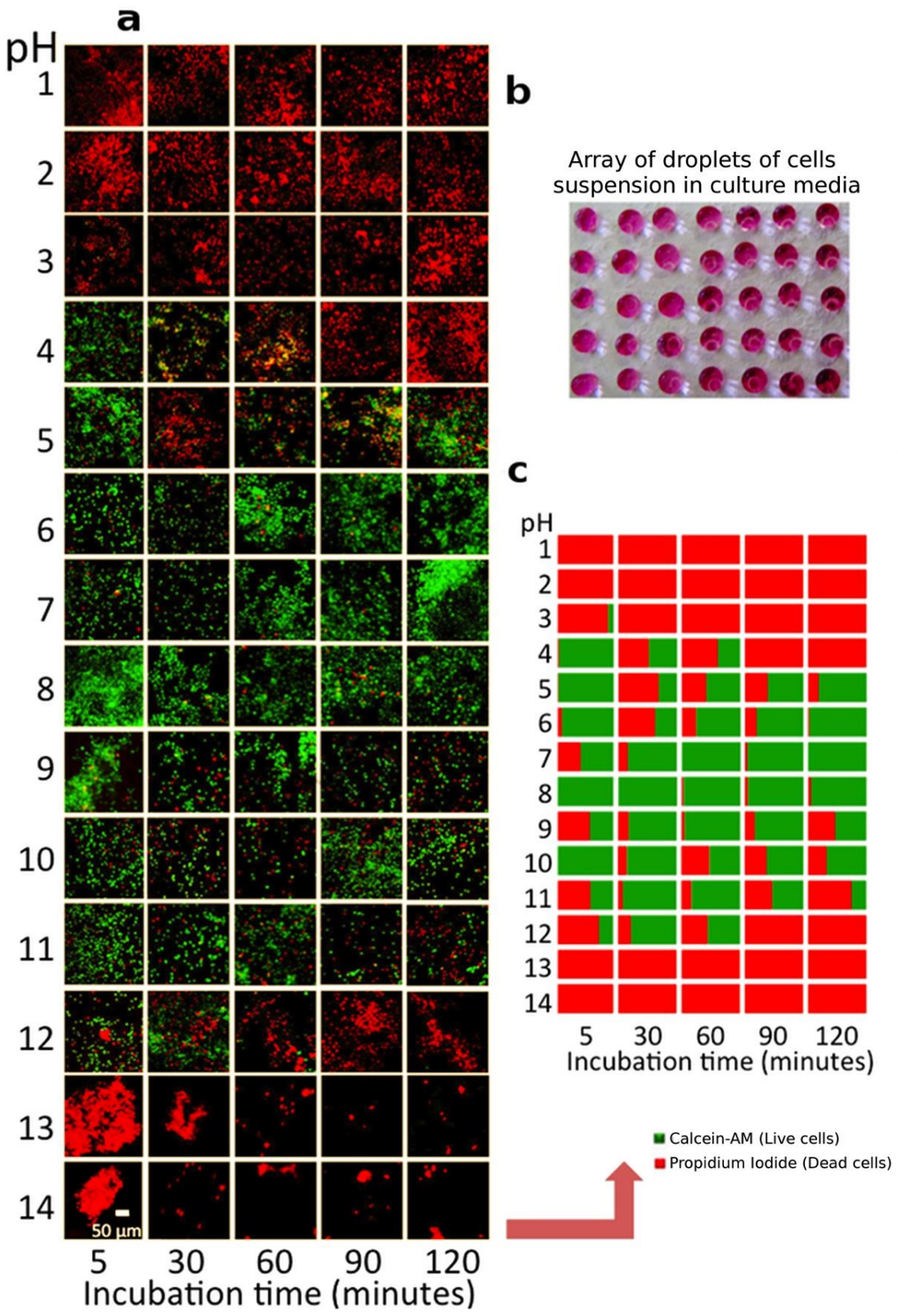

Figure 6.5 a) Fluorescence microscope images of the microarray composed of culture medium droplets at different pH (vertical axis) containing 1x10³ L929 cells/droplet taken at different incubation times (horizontal axis). b) Representative top-view image of the microarray where 10 µL of solution of individual cells suspension were dispensed in patterned SH surfaces. c) Intensity

map for the relative amount of live (green)/ dead (red) cells per spot corresponding to the same microarray tested with different pHs and culture times.

It is know that the effect of the pH in cells culture medium plays many critical roles in cell biological processes, such as viability, proliferation and apoptosis, ion transport and multidrug resistance [48]. Irregular pH values are usually associated with many diseases such as cancer [49]. Tumor microenvironments are often acidic, with pH levels as low as 6.2 [50]. Inside the cells, the variations of the pH can denature proteins or activate enzymes that normally are inactive around neutral pH. Knightom et al. [51] showed that acidic conditions promote angiogenesis of injured tissues. Figure 6.5 shows the viability of L929 cells suspended in culture media with different pH at different incubation times. Figure 6.5a shows the corresponding live/dead cell staining, obtained by the direct observation of the array of droplets dispensed in the platform (Figure 6.5b). As expected, and according to the literature [52-54], the fluorescence images confirmed that the favorable pH for cells to survive is between 6 and 8. In very acid and very alkaline medium, all cells died before 5 minutes. High-throughput image analysis of the micrographs permitted to built an intensity map of the values of the percentage of live/dead cells of the individual condition (Figure 6.5c), in which green and red colors represent the relative amount of living and dead cells. The results suggest that the proposed droplet-array chip may potentially be used to follow the cellular behavior of non-adherent cells, any cells in suspension or to investigate the effect of the surrounding atmosphere.

Most cell-based assays are currently performed on monolayer cultures (2D substrates) [13] or array plates [9, 55, 56] where cells adhere over a solid substrate, spread and form stress fibers between focal adhesions. The use of microarrays for combinatorial analysis present several advantages: high stability, well control and homogeneous cell environment, and facilitated microscope analysis and medium changes. However, in native tissues, many types of cells interact with other cells and with an extracellular matrix (ECM) within three-dimensional (3D) structures. The cell-cell and cell-ECM interactions provide mechanical and biochemical cue that can influence cellular functions and differentiation. Herein, we propose a new process for the formation of arrays of 3D cells agglomerates to be used in drug screening. In the developed platform, the cells are maintained in suspension, confined within a miniature liquid cage surrounded essentially by the gaseous environment of the device. The micro-indentations produced on the SH surfaces promote the fixation of the droplets over the high water repellent surfaces, even when the surface and cells suspension droplets are turned upside down. Therefore, it is possible to produce an array of microliter volume droplets with an inverse configuration that could be useful for high-throughput

monitoring. Extending the screening of cells in suspension of the last example, we employed the new arrangement to test the behavior of cells in an aggregated form- see Figure 6.6.

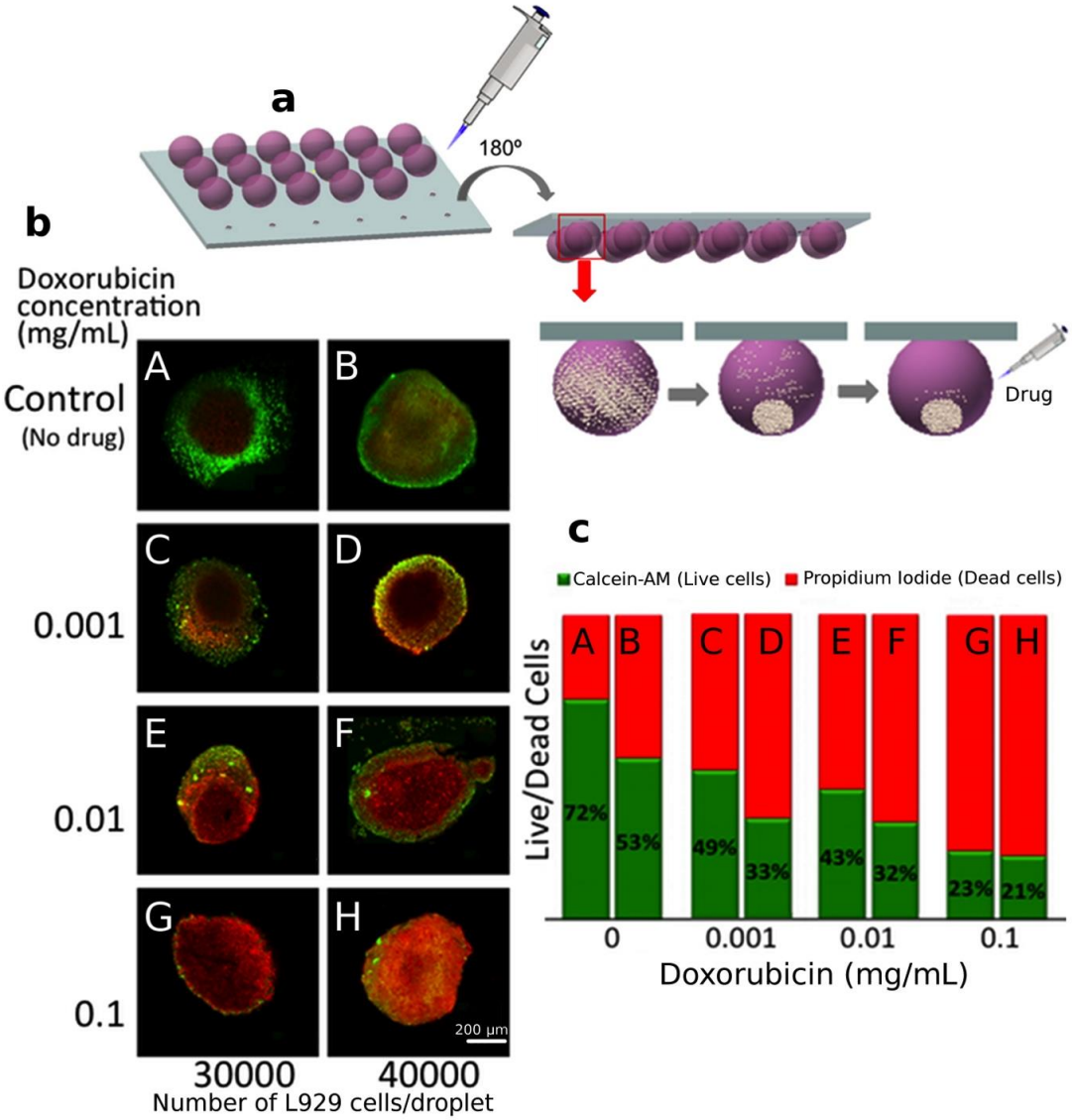

Figure 6.6 a) Scheme of SH surfaces patterned with micro-indentations able to suspend arrays of droplets containing cells; upon 24h spheroids are formed and drug-screening tests may be performed on the individual droplets. b) Fluorescent images of L929 spheroids obtained from confocal microscope 24h after the addition of various concentrations of doxorubicin. c) Percentage of live (green)/dead (red) cells per spot in the different conditions shown in b).

The commonly used methods to produce uniform cellular spheroids included: the hanging drop culture, microfluidic spheroid formation, non-adherent micropatterned surfaces and culture in microwell plates [56-61]. With the proposed platform it is possible to produce arrays of sedimented spheroids and test them in the same platform- see scheme in Figure 6.6a. Under this configuration, the cells in the suspended droplets give rise to spheroids formed by gravity. In this case, the cells do not have any contact

with solid substrate, and the clusters of cells, cultured in this environment, allow that cell-cell interactions dominate over cell-substrate interactions. The gravitational force applied on the cells in the hanging drop suspended cultures caused sedimentation and then aggregates became visible after 24h.

The platform used in this work present several advantages compared to the conventional methods used on the spheroids formation: the use of micro-size droplets for cell growth assays allow the drastic reduction of the volume in which the cells are grown; the use of SH surfaces mimicking the effect of rose petals, permits a minimum contact of the liquid to the surface, avoiding any interferences such as protein adsorption or release of molecules from the platform to the liquid media; cells culture medium can be changed easily without destroying the micro-tissues; drugs or other molecules can be added in any time, and if minimum precautions are taken, the mechanical impact in the spheroids is reduced; the platform is compatible or easily adapted with many analysis techniques, such as inverted confocal microscopes, in which droplets of cells suspension remain inverted on the SH surface; high-throughput combinatorial analysis may be performed *in situ* using different cells densities or drugs concentrations. For the proof-of-concept, droplets containing fibroblasts-like cells with two densities (30000 and 40000 cells/droplet) were dispensed on the inverted platform in order to promote the spheroids formation. After 24 h different amounts of doxorubicin were introduced in the droplets to assess the dose-dependent response of the formed tumor spheroids to this anticancer drug. The viability of the cells in the spheroids was measured after 24 hours using live/ dead staining images by confocal microscopy (Figure 6.6b). Images were selected out of the confocal stack to avoid overlapping of the same cells between images. Figure 6.6c shows the resulting analysis of the fraction of live and dead cells in the different conditions. As expected, with the increase of the doxorubicin concentration, cell viability decreased in both types of spheroids. The percentage of living cells is higher in the smaller spheroid. This should be due to the fact that assess of nutrients and the release of waste is less efficient in the larger and denser spheroid, giving rise to more extensive cell dead. The images of the Figure 6.6b clearly show that dead cells are mostly accumulated in the inner regions of the spheroids.

6.3 Conclusions

A new concept of substrates for anchoring aqueous-based microliter droplets was developed based on the use of superhydrophobic flat substrates with controlled positional adhesion. Such microarray chips are proposed to be used as a new low cost toolbox for high-throughput analysis in aqueous-based media. The platforms permit to screen physical, chemical and biological processes involving the combination of distinct elements and conditions, confined in spherical liquid mini-reactors. Events taking place in both

homogeneous and heterogeneous environments can be monitored inside the fixed droplets onto which relevant manipulations can be made including: mechanical agitations, mixture, adding/ removal of liquids and molecules or positioning the droplets at any angle relatively to the platform. Besides following more conventional chemical reactions the developed supports may also have potential to be used in biology or biomedical applications, including in the field of tissue engineering/regenerative medicine, biochemical and biological reactions, diagnosis, analytical analysis, drug discovery and drug delivery monitoring.

6.4 Experimental Section

Fabrication of patterned SH surfaces: Smooth polystyrene (PS) sheets, purchased from Goodfellow, UK, with 0.19 mm of thickness, ref. ST311190/1, were modified into SH substrates using a one-step phase-separation methodology under ambient condition. The surface modification was produced by dissolving 70% v/v solution of PS (Styrolution PS 158K) in tetrahydrofuran (THF, from Sigma-Aldrich) solvent for approx. 2 hours to form a pre-solution. Then, 1.4 mL of ethanol, from Panreac, was added into 2 mL of PS pre-solution and the mixed solution was stirred. A necessary volume to cover the PS substrate with this mixture was dipped onto a cleaned PS smooth sheet. After several seconds on air, the substrate with the mixture was immersed in ethanol for 1 min in order to force the polymer precipitation, leading to the formation of a rough and porous topography at both the nano and micro scale level. Afterwards the surface was dried at ambient temperature.

Micro-indentations over the SH surfaces were produced using a microhardeness tester equipment (Leica VMHT 30) applying loads of 2942 mN, 4903 mN and 19610 mN with a dwell time of 10 s. A sharp rigid Vickers diamond pyramid indenter (included angle α=136°) penetrated into the surface with a constant load during a complete loading–unloading cycle producing individual indentations. To produce the pedestals able to sustain arrays of droplets the indentations were placed in the surface at a distance of 5 mm from each other, with a square configuration.

The wettability of the smooth and polystyrene SH surfaces was assessed by contact angle measurements. Static water contact angle (WCA) measurements were carried out using an OCA15+ goniometer (DataPhysics, Germany) using the sessile drop method. Distilled water (4 μL) was dropped on the surfaces and pictures were taken after stabilization of the water drop. The adhesion of droplets with different volumes in the micro-indentations with different sizes of the SH surfaces were also studied: the sliding WCA of droplets with different volumes was analysed in each micro-indentations by sloping SH surfaces until 90°.

Surface morphology of the SH samples was analysed by scanning electron microscopy, SEM (Leica Cambridge, UK).

Preparation of micro-reactor based on patterned SH surfaces: Micro-indentations with 190 μm of size were produced in the SH surface using an indentation force of 2942 mN. Magnetic beads (Fe_3O_4, diameter ranging from 5-50 μm) were suspended and stirred until homogeneity in water with a concentration of 10 $mg.mL^{-1}$. A 10 μL water droplet with magnetic microspheres impregnated was deposited over a micro-indented SH surface using a microdispenser. The droplet suspension was subjected to a magnetic field by placing a magnetic stirrer (Fisher Scientific) with variable speed below the SH surface. The experience started with an increasing speed until 100 rpm allowing that the magnetic microspheres form chain-like structure under the influence of the imposed magnetic field. A cooper sulphate crystal was then incorporated into the droplet. Images of the droplets during the dissolution of the crystal were obtained using a Stereo Microscope + Lamp Schott KL 200 (model Stemi 1000 PG-HITEC, Zeiss) with 2.5X magnification, equipped with a digital camera with 5X optical zoom.

Chemically crosslinked hydrogels: Water-soluble highly purified chitosan, CHT (Protasan UP CL 213, viscosity 107 mPa.s, molecular weight Mw = $2.7x10^5$ $g.mol^{-1}$, 83% degree of deacetylation) was purchased from NovaMatrix. Genipin was purchased from Wako chemicals (ref n° 078-03021). Solutions of CHT were prepared using 1% v/v of acetic acid at concentrations of 0.1 $mg.mL^{-1}$, 1 $mg.mL^{-1}$, 5 $mg.mL^{-1}$, 7.5 $mg.mL^{-1}$ and 10 $mg.mL^{-1}$. Genipin solutions were prepared in ultra pure water at concentrations of 1 $mg.mL^{-1}$, 5 $mg.mL^{-1}$, 7.5 $mg.mL^{-1}$ and 10 $mg.mL^{-1}$. Both materials were mixed using the same quantity of the different concentrations leading to 20 different combinations. CHT solutions with the same concentrations without genipin were used as control.

The solutions were dropped in the chips prepared using the SH surfaces patterned with micro-indentations (190 μm size). The polymeric solutions were dispensed over the micro-indentations in a drop-by-drop logic in individual volumes of 10 μL. Each droplet separated by 5 mm, represents a different combination of CHT and genipin. After dispensing the solutions, the SH chips were placed in a desiccator with saturated humidity at 40°C. Images of the chip were captured in each 30 minutes until one of the conditions being completely crosslinked, confirmed by the unchanging of the color intensity. The percentage of reacted amine groups of CHT for each combination with genipin was quantified by colorimetric assay using the WCIF Image J software. A standard calibration curve (logarithmic curve, r^2=0.98) of pixel color intensity vs. glycine concentration was made. Different quantities of soluble glycine, ranging 0.2 to 2 $mg.mL^{-1}$ were prepared including genipin at a concentration of 10 $mg.mL^{-1}$. The measurements of the pixel intensity from each glycine concentration were performed over a total of 6

samples. The intensity of the pixels, grey scale 0-255, in which 0 correspond to dark color and 255 white color, was used to associate the color intensity of the solutions. The intensity color of the droplets of CHT with genipin was correlated with the pixels intensity of the standard curve. The percentage of reacted amine groups in each droplet was determined: the number of reacted amino molecules of the repeating unit of CHT obtained by the calibration curve was divided by the initial number of amine molecules.

Cell Expansion and Cell Culture: The immortalized mouse lung fibroblast cell line L929 was purchased from the European Collection of Cell Cultures and was used as well established cell line for viability studies. Cells were expanded in low glucose Dulbecco's Modified Eagle's Medium (DMEM), from Sigma-Aldrich, supplemented with 3.7 $g{\cdot}L^{-1}$ sodium bicarbonate, 10% heat-inactivated fetal bovine serum (FBS, Invitrogen) and 1% antibiotic/antimycotic (final concentration of penicillin 100 $units.mL^{-1}$ and streptomycin 100 $mg.mL^{-1}$; Gibco) at pH 7.4. Cells were grown in 75 cm^2 tissue culture flasks and incubated at 37 °C in a humidified air atmosphere of 5% CO2. Every 3–4 days, fresh medium was added. At 90% of confluence, L929 cells grown in tissue culture flasks were washed with PBS and subsequently detached by a chemical procedure with 0.05% trypsin-EDTA solution for 5 min at 37 °C in a humidified air atmosphere of 5% CO_2. To inactivate the trypsin effect, cell culture medium was added.

On-chip biological testing: Combinatorial analysis of fibroblasts-like cells on patterned SH surfaces was performed. Cells were re-suspended in culture medium with different pHs (pH ranging from 1-14) adjusted with HCl and NaOH solutions. Droplets of 5 µL with $1x10^3$ cells were seeded in the micro-indentations of patterned SH surfaces. Specimens were incubated at different times (5, 30, 60, 90 and 120 minutes) at 37°C in a humidified 5% CO_2 atmosphere. The cell viability was evaluated by a non-destructive live/dead assay. 2 µL of phosphate buffer saline PBS (Sigma-Aldrich) containing calcein-AM (1:500) and propidium iodide (1:1000) was placed at each droplet. Calcein-AM and propidium iodide dyes were purchased from Molecular Probes-Invitrogen. Samples were then incubated at 37°C for 10min and protected from the light. Droplets were visualized in the dark by fluorescence microscopy (Axioimage RZ1M, Zeiss). Living cells appeared in green and dead cells in red.

3D hanging droplet system: A hanging drops system used for the formation of spheroids was also performed using SH surfaces patterned with adhesive micro-indentations. Prior to cell seeding, the SH surfaces were sterilized by UV radiation for 30 min. Suspensions with different fibroblasts-like cell densities ($6x10^6$ and $8x10^6$ $cells.mL^{-1}$) were prepared. Droplets of 5 µL of each cell suspensions (in triplicate) were placed over the micro-indentations of the platform. Then, the platform was inverted 180° and incubated for 24h at 37°C in a humidified 5% CO_2 atmosphere. The platform containing droplets of cell suspensions was fixed into the lids of polystyrene petri dishes, and the bottom part was filled with

cell culture media, in order to create a saturated environment and avoid the evaporation of the droplets. After 24 hours of cell culture for spheroids formation, 2 µL of doxorubicin (Doxorubicin hydrochloride, Sigma-Aldrich) with different concentrations (0.1 $mg.mL^{-1}$, 0.01 $mg.mL^{-1}$ and 0.001 $mg.mL^{-1}$) were dispensed in the different droplets. The chip was again incubated for 24 hours at 37°C in a humidified 5% CO_2 atmosphere. The liquid content of the droplets with cell aggregates were carefully exchange with PBS. Afterwards, live/dead assay was performed. 2 µL of PBS containing calcein-AM and propidium was added to each condition to staining the spheroids. Pictures of the formed aggregates were taken in the confocal microscope to provide an accurate quantification (Olympus FluoView FV 1000).

Cell behaviour analysis: Image analysis tool (WCIF Image J software) was used to evaluate the percentage of live/dead cells of each droplet condition. Each image of stained cells with culture medium with different pHs obtained from fluorescent microscope was divided in green and red channels and transformed in a gray scale. The same procedure was made for each image of stained spheroid obtained from confocal microscope. The number in each channel (grey scale intensity 0-255, in which 0 correspond to black colour and 255 white colour) was counted and divided for the number of total analysed area (300 x 300 $pixels^2$). The same threshold criterion was used in all images.

6.5 Acknowledgements

The authors acknowledge the financial support from the FCT- Fundação para a Ciência e para a Tecnologia through the Ph.D. grants with the references SFRH/BD/73119/2010, SFRH/BD/69529/2010 and SFRH/BD/61390/2009. We also acknowledge the financial support of FEDER through the program Operacional Factores de Competitividade - COMPETE and from FCT - the Fundação para a Ciência e para a Tecnologia under the project PTDC/CTM-Bio/1814/2012.

6.6 References

[1] C.G. Simon, Jr., S. Lin-Gibson, Combinatorial And High-Throughput Screening Of Biomaterials, Adv Mater, 23 (2011) 369-387.

[2] M.R. Zonca, Jr., P.S. Yune, C.L. Heldt, G. Belfort, Y. Xie, High-Throughput Screening Of Substrate Chemistry For Embryonic Stem Cell Attachment, Expansion, And Maintaining Pluripotency, Macromol Biosci, 13 (2013) 177-190.

[3] S.W. Cranford, J. De Boer, C. Van Blitterswijk, M.J. Buehler, Materiomics: An -Omics Approach To Biomaterials Research, Adv Mater, 25 (2013) 802-824.

[4] M. Schenone, V. Dancik, B.K. Wagner, P.A. Clemons, Target Identification And Mechanism Of Action In Chemical Biology And Drug Discovery, Nature Chemical Biology, 9 (2013) 232-240.

[5] A.L. Hook, D.G. Anderson, R. Langer, P. Williams, M.C. Davies, M.R. Alexander, High Throughput Methods Applied In Biomaterial Development And Discovery, Biomaterials, 31 (2010) 187-198.

[6] A.N. Efremov, E. Stanganello, A. Welle, S. Scholpp, P.A. Levkin, Micropatterned Superhydrophobic Structures For The Simultaneous Culture Of Multiple Cell Types And The Study Of Cell-Cell Communication, Biomaterials, 34 (2013) 1757-1763.

[7] D.M. Titmarsh, H.Y. Chen, E.J. Wolvetang, J.J. Cooper-White, Arrayed Cellular Environments For Stem Cells And Regenerative Medicine, Biotechnology Journal, 8 (2013) 167-179.

[8] S.A. Sundberg, High-Throughput And Ultra-High-Throughput Screening: Solution- And Cell-Based Approaches, Current Opinion In Biotechnology, 11 (2000) 47-53.

[9] Y.C. Tung, A.Y. Hsiao, S.G. Allen, Y.S. Torisawa, M. Ho, S. Takayama, High-Throughput 3D Spheroid Culture And Drug Testing Using A 384 Hanging Drop Array, Analyst, 136 (2011) 473-478.

[10] C. Timm, C.M. Niemeyer, On-Chip Protein Biosynthesis, Angew Chem Int Ed Engl, 52 (2013) 2652-2654.

[11] Y.M. Foong, J. Fu, S.Q. Yao, M. Uttamchandani, Current Advances In Peptide And Small Molecule Microarray Technologies, Curr Opin Chem Biol, 16 (2012) 234-242.

[12] G.M. Luz, Á.J. Leite, A.I. Neto, W. Song, J.F. Mano, Wettable Arrays Onto Superhydrophobic Surfaces For Bioactivity Testing Of Inorganic Nanoparticles, Mater. Lett., 65 (2011) 296-299.

[13] A.I. Neto, C.A. Custódio, W. Song, J.F. Mano, High-Throughput Evaluation Of Interactions Between Biomaterials, Proteins And Cells Using Patterned Superhydrophobic Substrates, Soft Matter, 7 (2011) 4147.

[14] C.L. Salgado, M.B. Oliveira, J.F. Mano, Combinatorial Cell-3D Biomaterials Cytocompatibility Screening For Tissue Engineering Using Bioinspired Superhydrophobic Substrates, Integr Biol, 4 (2012) 318-327.

[15] M.B. Oliveira, J.F. Mano, On-Chip Assessment Of The Protein-Release Profile From 3D Hydrogel Arrays, Anal Chem, 85 (2013) 2391-2396.

[16] M.B. Oliveira, C.L. Salgado, W. Song, J.F. Mano, Combinatorial On-Chip Study Of Miniaturized 3D Porous Scaffolds Using A Patterned Superhydrophobic Platform, Small, 9 (2013) 768-778.

[17] N.M. Oliveira, A.I. Neto, W. Song, J.F. Mano, Two-Dimensional Open Microfluidic Devices By Tuning The Wettability On Patterned Superhydrophobic Polymeric Surface, Appl. Phys. Exp., 3 (2010) 085205.

[18] S.M. Oliveira, W.L. Song, N.M. Alves, J.F. Mano, Chemical Modification Of Bioinspired Superhydrophobic Polystyrene Surfaces To Control Cell Attachment/Proliferation, Soft Matter, 7 (2011) 8932-8941.

[19] A.I. Neto, H.J. Meredith, C.L. Jenkins, J.J. Wilker, J.F. Mano, Combining Biomimetic Principles From The Lotus Leaf And Mussel Adhesive: Polystyrene Films With Superhydrophobic And Adhesive Layers, RSC Advances, 3 (2013) 9352.

[20] X. Hong, X.F. Gao, L. Jiang, Application Of Superhydrophobic Surface With High Adhesive Force In No Lost Transport Of Superparamagnetic Microdroplet, Journal Of The American Chemical Society, 129 (2007) 1478-+.

[21] L. Feng, Y.A. Zhang, J.M. Xi, Y. Zhu, N. Wang, F. Xia, L. Jiang, Petal Effect: A Superhydrophobic State With High Adhesive Force, Langmuir, 24 (2008) 4114-4119.

[22] Y.Y. Yan, N. Gao, W. Barthlott, Mimicking Natural Superhydrophobic Surfaces And Grasping The Wetting Process: A Review On Recent Progress In Preparing Superhydrophobic Surfaces, Adv Colloid Interface Sci, 169 (2011) 80-105.

[23] M. Nosonovsky, B. Bhushan, Lotus Versus Rose: Biomimetic Surface Effects, In, 2012, Pp. 25-40.

[24] Z. Cheng, M. Du, H. Lai, N. Zhang, K. Sun, From Petal Effect To Lotus Effect: A Facile Solution Immersion Process For The Fabrication Of Super-Hydrophobic Surfaces With Controlled Adhesion, Nanoscale, 5 (2013) 2776-2783.

[25] H. Song, D.L. Chen, R.F. Ismagilov, Reactions In Droplets In Microfluidic Channels, Angew Chem Int Ed Engl, 45 (2006) 7336-7356.

[26] S.Y. Teh, R. Lin, L.H. Hung, A.P. Lee, Droplet Microfluidics, Lab Chip, 8 (2008) 198-220.

[27] B. Su, S. Wang, Y. Song, L. Jiang, A Miniature Droplet Reactor Built On Nanoparticle-Derived Superhydrophobic Pedestals, Nano Res, 4 (2010) 266-273.

[28] M.A.M. Gijs, F. Lacharme, U. Lehmann, Microfluidic Applications Of Magnetic Particles For Biological Analysis And Catalysis, Chemical Reviews, 110 (2010) 1518-1563.

[29] A. Accardo, F. Mecarini, M. Leoncini, F. Brandi, E. Di Cola, M. Burghammer, C. Riekel, E. Di Fabrizio, Fast, Active Droplet Interaction: Coalescence And Reactive Mixing Controlled By Electrowetting On A Superhydrophobic Surface, Lab Chip, 13 (2013) 332-335.

[30] Z. Long, A.M. Shetty, M.J. Solomon, R.G. Larson, Fundamentals Of Magnet-Actuated Droplet Manipulation On An Open Hydrophobic Surface, Lab Chip, 9 (2009) 1567-1575.

[31] D. De Bruyker, M.I. Recht, A.A. Bhagat, F.E. Torres, A.G. Bell, R.H. Bruce, Rapid Mixing Of Sub-Microlitre Drops By Magnetic Micro-Stirring, Lab Chip, 11 (2011) 3313-3319.

[32] M. Shikida, K. Takayanagi, K. Inouchi, H. Honda, K. Sato, Using Wettability And Interfacial Tension To Handle Droplets Of Magnetic Beads In A Micro-Chemical-Analysis System, Sens. Actuators, B, 113 (2006) 563-569.

[33] J. Schneider, A. Egatz-Gómez, S. Melle, S. Lindsay, P. Domínguez-García, M.A. Rubio, M. Márquez, A.A. García, Motion Of Viscous Drops On Superhydrophobic Surfaces Due To Magnetic Gradients, Colloids Surf., A, 323 (2008) 19-27.

[34] J.S. Sander, R.M. Erb, C. Denier, A.R. Studart, Magnetic Transport, Mixing And Release Of Cargo With Tailored Nanoliter Droplets, Adv Mater, 24 (2012) 2582-2587, 2510.

[35] F. Sarvi, Z. Yue, K. Hourigan, M.C. Thompson, P.P.Y. Chan, Surface-Functionalization Of PDMS For Potential Micro-Bioreactor And Embryonic Stem Cell Culture Applications, J. Mater. Chem. B, 1 (2013) 987.

[36] J.L. Drury, D.J. Mooney, Hydrogels For Tissue Engineering: Scaffold Design Variables And Applications, Biomaterials, 24 (2003) 4337-4351.

[37] A. Khademhosseini, R. Langer, Microengineered Hydrogels For Tissue Engineering, Biomaterials, 28 (2007) 5087-5092.

[38] D. Seliktar, Designing Cell-Compatible Hydrogels For Biomedical Applications, Science, 336 (2012) 1124-1128.

[39] J.K.F. Suh, H.W.T. Matthew, Application Of Chitosan-Based Polysaccharide Biomaterials In Cartilage Tissue Engineering: A Review, Biomaterials, 21 (2000) 2589-2598.

[40] J.F. Mano, G.A. Silva, H.S. Azevedo, P.B. Malafaya, R.A. Sousa, S.S. Silva, L.F. Boesel, J.M. Oliveira, T.C. Santos, A.P. Marques, N.M. Neves, R.L. Reis, Natural Origin Biodegradable Systems In Tissue Engineering And Regenerative Medicine: Present Status And Some Moving Trends, J R Soc Interface, 4 (2007) 999-1030.

[41] N.M. Alves, J.F. Mano, Chitosan Derivatives Obtained By Chemical Modifications For Biomedical And Environmental Applications, Int J Biol Macromol, 43 (2008) 401-414.

[42] S.S. Silva, A. Motta, M.T. Rodrigues, A.F.M. Pinheiro, M.E. Gomes, J.F. Mano, R.L. Reis, C. Migliaresi, Novel Genipin-Cross-Linked Chitosan/Silk Fibroin Sponges For Cartilage Engineering Strategies, Biomacromolecules, 9 (2008) 2764-2774.

[43] R.A.A. Muzzarelli, Genipin-Crosslinked Chitosan Hydrogels As Biomedical And Pharmaceutical Aids, Carbohydr Polym, 77 (2009) 1-9.

[44] L.P. Yan, Y.J. Wang, L. Ren, G. Wu, S.G. Caridade, J.B. Fan, L.Y. Wang, P.H. Ji, J.M. Oliveira, J.T. Oliveira, J.F. Mano, R.L. Reis, Genipin-Cross-Linked Collagen/Chitosan Biomimetic Scaffolds For Articular Cartilage Tissue Engineering Applications, J. Biomed. Mater. Res., Part A, 95A (2010) 465-475.

[45] M. Arteche Pujana, L. Perez-Alvarez, L.C. Cesteros Iturbe, I. Katime, Biodegradable Chitosan Nanogels Crosslinked With Genipin, Carbohydr Polym, 94 (2013) 836-842.

[46] F.L. Mi, Y.C. Tan, H.F. Liang, H.W. Sung, In Vivo Biocompatibility And Degradability Of A Novel Injectable-Chitosan-Based Implant, Biomaterials, 23 (2002) 181-191.

[47] T.G. Fernandes, M.M. Diogo, D.S. Clark, J.S. Dordick, J.M. Cabral, High-Throughput Cellular Microarray Platforms: Applications In Drug Discovery, Toxicology And Stem Cell Research, Trends Biotechnol, 27 (2009) 342-349.

[48] X.X. Zhang, Z. Wang, X. Yue, Y. Ma, D.O. Kiesewetter, X. Chen, Ph-Sensitive Fluorescent Dyes: Are They Really Ph-Sensitive In Cells?, Mol Pharm, 10 (2013) 1910-1917.

[49] A. Hulikova, A.L. Harris, R.D. Vaughan-Jones, P. Swietach, Regulation Of Intracellular Ph In Cancer Cell Lines Under Normoxia And Hypoxia, J Cell Physiol, 228 (2013) 743-752.

[50] T.M. Cao, T. Takatani, M.R. King, Effect Of Extracellular Ph On Selectin Adhesion: Theory And Experiment, Biophys J, 104 (2013) 292-299.

[51] D.R. Knighton, T.K. Hunt, H. Scheuenstuhl, B.J. Halliday, Z. Werb, M.J. Banda, Oxygen-Tension Regulates The Expression Of Angiogenesis Factor By Macrophages, Science, 221 (1983) 1283-1285.

[52] Y. Bae, S. Fukushima, A. Harada, K. Kataoka, Design Of Environment-Sensitive Supramolecular Assemblies For Intracellular Drug Delivery: Polymeric Micelles That Are Responsive To Intracellular Ph Change, Angew Chem Int Ed Engl, 42 (2003) 4640-4643.

[53] Y. Lu, J.J. Chen, L. Mu, Q. Xue, Y. Wu, P.H. Wu, J. Li, A.O. Vortmeyer, K. Miller-Jensen, D. Wirtz, R. Fan, High-Throughput Secretomic Analysis Of Single Cells To Assess Functional Cellular Heterogeneity, Anal Chem, 85 (2013) 2548-2556.

[54] J. Zhou, C. Fang, T. Chang, X. Liu, D. Shangguan, A Ph Sensitive Ratiometric Fluorophore And Its Application For Monitoring The Intracellular And Extracellular Phs Simultaneously, J. Mater. Chem. B, 1 (2013) 661.

[55] J. Kononen, L. Bubendorf, A. Kallioniemi, M. Barlund, P. Schraml, S. Leighton, J. Torhorst, M.J. Mihatsch, G. Sauter, O.P. Kallioniemi, Tissue Microarrays For High-Throughput Molecular Profiling Of Tumor Specimens, Nature Medicine, 4 (1998) 844-847.

[56] Z. Xu, Y. Gao, Y. Hao, E. Li, Y. Wang, J. Zhang, W. Wang, Z. Gao, Q. Wang, Application Of A Microfluidic Chip-Based 3D Co-Culture To Test Drug Sensitivity For Individualized Treatment Of Lung Cancer, Biomaterials, 34 (2013) 4109-4117.

[57] G. Cheng, J. Tse, R.K. Jain, L.L. Munn, Micro-Environmental Mechanical Stress Controls Tumor Spheroid Size And Morphology By Suppressing Proliferation And Inducing Apoptosis In Cancer Cells, Plos One, 4 (2009) E4632.

[58] A.Y. Hsiao, Y.C. Tung, C.H. Kuo, B. Mosadegh, R. Bedenis, K.J. Pienta, S. Takayama, Micro-Ring Structures Stabilize Microdroplets To Enable Long Term Spheroid Culture In 384 Hanging Drop Array Plates, Biomed Microdevices, 14 (2012) 313-323.

[59] J.C. Schulz, P.S. Stumpf, A. Katsen-Globa, A. Sachinidis, J. Hescheler, H. Zimmermann, First Steps Towards The Successful Surface-Based Cultivation Of Human Embryonic Stem Cells In Hanging Drop Systems, Eng Life Sci, 12 (2012) 584-587. [60] E. Fennema, N. Rivron, J. Rouwkema, C. Van Blitterswijk, J. De Boer, Spheroid Culture As A Tool For Creating 3D Complex Tissues, Trends Biotechnol, 31 (2013) 108-115. [61] Y. Morimoto, S. Takeuchi, Three-Dimensional Cell Culture Based On Microfluidic Techniques To Mimic Living Tissues, Biomaterials Science, 1 (2013) 257.

CHAPTER 7. A NOVEL HANGING SPHERICAL DROP SYSTEM FOR THE GENERATION OF CELLULAR SPHEROIDS AND HIGH THROUGHPUT COMBINATORIAL DRUG TESTING *

7.1 Abstract

We propose a novel hanging spherical drop system for anchoring arrays of droplets of cell suspension based on the use of biomimetic superhydrophobic flat substrates, with controlled positional adhesion and minimum contact with a solid substrate. By facing down the platform, it was possible to generate independent spheroids bodies in a high throughput manner, in order to mimic *in vivo* tumor models in a lab-on-chip scale. To validate this system for drug screening purposes, the toxicity of the anti-cancer drug doxorubicin in cell spheroids was tested and compared to cells in 2D culture. The advantages presented by this platform, such as feasibility of the system and the ability to control the size uniformity of the spheroid, emphasize its potential to be used as a new low cost toolbox for high-throughput drug screening and in cell or tissue engineering.

* *Neto A. I., Correia C. R., Oliveira M. B., Rial-Hermida I., Alvarez-Lorenzo C., Reis R. L. and Mano J. F. A novel hanging spherical drop system for the generation of cellular spheroids and high throughput combinatorial drug screening.* ***Biomaterials Science***, ***3***, *581-585, 2015.*

7.2 Introduction

Cell-based high throughput screening (HTS) has been proposed as a powerful tool for rapid identification of drug candidates from large biological and chemical libraries with desired efficacy, which can accelerate the drug discovery [1-4]. Most studies of cell and tissue regulation have relied on the analysis of cell behavior in two-dimensional (2D) cell culture models. However, the 2D model fails to simulate the *in vivo* cellular microenvironment, thus compromising cellular functions, namely metabolic activity, proliferation, differentiation and cell death. Efforts to address these limitations led to the development of three-dimensional (3D) cell culture models in which cells are grown within engineered extracellular matrix (ECM) [5]. HTS of anticancer drugs is usually performed using high-density multi-well plates with high-level and expensive robotic devices for cell seeding and drug management [6-10]. Recent advances in 3D cancer cell culture have used cellular spheroids as an adequate model, exhibiting a complex microenvironment similar to tumors *in vivo* and comparable drug responses [11-16]. Spheroids are self-assembled spherical clusters of cell colonies cultured in environments where cell-cell interactions dominate over cell-substrate interactions, and they naturally mimic avascular tumors with inherent metabolic (dependent on oxygen) and proliferative (dependent on nutrients) gradients [17].

3D spheroids can be easily produced by various simple methods, namely hanging drop cultures, engineered micro-fabrication of round-bottom and non-adherent platforms, microfluidic devices, spinner flasks, NASA rotary culture, thermo-responsible substrates and 3D scaffolds [18]. In particular, the hanging drop cultures offer an accessible and reliable method for generating higher numbers of spheroids with a precise and homogeneous size control and suitable compatibility for high throughput assays. Current developments in microarrays devices are directed towards further reductions in sample volumes, increasing analytical throughput and integration of pre- and post assay processing. Innovative technologies enable, for example, 384 spheroids to be cultured in a hanging drop fashion in the same platform [19]. However, the cost associated to the production and utilization of such innovative platforms requires high precision and expertise equipment that can be extremely costly.

In our group, we made advances in this field, creating an innovative low-cost platform for individually dispense of miniaturized biomaterials, cells and culture medium, based on the use of patterned superhydrophobic (SH) surfaces [20-24]. The topography of these SH surfaces exhibit peculiar features like micro- and nano- hierarchical roughness, leading to low surface energy, mimicking SH surfaces found in Nature, such as the Lotus leaf.

Herein, we propose the use of flat SH substrates to arrange arrays of quasi-spherical cell culture droplets with the capability to build-up 3D spheroids in a high throughput manner, in order to mimic *in vivo* tumor models in a lab-on-chip scale. Droplets of a cell culture suspension are fixed in defined positions by the action of micro-indentations patterned with an array arrangement on polystyrene SH surfaces. The SH platform is solely physically modified polystyrene (PS) [25-31], which guarantees the lack of cytotoxicity and the chemical stability of the platform. Such platform presents several advantages compared to the conventional methods used on spheroids formation. Micro-size droplets for cellular assays allow drastic reduction of the volume required for cell growth, while SH surfaces mimic the effect of rose petals allowing a minimum contact of the liquid to the surface, avoiding any interferences such as protein adsorption or release of molecules from the platform to the cell culture media. The cell culture medium can be changed easily without destroying the micro-tissues since the droplets are tightly linked to the substrates by strong capillary forces, and drugs or other molecules can be easily added in any time. Moreover, the platform is compatible or easily adapted with many analysis techniques, such as inverted confocal microscopy, in which droplets of cells suspension remain inverted on the SH surface; and high-throughput combinatorial analysis may be performed *in situ* using different cell densities or drug concentrations. The high stability, precise positional and adhesiveness of the droplets allow to invert the platform 180° according to hanging drop approaches. Under this configuration the cells initially suspended in the droplets give rise to spheroids formed by gravity. The innovation of our system relies on the spherical geometry ("hanging spherical drop" method) exhibited by the cell suspension droplets. The size and composition of each droplet can be easily controlled in an individual form.

To explore the capability of this platform, the cell behavior of 3D spheroids was compared to 2D culture upon being subjected to the effect of various concentrations of doxorubicin. Cell viability was evaluated using image-based analysis tools to assess the dose-dependent response of the formed tumor spheroids to this anticancer drug.

7.3 Results and Discussion

A platform was created following biomimetic principles [32]. Polystyrene (PS) superhydrophobic (SH) substrate mimicking the extreme water repellency of lotus leave was patterned with adhesive micro-indentations (Figure 7.1 A.II) simulating the effect of rose petals [33]. The low adhesion to droplets on the lotus leave is caused by the air pockets formed between cell papilla (Cassie-Baxter model) while in the rose petal surface the droplets penetrate into the cuticular folds by capillary forces (Wenzel model) [33]. The developed platform was used as a support for arrays of quasi-spherical droplets of cell

suspensions (Figure 7.1 A.I), for the generation of fibroblasts-like cell spheroids. PS sheets were treated by a phase separation methodology [34], resulting in a water contact angle (WCA) higher than 150°, mainly by the introduction of micro and nano roughness on the surface (Figure 7.1 A.III).

We hypothesize that the micro-indentations created on low surface-energy surfaces allow to confine and stabilize nearly spherical droplets only on the desired places with minimum contact area between droplet and surface, even when the surface with cells suspension droplets are turned upside down. (Figure 7.1 A.IV).

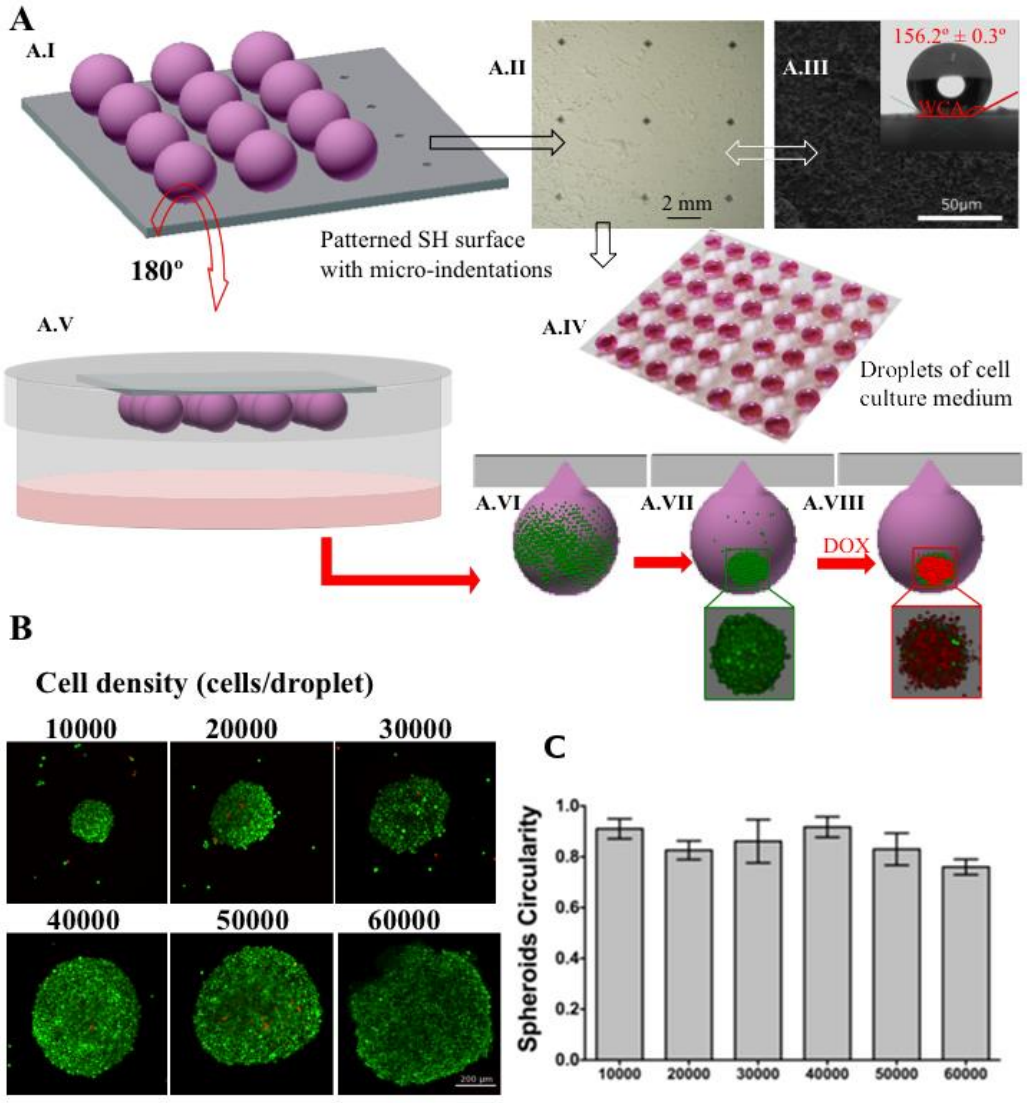

Figure 7.1 (A.I) Upper view scheme of the SH platform (A.II) patterned with micro-indentations able to suspend arrays of droplets containing cells. (A.III) The microstructure of PS SH surface observed by SEM and the representative image of a water droplet over the surface. (A.IV) Image of the hanging spherical drops system able to confine droplets on the desired places with minimum contact area between droplets and the surface. (A.V) Turning the platform 180°, (A.VI) the cell suspension inside the droplet (A.VII) leads to the formation of spheroids after 2 days due to the gravitational force applied to the cells. (A.VIII) Drug-screening tests by adding the anti-cancer drug, doxorubicin, in the droplets containing cell spheroids. (B)

Live/dead assay images after 48 hours of culture were taken in confocal microscopy of the formation of spheroids. Distinct cell densities were tested. Scale Bar: 200 μm. (C) Measurement of spheroids circularity using different densities of fibroblasts-like cells. The results were presented as mean ± standard deviation (n=3).

In the proposed device, the cells are maintained in suspension and confined within independent miniaturized cell culture droplets surrounded essentially by the gaseous environment of the device. The platform was fixed into the lids of polystyrene petri dishes (commercially available), and the bottom part was filled with cell culture media, in order to create a saturated environment and avoid the evaporation of the droplets (Figure 7.1 A.V-VI). The gravitational force applied on the cells in the hanged droplets induced its sedimentation and the formation of cell spheroids after 48h of seeding time (Figure 7.1 A.VII). Each droplet in the chip forms a singular spheroid with a consistent cell population that is generated without the need of any scaffold or adhesive substances. It was possible to produce arrays of individual sedimented spheroids and test distinct doses of an anti-cancer drug widely used in drug screening, doxorubicin (Dox), in the same device (Figure 7.1 A.VIII). Conventional methods to produce spheroids have common drawbacks, such as the formation of the spheroids with irregularly sizes, inaccessibility for testing in the platforms and difficulty to adapt to HTS platforms. The proposed hanging spherical drop system allows the growth of homogenously sized spheroids in an easy and non-invasive way. For the proof-of-concept, droplets containing fibroblasts-like cells suspension were dispensed on the inverted platform in order to promote the spheroids formation. Using distinct cell numbers, spheroids with different sizes and densities were obtained (Figure 7.1B). The pictures of the spheroids were taken using confocal microscope for precise cell quantification. The stained spheroids with calcein-AM (corresponding to green cells) and propidium iodide (corresponding to red cells) show that after 48 hours of incubation, the spheroids were entirely formed with high survival rates. As expected, the diameter of L929 spheroids increased with increasing cell density, from 10,000 to 60,000 cells/ droplet. Images of spheroids with more cell densities (from 5,000 to 60,000 cells per droplet), taken using fluorescent microscope, can be observed in Figure 7.S1. The micro-tissues produced by gravity-enforced hanging drop method with a density of 40,000 cells per drop present a perfect and uniform integration of single cells into a compact microstructure (Figure 7.2 A-C).

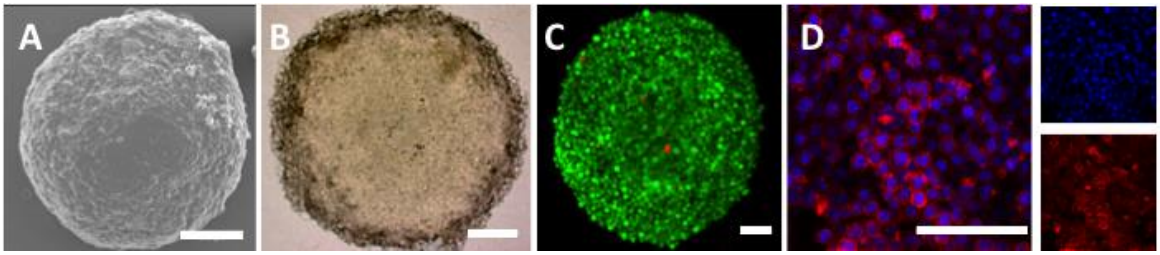

Figure 7.2 A) SEM, B) bright field, C) live/dead and D) DAPI/phalloidin representative images of L929 spheroids after 48 hours of culture. Scale bar: 100 µm.

Spheroids have become a "gold standard" model to investigate the cellular signalling mechanisms and effects of anti-tumour agents, mimicking the *in vivo* situation. Cancer cells live in a complex microenvironment consisting of non-cancer cells and tumour stroma. The tumour stroma consists of the basement membrane, immune cells, ECM, blood vasculature, inflammatory cells and fibroblasts. All are known to contribute for cancer development. Fibroblasts are the major component in the stroma and are responsible for the production of cytokines, ECM and growth factors that promotes tumour growth [35]. Under such conditions, fibroblasts can acquire a myofibroblastic phenotype and make direct cell-cell contact, via gap junction intercellular communication without intervening the ECM [36-38] (Figure 7.2D). However, when the fibroblasts are forced to cluster into a spheroid shape, they undergo a new pathway of cell activation beginning a process considered as necrosis-like death, induced by hypoxia or toxins (Figure 7.3 A.I). The limited flow of oxygen and nutrients into the core compromise the viability of the fibroblasts; as result, the viability of the cells decreases along the culture time. For this reason, a typical spheroid has an outer layer of proliferative cells, an internal layer of quiescent cells and hypoxic cells in the core.

The morphogenesis of 2D cell cultures (Figure 7.3 A.II) was evaluated along with the spheroids culture, as control. In both conditions 40,000 cells were used and live/dead assay was performed to determine the cell viability. The images of the cluster cells were taken using confocal microscopy, in order to provide accurate quantification of the 3D samples.

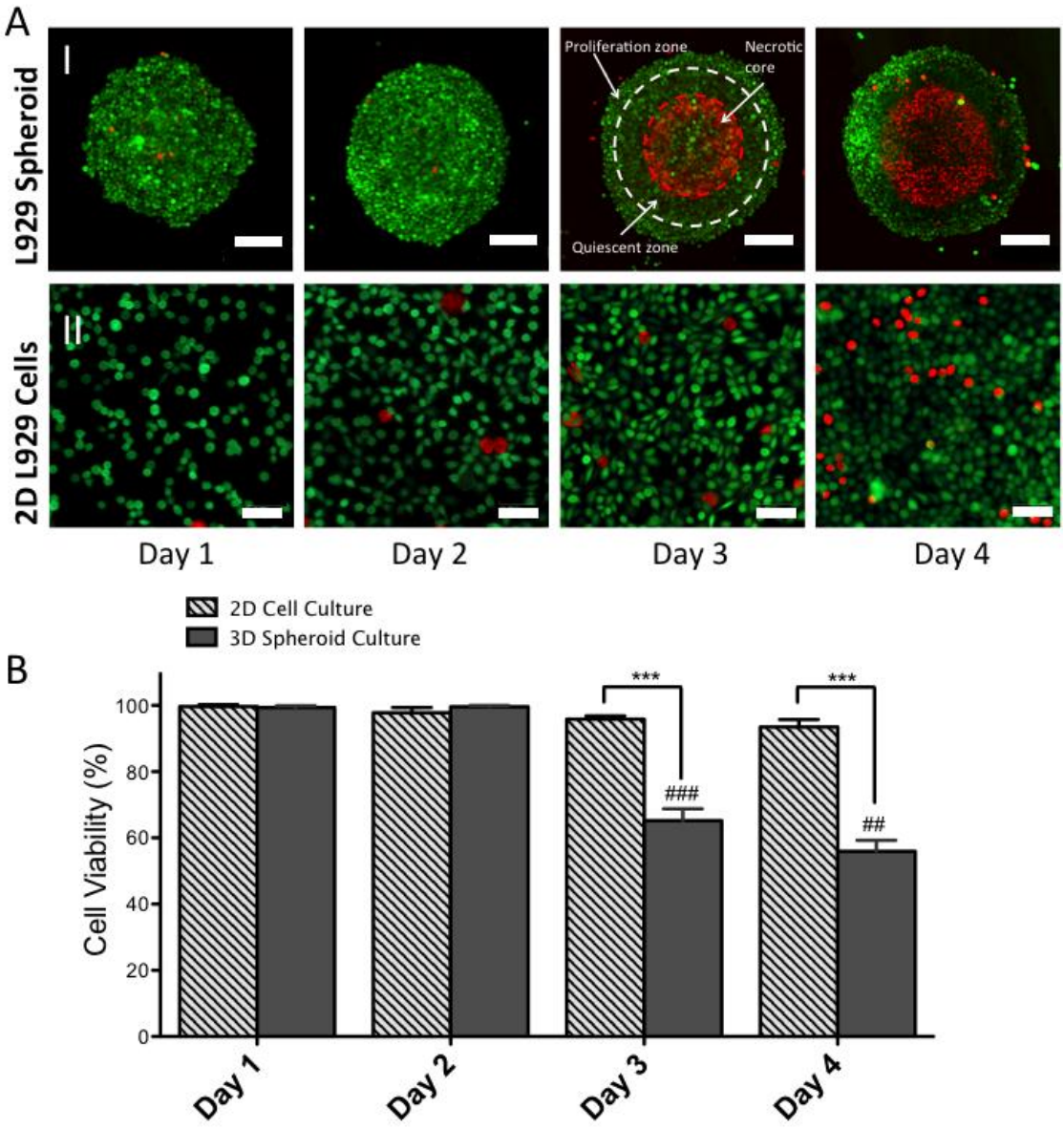

Figure 7.3 A.I) Representative images using live/ dead staining taken from confocal microscope of individual spheroids up to four days of culture time, with density of 40,000 cells per droplet. Scale bar: 200 μm A.II) Representative images of L929 monolayer cell culture along the same time points and cell density. Images using live/ dead staining were taken using fluorescent microscope. Scale bar: 50 μm B) Quantification of the viability of the cells in the spheroids and in the 2D cell cultures. Statistical differences were marked with (***), which stand for p-value < 0.001. To evaluate the statistical differences related to the previous time point double (##) and triple symbols (###) were used for p-value < 0.01 and p < 0.001, respectively. All results were presented as mean ± standard deviation.

The images of 2D cell culture were taken using fluorescence microscopy. With the increasing of the cell culture time, the cells in 2D monolayer presented higher viability compared to 3D spheroids (Figure 7.3B). This can be explained by the fact that cells cultured in monolayer have a higher surface area to adhere and proliferate, whereas 3D spheroids are limited to cell-cell interactions since are cultured in suspension.

Additionally, cells in monolayer have higher access to the nutrients of culture media, compared to the necrotic core of spheroids.

The cellular pathway targeted by a drug, such as doxorubicin (Dox), might differ from 2D to 3D condition. Dox is an anti-cancer agent, widely used in human cancer chemotherapy that inhibits RNA and DNA synthesis [39]. This drug induces an alternative cell death mechanism to apoptosis. Figure 7.4 shows the effect of distinct concentrations of Dox on the cells in spheroids with different densities. Different amounts of Dox were introduced in the droplets to assess the dose-dependent response of the formed tumour spheroids to this anticancer drug. The viability of the cells in the spheroids was measured after 24 hours by a live/dead assay (Figure 7.4 A). As expected, with the increase of the Dox concentration, cell viability of the spheroids decreased. However, L929 spheroids show a greater resistance to Dox compared to the monolayer L929 cultures (Figure 7.4 B-C).

Recent experiments have confirmed that tumor spheroid is more resistant to drugs compared with the corresponding 2D cell cultures [40, 41]. This increased Dox resistance in the spheroid cells may be due to cell-cell contact response, internal protective mechanisms, and/or mass transfer limitations.

Extending the screening of cells in suspension, we employed the new arrangement to test the behavior of cells in an aggregated form that could be useful for high-throughput monitoring. The proposed methodology could be easily extended to assess the time response of the cells to multiple drugs, drug screening on co-cultures, and study the effect of the gaseous environment on cell behavior (e.g. hypoxia, normoxia and hyperoxia).

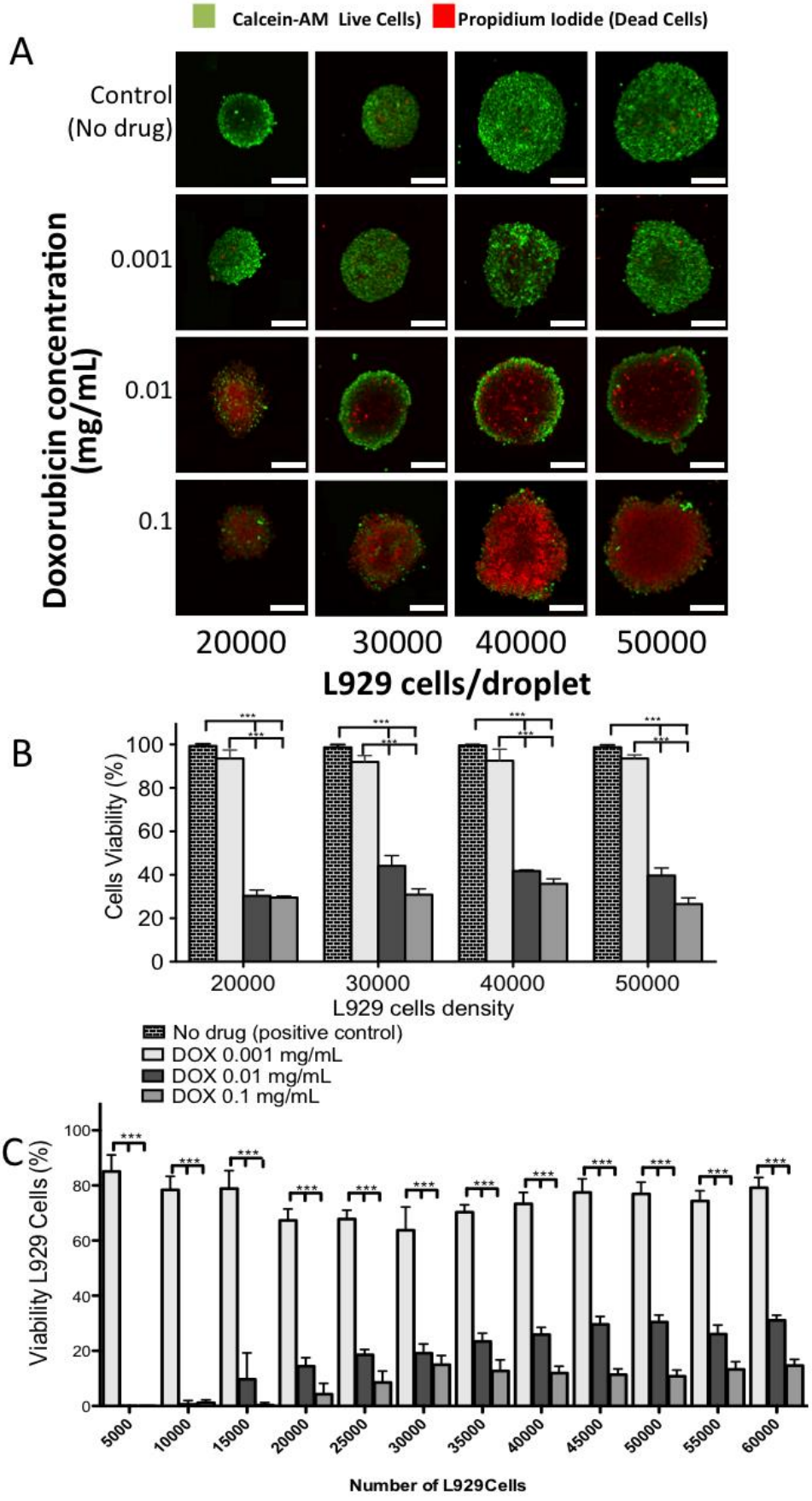
A
Calcein-AM Live Cells)
Propidium Iodide (Dead Cells)
Control
(No drug)
0.001
0.01
0.1
Doxorubicin concentration (mg/mL)
20000
30000
40000
50000
L929 cells/droplet
B
Cells Viability (%)
100
80
60
40
20
0
20000
30000
40000
50000
L929 cells density
No drug (positive control)
DOX 0.001 mg/mL
DOX 0.01 mg/mL
DOX 0.1 mg/mL
C
Viability L929 Cells (%)
100
80
60
40
20
0
5000
10000
15000
20000
25000
30000
35000
40000
45000
50000
55000
60000
Number of L929Cells

Figure 7. 4 A) Fluorescent images of L929 spheroids with distinct densities (48 hours of formation) obtained by confocal microscopy 24h after the addition of various concentrations of doxorubicin. Scale bar: 200 μm B) Percentage of live cells in the spheroids in the different conditions. C) Percentage of viable cells in the 2D cell culture using different densities and different concentrations of anti-cancer drug obtained by the alamar blue method. Absorbance was read at wavelength of 570 nm and 600 nm. Statistical differences were marked (***) $p < 0.001$. All results were presented as mean ± standard deviation.

7.4 Conclusions

Superhydrophobic biomimetic surface based on the so-called Lotus effect was produced onto which arrays of micro-indentations were generated to fix cell suspension droplets, based on the rose petals effect. By facing down the chip, it was possible to produce arrays of cells spheroids developed by gravity in the suspended droplets, according to an hanging spherical drop method. Spheroids provide a 3D cellular environment, which more accurately recapitulates the *in vivo* tumor, and have been used for drug screening tests. Using this platform, the dose-dependent cytotoxic effect of doxorubicin was measured, and we observed decreasing viability of the cells with increasing doxorubicin concentration. The spheroids also exhibit enhanced resistance to the drug over 2D standard monolayer cultures. We believe that such platform may also have potential to be used in several biological or biomedical applications, including in the field of tissue engineering and regenerative medicine, drug discovery, and drug delivery monitoring.

7.5 Experimental

Fabrication of patterned SH surfaces: SH polystyrene (PS) surfaces were produced using a one-step phase-separation methodology under ambient condition. 70 $mg.mL^{-1}$ solution of PS (Styrolution PS 158K) was prepared dissolving the granules in tetrahydrofuran (THF from Fluka, p.a. >99.5%) solvent for 2 hours to form a pre-solution at ambient temperature. Then, 1.3 mL of ethanol (from Panreac) was added into 2 mL of PS pre-solution and the mixed solution was stirred. A necessary volume to cover the PS substrate with this mixture was dipped onto a cleaned PS film (from Goodfellow, UK, with 0.25 mm of thickness, ref. ST311190/1). The substrate with the mixture was immersed in ethanol for 1 min. Afterwards the surface was dried at ambient temperature.

Micro-indentations over the SH surfaces were produced using a microhardeness tester equipment (Leica VMHT 30) applying loads of 2942 mN with a dwell time of 10 s. A sharp rigid Vickers diamond pyramid indenter (included angle α=136°) penetrated into the surface with a constant load during a complete loading–unloading cycle producing individual indentations. To produce the arrays to sustain droplets of cell culture medium, the micro-indentations were placed in the SH surface at a distance of 5 mm from each other, with a square configuration, in the total of 16 spots for each condition.

Surface characterization: Water contact angle measurements were also performed at room temperature using an OCA 15 plus goniometer (DataPhysics). The values were obtained by the sessile drop method. The used liquid was ultrapure water and the drop volume was 3 μL. At least five measurements were carried out.

The surface morphology of the SH sample and the spheroid formation was observed using a Leica Cambridge S-360 scanning electron microscope (SEM). All samples were coated with a conductive layer of sputtered gold. The SEM micrographs were taken at an accelerating voltage of 15 kV and at different magnifications.

Cell Expansion and Cell Culture: The immortalized mouse lung fibroblast cell line L929 was purchased from the European Collection of Cell Cultures and was used as well established cell line for viability studies. Cells were expanded in low glucose Dulbecco's Modified Eagle's Medium (DMEM), from Sigma-Aldrich, supplemented with 3.7 $g{\cdot}L^{-1}$ sodium bicarbonate, 10% heat-inactivated fetal bovine serum (FBS, Invitrogen) and 1% antibiotic/antimycotic (final concentration of penicillin 100 $units.mL^{-1}$ and streptomycin 100 $mg.mL^{-1}$; Gibco) at pH 7.4. Cells were grown in 75 cm^2 tissue culture flasks and incubated at 37 °C in a humidified air atmosphere of 5% CO_2. Every 3–4 days, fresh medium was added. At 90% of confluence, cells grown in tissue culture flasks were washed with phosphate buffer saline (PBS) and subsequently detached by a chemical procedure with 0.05% trypsin-EDTA solution for 5 min at 37 °C in a humidified air atmosphere of 5% CO_2. To inactivate the trypsin effect, cell culture medium was added. The cells were then centrifuged at 300 g and 25 °C for 5 min and the medium was decanted. Cell suspensions with distinct densities were prepared.

Monolayer Cell Culture: 1 mL of supplemented DMEM containing different cell suspensions was placed in a non-treated surface of 48-well cell plate (in triplicate). The plates were incubated at 37 °C in a humidified air atmosphere of 5% CO_2 at different incubation days. The fluorescent images of live/dead assay, were obtained by removing the cell culture media, and wash the culture plates carefully with PBS. Then, 1 mL of PBS containing 2 μL of calcein-AM and 1 μL of propidium iodide dyes were added to each well to staining the live cells with green and dead with red. After 10 minutes at 37 °C, samples were extensively washed with PBS solution and immediately visualized in the dark by transmitted light microscopy (Axio Imager Z1m, Zeiss). ImageJ software (NHI, USA) was used to quantify the cells adhered on the well plate.

Cytotoxicity of 2D cell culture: The 2D monolayers of cells were tested for cytotoxicity using alamarBlue colorimetric assay. Briefly, different cells density were placed in a treated surface 48-well cell culture plate

(in triplicate) and incubated at 37 °C and 5% CO_2. After 48 hours of culture, the assay was performed, protected from light. The culture medium was removed and 500 µL of supplemented DMEM containing 10 % v/v alamarBlue solution was added to each well. Samples were then incubated in the dark at 37 °C and 5% CO_2. After 4 h, 100 µL of each well (in triplicate) was transferred to a 96-well plate. The absorbance was monitored at 570 nm and 600 nm using a microplate reader (Synergy HT, Bio-TEK).

On-chip spheroids formation: A hanging drops approach used for the formation of spheroids was performed using SH surfaces patterned with adhesive micro-indentations. Prior to cell seeding, the SH surfaces were sterilized by UV radiation for 30 min. Suspensions with different fibroblasts-like cell densities were prepared. Droplets of 5 µL of cell suspensions (in triplicate) were placed over the micro-indentations of the platforms. The platform with different cell suspensions was inverted 180° and incubated for 48 hours at 37°C in a humidified 5% CO_2 atmosphere. The platform containing droplets of cell suspensions was fixed into the lids of polystyrene petri dishes, and the bottom part was filled with cell culture media, in order to create a saturated environment and avoid the evaporation of the droplets The representative images of the formed spheroid in the droplet with 40,000 L929 cells after 48 hours of incubation (Figure 7.2) were taken using scanning electron microscope (JSM-6010LV, JEOL), transmitted light microscopy (Axio Imager Z1m, Zeiss) and inverted confocal microscopy (Leica, TCS SP8). For the SEM analysis, after the spheroid formation, 5 µL of 10% formalin was dispensed to the droplets. The spheroids were dehydrated with a series of increasing ethanol concentrations (50%, 70%, 80%, 95% and 100%). Live/dead assay was assessed. 2 µL of PBS containing calcein-AM and propidium iodide was added to the spheroids. DAPI and phalloidin assay was also performed. DAPI stains preferentially double-stranded DNA by delineating cells nuclei in blue and phalloidin stains with the red color the actin filaments of the cells and is used to evaluate the function of cytoplasmic actin. Prior to staining, the culture medium was removed and 5 µL of 10% formalin was dispensed to the droplets. Then, 2 µL of PBS containing DAPI and phalloidin was added.

Drug screening tests: After 48 hours of cell culture for spheroids formation, 2 µL of doxorubicin (Doxorubicin hydrochloride, Sigma-Aldrich) with different concentrations (0.1 $mg.mL^{-1}$, 0.01 $mg.mL^{-1}$ and 0.001 $mg.mL^{-1}$) were dispensed in the different droplets. The chips were incubated for 24h at 37°C in a humidified 5% CO_2 atmosphere. The liquid content of the droplets with cell aggregates were carefully exchange with PBS. Afterwards, 2 µL of PBS containing calcein-AM and propidium iodide was added to each condition to staining the spheroids. The same procedure was made to 2D cell culture.

3D spheroids analysis: Image analysis tool (WCIF ImageJ software, NHI) was used to evaluate the percentage of live/dead cells of each droplet condition. Each image of stained spheroids obtained from confocal microscope was divided in green and red channels and transformed in a gray scale. The number in each channel (grey scale intensity 0-255, in which 0 correspond to black color and 255 white color) was counted and divided for the number of total analyzed area. The same threshold criterion was used in all images.

Statistical analysis: The statistical analysis of both cell cultures data was performed using two-way analysis of variance (ANOVA) with Bonferroni post-test using GraphPad Prism 5.0 software. The adopted nomenclature was the following: statistical differences in grouped by time point analysis were marked with (**) and (***), which stand for p-value < 0.01 and p < 0.001, respectively. For evaluate the statistical differences relating to the time point before, the symbol "#" was used to represent 3D spheroid. Double symbols (##) represent p < 0.01 and triple symbols (###) represent p < 0.001. All results were presented as mean ± standard deviation.

7.6 Acknowledgements

The authors thank the precious help of Alessandra Zonari and Rui Domingues on capturing of the confocal images. The authors acknowledge the financial support from the FCT- Fundação para a Ciência e para a Tecnologia through the Ph.D. grants with the references SFRH/BD/73119/2010, SFRH/BD/69529/2010 and SFRH/BD/71396/2010. We acknowledge the financial support of FEDER through the program Operacional Factores de Competitividade - COMPETE and from FCT - the Fundação para a Ciência e a Tecnologia under the project PTDC/CTM-BIO/1814/2012. We also thank the support by the European Research Council grant agreement ERC-2012-ADG 20120216-321266 for the project ComplexiTE.

7.7 Supporting information

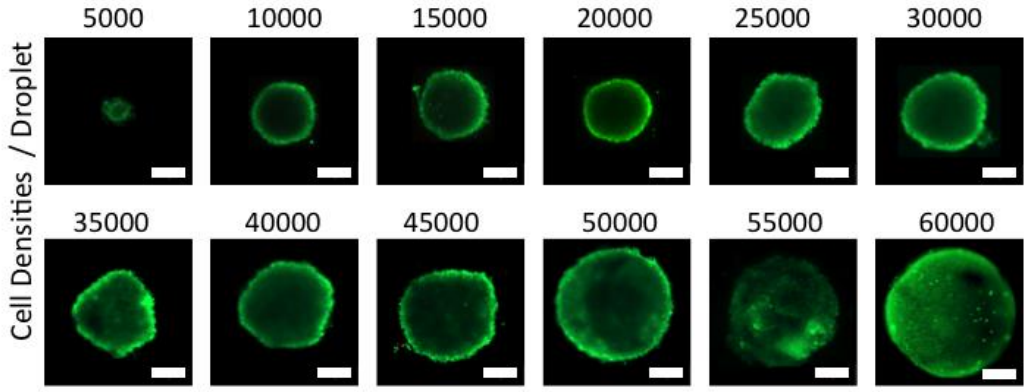

Figure S7.1 Representative images of spheroid formation, after 48 hours, using different densities of fibroblasts-like cells. Scale bar: 200 µm

7.8 References

[1] B.G. Chung, L.F. Kang, A. Khademhosseini, Micro- And Nanoscale Technologies For Tissue Engineering And Drug Discovery Applications, Expert Opinion On Drug Discovery, 2 (2007) 1653-1668.

[2] S.W. Cranford, J. De Boer, C. Van Blitterswijk, M.J. Buehler, Materiomics: An -Omics Approach To Biomaterials Research, Advanced Materials, 25 (2013) 802-824.

[3] A.N. Efremov, E. Stanganello, A. Welle, S. Scholpp, P.A. Levkin, Micropatterned Superhydrophobic Structures For The Simultaneous Culture Of Multiple Cell Types And The Study Of Cell-Cell Communication, Biomaterials, 34 (2013) 1757-1763.

[4] M. Schenone, V. Dancik, B.K. Wagner, P.A. Clemons, Target Identification And Mechanism Of Action In Chemical Biology And Drug Discovery, Nature Chemical Biology, 9 (2013) 232-240.

[5] F. Pampaloni, E.G. Reynaud, E.H.K. Stelzer, The Third Dimension Bridges The Gap Between Cell Culture And Live Tissue, Nature Reviews Molecular Cell Biology, 8 (2007) 839-845.

[6] C.J. Torrance, V. Agrawal, B. Vogelstein, K.W. Kinzler, Use Of Isogenic Human Cancer Cells For High-Throughput Screening And Drug Discovery, Nature Biotechnology, 19 (2001) 940-945.

[7] H.M. Dunstan, C. Ludlow, S. Goehle, M. Cronk, P. Szankasi, D.R.H. Evans, J.R. Simon, J.R. Lamb, Cell-Based Assays For Identification Of Novel Double-Strand Break-Inducing Agents, Journal Of The National Cancer Institute, 94 (2002) 88-94.

[8] H. Tian, L. Ip, H. Luo, D.C. Chang, K.Q. Luo, A High Throughput Drug Screen Based On Fluorescence Resonance Energy Transfer (FRET) For Anticancer Activity Of Compounds From Herbal Medicine, British Journal Of Pharmacology, 150 (2007) 321-334.

[9] H.R. Li, H.Y. Zhou, D. Wang, J.S. Qiu, Y. Zhou, X.Q. Li, M.G. Rosenfeld, S. Ding, X.D. Fu, Versatile Pathway-Centric Approach Based On High-Throughput Sequencing To Anticancer Drug Discovery, Proceedings Of The National Academy Of Sciences Of The United States Of America, 109 (2012) 4609-4614.

[10] L.F. Willoughby, T. Schlosser, S.A. Manning, J.P. Parisot, I.P. Street, H.E. Richardson, P.O. Humbert, A.M. Brumby, An In Vivo Large-Scale Chemical Screening Platform Using Drosophila For Anti-Cancer Drug Discovery, Disease Models & Mechanisms, 6 (2013) 521-529.

[11] M.T. Santini, G. Rainaldi, P.L. Indovina, Apoptosis, Cell Adhesion And The Extracellular Matrix In The Three-Dimensional Growth Of Multicellular Tumor Spheroids, Critical Reviews In Oncology Hematology, 36 (2000) 75-87.

[12] L.G. Griffith, M.A. Swartz, Capturing Complex 3D Tissue Physiology In Vitro, Nature Reviews Molecular Cell Biology, 7 (2006) 211-224.

[13] K.M. Yamada, E. Cukierman, Modeling Tissue Morphogenesis And Cancer In 3D, Cell, 130 (2007) 601-610.

[14] M. Rimann, U. Graf-Hausner, Synthetic 3D Multicellular Systems For Drug Development, Current Opinion In Biotechnology, 23 (2012) 803-809.

[15] E. Fennema, N. Rivron, J. Rouwkema, C. Van Blitterswijk, J. De Boer, Spheroid Culture As A Tool For Creating 3D Complex Tissues, Trends In Biotechnology, 31 (2013) 108-115.

[16] E.W.K. Young, Cells, Tissues, And Organs On Chips: Challenges And Opportunities For The Cancer Tumor Microenvironment, Integrative Biology, 5 (2013) 1096-1109.

[17] J. Friedrich, C. Seidel, R. Ebner, L.A. Kunz-Schughart, Spheroid-Based Drug Screen: Considerations And Practical Approach, Nature Protocols, 4 (2009) 309-324.

[18] R.Z. Lin, H.Y. Chang, Recent Advances In Three-Dimensional Multicellular Spheroid Culture For Biomedical Research, Biotechnology Journal, 3 (2008) 1172-1184.

[19] Y.C. Tung, A.Y. Hsiao, S.G. Allen, Y.S. Torisawa, M. Ho, S. Takayama, High-Throughput 3D Spheroid Culture And Drug Testing Using A 384 Hanging Drop Array, Analyst, 136 (2011) 473-478.

[20] G.M. Luz, A.J. Leite, A.I. Neto, W.L. Song, J.F. Mano, Wettable Arrays Onto Superhydrophobic Surfaces For Bioactivity Testing Of Inorganic Nanoparticles, Materials Letters, 65 (2011) 296-299.

[21] A.I. Neto, C.A. Custodio, W.L. Song, J.F. Mano, High-Throughput Evaluation Of Interactions Between Biomaterials, Proteins And Cells Using Patterned Superhydrophobic Substrates, Soft Matter, 7 (2011) 4147-4151.

[22] C.L. Salgado, M.B. Oliveira, J.F. Mano, Combinatorial Cell-3D Biomaterials Cytocompatibility Screening For Tissue Engineering Using Bioinspired Superhydrophobic Substrates, Integrative Biology, 4 (2012) 318-327.

[23] M.B. Oliveira, J.F. Mano, On-Chip Assessment Of The Protein-Release Profile From 3D Hydrogel Arrays, Analytical Chemistry, 85 (2013) 2391-2396.

[24] M.B. Oliveira, C.L. Salgado, W.L. Song, J.F. Mano, Combinatorial On-Chip Study Of Miniaturized 3D Porous Scaffolds Using A Patterned Superhydrophobic Platform, Small, 9 (2013) 768-778.

[25] W.L. Song, A.C. Lima, J.F. Mano, Bioinspired Methodology To Fabricate Hydrogel Spheres For Multi-Applications Using Superhydrophobic Substrates, Soft Matter, 6 (2010) 5868-5871.

[26] A.C. Lima, W. Song, B. Blanco-Fernandez, C. Alvarez-Lorenzo, J.F. Mano, Synthesis Of Temperature-Responsive Dextran-MA/Pnipaam Particles For Controlled Drug Delivery Using Superhydrophobic Surfaces, Pharmaceutical Research, 28 (2011) 1294-1305.

[27] S.M. Oliveira, W.L. Song, N.M. Alves, J.F. Mano, Chemical Modification Of Bioinspired Superhydrophobic Polystyrene Surfaces To Control Cell Attachment/Proliferation, Soft Matter, 7 (2011) 8932-8941.

[28] A.C. Lima, P. Sher, J.F. Mano, Production Methodologies Of Polymeric And Hydrogel Particles For Drug Delivery Applications, Expert Opinion On Drug Delivery, 9 (2012) 231-248.

[29] A.C. Lima, C.A. Custodio, C. Alvarez-Lorenzo, J.F. Mano, Biomimetic Methodology To Produce Polymeric Multilayered Particles For Biotechnological And Biomedical Applications, Small, 9 (2013) 2487-2492.

[30] A.C. Lima, C.R. Correia, M.B. Oliveira, J.F. Mano, Sequential Ionic And Thermogelation Of Chitosan Spherical Hydrogels Prepared Using Superhydrophobic Surfaces To Immobilize Cells And Drugs, Journal Of Bioactive And Compatible Polymers, 29 (2014) 50-65.

[31] S.M. Oliveira, N.M. Alves, J.F. Mano, Cell Interactions With Superhydrophilic And Superhydrophobic Surfaces, Journal Of Adhesion Science And Technology, 28 (2014) 843-863.

[32] A.I. Neto, H.J. Meredith, C.L. Jenkins, J.J. Wilker, J.F. Mano, Combining Biomimetic Principles From The Lotus Leaf And Mussel Adhesive: Polystyrene Films With Superhydrophobic And Adhesive Layers, Rsc Advances, 3 (2013) 9352-9356.

[33] Z.J. Cheng, M. Du, H. Lai, N.Q. Zhang, K.N. Sun, From Petal Effect To Lotus Effect: A Facile Solution Immersion Process For The Fabrication Of Super-Hydrophobic Surfaces With Controlled Adhesion, Nanoscale, 5 (2013) 2776-2783.

[34] N.M. Oliveira, A.I. Neto, W.L. Song, J.F. Mano, Two-Dimensional Open Microfluidic Devices By Tuning The Wettability On Patterned Superhydrophobic Polymeric Surface, Applied Physics Express, 3 (2010).

[35] K. Rasanen, A. Vaheri, Activation Of Fibroblasts In Cancer Stroma, Experimental Cell Research, 316 (2010) 2713-2722.

[36] S. Yonemura, M. Itoh, A. Nagafuchi, S. Tsukita, Cell-To-Cell Adherens Junction Formation And Actin Filament Organization - Similarities And Differences Between Non-Polarized Fibroblasts And Polarized Epithelial-Cells, Journal Of Cell Science, 108 (1995) 127-142.

[37] S.G. Spanakis, S. Petridou, S.K. Masur, Functional Gap Junctions In Corneal Fibroblasts And Myofibroblasts, Investigative Ophthalmology & Visual Science, 39 (1998) 1320-1328.

[38] V.A. Krutovskikh, C. Piccoli, H. Yamasaki, Gap Junction Intercellular Communication Propagates Cell Death In Cancerous Cells, Oncogene, 21 (2002) 1989-1999.

[39] G. Aubelsadron, D. Londosgagliardi, Daunorubicin And Doxorubicin, Anthracycline Antibiotics, A Physicochemical And Biological Review, Biochimie, 66 (1984) 333-352.

[40] L.F. Yu, M.C.W. Chen, K.C. Cheung, Droplet-Based Microfluidic System For Multicellular Tumor Spheroid Formation And Anticancer Drug Testing, Lab On A Chip, 10 (2010) 2424-2432.

[41] I. Amjadi, M. Rabiee, M.S. Hosseini, M. Mozafari, Synthesis And Characterization Of Doxorubicin-Loaded Poly(Lactide-Co-Glycolide) Nanoparticles As A Sustained-Release Anticancer Drug Delivery System, Applied Biochemistry And Biotechnology, 168 (2012) 1434-1447.

CHAPTER 8. FABRICATION OF HYDROGEL PARTICLES OF DEFINED SHAPES USING HYDROPHILIC-SUPERHYDROPHOBIC MICROPATTERNS *

8.1 Abstract

We report a method to rapidly fabricate alginate hydrogel microparticles of specific sizes and shapes. Our method is based on the formation of arrays of microdroplets of pre-hydrogel solutions on superhydrophobic-hydrophilic patterns using the process of discontinuous dewetting, followed by their gelation via the parallel addition of $CaCl_2$ to the individual droplets via the sandwiching method. We demonstrate that viability of living cells incorporated within the hydrogel particles is higher during the long-term cultivation than in the case of cells cultured in the bulk three-dimensional hydrogel matrix. Incorporation of magnetic particles into free-standing hydrogels containing living cells enabled ease manipulation of the particles using an external magnetic field.

* *Neto A. I., Demir K., Popova A. A., Oliveira M. B., Mano J. F. and Levkin P. A. Fabrication of Hydrogel Particles of Defined Shapes using Hydrophilic -Superhydrophobic Micropatterns.* ***Advanced Materials****. 2016, Accepted manuscript.*

8.2 Introduction

Hydrogels are hydrated three-dimensional (3D) cross-linked polymers resembling natural extracellular matrix (ECM) that provide soft 3D support for cellular growth and tissue formation [1]. Due to their unique properties such as high porosity, permeability for gases, nutrients and metabolites, as well as their compatibility with physiological conditions, hydrogels have been extensively studied as material support for immobilizing cells, cultivating cells in 3D [2], biomedical applications, drug delivery and tissue engineering [3].

Two distinct approaches namely "top-down" or "bottom-up" have recently emerged in hydrogel engineering. Top-down approaches control the microscale features (i.e. size and shape) of relatively large pieces of bulk hydrogels [4], whereas bottom-up approaches aim to generate larger tissue constructs via the assembly of smaller building blocks (usually cell-laden hydrogels) which mimic the *in vivo* tissue structure of repeating functional units [5].

The limitations of bulk hydrogels are that they usually lack the hierarchical architecture of *in vivo* tissues and suffer from the slow diffusion of nutrients and other biological signaling molecules (e.g., growth factors) from the surrounding medium into the entrapped cells, leading to higher toxicity and incompatibility with long-term cell cultivation. These drawbacks undermine the concept of employing hydrogels for 3D cell cultivation [6, 7].

Several attempts have been proposed to solve this problem [8-12]. The Doyle group developed methods to generate hydrogel microparticles with specific shapes using continuous flow or stop-flow lithography [13]. A droplet-based microfluidic system was proposed to construct alginate gel beads encapsulating cells [14]. Cell-encapsulating hydrogel particles have recently been used in several fields such as 3D cell culture and in vitro micro-physiological models [15, 16].

However, there are still too few methods allowing for the fabrication of hydrogel particles with different geometries and dimensions and compatible with the cell encapsulation [17]. New approaches combining the encapsulation of cells into structures with complex geometries and long-term cell analysis are also required.

We recently demonstrated a versatile platform for creating thousands of isolated microdroplets of specific geometry and volume, based on the use of superhydrophobic (SH) surfaces patterned with wettable superhydrophilic (SL) domains [18-22]. The extreme wettability contrast of the SH-SL patterns allows the spontaneous separation of an aqueous solution into high-density arrays of microdroplets using the effect

of discontinuous dewetting. This rapid and facile droplet formation does not require multiple pipetting or a liquid handling device. The handling of small volumes of droplets requires fewer reagents than with conventional microplates.

Microarray platforms can be used to study cellular behavior by creating distinct combinations of chemical/biochemical microenvironments [23, 24]. Micropatterning and microfluidic systems have been used to create hydrogels with spatially controlled organization as well as numerous cell-material or cell-cell combinations to analyze distinct biological issues [25, 26]. Micro-patterned arrays have been generated by immobilizing hydrogels on different micro-domains within a plane surface, and they have been used for disease diagnosis, prognosis, biochemical analysis, and therapeutic regimes, and have become an alternative approach for high-throughput multiplexed assays [27-30]. Strategies avoiding such 2D fixation of various hydrogels have employed shape-coded hydrogel particles as a suspension microarray format for multiplexed bioassays [31, 32].

Here we describe a method for the rapid fabrication of alginate hydrogel particles of defined sizes and shapes using the effect of discontinuous dewetting on an SH-SL microarray combined with the sandwiching method to achieve the simultaneous gelation of the pre-hydrogel droplets. We applied this method in three demonstrations: (1) preparing an array of hydrogel particles and free-standing hydrogel particles with distinct geometries and sizes defined by the photomask features; (2) examining the cells' *in situ* viability encapsulated into free-standing hydrogel particles, and (3) constructing magnetic responsive hydrogel particles for modular tissue engineering and shape-coded free-standing hydrogels of distinct cell types.

8.3 Results and Discussion

To produce the SH-SL array, a nanoporous poly(2-hydroxylethyl methacrylate-*co*-ethylene dimethacrylate) (HEMA-EDMA) polymer layer was formed on a microscope glass slide followed by modifying the polymer surface with alkyne groups via esterification [18]. Afterwards, an SH pattern with specific geometry was formed by functionalizing the surface with 1*H*,1*H*,2*H*,2*H*-perfluorodecanethiol using the thiol-yne photo-click reaction [18] and by applying a corresponding quartz photomask. The remaining alkyne groups were reacted with 2-mercaptoethanol under UV light to form the desired pattern of superhydrophilic (SL) areas separated by superhydrophobic (SH) borders. The porous SH regions possessed advancing (θ_{adv}), static (θ_{st}) and receding (θ_{rec}) WCAs of 173°, 170° and 164°, respectively, while the SL areas showed WCAs close to zero.[20]

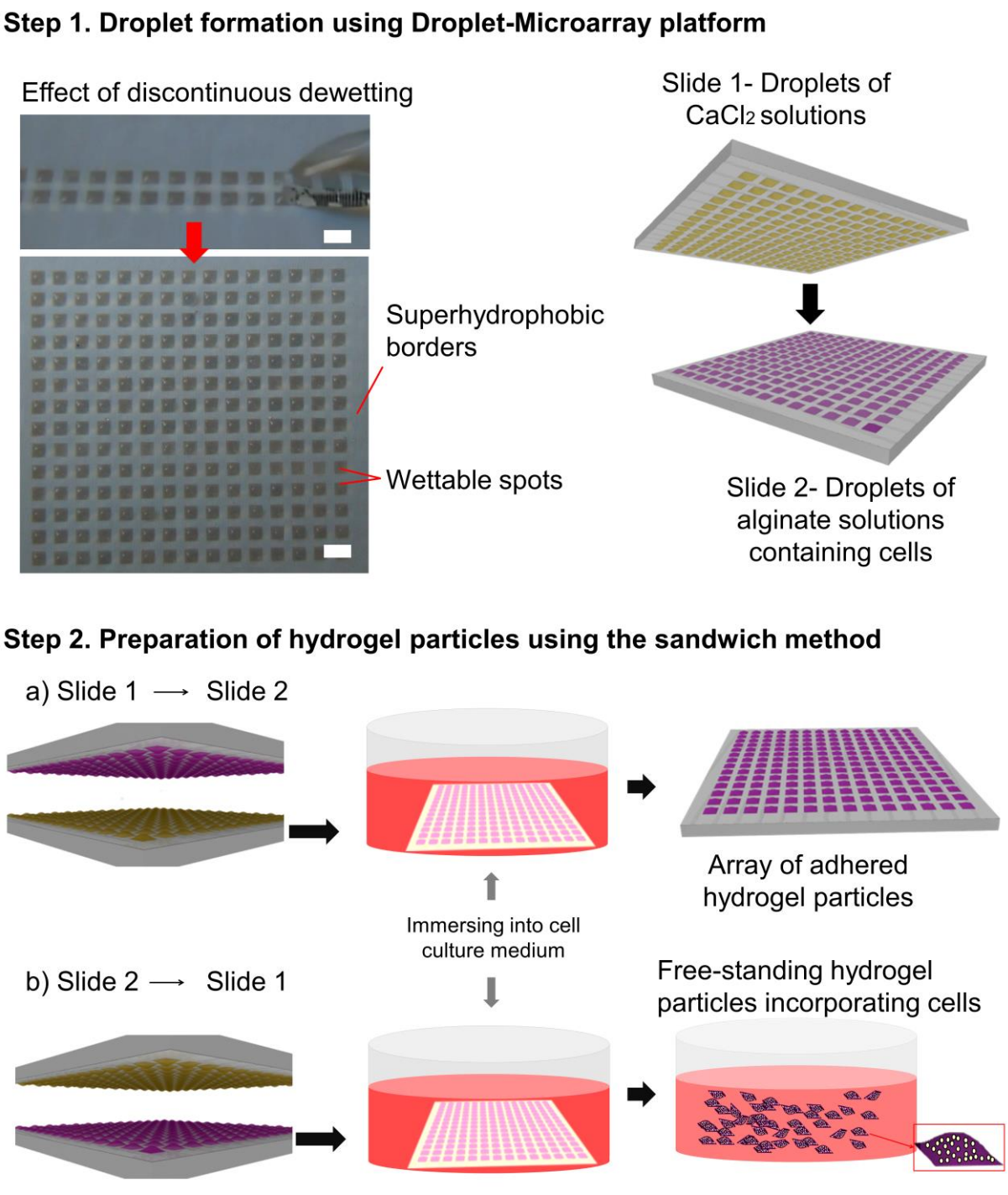

Figure 8.1 Schematic representation of the DMA platform and workflow for the high-throughput fabrication of hydrogel particles via the sandwiching method. Step 1: Formation of an array of droplets of a pre-hydrogel solution on a superhydrophobic-superhydrophilic array. Step 2: Crosslinking of alginate droplets by performing parallel addition of $CaCl_2$ solutions into the individual droplets via the sandwiching method. By changing the position of the slide 1 (bottom vs top) containing $CaCl_2$ droplets, it is possible to form either an array of fixed hydrogel particles (Step 2a) or detach hydrogel particles to form free-floating hydrogel particles (Step 2b). Scale bar: 2 mm.

The extreme difference in wettability between the SL spots and SH background creates a means of forming arrays of microdroplets using the effect of discontinuous dewetting [33] (Figure 8.1, Step 1). The size and volume of the droplets depend on the geometry and surface area of the hydrophilic regions and

is controllable from 700 pL up to 3 µL.[18] This allows for the dispensing of aqueous solutions into thousands of droplets without the need for manual pipetting or robotic devices. As soon as the nanoporous SL areas become wet, the porous polymer becomes transparent due to reduced light scattering caused by matched refractive indexes, thereby making SL spots visible and enabling light and fluorescent microscopy analysis. In this project we prepared arrays of droplets of different shapes and sizes (Figure 8.2, S2) with droplet height of 14.2 ± 1.3 µL (Figure 8.S1) [20].

The workflow of the high-throughput fabrication of hydrogel particles is illustrated in Figure 8.1. In the first step, two separated arrays of droplets were formed. Slide 1 was prepared using $CaCl_2$ solution (1 mol/L) as a crosslinker. The second slide (Slide 2) contained cells suspended in 2 mg.mL-1 of alginate solution. Afterwards, the two slides were aligned to come briefly into contact (Slide 1 – bottom, Slide 2 – top) to mix and form separated hydrogel droplets (Figure 8.1). The droplets' gelation occurred within seconds (~10 sec) after the addition of $CaCl_2$ solution. Then, the two slides were separated and an array of adhered hydrogel particles formed on the slide, which was located at the bottom during sandwiching (Figure 8.1, step 2a). In this case, our hypothesis is that $CaCl_2$ trapped in the porous polymer continues to diffuse into the droplets after the sandwiching step, leading to the formation of a stronger hydrogel layer at the surface, which anchors hydrogel to the polymer substrate even when the slide is immersed into solution. The stability of hydrogels-on-chip was tested for 7 days of culturing fully immersed in medium, which did not result in detachment. By changing the position of the two slides (Slide 1 – top, Slide 2 - bottom) an array of hydrogel particles formed again (Figure 8.1, step 2b). During the sandwiching step, the DMA slide containing alginate droplets is placed at the bottom. In this case, hydrogel particles could be easily detached from the DMA slide by immersing in culture medium or buffer. Free-standing hydrogel particles containing cells could be also formed using this method. We hypothesize that the reason for the different gelation and adhesion strengths of the hydrogel particles is caused by fast consumption of $CaCl_2$ during the crosslinking process in the droplets resulting in a weaker hydrogel layer at the bottom of droplets and their easy detachment.

To demonstrate the broad applicability of this method, we used the DMA platform to fabricate a variety of hydrogel particles with different geometries (Figure 8.2).

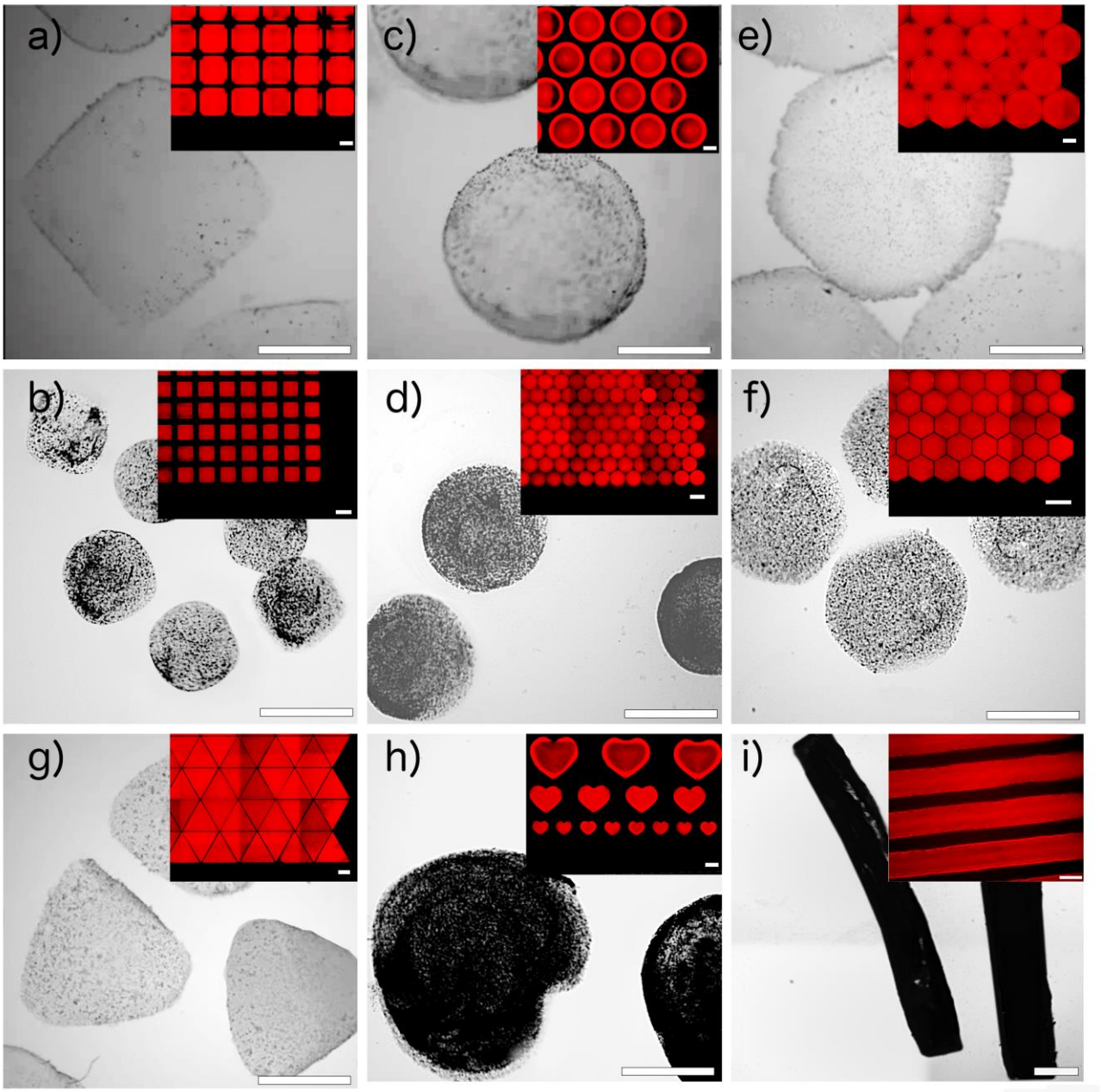

Figure 8.2 Microscopic images of free-standing hydrogel particles (bright-field images) containing magnetic beads and arrays of fluorescent hydrogel particles anchored to the patterned surfaces (insets). Fluorescent hydrogel particles contain 0.25 wt % of rhodamine 6G as additive. The following geometries were used: squares with 3 mm (a) and 1 mm (b) side length, circle with 3 mm (c) and 1 mm (d) diameter, hexagon of 3 mm (e) and 2 mm (f) side length, triangle with 3 mm side length (g), hearts with width of 3 mm (h) and stripes of 1 mm width. Scale bar 1 mm.

Both free-standing and on-array hydrogel particles of different sizes and geometries could be prepared. The dimension and shape of the hydrogel particles can be controlled by the photomask design. Comparison of the fluorescence intensity of hydrogels formed on distinct SL spots, as well as the dimensions of the free-standing hydrogels proved the homogeneous size distribution of hydrogel particles of different shapes (Figure 8.S2).

Figure 8.2 demonstrates that the droplet array method is not perfectly suited for the formation of hydrogel particles with sharp corners. This is a result of the surface tension of water solutions that tries to round off the corners of liquid droplets at the sharp edges of the hydrophilic-hydrophobic patterns. However, the shapes of hydrogel particles are easily recognizable and could be distinguished automatically by an image-recognition software. It is also evident from the images in Figure 8.2 that the geometry of edges of the pattern (straight lines – triangles and hexagons, round, or even concave in the case of hearts) is transferred to the hydrogel particles.

The shape of hydrogel particles can be applied in various ways and can also have an effect of cells or cell encapsulation. For example, the shape and size of particles will determine the number of cells per particle. The shape of particles will be important for constructing macro assemblies with diverse architectures, inter-particulate distances or particle-to-particle interactions. This method can be used as a toolbox of cell bearing hydrogel bricks of different shapes to enable diversity of multi-particle assemblies for modular tissue engineering [30]. In addition, shape of such building blocks can be used to encode information about the composition of the individual blocks without the need for separate fluorescent labeling (*vide infra*).

The mechanical properties of hydrogels are important for mimicking the *in-vivo* cellular environment and for achieving higher cell viability during long-term cell culture. The stiffness of hydrogels depends on the concentration of $CaCl_2$ used for gelation. Dynamic mechanical analysis see supplementary information and Figures 8.S1e-f for details) was used as a non-destructive technique to characterize the viscoelasticity of the hydrogels fabricated using different concentrations of $CaCl_2$. To check the long-term stability of free-standing hydrogels, we assessed the mechanical and viscoelastic properties on hydrogels immersed in cell culture medium with or without the supplementation of 1% (v/v) of $CaCl_2$ solution for 1, 3, 5 and 7 days (see Figure 8.S3 for details). Our results revealed that after immersion of crosslinked alginate hydrogels into cell culture medium the hydrogels' storage modulus decreased from 95 kPa (day 1) to approximately 19 kPa on day 7 (Figure 8.S3a) [34]. This could be explained by ionic exchange between calcium and monovalent ions (such as sodium ions). However, this tendency seemed to be reversed by a possible continuation of the crosslinking, by adding calcium ions to the medium. The hydrogels' storage modulus increased with the duration of immersion in the calcium-supplemented medium, to approximately 200 kPa, after 7 days of immersion (Figure 8.S3b). Moreover, in hydrogels immersed in calcium-containing medium, the loss-factor values did not vary significantly with time (Figures 8.S3c-d).

In the next step we also fabricated free-standing hydrogel particles incorporating living cells (Figure 8.3a). We first demonstrated that alginate and $CaCl_2$ exerted no cytotoxic effect on live human cervical tumor cell line expressing GFP (HeLa-GFP) (Figure 8.S4). Then, cells were seeded onto the SH-SL patterned surface containing round SL spots of 3 mm diameter by applying cell suspension containing 2 mg.mL-1 of alginate to form an array of separated droplets. $CaCl_2$ solution was spread on a separate DMA slide. Hydrogels were formed by sandwiching both slides using the sandwiching device (Figure 8.1). This led to the formation of an array of round, free-standing hydrogel particles particles of 3 mm diameter at the base. Each hydrogel particle incorporated on average 588 ± 62 cells (Figure 8.S5). The hydrogel array slide was immersed in cell culture medium supplemented with 1% of $CaCl_2$ for a few seconds, leading to the immediate detachment of hydrogel particles. $CaCl_2$ was added to the medium to keep the hydrogel particles from dissociating. The medium supplemented with calcium was exchanged every 2 days. Square hydrogel particles whose sides measured 1 mm were also fabricated using this method (Figure 8.S6). The viability of cells cultured in free-floating hydrogel particles was monitored for up to 7 days via propidium iodide staining and MTT assay (Figure 8.3b,c). These results were compared with the viability of HeLa-GFP cells cultured in a standard petri dish (2D positive control) and cells cultured in bulk 2 mm thick alginate hydrogel layers prepared in a 24-well microtiter plate. Already 24h after the onset of culturing, the viability of cells in free-standing hydrogels was more than 20% higher than that of the bulk hydrogels. The toxicity of cells cultured in the bulk hydrogel rose to 60% after 5 days and 80-90% after 7 days of culturing, while that of cells in the hydrogel particles rose to just about 20% and 30%, respectively. This is attributable to the cells' superior accessibility to oxygen and nutrients when cultured in the thin free-standing hydrogel particles compared with the limited nutrient and gas exchange in the bulk hydrogel system. The difference in cell viability can be explained by much higher surface area-to-volume ratio of free-standing hydrogels (app. 11) compared to bulk hydrogel (app. 0.9), which reflects in exchange rate of nutrients and oxygen. One property of ionically cross-linked alginate hydrogel particles is that they dissolve when cultured in standard Ca-negative culture medium. This happens due to the release of calcium ions into the surrounding media caused by the exchange with monovalent cations (such as sodium ions present in the medium) [34]. This could be either an advantage (enabling cell release from the hydrogel) or a disadvantage (when long-term cultivation is required). To address this problem, we supplemented the culture medium with 1% (v/v) solution of $CaCl_2$ (Figure 8.S7). Those results revealed no significant differences in the cells' viability, whereas the viability of cells cultured in cell culture medium (without calcium addition) dropped to 70% of viability on day 7. Thus, the addition of calcium ions to physiological media promotes mechanical integrity without affecting cellular viability.

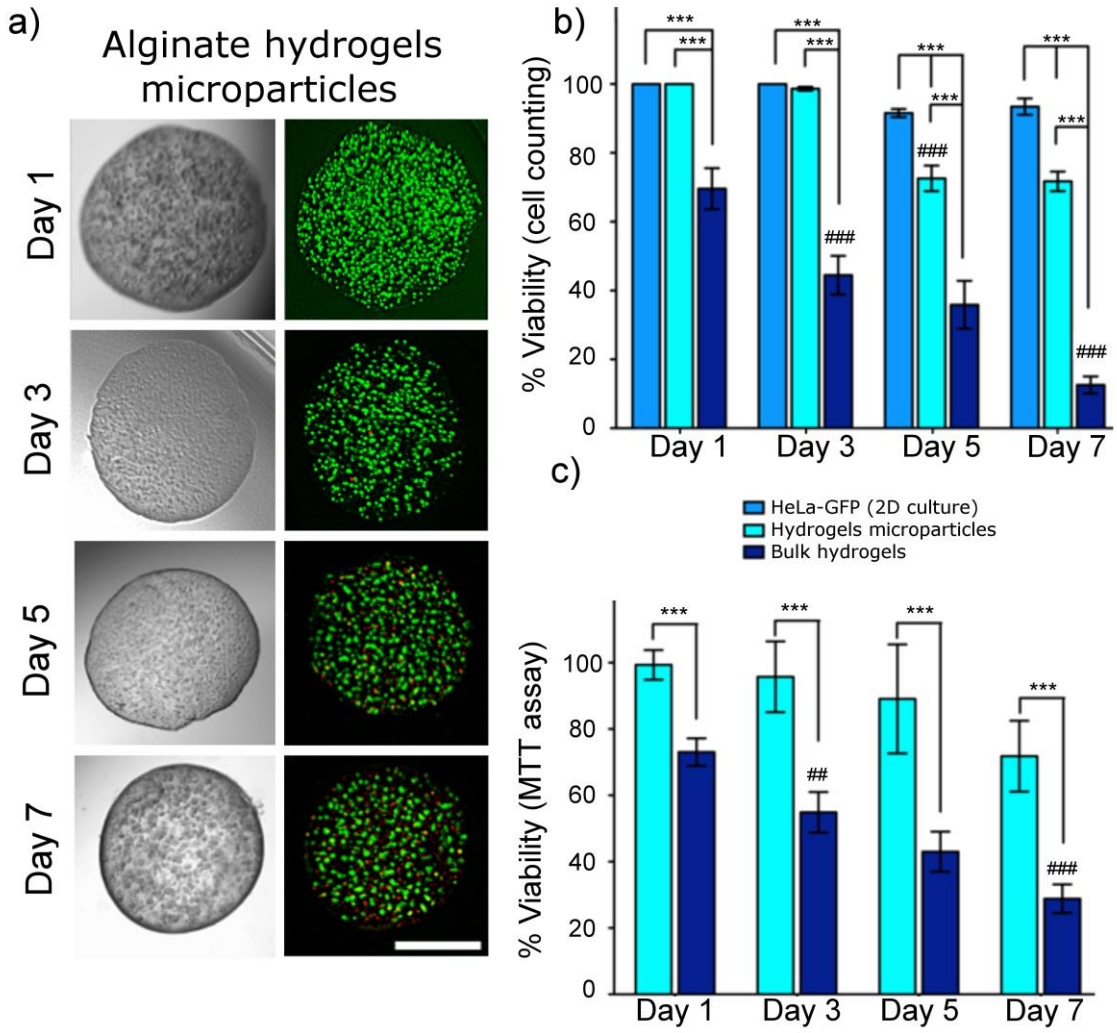

Figure 8.3 a) Representative brightfield and corresponding fluorescence images of free-standing hydrogels encapsulating HeLa-GFP cells for up to 7 days of culturing time. Dead cells are visualized using PI staining. Scale bar: 1 mm. b) Percentage of live cells obtained using image-based analysis and c) MTT colorimetric assay. Statistical differences by time point analysis were marked with (*), (**), (***), which stand for p-values <0.05; p<0.01; p<0.001, respectively. Statistical differences related to the previous time points are indicated by ## (p<0.01) or ### (p<0.001). All results are presented as ± standard deviation.

Magnetic field has been used in various cellular applications, cell sorting, 3D cell cultures, tissue engineering, local hyperthermia therapies, and clinical imaging applications [35-38]. Using the droplet microarray method, free-standing hydrogels can be loaded with functional magnetic or other nanoparticles to enable the use of magnetic field for the remote manipulation of the hydrogels (Figure 8.4).

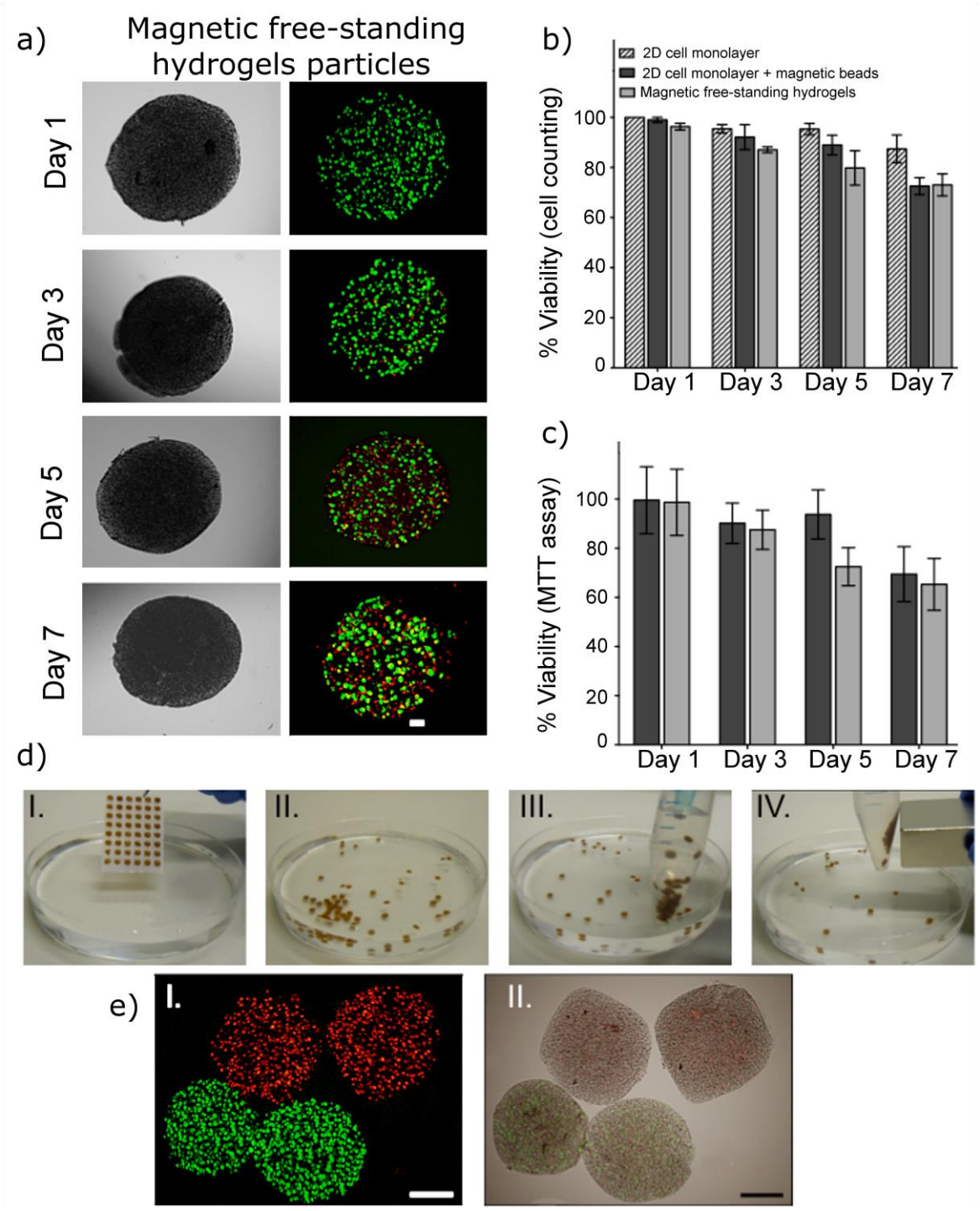

Figure 8.4 Magnetic free-standing hydrogel particles fabricated using the droplet-microarray approach. a) Representative brightfield and correspondent fluorescence images of magnetic hydrogels encapsulating HeLa-GFP cells and magnetic particles for 7 days of culturing time. Live and dead cells are represented by green (GFP) and red (PI) color, respectively. Scale bar: 200 μm b) Percentage of live/dead cells using image-based analysis (cell counting) and c) MTT colorimetric assay. Absorbance was read at wavelength of 570 nm. All results are presented as ± standard deviation. d) (I.) An array of square-shaped magnetic hydrogel particles (3 mm size length), (II) free-standing hydrogel particles formed by immersion the array in buffer, (III) manipulation of the particles by pipetting or (IV) an external magnetic field. e) Representative images of (i) brightfield, (ii) fluorescent and (iii) overlay of co-culture hydrogels with circle and square shapes. HeLa cells expressing GFP cells (green)

were immobilized in circle-shaped free-standing hydrogels and MLIy-mCherry cells (expressing fluorescent red) were immobilized in squared-shaped free-standing hydrogels. Scale bars: 1 mm.

Magnetic beads measuring 2 μm were added to alginate solution containing living Hela-GFP cells. The viability of cells cultured in free-floating magnetic hydrogel particles was evaluated for up to 7 days using propidium iodide staining, followed by fluorescence microscopy (Figure 8.4b). MTT colorimetric assay was performed separately (Figure 8.4c). We observed no significant differences in the viability of the cells cultured in the presence of magnetic beads in comparison to 2D cell culture (Figure 8.S8). After 1 day of cell culturing in a 2D and 3D environment, viability remained at 100%, dropping to 70% on day 7.

Magnetic hydrogel particles can be useful for the Modular Tissue Engineering [39] due to the possibility to manipulate both single particles and particle assemblies using external magnetic field. Thus, it is also possible to remotely control exchange of the medium, collection of hydrogel particles and active movement of particles across culture medium. On the other hand, application of the external magnetic field to a suspension of free-standing magnetic hydrogel particles permits rapid assembly of the particles into stable macroscopic 3D architectures (Figure 8.S11). The ability to remotely modulate the density and interparticulate volume of 3D hydrogel architectures using external magnetic field has been also demonstrated in a proof-of-concept experiment (Figure 8.S11). We showed that this method could be used to remotely compress or expand 3D hydrogel particle assemblies (3 mm diameter, n=250), which is important, for example, for achieving active perfusion of large 3D hydrogel particle assemblies with medium for long-term cell culturing (Figure 8.S11). The remotely controlled compression-expansion cycles could be repeated at least 50 times (Figure 8.S11). Finally, the ability to remotely compress hydrogel particle assemblies was applied to demonstrate the stimuli-responsive release of a small molecule drug incorporated inside the hydrogel using an external magnetic field as the stimulus (Figure 8.S9).

In order to demonstrate the ability to use hydrogel particles of diverse geometries for shape-coding to distinguish between hydrogels´ different compositions, we prepared two types of free-standing hydrogels: round 3 mm hydrogel particles encapsulating HeLa-GFP cells and square 3 mm hydrogel particles incorporating MLTy-CMV-mCherry-neo cells expressing cherry fluorescent protein (Figure 8.4e). The density of both cell types inside the distinctly shaped hydrogel particles was set to 6 x 10^5 cells per mL of alginate solution. The same amounts of free-standing hydrogel particles were mixed in a Petri dish. The fluorescence images show that no cross-contamination occurred between hydrogels, and that the cells remained immobile inside the particles (Figure 8.4). It is also evident that the shape difference opens the

way to differentiate between particles´ various compositions and encapsulated cell types without special fluorescence labeling.

8.4 Conclusions

We have demonstrated a new method to fabricate free-standing hydrogel particles with defined geometries and sizes, while maintaining control of the elastic modulus and the composition of the hydrogel. This platform offers several advantages: (i) thousands of hydrogel particles can be rapidly formed without the need for multiple pipetting; (ii) their size and composition can be controlled using the geometry of the hydrophilic areas; (iii) cells can be encapsulated inside hydrogel particles; (iv) the volume of the hydrogel particles can be in the nanoliter range scale, which is one order of magnitude less than that of a standard well in a 96-well plate; (v) sample cross-contamination is prevented by the use of superhydrophobic barriers; (vi) the hydrogel particles can be used either in the form of an array for screening applications or as free-standing particles. The presented technology was also used to form magnetic hydrogel particles incorporating live cells. These particles can be employed for the modular tissue engineering due to the possibility to manipulate both single particles and particles assemblies using external magnetic field. We believe that the ability to easily create and manipulate thousands of hydrogel particles of controlled size and geometry will be essential for 3D cell studies and modular tissue engineering. Finally, such a platform can potentially be applied to different types of biomaterials, hydrogels and cells.

8.5 Materials and Methods

Materials: Low viscosity sodium alginate from brown algae (~250 cP) was purchased from Sigma-Aldrich (USA). Magnetic beads (2 µm, chemagen) in a concentration of 100 mg.mL-1 were kindly provided by Prof. Dr. Matthias Franzreb (Institute of Functional Interfaces, KIT). Glass slides were purchased from Schott Nexterion. Sodium hydroxide (NaOH) was purchased from Carl Roth GmbH + Co. KG (Germany). Calcium chloride ($CaCl_2$), sodium chloride ($NaCl_2$) (p.a. ≥ 99,5%), *hydrochloric acid* (HCl), dichloromethane and 4-(dimethylamino)pyridine were purchased from Merck (Germany). 3-(trimethoxysilyl)propyl methacrylate, 2-hydroxyethyl methacrylate (HEMA), ethylene dimethacrylate (EDMA), cyclohexanol, 2,2-dimethoxy-2-phenylacetophenone, trichloro(1H,1H,2H,2H-perfluorooctyl) silane, 4-pentynoic acid, perfluorodecanthiol and fetal bovine serum (FBS) were purchased from Sigma-Aldrich Chemie (Germany). Silica beads (SilicaSphere 100 Å) was purchased from SiliCycle Dichrom GmbH (Germany). Adhesive film was purchased from Tesa (Germany). N,N'-diisopropylcarbodiimine and ß-mercaptoethanol were purchased from Alfa Aesar GmbH & Co KG (Germany). Quartz photomask was

developed with Autodesk Inventor 2011 software and manufactured by Rose Fotomasken (Germany). Dulbecco's Modified Eagle's Medium DMEM, Penicillin/ Streptomycin and trypsin/ EDTA were purchased from Gibco, Life Technologies GmbH (Germany). Red fluorescent rat mammary carcinoma MLIy-CMV-mCherry-neo was kindly donated by Prof. Jonathan P. Sleeman and Dr. Olivier Kassel (Institute of Toxicology and Genetics, KIT,Germany). Human Cervical tumor cell line HeLa expressing GFP was purchased from BioCat (Germany).

Preparation of the Droplet Microarray (DMA): Briefly, glass slides were first activated by immersing them in 1M NaOH for 1 hour followed by neutralization immersing them in 1M HCl for 30 minutes. Activated glass slides were modified with 20% v/v solution of 3-(trimethoxysilyl)propyl methacrylate in ethanol for 30 minutes at room temperature. In order to create a thin polymer thin atop of the modified glass slides, a polymerization mixture solution was prepared based on: 24 wt% 2-hydroxyethyl methacrylate (HEMA), 16 wt% ethylene dimethacrylate (EDMA), 12 wt% 1-decanol, 48 wt% cyclohexanol and 0,4 wt% 2,2-dimethoxy-2-phenylacetophenone. The polymer layer's thickness was controlled by applying 15 μm monodispersed silica beads on corners of fluorinated glass slide, which was prepared in trichloro(1H,1H,2H,2H-perfluorooctyl)silane vapor in desiccators under 50 mbar vacuum for 3 hours. Afterwards, a few droplets (70 μL) of polymerization solution were dispensed applied onto a fluorinated glass slide containing the silica beads and covered with a modified slide. Polymerization was performed by crosslinking a HEMA-EDMA polymer mixture via UV irradiation with 12 mW/cm^2 intensity and 260 nm wavelength for 15 minutes. The polymer surface was washed with ethanol and dried with an air gun. To increase the roughness, the polymer surface was taped with commercial adhesive tape. Then, the polymer surface was modified by immersing the entire glass slide in an esterification solution containing 45 mL of dichloromethane 56 mg of 4-(dimethylamino)pyridine, 111,6 mg of pentynoic acid and 180 μL of N,N'-diisopropylcarbodiimine for 4 hours while stirring at room temperature. A superhydrophobic pattern was obtained by dripping 5% v/v solution of perfluorodecanthiol in acetone onto the polymer surface and irradiating the slide with a photomask under 260 nm of UV light at 12 mW/cm^2 for 1 min. Superhydrophilic spots were created by applying 10% v/v ß-mercaptoethanol solution in 1:1 water:ethanol onto the patterned surface and irradiating the slide with 260 nm UV light at 12 mW/cm^2 for 1 min.

On-chip alginate hydrogel particles preparation ("Sandwich method"): A 2% w/v of alginate was dissolved in 0.15 M of NaCl. The pH of the alginate solution was adjusted to 7. Hydrogel particles were produced using patterned DMA by a sandwich method. Briefly, Slide 1 was prepared via the rolling droplet technique, simply by rolling a drop of 1M $CaCl_2$, in which liquid solution fills only the DMA slide's wettable areas. Slide 2 was prepared using the standing droplet technique, where a droplet of 1 mL of alginate

solution was lying on the top of a patterned array followed by slightly tilting the slide, thus enabling droplets to from spontaneously – see step 1 in Figure 8.1. For the precise alignment and sandwiching of $CaCl_2$ and alginate slides, both surfaces were mounted on a vacuum clamping system to ensure proper handling. First, the $CaCl_2$ slide was positioned laterally on a manual x,y linear stage PKT 130 (Owis GmbH, Staufen, Germany) mounted on a bottom plate. Then alginate slide was positioned vertically on the top place, so that its pre-printed pattern matched the geometry of the $CaCl_2$ slide. With the goniometer TP 65 (Owis GmbH, Staufen, Germany) the surfaces were positioned co-planar to enable the droplets' homogeneous diffusion. Using a UI-5490-SE camera (IDS Imaging Development Systems GmbH, Obersulm, Germany), we could monitor the sandwiching process in real time. The camera also enabled us to align both patterned slides. Once the droplets on different slides had remained in contact for 30 seconds, the patterned slides were separated from each other. The vacuum clamping system enabled fast and reproducible handling, allowing for highly coplanar removal of the upper glass slide and preventing the risk of cross contamination between droplets. This procedure makes it possible to produce immediately an array of hydrogel particles that remain fixed within the DMA even when the slide is immersed in liquid solution- see schematic representation of step 2a in Figure1. Detached hydrogels particles were obtained by moving the $CaCl_2$ slide to the top of the device- see schematic representation of step 2b of the Figure1.

Preparation of alginate hydrogels for dynamic mechanical analysis: A solution of 2% (w/v) sodium alginate was prepared. Portions of 200 μL of the alginate solution were poured into silicon molds with 7 mm diameter, and 2 mm height. Each circular well was then covered with 200 μL of $CaCl_2$. Different hydrogels were prepared by using $CaCl_2$ in concentrations of 0.1, 0.5, 1 and 2 M. The reaction occurred for 15 minutes, and the hydrogels were then rinsed with PBS. After their processing, the alginate hydrogels were tested for their storage modulus (E') and loss factor (tan δ) under cyclic compression using a Tritec 8000B (Triton Technology, United Kingdom) dynamic mechanical analyzer. To avoid any ionic exchange phenomena with the immersion media, the tests were performed under environmental conditions (not immersed, at room temperature). The assays were conducted through three compressive cycles of increasing frequencies ranging from 0.5 to 15 Hz. The experiments were done under constant strain amplitude, corresponding to 1% of the total height of the hydrogels, which was accurately measured for each specimen. At least 4 specimens were measured per condition. For the second characterization, hydrogels prepared with 1 M $CaCl_2$ were immersed in (i) DMEM cell culture medium and (ii) DMEM cell culture medium supplemented 1% of $CaCl_2$. Both immersion conditions aimed at mimicking the cell culture conditions used in this experiment. Cell culture media in both formulations were exchanged every

3 days at the same frequency as that in the cell culture experiments. The hydrogels were tested for their E' and tan delta after 1, 3, 5 and 7 days of immersion in cell culture media, at 37°C. The hydrogels were tested under immersion in DMEM (with or without calcium supplementation, similarly to the immersion medium during the experiment), at 37°C.

In vitro cell expansion and cell culture: Cells were routinely cultured in complete Dulbecco's Modified Eagle's Medium DMEM containing 10% of fetal bovine serum FBS and 1% of Penicillin/Streptomycin at pH 7.4. Cells were grown in 75cm^2 tissue culture flasks and incubated at 37°C in a humidified air atmosphere of 5% CO_2. Fresh medium was added every 2 to 3 days.

Cell encapsulation inside hydrogel particles: At 90% of confluence, cells grown in tissue culture flasks were washed with PBS and subsequently detached by a chemical procedure with 0.05% trypsin-EDTA solution for 2 minutes at 37°C in a humidified air atmosphere of 5% CO_2. To inactivate the trypsin effect, cell culture medium was added. Cells were then centrifuged at 1200 rpm and 25°C for 3 minutes and the medium was decanted. Afterwards, cells were mixed with 2% w/v alginate. Cell density was set to 6 x 10^5 cells per mL of alginate. This solution was then used to produce alginate hydrogels particles with the sandwich method previously described. Fixed and detached alginate hydrogel particles prepared in 1 x 1 mm size DMA with HeLa expressing GFP encapsulated cells were immersed in culture medium. The detached alginate hydrogels particles prepared in 3 x 3 mm circle-sized DMA containing HeLa-GFP encapsulated cells were immersed in cell culture medium, with and without supplementation of $CaCl_2$. Bulk alginate hydrogels (negative control) with HeLa-GFP cells were prepared in 24 well-plate using 1M of $CaCl_2$ solution and 2 % w/v alginate solution with cells in a ratio of 1:1 and cell culture medium. 200 µL of alginate solution containing cells was added into individual well (in triplicate) and further 200 µL $CaCl_2$ solution was added in order to crosslink the polymer solution. Afterwards, 500 µL of cell culture medium was added on the top of bulk hydrogel. Bulk hydrogels with 2 mm thick was prepared. During the incubation time, the cell culture medium was decanted and changed for fresh medium every 2 to 3 days. The entire procedure was performed under sterile conditions. All the solutions used in this step were sterilized by filtering them through a 0.22 µm filter.

Magnetic hydrogel particles (cell co-culture): We carried out the same procedure used to produce detached alginate hydrogel particles described previously to make the magnetic hydrogel particles. Magnetic bead solution was diluted to a final concentration of 10 mg.mL-1 and then centrifuged at 4000 rpm and 25°C for 10 minutes. The liquid was decanted and 2% w/v alginate added. Two different solutions of magnetic beads containing alginate were prepared. The first solution red fluorescent rat mammary carcinoma MLIy-CMV-mCherry-neo was mixed, and the second green fluorescent HeLa-GFP

was added. Green fluorescent cells were encapsulated inside alginate hydrogel particles prepared in 3 x 3 mm circular DMA, whereas red fluorescent cells were encapsulated inside alginate hydrogel particles prepared in 3 x 3 square-sized DMA. The hydrogels of different geometries with distinct cell types were then immersed in the same culture medium.

MTT viability assay: alginate hydrogel particles were tested for cytotoxicity and suitability for live cell encapsulation using a MTT colorimetric assay. This assay is based on the bioreductive ability of mitochondrial dehydrogenase enzymes present in viable cells to convert the (3-(4,5-dimethylthiazol-2-yl)-2,5-diphenyltetrazolium bromide) tetrazolium (MTT) compound into a cell culture-soluble purple formazan product. Circular alginate hydrogel particles prepared in 3 x 3 mm size DMA with HeLa expressing GFP encapsulated cells were placed in a non-treated surface 24-well cell culture plate (n = 3 per well, in triplicate) and incubated at 37°C and 5% CO_2. At 1, 3, 5 and 7 days of culture, the MTT assay was performed protected from the light. Briefly, culture medium was removed and 500 µL of serum-free DMEM containing MTT solution with a dilution ratio of 1:10 added to each well. Samples were then incubated in the dark at 37°C and 5% CO_2. The wells containing hydrogel participles were re-suspended using a pipette in order to release the cells encapsulated. After 3h, 100 µL of each well (in triplicate) was transferred to a 96-well plate. Then, 100 µL of dimethyl sulfoxide (DMSO) was added to each well to dissolve formazan crystals, and incubated for 1h at 37°C and 5% CO_2. The amount of formazan product was measured by absorbance at a wavelength of 570 nm using a multiwell spectrophotometer. The background was corrected by subtracting MTT blank solution. All these procedures took place for hydrogel particles cultured in culture medium with and without supplementation of $CaCl_2$, bulk hydrogels, cells suspended in culture medium with and without $CaCl_2$ supplementation, hydrogel particles with and without incorporation of magnetic beads, and cells suspended in culture medium with and without the supplementation of magnetic beads.

Fluorescence assay: Alginate particles (n = 3 per well in triplicate) and controls (n = 3 of cells suspensions and bulk hydrogels) were incubated for 1, 3, 5 and 7 days at 37°C and in a humidified 5% of CO_2 atmosphere. Live-dead assays were performed during each time culture period. HeLa-expressing GFP cells contain a green fluorescent cell marker retained in the cytoplasm. The unviable cells lose their green fluorescence. Propidium Iodide (PI) is a membrane impermeant and thus binds to the dead cells' DNA. At each time point, PI was added to each well at a ratio of 1:1000. Samples were incubated at 37°C for 10 minutes protected from the light. Images of the formed hydrogels were taken with the fluorescent microscope BZ-9000 Keyence (Japan) to enable accurate quantification. Double staining was obtained in Z-stack mode with a resolution of 90 µm between the slides for the hydrogel particles.

Cell behavior analysis: Image analysis tool (WCIF ImageJ software) was used to evaluate the percentage of live/dead cells in each hydrogel condition and the controls. Each image obtained from fluorescent microscope was divided in green and red channels and transformed into a gray scale (grey scale intensity 0-255, which 0 correspond to black and 255 white color). The number of cells counted in the each channel was divided to arrive at the number of total cells counted in the both channels. The counting was performed over total of 5 samples. The same threshold criterion was used in all images.

Dexamethasone diffusion: Magnetic bead solution was diluted to a final concentration of 10 mg.mL-1 and then centrifuged at 4000 rpm and 25°C for 10 minutes. The liquid was decanted and 2% w/v alginate added. 10 µL of dexamethasone solution was mixed with 1 mL of prepared alginate solution with a final drug concentration of 25 $\mu g.mL^{-1}$. Magnetic hydrogel particles containing dexamethasone (n=40, 5µL of each hydrogel particles) were prepared in 3 x 3 mm circular DMA slide. Bulk alginate hydrogels was prepared in falcon tube using 100 µL of 1M of $CaCl_2$ solution and 100 µL of 2 % w/v alginate solution containing magnetic beads and dexamethasone solution. The magnetic hydrogel particles and bulk hydrogel produced were immersed in 10 mL of pure water solution up to 240 minutes at room temperature. The absorbance of both formulations was measured at 241 nm over time, with and without the application of external magnetic field.

Modular building blocks: The magnetic hydrogel particles with 3 mm of diameter (n=250) were placed in glass capsule (usually used for GPC analysis) and the assembly of hydrogels was carried out using a stereo microscope. An external magnetic field was applied 50 times and the length of the modular tissue assembly was measured using ImageJ program.

Statistical analysis: MTT and fluorescent assay data were grouped by time point, namely, 1, 3, 5 and 7 days to analyze significant differences between formulations. Statistical analysis was performed using one-way analysis of variance (ANOVA) with Bonferroni post-test using GraphPad Prism 5.0 software. The adopted nomenclature was the following: statistical differences in grouped by time point analysis were marked with (*), (**) and (***), which stand for value p-value < 0.05, p < 0.01 and p < 0.001, respectively. To evaluate the statistical differences relating to the time point before, the # symbol was used. Single symbol (#) represent p < 0.05, double symbols (##) p < 0.01 and triple symbols (###) p < 0.001. All the results were presented as mean ± standard deviation.

8.6 Supplementary Figures

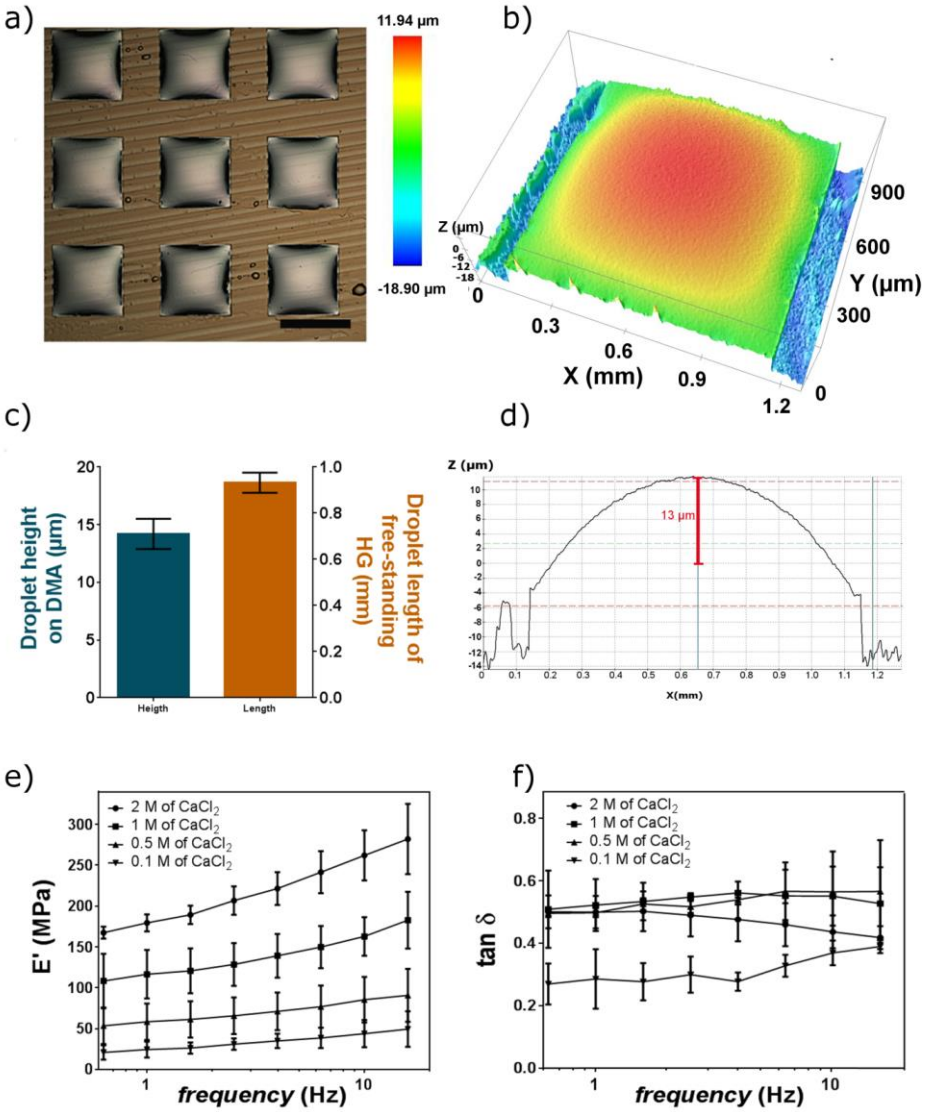

Figure S8.1 Representative brightfield image of a DMA containing hydrogel alginate particles. b) Figure obtained taken directly from the DMA using profilometry device, showing the homogeneous size distribution of the HG particles (c-d). Dynamic mechanical analysis measurements of e) Storage modulus (E´) and f) loss factor (tan δ) for alginate hydrogels obtained using different concentrations of calcium chloride.

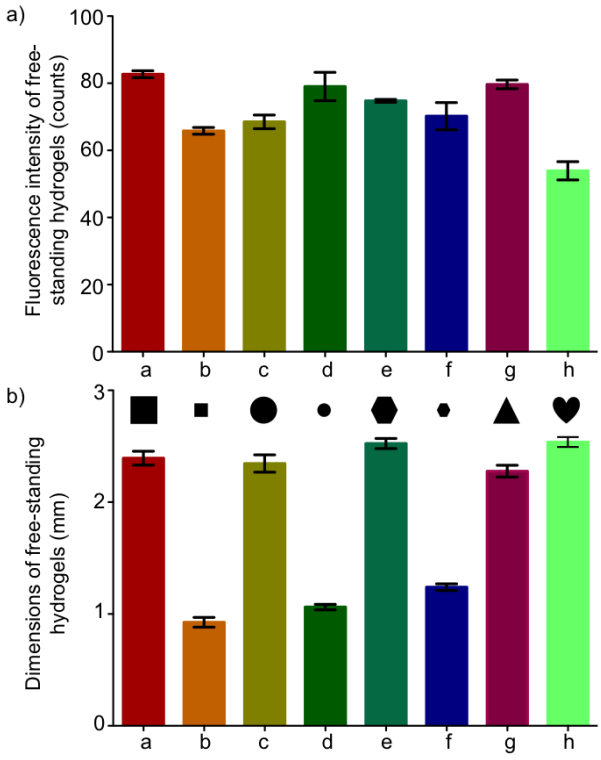

Figure S8.2 a) Fluorescence intensity and b) size measurements of the HG particles represented on the Figure 8.2 of the main text.

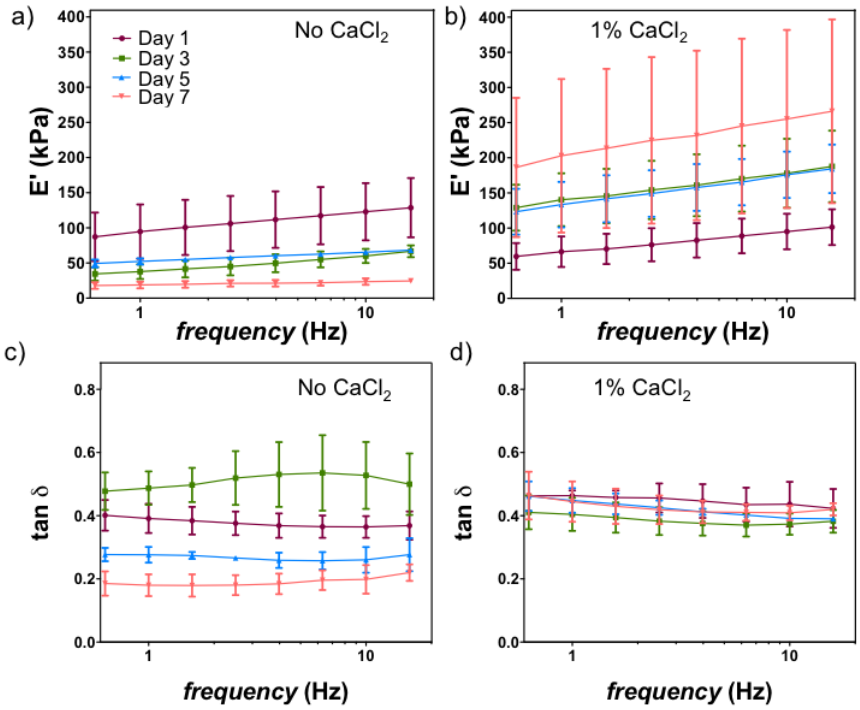

Figure S8.3 Dynamic mechanical analysis of a-b) storage modulus (E´) and c-d) loss factor (tan δ) for HG particles immersed in cell culture medium with and without calcium supplementation for up to 7 days' incubation time.

Figure S3 details:

Using more calcium chloride led to an increase in the hydrogel's storage modulus (E') , probably due to the establishment of more crosslinking points between the polymer chains and calcium ions. The use of increasing concentrations of $CaCl_2$ ranging from 0.1 M to 2 M led to a linear increase in the final storage modulus of the hydrogel ranging from 24 kPa to 180 kPa, for a frequency of 1 Hz (Figure 8.S1e). The hydrogel's loss factor was kept stable at a 1 Hz frequency, with values close to 0.5, for samples prepared with 2, 1 and 0.5 M of $CaCl_2$ (Figure 8.S1f). The tan δ values of the hydrogel prepared with 0.1 M $CaCl_2$ were lower (0.3, for 1 Hz), revealing their lower capacity to dissipate energy.

To check the long-term stability of free-standing hydrogels, we assessed the mechanical and viscoelastic properties of hydrogels immersed in cell culture medium with or without the supplementation of 1% $CaCl_2$ for 1, 3, 5 and 7 days. This study aimed at assessing the variations in the mechanical and viscoelastic properties of alginate hydrogels during cell culturing. In hydrogels immersed in cell culture medium without calcium supplementation, E' values dropped progressively over time, from 95 kPa (at 1 Hz) on day 1 to approximately 19 kPa on day 7. This behavior may be explained by the ionic exchange of the crosslinking divalent ion – calcium by monovalent ions present in the cell culture medium. A similar phenomenon has been reported as the reason for the lack of stability of ionically-crosslinked hydrogels during in vivo implantation. The hydrogels' dampening ability also decreased in conjunction with the immersion time in cell culture medium, from values ranging from 0.4-0.5 (for 1 Hz), to 0.2 (for 1 Hz). We detected the opposite trend in hydrogels incubated in cell culture medium supplemented with 1% of $CaCl_2$. Although the immersion in calcium-supplemented medium first led to a greater decrease in the E' values from 120 kPa (post-processing, at 1 Hz) to 66 kPa (day 1 after immersion, at 1 Hz), the hydrogels' storage modulus then increased with the duration of immersion in the calcium-supplemented medium, up to approximately 200 kPa, after 7 days of immersion.

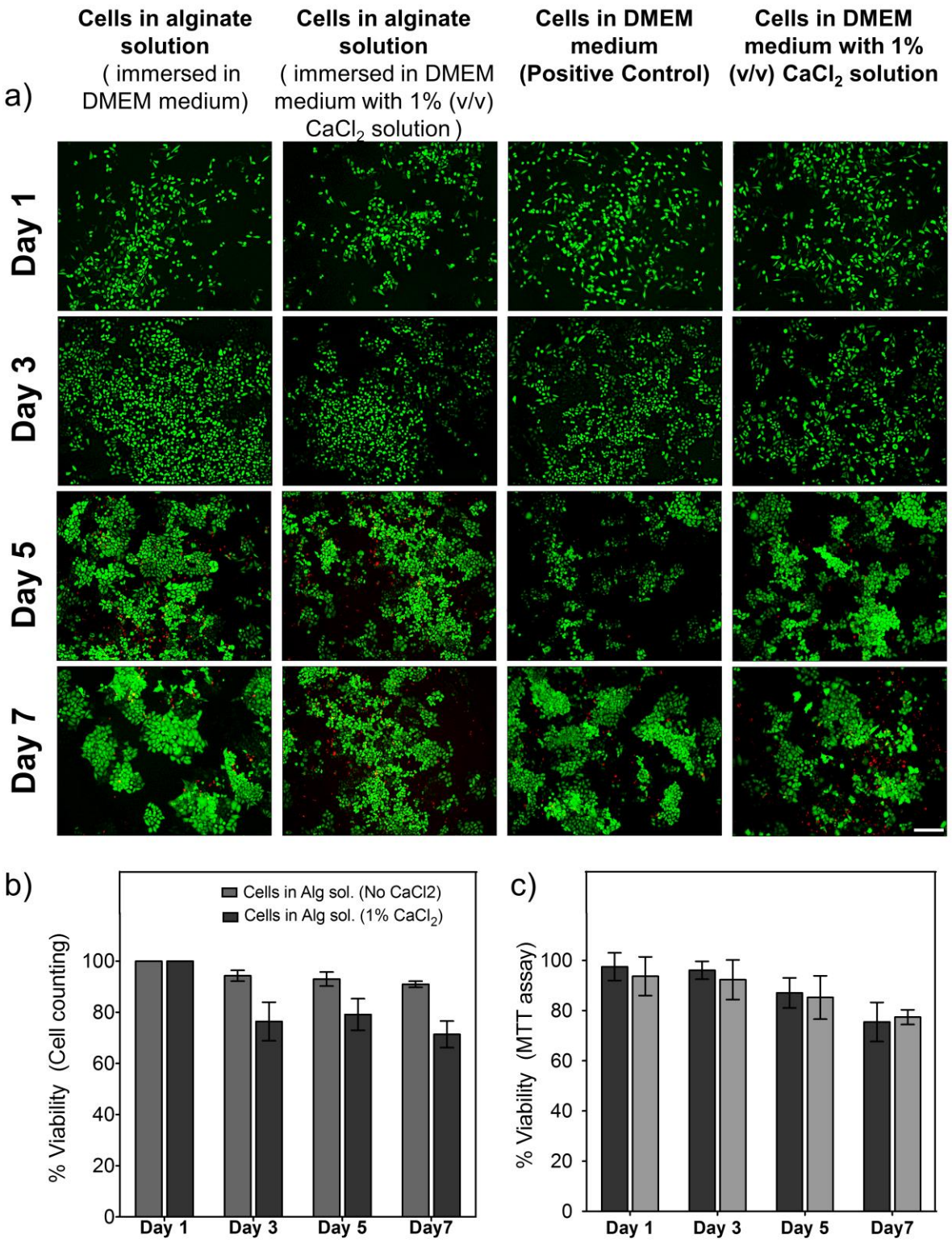

Figure S8.4 a) Representative fluorescence images of 2D monolayer culture of HeLa-GFP cells in alginate solution, with and without adding calcium chloride, to 7 days of culturing time. Live and dead cells are represented by green and red color, respectively. Scale bar: 1 mm. b) Percentage of live/dead cells using image-based analysis (cell counting) and c) MTT colorimetric assay. Absorbance was read at wavelength of 570 nm. All results are presented as ± standard deviation.

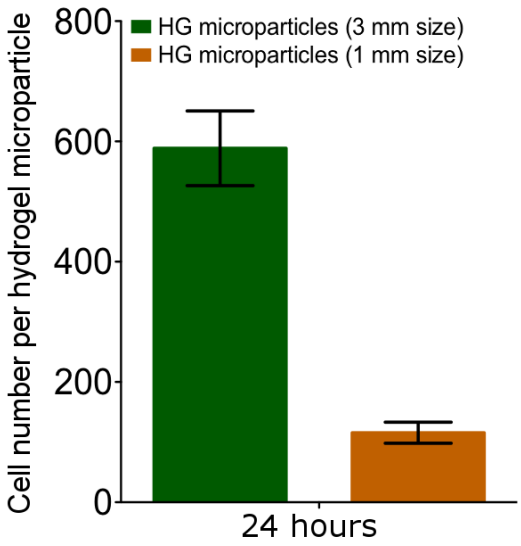

Figure S8.5 Quantification of cell numbers inside each 3 mm and 1 mm HG particles.

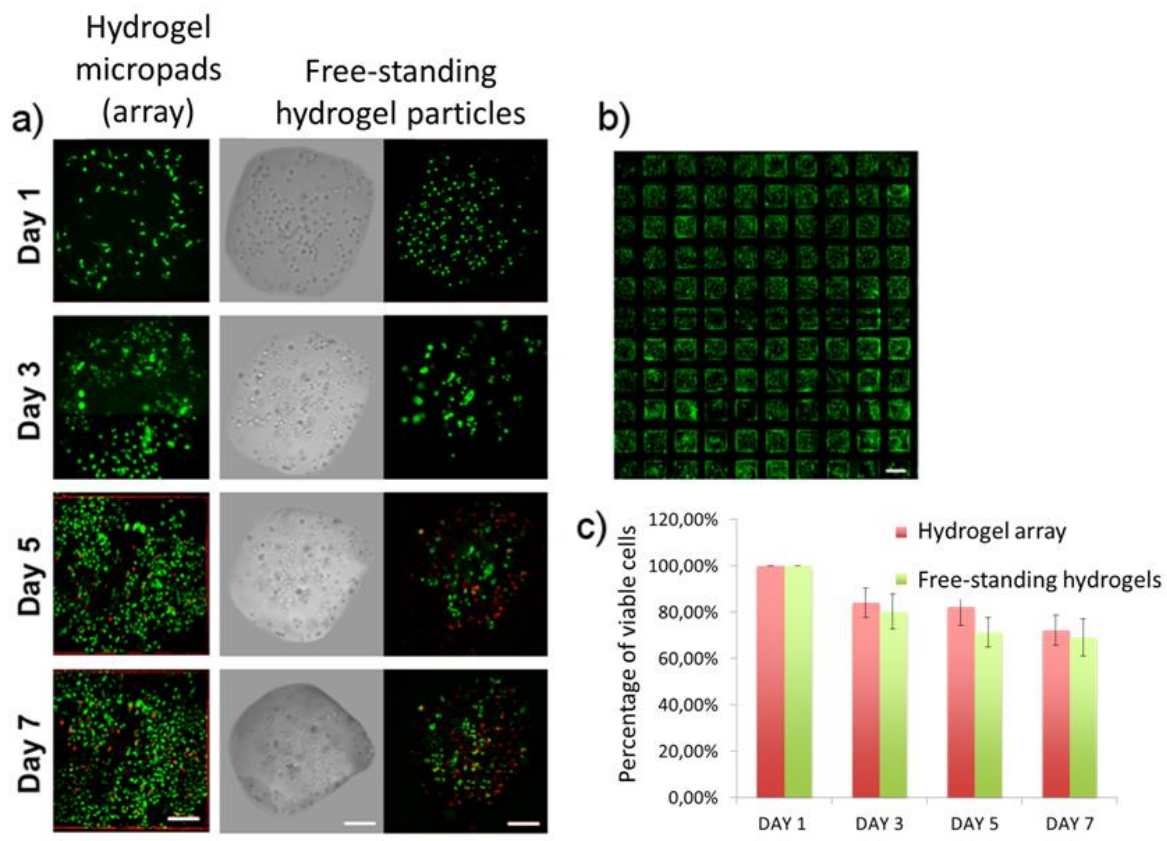

Figure S8.6 a) Hydrogel particles in Droplet-Microarray with square shape encapsulating HeLa-GFP cells up to 7 days of culturing time. Live and dead cells are represented by green and red color, respectively. Representative fluorescence images of the same cells-encapsulating hydrogel particle up to 7 days of culture time. b) Representative brightfield and fluorescence images of the same free-standing hydrogel particle up to 7 days of culturing time are also shown. Scale bar: 200 µm b) DMA slide containing anchored hydrogels with a square shape with HeLa cells encapsulated without any cross-contamination

between wettable spots. Scale bar: 1 mm. c) Percentage of live/dead cells using image-based analysis (cell counting). All results are presented as ± standard deviation.

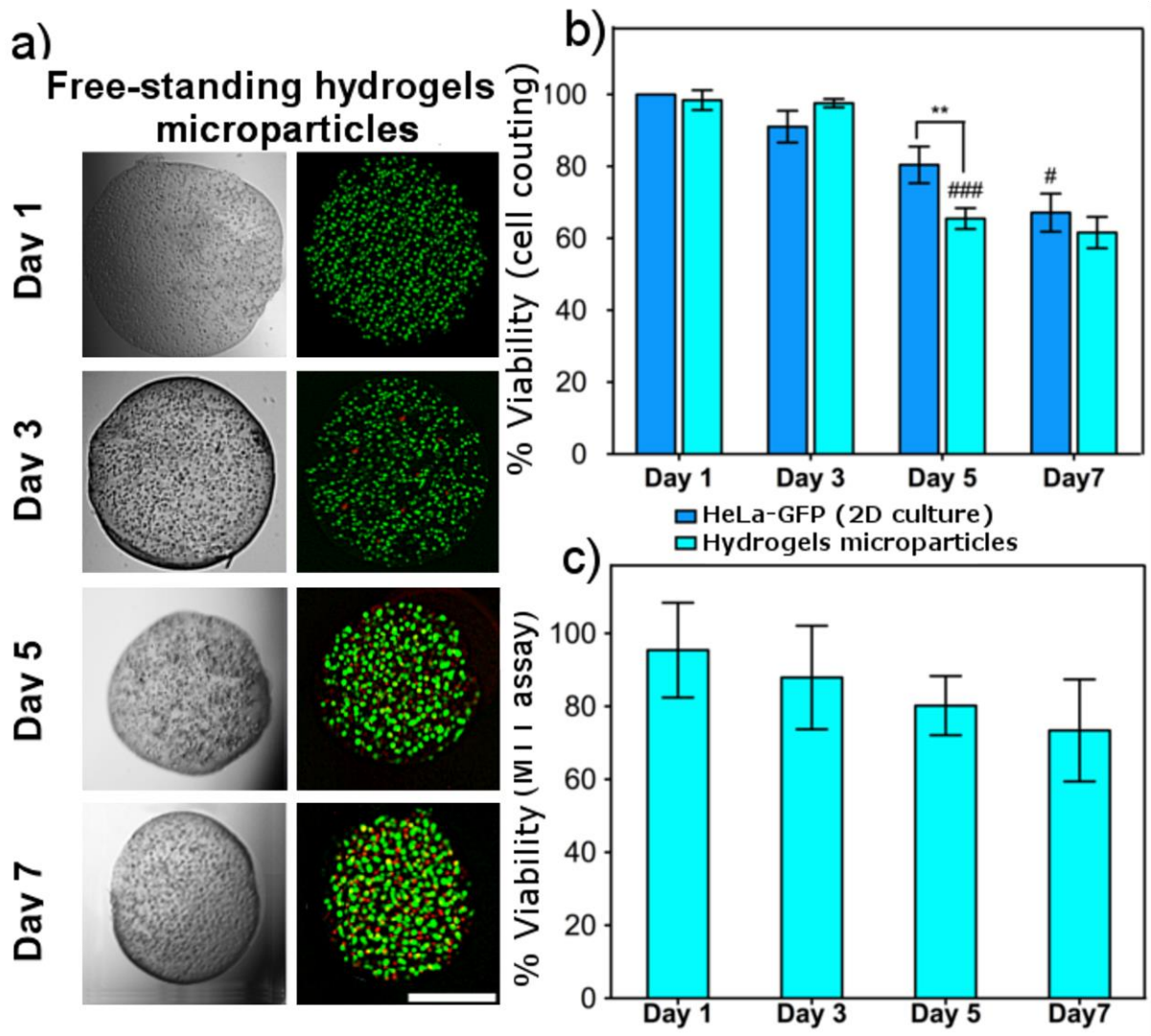

Figure S8.7 a) Representative brightfield and correspondent fluorescence images of free-standing hydrogels encapsulating HeLa-GFP cells, immersed in cell culture medium supplemented with 1% of calcium chloride, for up to 7 days of culturing time. Live and dead cells are represented by green and red color, respectively. Scale bar: 1 mm. b) Percentage of live/dead cells using image-based analysis (cell counting) and c) MTT colorimetric assay. Absorbance was read at wavelength of 570 nm. Statistical differences by time point analysis were marked with (**) which stand for a p-value <0.01. To determine the statistical differences relating to the previous time point, a single symbol (#) and triple symbol (###) represent p-value <0.05 and p<0.001, respectively. All results are presented as ± standard deviation.

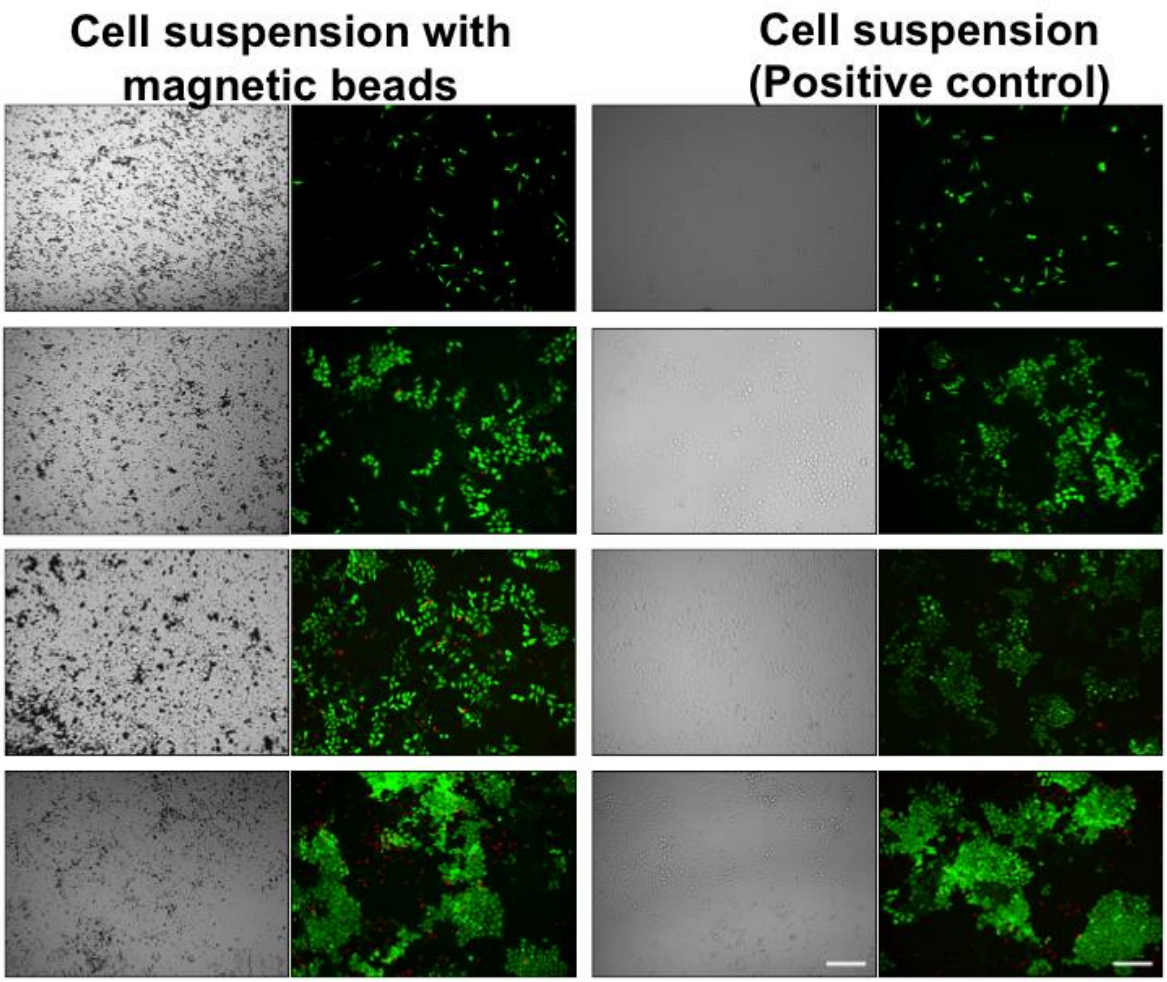

Figure S8.8 a) Representative brightfield and correspondent fluorescence images of 2D monolayer culture of HeLa-GFP cells after 7 days of culturing with and without magnetic particles. Dead cells (stained with PI) show red fluorescence, respectively. Scale bar: 1 mm.

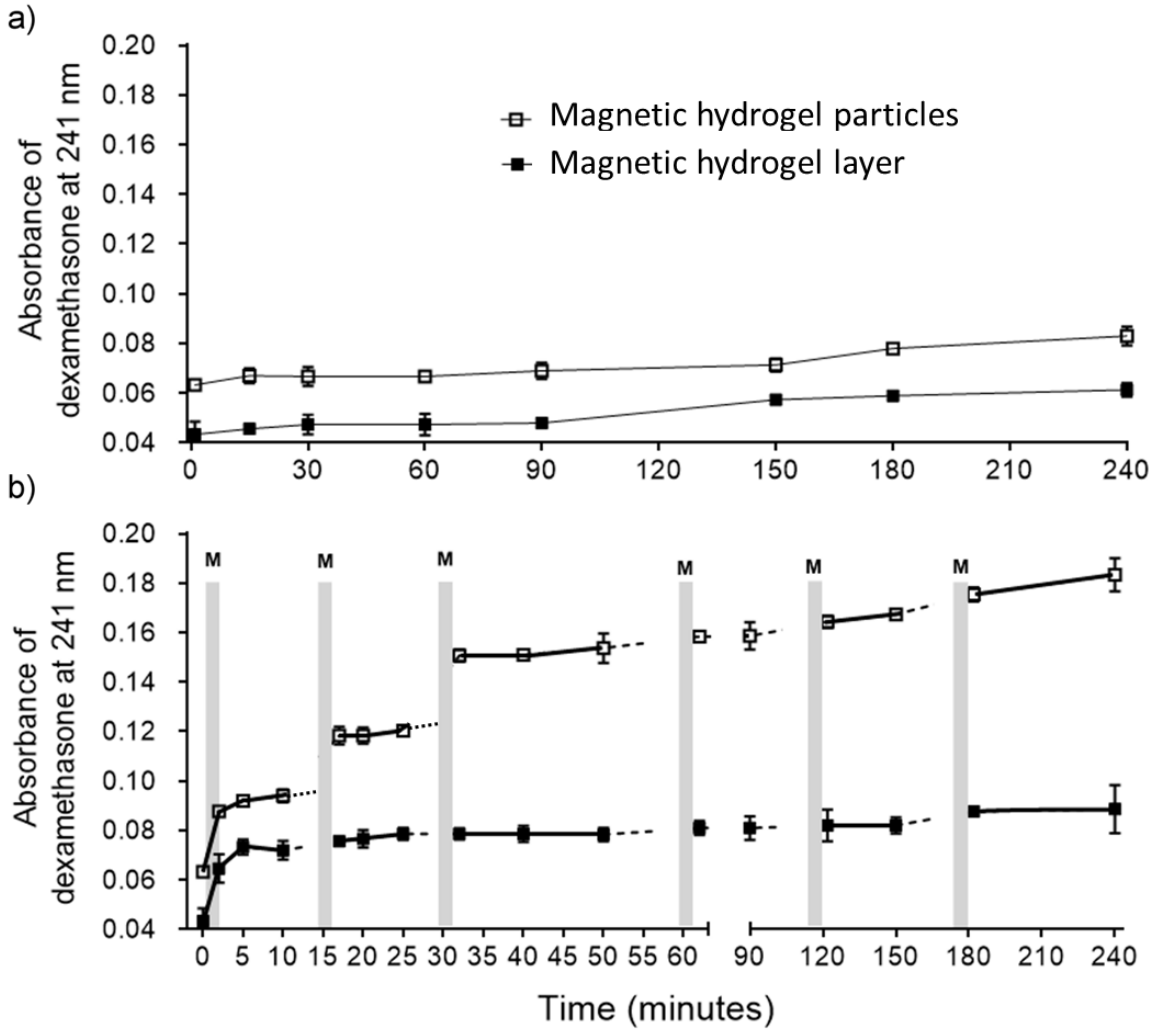

Figure S8.9 UV Absorbance measured at 241 nm of a supernatant above either hydrogel particles or bulk hydrogel layer. a) Magnetic hydrogel particles (n=40, $V_{particle}$= 5 µL) and bulk hydrogel layer incorporating magnetic beads (thickness 2 mm, V_{bulk}= 200 µL) containing dexamethasone (25 µg/mL) were incubated in DI water at room temperature. No magnetic field applied. b) The same as in (a) but with application of external magnetic field at different time points: 1, 15, 30, 60, 120 and 180 minutes. M – indicates the application of magnetic field for 2 min.

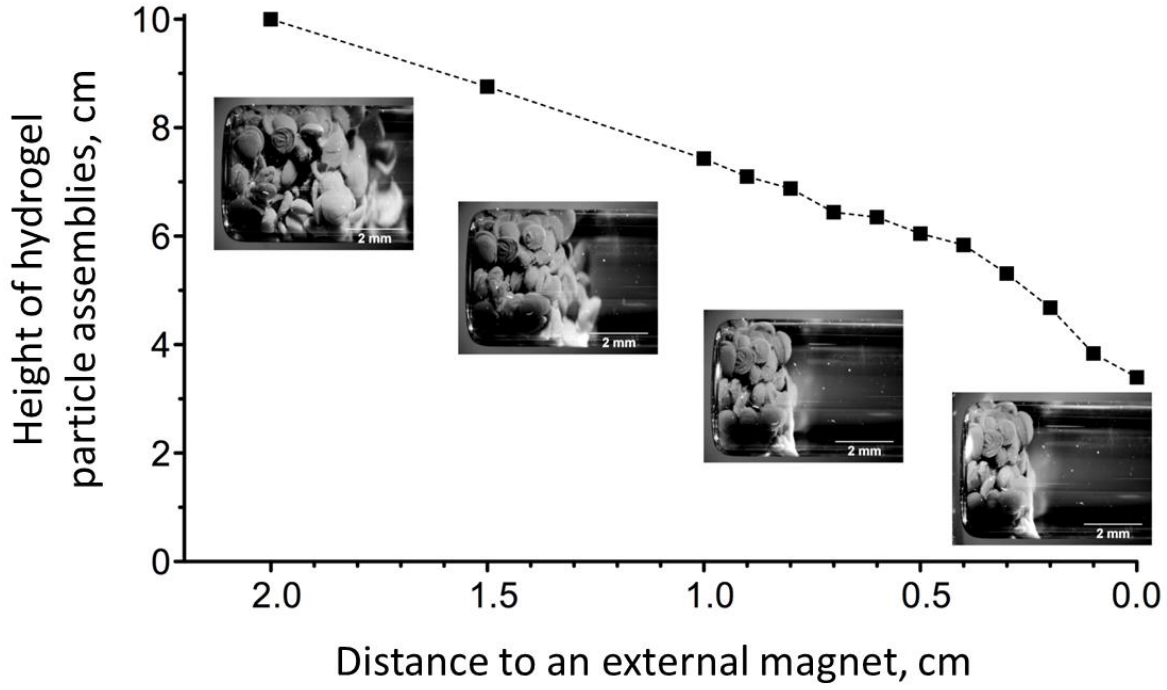

Figure S8.10 Plot showing the possibility to control the density of assembly of magnetic hydrogel particles using an external magnet applied at different distances from the particles. Plot of the height of an assembly of magnetic hydrogel particles (n= 250) in a glass tube with an external magnet positioned at different distances from the bottom of the glass tube. Corresponding images of the particles in the tube are shown.

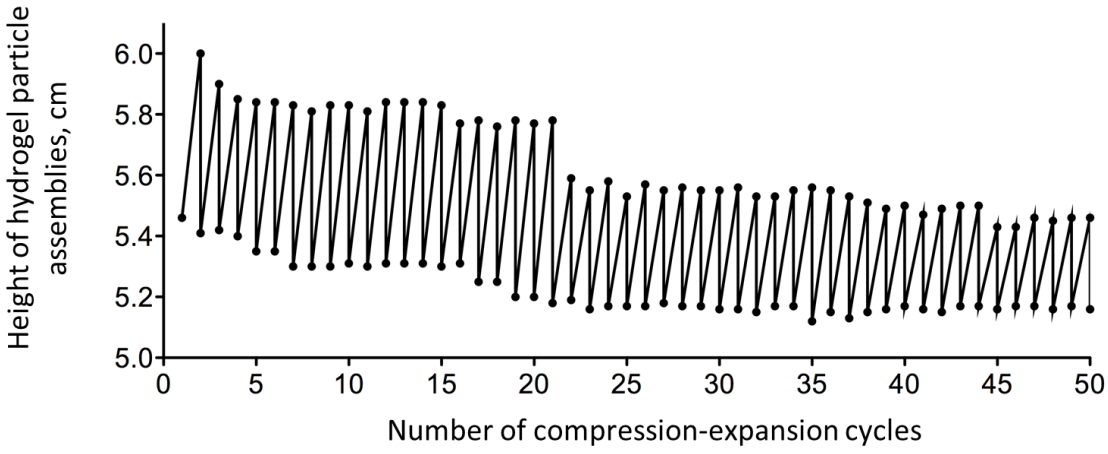

Figure S8.11 Reversible compression-expansion of an assembly of magnetic hydrogel particles (n = 250) by the application of external magnetic field.

8.6 Acknowledgments

The authors acknowledge financial support from the FCT- Fundação para a Ciência e para a Tecnologia through a Ph.D. grant with the reference SFRH/BD/73119/2010. This work was funded by the Helmholtz Association's Initiative and Networking Fund (grant VH-NG-621) and European Research Council Starting Grant (ERC-2013-StG 337077 DropCellArray). We are grateful to Dr. Christian Greiner's group of (KIT) for their help with optical profilometry measurements and to Dr. Gary Davidson and Dr. Olivier Kassel (Institute of Toxicology and Genetics, KIT) for providing the cell lines.

8.7 References

[1] O. Smidsrød, G. Skja, Alginate As Immobilization Matrix For Cells, Trends In Biotechnology, 8 (1990) 71-78.

[2] K.Y. Lee, D.J. Mooney, Hydrogels For Tissue Engineering, Chemical Reviews, 101 (2001) 1869-1879.

[3] J.L. Drury, D.J. Mooney, Hydrogels For Tissue Engineering: Scaffold Design Variables And Applications, Biomaterials, 24 (2003) 4337-4351.

[4] V. Chan, P. Zorlutuna, J.H. Jeong, H. Kong, R. Bashir, Three-Dimensional Photopatterning Of Hydrogels Using Stereolithography For Long-Term Cell Encapsulation, Lab On A Chip, 10 (2010) 2062-2070.

[5] R. Gauvin, R. Parenteau-Bareil, M.R. Dokmeci, W.D. Merryman, A. Khademhosseini, Hydrogels And Microtechnologies For Engineering The Cellular Microenvironment, Wiley Interdisciplinary Reviews-Nanomedicine And Nanobiotechnology, 4 (2012) 235-246.

[6] T.R. Hoare, D.S. Kohane, Hydrogels In Drug Delivery: Progress And Challenges, Polymer, 49 (2008) 1993-2007.

[7] T. Billiet, M. Vandenhaute, J. Schelfhout, S. Van Vlierberghe, P. Dubruel, A Review Of Trends And Limitations In Hydrogel-Rapid Prototyping For Tissue Engineering, Biomaterials, 33 (2012) 6020-6041.

[8] M.E. Helgeson, S.C. Chapin, P.S. Doyle, Hydrogel Microparticles From Lithographic Processes: Novel Materials For Fundamental And Applied Colloid Science, Current Opinion In Colloid & Interface Science, 16 (2011) 106-117.

[9] W. Lee, D. Choi, J.-H. Kim, W.-G. Koh, Suspension Arrays Of Hydrogel Microparticles Prepared By Photopatterning For Multiplexed Protein-Based Bioassays, Biomedical Microdevices, 10 (2008) 813-822.

[10] P. Panda, S. Ali, E. Lo, B.G. Chung, T.A. Hatton, A. Khademhosseini, P.S. Doyle, Stop-Flow Lithography To Generate Cell-Laden Microgel Particles, Lab On A Chip, 8 (2008) 1056-1061.

[11] J.Y. Sim, J.-H. Choi, J.-M. Lim, S. Cho, S.-H. Kim, S.-M. Yang, Microfluidic Molding Of Photonic Microparticles With Engraved Elastomeric Membranes, Small, 10 (2014) 3979-3985.

[12] Y. Du, E. Lo, S. Ali, A. Khademhosseini, Directed Assembly Of Cell-Laden Microgels For Fabrication Of 3d Tissue Constructs, Proceedings Of The National Academy Of Sciences Of The United States Of America, 105 (2008) 9522-9527.

[13] D. Dendukuri, D.C. Pregibon, J. Collins, T.A. Hatton, P.S. Doyle, Continuous-Flow Lithography For High-Throughput Microparticle Synthesis, Nature Materials, 5 (2006) 365-369.

[14] L. Yu, M.C.W. Chen, K.C. Cheung, Droplet-Based Microfluidic System For Multicellular Tumor Spheroid Formation And Anticancer Drug Testing, Lab On A Chip, 10 (2010) 2424-2432.

[15] A. Kumachev, J. Greener, E. Tumarkin, E. Eiser, P.W. Zandstra, E. Kumacheva, Biomaterials, 32 (2011) 1477-1483.

[16] D. Wei, W. Xiao, J. Sun, M. Zhong, L. Guo, H. Fan, X. Zhang, A Biocompatible Hydrogel With Improved Stiffness And Hydrophilicity For Modular Tissue Engineering Assembly, Journal Of Materials Chemistry B, 3 (2015) 2753-2763.

[17] S.P.R. Kobaku, G. Kwon, A.K. Kota, R.G. Karunakaran, P. Wong, D.H. Lee, A. Tuteja, Wettability Engendered Templated Self-Assembly (Wets) For Fabricating Multiphasic Particles, Acs Applied Materials & Interfaces, 7 (2015) 4075-4080.

[18] W. Feng, L. Li, E. Ueda, J. Li, S. Heissler, A. Welle, O. Trapp, P.A. Levkin, Surface Patterning Via Thiol-Yne Click Chemistry: An Extremely Fast And Versatile Approach To Superhydrophilic-Superhydrophobic Micropatterns, Advanced Materials Interfaces, 1 (2014).

[19] A.N. Efremov, E. Stanganello, A. Welle, S. Scholpp, P.A. Levkin, Micropatterned Superhydrophobic Structures For The Simultaneous Culture Of Multiple Cell Types And The Study Of Cell-Cell Communication, Biomaterials, 34 (2013) 1757-1763.

[20] A.A. Popova, S.M. Schillo, K. Demir, E. Ueda, A. Nesterov-Mueller, P.A. Levkin, Droplet-Array (Da) Sandwich Chip: A Versatile Platform For High-Throughput Cell Screening Based On Superhydrophobic-Superhydrophilic Micropatterning, Advanced Materials, 27 (2015) 5217-5222.

[21] E. Ueda, F.L. Geyer, V. Nedashkivska, P.A. Levkin, Droplet Microarray: Facile Formation Of Arrays Of Microdroplets And Hydrogel Micropads For Cell Screening Applications, Lab On A Chip, 12 (2012) 5218-5224.

[22] F.L. Geyer, E. Ueda, U. Liebel, N. Grau, P.A. Levkin, Superhydrophobic-Superhydrophilic Micropatterning: Towards Genome-On-A-Chip Cell Microarrays, Angewandte Chemie-International Edition, 50 (2011) 8424-8427.

[23] M.B. Oliveira, J.F. Mano, High-Throughput Screening For Integrative Biomaterials Design: Exploring Advances And New Trends, Trends In Biotechnology, 32 (2014) 627-636.

[24] F. Xu, J. Wu, S. Wang, N.G. Durmus, U.A. Gurkan, U. Demirci, Microengineering Methods For Cell-Based Microarrays And High-Throughput Drug-Screening Applications, Biofabrication, 3 (2011) 034101.

[25] G.T. Vladisavljevic, I. Kobayashi, M. Nakajima, Production Of Uniform Droplets Using Membrane, Microchannel And Microfluidic Emulsification Devices, Microfluidics And Nanofluidics, 13 (2012) 151-178.

[26] L. Wang, M. Qiu, Q. Yang, Y. Li, G. Huang, M. Lin, T.J. Lu, F. Xu, Fabrication Of Microscale Hydrogels With Tailored Microstructures Based On Liquid Bridge Phenomenon, Acs Applied Materials & Interfaces, 7 (2015) 11134-11140.

[27] A. Peters, D.M. Brey, J.A. Burdick, High-Throughput And Combinatorial Technologies For Tissue Engineering Applications, Tissue Engineering Part B-Reviews, 15 (2009) 225-239.

[28] C.L. Salgado, M.B. Oliveira, J.F. Mano, Combinatorial Cell–3d Biomaterials Cytocompatibility Screening For Tissue Engineering Using Bioinspired Superhydrophobic Substrates, Integrative Biology, 4 (2012) 318-327.

[29] H. Moch, P. Schraml, L. Bubendorf, M. Mirlacher, J. Kononen, T. Gasser, M.J. Mihatsch, O.P. Kallioniemi, G. Sauter, High-Throughput Tissue Microarray Analysis To Evaluate Genes Uncovered By Cdna Microarray Screening In Renal Cell Carcinoma, American Journal Of Pathology, 154 (1999) 981-986.

[30] F. Deiss, A. Mazzeo, E. Hong, D.E. Ingber, R. Derda, G.M. Whitesides, Platform For High-Throughput Testing Of The Effect Of Soluble Compounds On 3d Cell Cultures, Analytical Chemistry, 85 (2013) 8085-8094.

[31] D.C. Pregibon, M. Toner, P.S. Doyle, Multifunctional Encoded Particles For High-Throughput Biomolecule Analysis, Science, 315 (2007) 1393-1396.

[32] C.L. Lewis, C.-H. Choi, Y. Lin, C.-S. Lee, H. Yi, Fabrication Of Uniform Dna-Conjugated Hydrogel Microparticles Via Replica Molding For Facile Nucleic Acid Hybridization Assays, Analytical Chemistry, 82 (2010) 5851-5858.

[33] R.J. Jackman, D.C. Duffy, E. Ostuni, N.D. Willmore, G.M. Whitesides, Fabricating Large Arrays Of Microwells With Arbitrary Dimensions And Filling Them Using Discontinuous Dewetting, Analytical Chemistry, 70 (1998) 2280-2287.

[34] K.Y. Lee, D.J. Mooney, Alginate: Properties And Biomedical Applications, Progress In Polymer Science, 37 (2012) 106-126.

[35] A. Ito, M. Shinkai, H. Honda, T. Kobayashi, Medical Application Of Functionalized Magnetic Nanoparticles, Journal Of Bioscience And Bioengineering, 100 (2005) 1-11.

[36] J. Dobson, Remote Control Of Cellular Behaviour With Magnetic Nanoparticles, Nature Nanotechnology, 3 (2008) 139-143.

[37] F. Xu, C.-A.M. Wu, V. Rengarajan, T.D. Finley, H.O. Keles, Y. Sung, B. Li, U.A. Gurkan, U. Demirci, Three-Dimensional Magnetic Assembly Of Microscale Hydrogels, Advanced Materials, 23 (2011) 4254-4260.

[38] S. Gil, J.F. Mano, Magnetic Composite Biomaterials For Tissue Engineering, Biomaterials Science, 2 (2014) 812-818.

[39] J.W. Nichol, A. Khademhosseini, Modular Tissue Engineering: Engineering Biological Tissues From The Bottom Up, Soft Matter, 5 (2009) 1312-1319.

SECTION IV. CONCLUDING REMARKS AND FUTURE PRESPECTIVES

CHAPTER 9. CONCLUSIONS AND FUTURE PERSPECTIVES

Tissue Engineering (TE) involves numerous chemical, physical and biological events of remarkable complexity, which controls cell function, and facilitates the formation of tissue architectures, which are extremely important for the development of functional tissues. The ultimate goal of TE is to recreate such heterogeneous environments for engineering artificial tissues to replace or regenerate dysfunctional/damaged tissues and organs. Microarrays can significantly improve the identification of such formulations in the shortest possible time by enabling the high throughput screening of cell-matrix, cell-ECM and cell-drug interactions within heterogeneous tissue-like environment, in a cost-effective manner. In this thesis, interactions of cells with many diverse materials in both 2D- and 3D-dimensions were assessed rapidly through the use of SH microarrays for rapid outcome measures of cell-material or cell-cell combinations.

In Chapter 3, we reported the preparation of discrete and structured multilayered on glass slides. The formation of multilayers films of conjugate dopamine-modified hyaluronic acid and chitosan produced coatings with distinct properties, when compared with the conventional ones (chitosan and hyaluronic acid). The benefit of this work was to combine an enhanced cell response with a significantly improved adhesive strength, whereas the other reported methods have only showed improvements on cell behaviour. Afterwards, as proof-of-concept, structured multilayered regions were patterned on a single microarray. In Chapter 5, flat biomimetic SH surfaces patterned with transparent spots were produced by a bench-top methodology and were used for the build-up of arrays of multilayer films. The wettability contrast imprinted onto the chips allowed to produce individual and positional controlled, multilayer films in the wettable regions. In addition, the flat configuration of the microarray permitted to perform a series of non-destructive measurements directly on the individual spots. In this work, the influence of functional dopamine molecules on three specific LbL properties of interest was demonstrated: (1) final roughness, wettability, and morphology; (2) discrete measurement of adhesion properties of the films and (3) in situ examination of cells adhesion. Multilayer films containing catechol groups presented higher mechanical adhesion strength and enhanced cell adhesion, showing potential to be used as a new generation of wound healing bandages or surgical sealants, or even, as surface coatings for optimized cell-substrate interaction. The preparation of multilayer films on microarrays (Chapter 5) present several advantages compared with conventional glass slides (Chapter 3): ability to control the uniformity and size of the multilayers films; it's suitability to be used as a new low cost toolbox and for high-content cellular screening; and capability for monitoring *in situ* a variety of distinct material properties.

In this thesis two biomimetic approaches were created. First, in Chapter 4, polystyrene membranes with both SH properties of a lotus leaf and adhesive domains of marine mussels were designed into 3D tube structure by employing the adhesion to provide bonding for construction. SH and hydrophilic features were patterned onto one surface, thereby constraining the localization of water. We hypothesize that such efforts will contribute to future advances in materials development, especially the biomedical management of fluid flow, by showing that multiple bioinspired approaches can be combined into one system. On a second approach, Chapter 6, a new concept of microarray platform for anchoring aqueous-based microliter droplets was developed based on SH substrate mimicking the extreme water repellency of lotus leave patterned with adhesive micro-indentations simulating the effect of rose petals. The platforms allowed to screen physical, chemical and biological processes involving the combination of distinct elements and conditions, confined in spherical liquid mini-reactors. The high stability, precise positional and adhesiveness of the droplets allow to invert the platform 180° according to hanging drop approaches. Under this configuration the cells initially suspended in the droplets give rise to spheroids formed by gravity. In Chapter 7, the innovation of this system relies on the spherical geometry ("hanging spherical drop" method) exhibited by the cell suspension droplets. The size and composition of each droplet could be easily controlled in an individual form. The dose-dependent cytotoxic effect of doxorubicin was measured, and, as expected, we observed a decreasing viability of the cells with increasing doxorubicin concentration. The spheroids also exhibited enhanced resistance to the drug over standard monolayer cultures.

In Chapter 8, a new method was developed to fabricate free-standing hydrogel particles with defined geometries and sizes, while maintaining control of the elastic modulus and the composition of the hydrogel. The method was based on the effect of discontinuous dewetting on an SH-SL microarray combined with the sandwiching method to achieve the simultaneous gelation of the pre-hydrogel droplets. We applied this method in three demonstrations: (1) preparing an array of hydrogel particles and free-standing hydrogel particles with distinct shapes and sizes defined by the photomask geometrical features; (2) examining the cells' *in situ* viability encapsulated into free-standing hydrogel particles, and (3) constructing magnetic responsive hydrogel particles for modular tissue engineering and shape-coded free-standing hydrogels of distinct cell types. Using this platform several hydrogel particles were rapidly formed without the need for multiple pipetting. The size and composition of the hydrogel particles was controlled depending on the geometry of the hydrophilic areas. The volume of the formed hydrogel particles was in the nanoliter range scale, which is one order of magnitude less than that of a standard well in a 96-well plate. In this work hydrogel particles were produced either in the form of an array for screening

applications or as free-standing particles. Free-standing hydrogels incorporating magnetics beads were formed. We believe that the ability to easily create and manipulate a large amount of hydrogel particles of controlled size and geometry will be essential for 3D cell studies and modular tissue engineering.

Several advantages are drawn from the use of SH surfaces as chips for high-throughput analysis. The size and composition of the platform, as well as, the geometry of the wettable spots, can be easily controlled in an individual form, and the assays in the liquid state occur only in the desired wettable area without cross-talking between spots. The use of micro-size droplets for the production of multilayer films/ spheroids or hydrogels, as well as for biological assays, allows a drastic reduction of the volume in which the cells are grown; cell culture media can be changed easily without destroying the integrity of formed 3D structured. The platform is compatible with or easily adapted to many characterization can be performed using image-based analysis directly on the chip taking the benefit of the transparency of the spots (Chapter 5 and 8) and high-throughput combinatorial analysis may be performed *in situ* using different cell types. The cost associated with the production of the SH chips is low, and the technology is amenable to be easily scaled- up. The high contrast of wettability allows having biomaterials with different sizes simply by varying its volume to be dispensed in the wettable spot, while maintain the same contact area with the substrate.

In the Future, patterned microarrays could be created using digital liquid patterning as it offers simple and maskless approach for manual generation of micrometer precise liquid patterns without the need of manufacturing photomasks or changing substrate every time when geometry of liquid pattern has to be changed or modified. Therefore, this approach can reduce experimental time for the production of arbitrary liquid patterns of variety biomaterials and cells. Digital liquid patterning is also suitable for the generation of multi-component gradients with complex geometry of different materials compatible with biological studies. In addition, the method does not require special training or sophisticated equipment for generation liquid patterns or gradients, thus the technique is easy accessible to virtually any user.

In conclusion, patterned SH surfaces as high-throughput platforms for TE studies were successfully created and opened several perspectives that may be developed in future works. A possibility is the ability to create 3D biomaterial microchips that can be implanted clinically for cost-effective screening of the host response to new biomaterials, in a personalized medicine perspective. It would be interesting to develop an array of miniaturized 3D micro tissues (e.g spheroids) on 3D biomaterial microchip (porous scaffold or hydrogel), where cell co-culture could be implemented (on both porous platform and on formed micro tissues) to examine specific tissue regeneration in HTS manner. To enhance the function of

engineered tissues there is a need to generate structures that mimic the intricate architecture and complexity of native organs and tissues. With the desire to create more complex tissues with features such as developed and functional microvasculature, cell binding motifs and tissue specific morphology, TE techniques have evolved on building modular microtissues with repeated functional units. Therefore, patterned SH surfaces could be used for HTS formation of core-shell hydrogel beads incorporating elements of the extracellular matrix and support the formation of multicellular spheroids. For example, using temperature-responsive polymers as hydrogel core, the polymer shell could be formed using a different polymer and through by ionic crosslinking. Warming-up the hydrogels, the core would be dissolved, maintaining the multicellular spheroids protected inside the bead shell with cell culture medium surrounding. In addition, hydrogels with different sizes and shapes may be used to create shape-controlled tissue modules from modular microscale units. Such approach could be advantageous because cells can create their own microarchitecture through ECM remodeling and cell migration/aggregation.